Cardiff University

School of Chemistry

Luminescent and Electrochemical Probes Based on Au(I), Ir(III) and Fe(II) Coordination Complexes for Bioimaging, Diagnostics and Therapeutics

Thesis submitted for the degree of Doctor of Philosophy by:

Lara May Groves

September 2017

CARDIFF UNIVERSITY

SCHOOL OF CHEMISTRY

ABSTRACT

Doctor of Philosophy

By Lara May Groves

This thesis describes the development and synthesis of a range of novel fluorophores based on 1,8-naphthalimide, N-heterocyclic carbene (NHC) and phosphine derivatives, as well as coordination chemistry with Au(I), Ir(III) and Fe(II). Detailed discussions on the characterisation and the photophysical properties are described, with reference to applications including bioimaging, diagnostics and therapeutics.

Chapter 2 describes the synthetic development and spectroscopic analysis of a series of NHC-functionalised 1,8-naphthalimide fluorophores, generating ten new ligands that were successfully utilised for Au(I) coordination chemistry. The optical properties of the compounds were dictated by ligand-centred transitions. Cytotoxicity assessments revealed that compounds were the most toxic to LOVO and MCF-7 cell lines. In addition, lysosomal localisation was observed in cell imaging studies with MCF-7 cells, as seen with structurally related anticancer compounds.

Chapter 3 describes the synthetic development and spectroscopic analysis of a series of aminophosphine and phosphinite fluorophores, generating six new ligands, with some successfully utilised for Au(I) coordination chemistry. The photophysical properties were explored in detail due to the presence of different fluorescent groups, including naphthalene, anthracene, pyrene and anthraquinone. In this chapter, ^{31}P NMR was particularly important in confirming the success of the synthetic routes.

Chapter 4 describes the comparative syntheses of six new phenyl-1*H*-pyrazoles and their corresponding cyclometalated iridium(III) complexes using both batch and, successfully applied, flow-microwave methodologies. Isolation of spectroscopically pure species in less than 1 hour of reaction time from $IrCl_3$ was observed, along with ligand-dependent, tuneable green-yellow luminescence.

Chapter 5 outlines determination of a successful synthetic route to a series of fluorescent electrochemical biosensors that incorporate both a redox active ferrocene unit and a naphthalimide moiety, with the intention to be applied as an electrochemical detection method for Clostridium Difficile (CDF). Detailed photophysical and electrochemical investigations were used to determine suitability for the desired application.

Contents

Acknowledgements

Firstly, my utmost thanks are to my supervisor, Simon Pope. Thank you for encouraging me to do a PhD, and for being there every step of the way for the past three years. I am extremely grateful for your intelligence and commitment which has endlessly supported me academically, and for your friendship which has been a lovely and meaningful part of my time at Cardiff.

Alongside my supervisors I'd like to say a huge thank you to Jamie Platts, Ben Ward and Joe Beames for your invaluable DFT and TA calculations. In addition, thank you to Catrin, David and Tony for all your knowledge, support and guidance with cell imaging studies; the days in the suite were always enjoyable. I am also extremely grateful to Christiane Schotten and Duncan Browne, with whom I collaborated to complete my first 'first author' paper! Special thanks also to one of my MChem students, Beth Seccombe, for persisting on the ferrocene chemistry with me.

A massive thank you to all of the chemistry technical staff: Rob, Simon W., Jamie, Robin, Simon J. & Tom. The department would not function without you guys and it was always lovely to see your faces in the corridor. That also applies to other staff members in the inorganic department; Angelo, Ian, Nancy, Ben, Dayna and Tim. More thanks to all my PhD and post-doc colleagues, past and present, most of whom I have enjoyed a healthy debate with – there are a lot to list but you're all great and I hope there are many continuing friendships!

To previous and current members of the Pope group, you're all spectacular. I started with Emily, Ollie and Stokes and the team has gone on to grow including Corey (my first lovely lab baby – I'm so proud of you and Alex bossing the Easun Lab), Sam, Adam and Kaitlin. Thank you all for making time in the lab so enjoyable, enjoy the round bottom flasks that are back in circulation after my departure. A big special thank you to Stokes: there were a few dark days during the last three years that I couldn't have got through without you – I'll thank you with many future burgers!

I am also eternally grateful to my incredible friends outside my PhD, all of whom I love and am inspired by every day. Thank you to Gianna, Lucy and Caz for a great first year living together and for being amazingly supportive friends and incredible human beings:

here's to many years as a Wyeverne Family. Thank you to Abbie, my oldest friend who is one of the most spectacular people on the planet, I don't think I would be the person I am today if it wasn't for our 21 years of faultless friendship and your endless kindness. Thank you also to Stacey, Emily and Fooks; you're all wonderful friends, thank you for making me endless dinners over the past three years, I promise I'll stop slacking now! Finally, thank you to James for putting up with my consistently excessive excitement to see you after spending many of my writing days with no human contact, maybe I'll calm down now?

My biggest thank you of all goes to my outstanding family: Mum, Dad and Sophie. Soph, I am constantly inspired by your determination, kindness and hilarity. Thank you for always being there for me, I was so proud to see you become Mrs Butterfield this month. And to Mum and Dad, thank you for always encouraging me and for making my life so happy. You are the most important friends in my life and the best parents I could ask for. Words cannot possibly express my gratitude for your unfaltering guidance, support and love. I love you both infinitely.

List of Figures

List of Schemes

List of Tables

List of Abbreviations

Spectroscopy and Techniques

NMR – Nuclear Magnetic Resonance

FT – Fourier Transform

UV-Vis – Ultraviolet-Visible

IR – Infra-red

ATR – Attenuated Total Reflectance

MS – Mass Spectrometry

TA – Transient Absorption

ES - Electrospray

LR – Low Resolution

HR – High Resolution

TLC – Thin Layer Chromatography

CV – Cyclic Voltammetry

TD – Time Dependant

DFT – Density Functional Theory

PET – Positron Emission Tomography

MRI - Magnetic Resonance Imaging

CT – Computed Tomography

CFM – Confocal Fluorescence Microscopy

FLIM – Fluorescence Lifetime Imaging Mapping

CCD – Charge Coupled Device

TIRF – Total Internal Reflection Fluorescence

NLO – Non-Linear Optical

STED - Stimulated Emission Depletion

SAR – Structure Activity Relationship

MTT Assay – Microculture Tetrazolium Assay

2D – 2 Dimensional

3D – Three Dimensional

m/z – Mass/Charge Ratio

δ – Chemical Shift

ppm – parts per million

s - singlet

d - doublet

t - triplet

q - quartet

m - multiplet

$\{H^1\}$ – proton decoupled

λ - wavelength

IC_{50} – concentration of drug where 50 % of cells are viable

Photophysical and Chemical Properties

IC – Internal Conversion

ISC – Intersystem Crossing

SOC – Spin Orbit Coupling

ES – Excited State

GS – Ground State

LED – Light Emitting Diode

OLED – Organic Light Emitting Diode

OLEC – Organic Light Emitting Electrochemical Cell

MC – Metal Centred

IL – Intra-Ligand

CT – Charge Transfer

ICT – Intra-ligand Charge Transfer

MLCT – Metal-to-ligand Charge Transfer

^{3}MLCT – triplet Metal-to-ligand Charge Transfer

LLCT - Ligand-to-Ligand Charge Transfer

^{3}ILCT - Triplet Intra-Ligand Charge Transfer

^{3}SBLCT - Triplet Sigma Bond to Ligand Charge Transfer

HOMO – Highest Occupied Molecular Orbital

LUMO – Lowest Unoccupied Molecular Orbital

abs – absorption

em – emission

exc – excitation

τ – Lifetime

ϕ – Quantum yield

S_0 – singlet ground state

S_1 – first singlet excited state

T_1 – first triplet excited state

PeT – photoinduced electron transfer

RET – Resonance Energy Transfer

FRET – Förster Resonance Energy Transfer

CFSE – Crystal Field Stabilisation Energy

OD – Optical Density

<u>Solvents, Chemicals and Biological Substances</u>

DCM – dichloromethane

DMF – dimethylformamide

DMSO – dimethylsulfoxide

THF - tetrahydrofuran

MeCN – acetonitrile

MeOH – methanol

EtOH – ethanol

$CHCl_3$ – chloroform

STAB - sodium triacetoxyborohydride

NaI – sodium iodide

^{t}Bu – tert-butyl

IAd - 1,3-di(adamantyl)imidazole-2-ylidene

tht – tetrahydrothiophene

bpy – 2,2'-bipyridine

phen – 1,10-phenanthroline

Me – methyl

Et – ethyl

Ph – Phenyl

PPh_3 – triphenylphosphine

ppy – 2-phenylpyridine

acac - acetylacetone

Cp – cyclopentadiene

pyr – pyridyl

NO – nitrous oxide

TrxR – thioredoxin reductase

NHC – N-heterocyclic carbene

L – ligand

DNA – deoxyribosenucleic acid

ctDNA – circulating tumour deoxyribosenucleic acid

RNA – ribonucleic acid

HIV – Human Immunodeficiency Virus

TMRE – Tetramethylrhodium ethyl ester

HEK – Human Embryonic Kidney

LOVO – human colon cancer cell line

HeLa – human cervical cancer cell line

MCF7 – human breast cancer cell line

A549 – human lung cancer cell line

PC3 – human prostate cancer cells

CDF - Clostridium Difficile

GFP – green fluorescent protein

DAPI - 4',6-diamidino-2-phenylindole

CX1- human colon carcinoma cell line

LX1 – human lung carcinoma cell line

Bel7402 – human hepatoceullular carcinoma cells

HL60 – human promyelocytic leukemia cell line

HT29 – human colon carcinoma cells

HepG2 – human liver cancer cell line

ICB2 – site of topoisomerase II alpha promotor

Chapter 1 - Introduction

1.1 Luminescence

Luminescence is defined as the emission of light from any substance.[1] This light comes from the emission of photons by a molecule as it relaxes from its excited state (ES) to ground state (GS). This can be achieved *via* a number of pathways, as described by the Jablonski energy level diagram in Figure 1.2. Many different types of luminescence are possible: electroluminescence, chemiluminescence, bioluminescence, radioluminescence and photoluminescence.[2,3] The work described herein concentrates on photoluminescence and its applications.

1.1.1 Photoluminescence

Each type of luminescence initially requires the promotion of an electron to excited energy levels.[4] For photoluminescence, absorption of light by a molecule is required in order for electrons to occupy excited state energy levels,[3,5] because the energy gap is too great to be exceeded thermally. Excitation is likely to be from the ground singlet state (S_0) to the first excited singlet energy level (S_1). This is defined by the Franck-Condon principle (Figure 1.1), which describes that: i) nuclei are much larger than electrons; and ii) a shift of internuclear separation occurs if the bonding character is different in the ground and excited states (i.e. increased antibonding character). For these reasons, the Franck-Condon principle states that electronic transitions must be vertical[1] because the transition is so rapid (10^{-15} s) that the nuclei do not have sufficient time to react, instead they remain in a stationary framework.

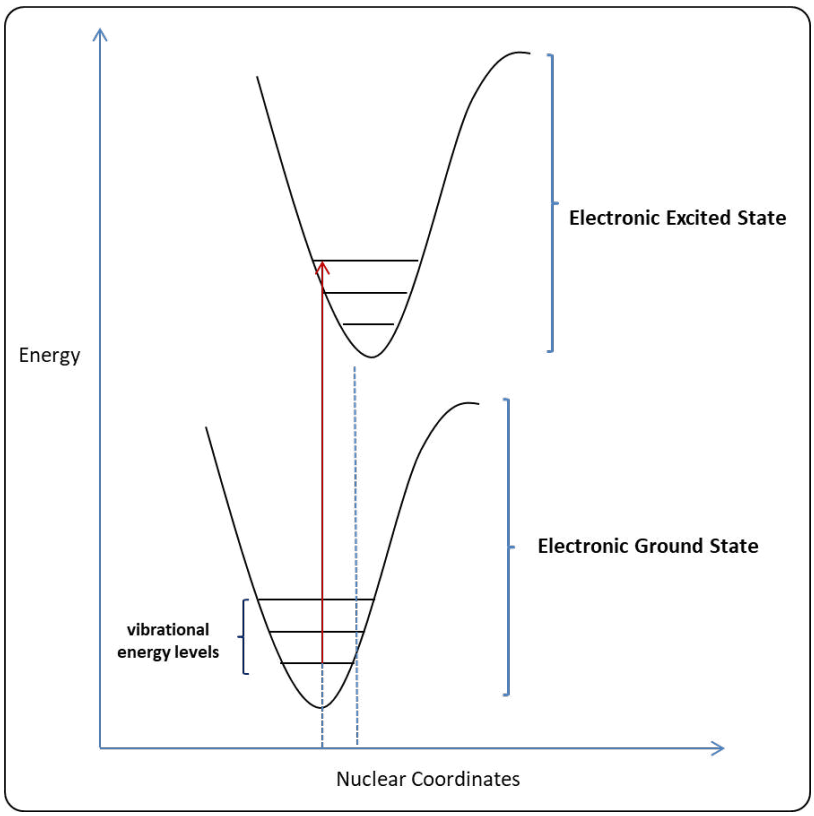

Figure 1.1: Illustration of the Franck-Condon Principle

The Jablonski energy level diagram (Figure 1.2) describes the processes that occur between the absorption and emission of light *via* photoluminescence, the transitions in which are shown as vertical lines to demonstrate the instantaneous nature of light absorption, as described above. Energy levels marked with an S represent singlet electronic states, whereas those marked with a T represent triplet electronic states.[1]

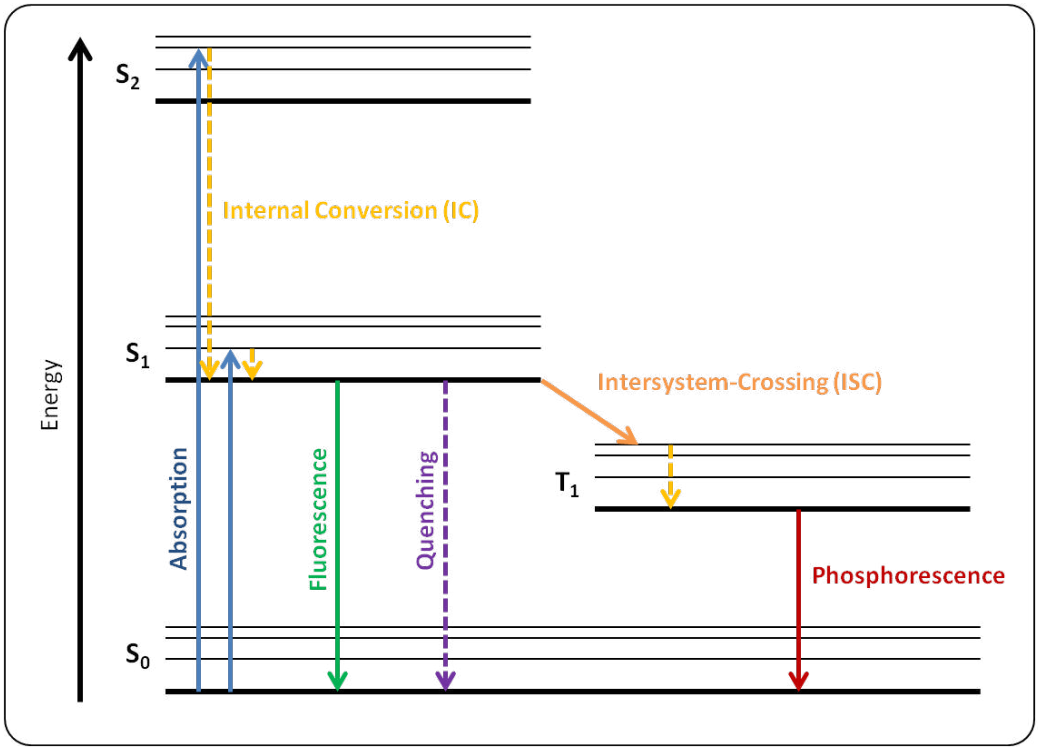

Figure 1.2: Jablonski energy level diagram

Upon light absorption, a luminophore is excited from the ground state level S_0 to a higher energy vibrational level of S_1. The higher energy excited state is relatively unstable, therefore deactivation is favourable and can occur *via* several processes.[2] Firstly, molecules can quickly relax to the lowest vibrational level of S_1 through non-radiative internal conversion (IC) where energy is lost in the form of heat, usually occurring within 10^{-12} s or less. This process usually occurs before emission, and then emission usually occurs from the lowest vibrational state of S_1 (*i.e.* after reaching thermal equilibrium).[1,3] In addition, it is observed that the wavelength at which luminescence emission occurs is generally independent of excitation wavelength due to the speed of IC, known as Kasha's rule.[1]

Following IC, the electron can undergo one of two processes. One of these is fluorescence, which occurs from the lowest energy vibration state of S_1 back to an excited vibrational ground state in level S_0, and occurs for most organic fluorophores.[5] During fluorescence, overall electron spin is conserved and therefore allowed according to selection rules rules.[4] This results in an efficient process with decay rates in the region of 10^{-8} s,[1,2,6] which leads to lifetimes below 10 ns.

Another option following IC is intersystem crossing (ISC), where molecules residing in the S_1 state undergo spin conversion to the T_1 state in a non-radiative process. In the absence of spin-orbit coupling or an external magnetic field the singlet and triplet states are close in energy, with the triplet state usually lower in energy than the singlet state.[3] ISC is spectroscopically spin forbidden, but facilitated by heavy atoms,[1] and is a kinetic process occurring *via* collisions.[6] After ISC, further energy can be lost by the emission of a photon to allow the electron to relax from the T_1 state to S_0.[1] This process is known as phosphorescence and is also a spin forbidden process and therefore lifetimes are longer than fluorescence (ms-s). Furthermore, the additional energy loss results in a lower energy of phosphorescence emission when compared to fluorescence emission. Due to the aforementioned heavy atom facilitation of ICS, most emissive transition metal complexes undergo spin change and exhibit phosphorescence. [4]

1.1.2 Measuring Photophysical Characteristics

Important photophysical properties of luminescent compounds are measured using two main techniques: steady state and time resolved measurements.[1] The most common of these, steady state measurements, are performed *via* constant illumination of a sample. This process allows a steady excited state to be reached, thus resulting in constant emission. On the other hand, time-resolved measurements require exceptionally short timeframes and therefore involve more sophisticated equipment. The technique involves exposure of a sample to a pulse of light that must be shorter than the decay time to allow the decay profile to be recorded. The nature of these two techniques renders steady state measurements an average of time-resolved measurements for the period of the decay, therefore combination of the two can give information on several significant parameters.

1.1.2.1 Quantum Yield (Φ)

An extremely important photophysical parameter is quantum yield, which describes the ratio of the number of emitted photons relative to the number of absorbed photons.[1,3,5] It describes the efficiency of the radiative decay process and takes into account the radiative decay rate (Γ) and the rate of non-radiative decay (k_{nr}), as explained by Equation 1.[7] High Φ values give rise to the brightest emission, for example values

approaching unity can be seen in rhodamine species where Γ is much greater than k_{nr}. However, due to quenching (see Section 1.1.2.3) it is impossible to reach perfect unity.[1]

$$\Phi = \frac{number\ of\ emitted\ photons}{number\ of\ absorbed\ photons} \qquad (1)$$

$$\Phi = \frac{\Gamma}{\Gamma + k_{nr}} \qquad (2)$$

Quantum yields can be calculated experimentally by comparison with a standard such as $[Ru(bpy)_3][PF_6]_2$ (denoted by subscript R) by using Equation 3, where S is the area below the emission spectrum, A is the absorbance at the excitation wavelength and n is the refractive index of the solvent.[8]

$$\Phi = \Phi_R \frac{S}{S_R}\frac{A_R}{A}\frac{n^2}{n_R^2} \qquad (3)$$

1.1.2.2 Lifetime (τ)

Different systems have varying emissive characteristics which are dominated by the length of the luminescence lifetime. Measurement of luminescent lifetimes allows a distinction to be made between fluorescence and phosphorescence, as well as determining the time available for the ES to interact with the environment. The lifetime (τ) is defined as the average time molecules spend in the excited state before returning to the ground state, as described by Equation 4.[1,5]

$$\Upsilon = \frac{1}{\Gamma + k_{nr}} \qquad (4)$$

Despite being useful for probe applications, long lifetimes can be a disadvantage because the ES is more accessible to quenching deactivation pathways. Lifetimes can also offer an additional contrast parameter for cellular imaging techniques such as fluorescence lifetime imaging microscopy (FLIM).[5]

1.1.2.3 Quenching

As well as non-radiative processes, the luminescence lifetime of a compound is affected by quenching. Quenching is defined as a decrease in emission intensity through a variety of processes, and is most common when in solution. The most common form of quenching is collisional, otherwise known as dynamic, and involves the ES being deactivated following contact with another molecule and hence is accelerated by diffusion effects in solution.[5] The most frequently encountered quenching species is molecular oxygen and therefore it is common practise to remove dissolved oxygen to obtain luminescent spectra. Although often debated, the most probable cause of O_2 quenching is paramagnetic O_2 causing ISC,[1] which can also be facilitated by halogens. In these cases, once ISC has occurred the long-lived triplet state is completely quenched before phosphorescence can occur.

Collisional quenching is defined by the Stern-Volmer equation (Equation 5):[1]

$$\frac{F_0}{F} = 1 + K\,[Q] = 1 + \, k_q \tau_0 [Q] \qquad (5)$$

In this equation, K is the Stern-Volmer quenching constant and informs on the sensitivity of the fluorophore to collisional quenching. F and F_0 are the fluorescence intensity with and without the quencher, respectively. [Q] refers to the concentration of the quencher, τ_0 is the unquenched lifetime and k_q is the bimolecular quenching constant.

There are several other quenching mechanisms in addition to collisional quenching. One example is static quenching, which involves the formation of non-emissive complexes of luminophores with a quencher.[5] Amines can demonstrate this form of quenching as they are able to form ES charge transfer complexes for which the exciplex is quenched in polar solvents. Amines are also able to quench fluorophores *via* photoinduced electron transfer (PeT). Another quenching mechanism is resonance energy transfer (RET), also referred to as Förster RET (FRET).[1,5] This mechanism is defined as non-radiative transfer of energy between an excited donor and acceptor molecule; hence it only occurs when there is sufficient overlap of the absorption profiles of the donor and the acceptor.[9]

As discussed above, quenching mechanisms can be problematic with regards to luminescent properties, but can also lead to a variety of important applications, for

example on-off fluorescent probes or in photodynamic therapy. These can be used for a number of processes:[1] i) diffusion membrane probes; ii) DNA and protein binding probes; and iii) quenching of fluorescence due to specific binding events, for example binding to metal ions.

1.1.2.4 Stokes' Shift

It can be seen from the Jablonski energy level diagram (Figure 1.2) that the energy of emission is generally less than that of absorption. In 1852 Sir G. G. Stokes noted this as the emission wavelength is always longer than that of the excitation. Stokes' shift is therefore defined as the difference between the wavelength/frequency of the absorbed and emitted photons.[4] The emission energy is always lower than the excitation due to the energy lost by IC and thermalisation of excess vibrational energy.[1] The Stokes' shift is an essential property for consideration in the application of a ligand as a fluorophore, as large value shifts are able to reduce the self-quenching of luminescence by the molecule. Organic fluorophores tend to have small to moderate Stokes' shifts due to their tendency for spin conservation. However ES changes in geometry can give rise to larger values.[4] In addition, large shifts allow distinction between fluorescence and autofluorescence in cellular imaging applications, where autofluoresence describes the intrinsic fluorescence of natural cellular objects.[4] An optical filter of FLIM techniques can be employed to selectively filter out autofluorescence of luminophores with large Stokes' shifts.[5]

1.1.2.5 Environmental Considerations

There are several environmental factors that can affect the emission wavelength of a luminophore, for example other fluorophores, solvent molecules, ions and pH.[5] Shifts in the wavelength can be described as either bathochromic or hypsochromic, and changes in intensity are referred to as hyperchromic or hypochromic (Figure 1.3).[1] Controlling the nature of a fluorophore can give rise to desirable applications, for example hyperchromic and bathochromic shifts are desirable for biological systems and hence ideal for cell imaging applications.[10]

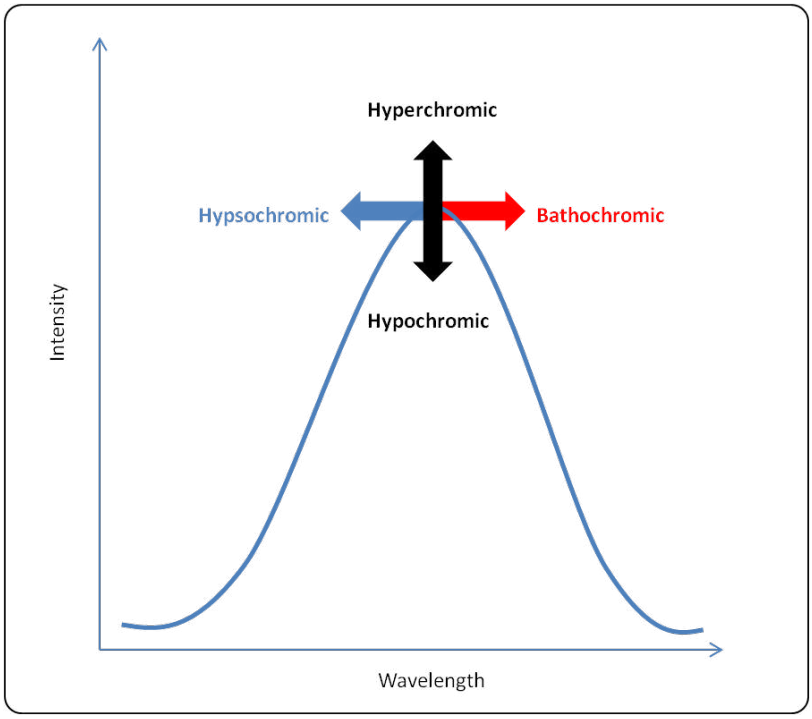

Figure 1.3: Shifts of absorption and emission spectra

Absorption and emission spectra of samples in solution are highly dependent on the nature of the solvent. This is due to the fact that irradiation by light leads to the redistribution of electron density within a molecule.[1] This changes the interactions between the solute and any molecules that are solvating the excited molecules. For these reasons, the dipole moment of the luminophore can change during excitation, which is common in samples that show charge transfer (CT) character.[11] Perturbation of the emission band is known as solvatochromism, where the extent depends on a number of factors: i) solvent nature; ii) nature of the luminophore; and iii) type of transition that occurs.[1] When the ES is more polar in nature and can therefore be stabilised by solvent reorientation around the molecule, the result is lowering the energy of ES resulting in a bathochromic shift. This type of shift is described as positive solvatochromism and can make a significant contribution to the Stokes' shift. When the GS is more polar than the excited state, negative solvatochromism occurs.

In addition to the previously mentioned environmental factors, photobleaching can also reduce the emission intensity. This is a frequently encountered problem for fluorescence imaging techniques and occurs when an irreversible chemical change is induced after

excitation. Increasing the sensitivity of the imaging technique and designing a low illumination level fluorophore can reduce the amount of photobleaching.[5,12]

1.1.2.6 Organic Luminophores and their Substituents

There is a huge variety of organic luminophores based on aromatic species that can be conjugated, substituted and functionalised. The unsaturated nature of aromatic species means they possess strong π-π* absorptions[3] and commonly exhibit fluorescence from the lowest lying π* ES and/or intra-ligand charge transfer (ICT). Larger bathochromic shifts and emission intensities are observed with highly conjugated molecules,[3] in addition to the introduction of vibronic structures due to rigidity.[13] Although organic luminophores usually exhibit fluorescence emission, there are rare examples where triplet emission is possible but often readily quenched.

The nature of the substituents on the aromatic unit can have a significant effect on the luminescent behaviour of a luminophore due to the effect on electron density.[3,14] Electron donating groups, such as alcohols or amines, cause a shift in the absorption and emission spectra, in addition to an increase in the molar absorption coefficients. Furthermore, electron donating groups can cause spectra to become broad and pH sensitive due to a significant l-π* contribution – which is essentially an ICT process. On the other hand, electron withdrawing groups such as carbonyls or imides give rise to low lying n- π* ES. This results in lower extinction coefficients and quantum yields.[3] The quantum yield will be highly dependent on solvent when the n-π* ES lies close in energy to the π-π*.[15] It is also possible for organic compounds to aggregate and form excimers, which often exhibit bathochromic and hyperchromic shift[16] combined with a broadening of emission profiles.[17] There are numerous examples of organic fluorophores based on 1,8-naphthalimide derivatives, which are discussed in Section 1.4.

1.1.3 Luminescent Probes

There has been extensive research into the applications of optical probes for biochemical and medicinal studies,[18] for example to sense either: i) biological conditions (pH,[19] O_2 levels[18]) or biological processes; or ii) specific species of biological interest (such as Zn(II),[20] Cu(II)[19,21] and sugars[22]). There are three main requirements that must

be met in order for a luminophore to become an effective luminescent probe: i) obvious change in the photophysical properties upon the sensing event; ii) a high affinity and selectivity for the chosen analyte; and iii) easy delivery to the subject matter.[1,23] With rational design, fluorescent probes can exhibit high sensitivity, resolution and good acquisition times, in addition to their use at relatively low concentrations.[24] Due to advances in biological imaging technologies (see section 1.3), they are also capable of imaging at intracellular level in real time, with excellent spatial resolution.[23,25]

1.2 Coordination Chemistry

Coordination chemistry is the study of coordination compounds or complexes, which are defined according to IUPAC recommendations as: "*an ion or neutral molecule that is composed of a central atom, usually that of a metal, to which is attached a surrounding array or other atoms or groups of atoms, each of which is called a ligand*".[26] Coordination chemistry was first developed in the 19th century when Werner, for example, disbanded the link between metal oxidation state and coordination number and began use of the term coordination compounds.[27] Today, coordination compounds are the subject of a vast amount of varied research. In particular, there is a rich array of coordination compounds that exhibit extremely interesting spectroscopic properties.

1.2.1 d-Block Metal Complexes

As discussed above, most organic fluorophores possess a singlet excited state that is short lived, giving rise to small Stokes' shifts. Luminescent coordination compounds containing d-block metals typically emit from triplet excited states, and are thus suitable for sensing and imaging properties due to a number of inherent properties.

1.2.2 Crystal Field Theory

Metal complexes are made up of a number of ligands, each of which forms coordinative dative bonds to a metal ion.[28] Crystal field theory describes a ligand lone pair modelled as a point negative charge (or as the partial charge of an electric dipole) that repels electrons in the d-orbitals of the central metal ion.[29] Thus, the formation of bonds occurs through the donation of a lone pair of electrons for σ- and π-donors, which are complemented by a π-acceptor component.[28] The theory focuses on how the nature of

a ligand affects the resultant splitting of d-orbitals into groups with non-degenerate energies, thus helping to rationalise the optical spectra, thermodynamic stability and magnetic properties of complexes.[29] For example, in 6-coordinate, octahedral complexes (O_h), the five d orbitals split into two non-degenerate energies where three non-bonding orbitals with t_{2g} symmetry lie at lower energies and correspond to d_{xy}, d_{xz} and d_{yz}, whilst the two e_g symmetric anti-bonding orbitals, d_{x2-y2} and d_{z2} orbitals lie at higher energy.

Rationalisation of the stability of a complex uses the crystal field splitting energy (Δ), which is dependent on the principle quantum number, charge of the metal and the nature of the ligand.[30] With octahedral complexes, for example, this is denoted as Δ_o. The partial filling of the aforementioned t_{2g} and e_g orbitals allows for electronic transitions to occur when the irraditation energy is equal to Δ_o. With careful ligand design, the photophysical properties of a complex can be controlled due to the dependant nature of Δ on the nature of the ligand. The Spectrochemical Series (Figure 1.4) represents the effects that different ligand types have on the perturbation of the d orbitals , and ranks them in order of their effect on Δ.[28] The general trend is as follows:

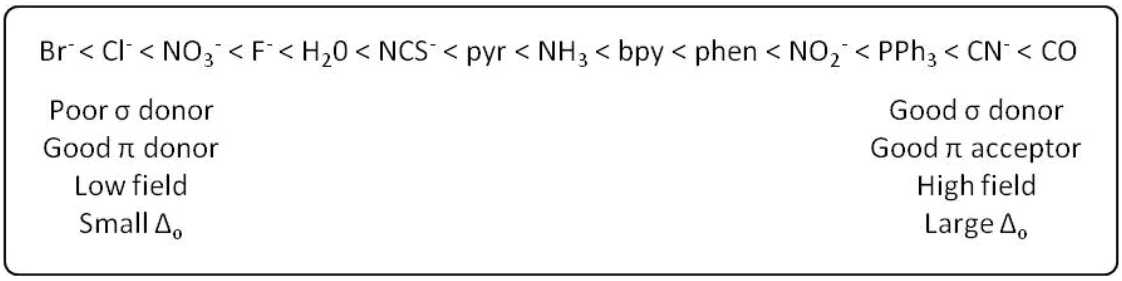

Figure 1.4: Spectrochemical Series

In addition, polydentate ligands, for example bipyridine (bpy) and 1,10-phenanthroline (phen), donate electron density from more than one site.[28] They are often preferred because they increase the thermodynamic stability of a coordination complex; this is known as the chelate effect, which was first described by Curtis in 1964.[31] These types of ligands are further explored in Chapter 4. The increase in thermodynamic stability

can be related to the Gibbs free energy of a system, where a lower ΔG leads to a higher stability, as denoted in Equation 6.[29]

$$\Delta G = \Delta H - T\Delta S \qquad (6)$$

The entropic contribution towards increased disorder is favourable for polydentate ligands, as moving from a MX_6 complex to ML_3 complex (where X is a mondentate ligand and L is a bidentate ligand), for example, results in an increase in molar equivalents of the reaction products. The enthalpic contribution originates from breaking each of the coordinative bonds in order to fully dissociate a polydentate ligand.

1.3 Diagnostic Medicine – Medical Imaging

Coordination compounds and organic luminophores have been applied for a variety of medical imaging techniques. The last few decades of the twentieth century saw huge development and commercialization of a range of new medical imaging technologies. In part, this acceleration is attributed to advances in understanding the fundamentals of the physical phenomena on which the imaging technologies are based.[32] Medical imaging is reliant upon detecting the differences between the compositions of different tissues within the body, using an external source.[33] Classical forms of imaging are known as anatomical imaging which involves the detection of internal structural consequences from outside the body. In recent years, molecular imaging has emerged as a successful technique, and involves the detection of the biological or physical abnormalities underlying the disease.[34] A key difference between these two imaging techniques is that molecular imaging always requires a probe that must be specific to the molecular event to be detected, thus chemistry plays a crucial role in the development of new approaches. There are many imaging modalities that are currently available to the clinician; examples include Positron Emission Tomography (PET), Magnetic Resonance Imaging (MRI), Computed Tomography (CT), X-Ray and fluorescence microscopy. Specifically, there has been a remarkable growth in the use of fluorescence spectroscopy during the past 20 years.[1] One protocol is by no means an isolated or independent mode of imaging,[35] and each technique has distinct advantages and disadvantages.

1.3.1 Fluorescence Microscopy

Fluorescence microscopy is a powerful, highly sensitive[36] imaging technique that utilises fluorescent probes for biological or medicinal applications.[2,5] In rare cases, the technique utilises the intrinsic fluorescence of a biological sample upon excitation, rather than a fluorescent probe.[4,37] Its use in the screening of chemical and biochemical analytes has become a quickly advancing area over the past few decades.[32] It has become an ideal microscopy technique for the assessment of biological specimens because it provides a technique for specific detection of non-emissive cells, with advantages including increased contrast and signal-to-noise ratio when compared to standard microscopy techniques.[4,19] In addition, fluorescence microscopy offers high nanometer resolution (*ca*. half of the emission wavelength),[2,5,38] non-invasive character and requires a relatively low concentration of probe. The high degree of sensitivity is due to the detection of emitted light as opposed to reflected light used for normal spectroscopy, thus allowing visualisation at molecular level for a relatively low cost.[38] The technique is used in industry for inspection of surfaces and coatings, but in a biological context it dynamically notifies on the localisation and uptake of molecules within cells.[36,39]

Despite its advantages, the technique is inherently limited due to the requirement for both excitation and emission wavelengths to be tissue compatible, thus confining its use to largely imaging at a cellular or thin tissue level, as opposed to being a whole-body technique.[40] In addition, tissue compatible wavelengths are generally in the near-IR region and have poor penetration through tissue.[4]

1.3.2 Confocal Fluorescence Microscopy (CFM)

There has been substantial improvements in fluorescence microscopy techniques due to advances in technologies such as probe chemistry, confocal optics, multiphoton excitation, detectors and genetically expressed fluorophores such as green fluorescent protein (GFP).[41] Confocal fluorescence microscopy has helped to address the problems associated with the traditional technique as it limits photon detection to light that is emitted from the focal point by actively supressing signal coming from out-of-focus planes,[42] thus giving rise to a significant increase in the contrast and resolution. This

technique allowed the introduction of optical sectioning and gave rise to three-dimensional microscopic reconstructions of biological tissue.[2] The confocal principle was first discovered in 1957 by Martin Minsky and the first commercial instrument was created in 1982.[2] The modern microscope utilises either the output of photomultiplier tubes or a digital charge-coupled device (CCD) camera to build up the image, which is then directly processed in a computer imaging system and displayed on a high-resolution video monitor.[43] In addition to CFM, advances have been made in two-photon microscopy, which involves the excitation of a chromophore by two photons simultaneously. The success of this technique relies on a very high concentration of photons, a property that only occurs at the focal point, thus giving rise to focused, sectioned images.[40] The technique has been described as the 'optical magic wand' due to the avoidance of the photo damage and photobleaching.[40] As mentioned above, the development of genetically encoded fluorophores such as GFP are said to have revolutionised fluorescence microscopy.[40] The protein is naturally occurring in the bioluminescent jellyfish *Aequorea Victoria* and absorbs blue light and emits green.[41] It has provided a basis for the synthesis for a wide number of variants, giving rise to a wide choice for the microscopist. Besides GPF and two-photon, the past decade has seen advancement in other fields of fluorescence microscopy, such as total internal fluorescence (TIRF), which monitors the movement of single molecules in very thin samples;[44] as well as imaging deconvolution and analysis, which has had a profound impact in cytogenetics.[45] Other recent developments have been focused around quantum dots and fluorescent nano-crystals.[37]

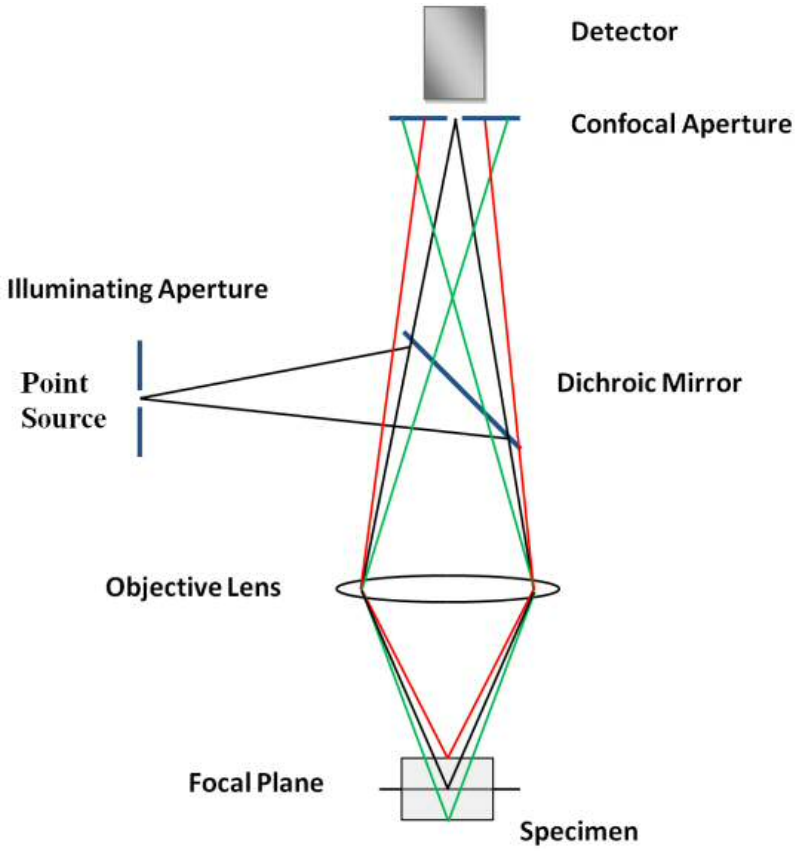

Figure 1.5: Illustration of CFM[46]

The basic structure of CFM equipment is displayed in Figure 1.5.[46] The excitation photons firstly pass through a pinhole before focusing through an objective lens onto a precise location in one focal plane. The emission is then passed through a second pinhole to reject any out-of-focus light.[2,36,38] This gives rise to 2D optical slices (z-stacks) that are collected and reconstructed to form a false-colour, 3D image.[4,5,36]

Importantly, CFM can perform multi-channel detection *via* a master beam splitter that reflects selected wavelengths. The selected wavelengths are split using dichromic mirrors and distinguished using different detectors. This ability gives rise to the detection of specific staining and co-localisation experiments, which are extensively explored in Chapter 2. Co-localisation studies work by using two fluorescent probes simultaneously, where one is hypothesised to localise in a certain cellular substructure, and another with different emissive properties that is known to target the same substructure.[5] Following this, the degree of co-localisation can be determined by overlaying the corresponding images, thus concluding the target of the new probe.[38]

A more recently developed technique, known as super-resolution fluorescence microscopy, encompasses a variety of sub-techniques based on tailored illumination, non-linear optical (NLO) devices and the accurate localisation of single molecule probes.[47] The Nobel Prize in 2014 was won by Betzig, Moerner and Hell for development of some of the techniques, including stimulated emission depletion (STED) microscopy and single molecule microscopy.[47,48]

1.3.3 Luminescent Probes for Cell Imaging

Fluorescent probes must possess a number of requirements for biological applications, including: i) bright emission at tissue compatible wavelengths; ii) tissue and laser compatible excitation wavelengths; iii) a low tendency of photobleaching; and iv) a method of differentiating from autofluorescence *via* large Stokes' shifts or long lifetimes.[5,36,38] In addition, probes must exhibit good membrane permeability, solubility in aqueous media and low toxicity. It is possible for probes to target specific cell substructures according to their design, for example Golgi apparatus and endoplasmic reticulum require lipids or inhibitors of protein movement, and the nucleus requires DNA binding properties.[5]

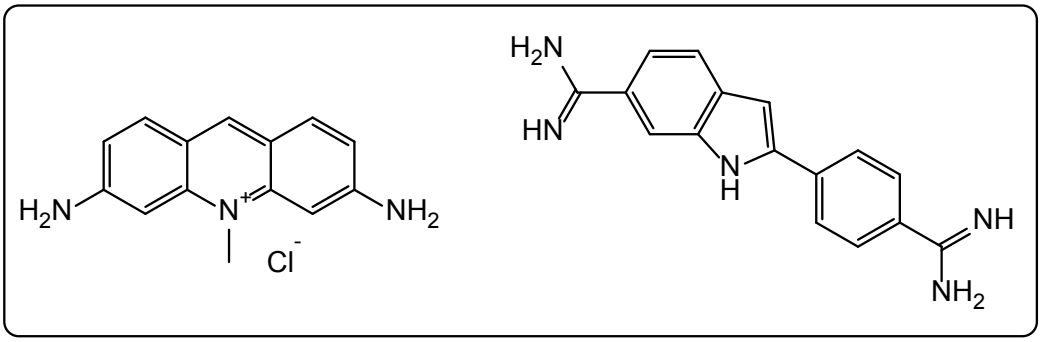

Figure 1.6: Acriflavine (left) and DAPI (right)

Bommer used an acriflavine dye as the probe for the first fluorescent imaging of a fixed tissue sample in 1929 (Figure 1.6).[2] Today, most probes are organic structures with fused aromatic or heterocyclic rings, for example 4',6-diamidino-2-phenylindole (DAPI), a nuclear fluorescent stain (Figure 1.6).[4] Inorganic species have also been applied to cell imaging applications due to their desirable photophysical properties and tunable nature.

1.4 1,8-Naphthalimides

Naphthalimides are a class of polycyclic imides containing a π-deficient flat aromatic or heteroaromatic ring system (Figure 1.7). In general, they are characterised by the presence of a planar aromatic chromophore and one or two flexible basic side chains which promote DNA affinity through electrostatic or hydrophobic interactions.[49] 1,8-Naphthalimide derivatives make up an extremely important family of fluorescent compounds with multiple applications, such as DNA targeting, anticancer and cellular imaging.[50] In particular, they are a category of compounds which exhibit high levels of anti-tumour activities centred around their effective intercalation into DNA and other effects such as apoptosis induction.[49] Many derivatives in the literature focus on mono- or bis-naphthalimide structures, where substituents include amines, polyamine conjugates, heterocycles, oligonucleotides, peptides and metal complexes. They are ideal candidates as probes because they have rich photophysical properties that are dependent on the nature and the substitution pattern of the aryl ring.

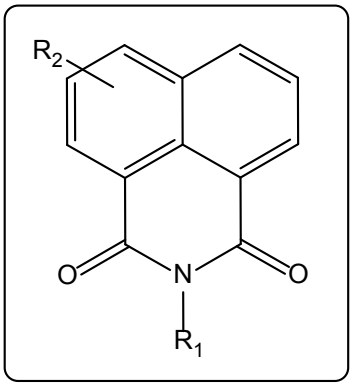

Figure 1.7: General structure of a 1,8-naphthalimide

In addition to their photophysical properties, the prevalence of 1,8-naphthalimides in recent literature is partly due to their ease of synthesis from the corresponding 1,8-naphthalic anhydride.[51] This is able to react with a range of amines, which can in turn be followed by substitution of the aryl ring, most commonly at the 2- or 4-position to give compounds of high purity and with high yields.[50] These synthetic protocols give rise to a vast array of possibilities, which means it is possible to control electronic properties, spectroscopic properties and photochemical behaviour *via* the use of specific moieties.

It is this type of tuneable behaviour that allows these compounds to be exploited as dual therapeutic and fluorescent imaging agents.

1.4.1 1,8-Naphthalimides as anticancer agents

The discovery of novel and effective anti-cancer drugs is a primary focus amongst researchers as clinically used drugs exhibit poor pharmacokinetics, dangerous side effects and drug resistance.[49] As discussed above, naphthalimides are highly active anticancer drugs based upon effective intercalation with DNA, which can be investigated in terms of structural modifications and structure activity relationships (SAR).

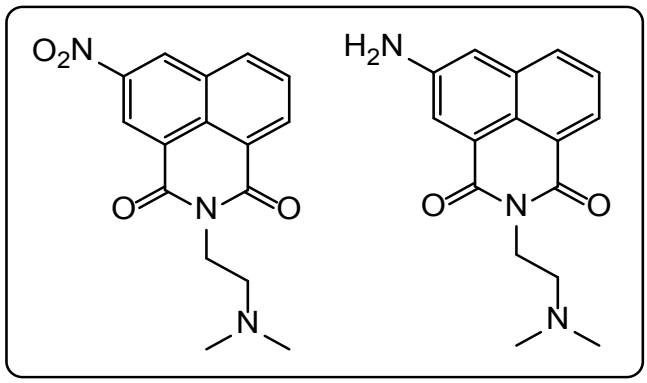

Figure 1.8: Amonafide (left) and Mitonafide (right)

1,8-Naphthalimides as DNA-binding agents were originally established by Brana *et al*.[52] Some derivatives have entered into phase III and phase II clinical trials, including *amonafide* and *mitonafide* (Figure 1.8). Clinical trials have shown that both show high anti-tumour activity and have desirable IC_{50} values (concentration of a drug required to inhibit a biological process by 50%) against HeLa cell lines.[53] Both are able to bind to DNA through intercalation into minor grooves, thus inhibiting topoisomerase activity by affecting the breakage-rejoining step.[54] Amonafide is commercially known as Quinamed®, a dichloride salt of amonafide developed by *ChemGenex Pharmaceuticals* as a treatment for acute myeloid leukaemia which has reached phase III clinical trials.[55] It has been found by SAR studies that the presence of a basic terminal group in the side chain has a significant effect on the anticancer activity, hence a large number of these types of compounds have been synthesised.[53] It has also been observed that if there is a nitro-substituted analogue present, there will be a higher anticancer activity in the 3-

substituted position in comparison to the 4-. It is thought that this is due to the ease of co-planar orientation and hence more effective stacking interactions between the 3-nitro-1,8-naphthalimides and DNA.[56]

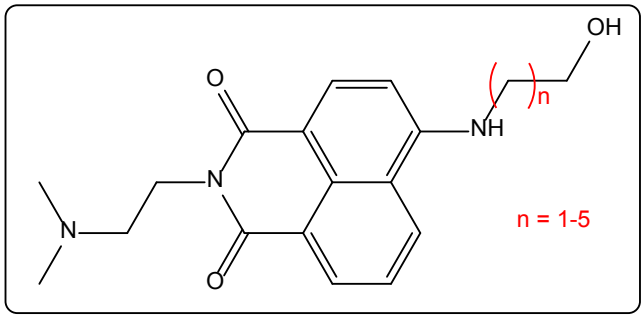

Figure 1.9: Derivatives by Wang et al.[57]

DNA binders showing high anticancer activity against leukaemia have also been developed by Zee-Cheng and Cheng. The structures were reported as N-(dialkylaminoethyl)-derivatives of 3,6-dinitro and 3,6-diamino-1,8-naphthalimides, again with low IC_{50} values.[58] Following this, a series of 3-amino-6-nitro-1,8-naphthalimide derivatives showed high cytotoxicity against human colon carcinoma (CX1) and lung carcinoma cell lines (LX1).[59] In recent work, Wang *et al.* reported the ct-DNA binding properties of naphthalimide derivatives containing hydroxyl-alkylamines at the 4-position (Figure 1.9).[57] Spectral changes in the UV-Vis and emission profiles suggested intercalation of the compounds into the base pairs of DNA, where an increase in the fluorescence intensity in the presence of ct-DNA was observed. In addition, the derivatives were found to be more cytotoxic than cis-platin in Bel-7402 and HL-60 cell lines, where anti-cancer activities increased with increasing length of the side chain.

1.4.2 Bis-naphthalimide anticancer agents

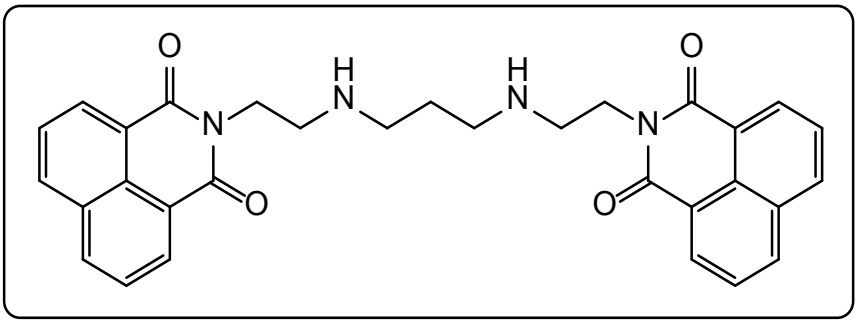

Figure 1.10: Elifinide

Bis-naphthalimides describe a class of compounds where two 1,8-naphthalimides are connected by a polyamine spacer in order to exploit the DNA binding and anti-tumour activity and were initially developed by Brana and co-workers,[60] for example *elifinide* (Figure 1.10) shows high activity against a range of human xenograft models such as lung, colon, and melanoma.[61] It is able to unwind and change the viscosity of closed circular plasmid DNA by binding along the major groove, and shows a preferential DNA interaction for alternating purine-pyrimidine dinucleotide steps.[62] This goes against the trend that the nitro/amino substituted derivatives display better antitumour activity.[63] Within this family of structures comes an efficient DNA binder incorporating a phenanthrene chromophore (Figure 1.11) that displayed excellent L1210 activity with a significant $IC_{50.}$[64] A noteworthy extension to the bis-naphthalimide derivatives comes from Gunnlaugsson *et al*., which involved the inclusion of a Troger's base linker for DNA targeting. Compounds were designed to ensure that the terminal nitrogen atom in the side chain is protonated at physiological pH, meaning that water solubility is enhanced and electrostatic interactions with the negatively charged phosphate backbone of DNA are favoured.[65] In this research, binding with specifically high affinity to calf thymus DNA was observed. In addition, rapid uptake into leukaemia cells was observed with nuclear localisation, as monitored by commercially available co-stains.

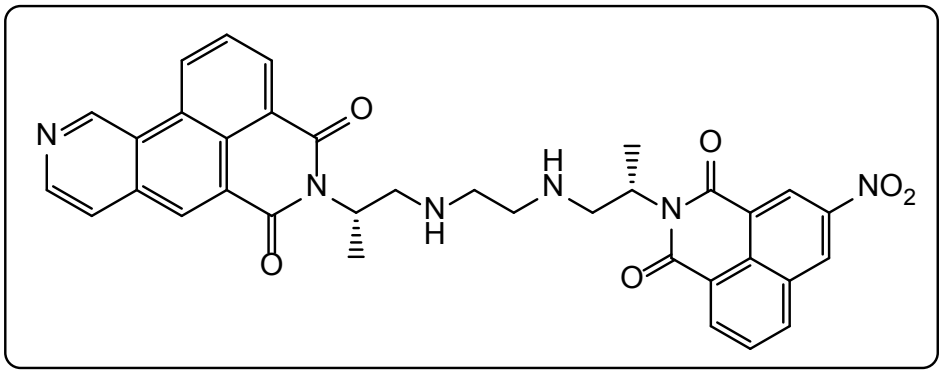

Figure 1.11: Phenanthrene derivative[64]

Ethidium bromide displacement assay has been used to study the interaction between naphthimidobenzamide derivatives (Figure 1.12) and various DNA sequences.[66] Binding was 350 times stronger to G-C repeats than to A-T and A-A repeating oligomers. The contact of the ligand with a specific DNA sequence showed p300 gene expression and significant anti-cancer activity in human solid xenografts was observed. This research interestingly concluded that DNA binding agents can be sequence specific and may be used as a possible control mechanism for transcription of tumour related genes.

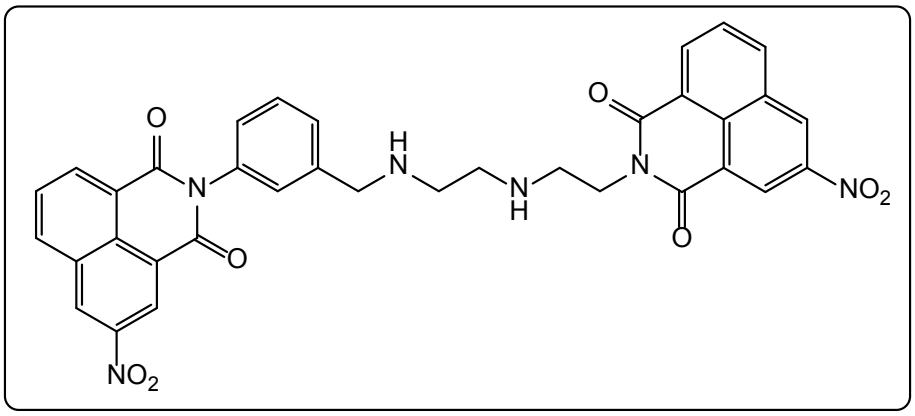

Figure 1.12:Naphthalimidobenzamide derivative[66]

1.4.3 Naphthalimide-Metal Complex Conjugates

Transition metal complexes of 1,8-naphthalimides have also received a considerable amount of interest in the past couple of decades for developing cancer and

chemotherapeutic agents.[67,68] Cis-platin is a well-known chemotherapeutic that has encountered frequent problems, mainly due to cellular resistance. Perez *et al.* have developed novel Pt-bis-naphthalimide complexes (Figure 1.13) to enhance DNA binding and cytotoxicity in an attempt overcome the issues associated with cis-platin,[69] through intercalation of the bis-naphthalimide unit in addition to the platination of DNA bases.

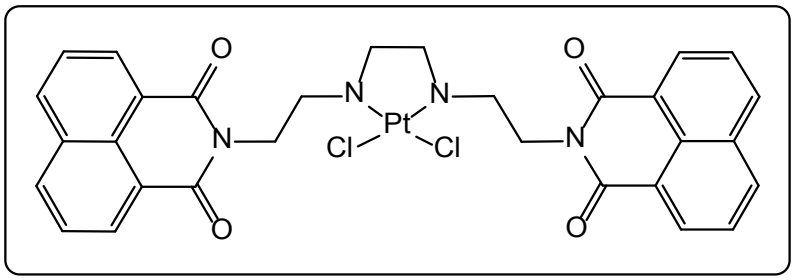

Figure 1.13: Naphthalimide-Pt conjugate bby Perez et al.[69]

The antiproliferative activity of gold(I)-complexes has also been explored during development of gold(I)-phosphine complexes bearing a thio-naphthalimide ligand (Figure 1.14),[70] where compounds exhibited growth inhibitory effects in MCF-7 breast cancer and HT-29 colon carcinoma cells. In comparison to the free naphthalimide analogue, there was increased cellular uptake and accumulation of gold in the nucleus of tumour cells due to the presence of a thiol moiety.

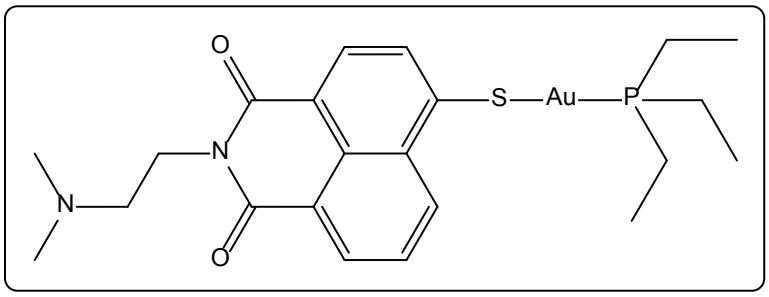

Figure 1.14: Gold(I)-phosphine naphthalimide derivative[70]

Ruthenium has also been investigated extensively in this field, namely by Gunnlaugsson *et al.* for use as potential DNA-binders and photocleaving agents. Flexible and rigid linkers have been used in the development of Ru(II) polypyridyl complexes with 1,8-

naphthalimide derivatives. One example includes the use of an aromatic linker as shown by Quinn and Gunnlaugsson, which was shown to possess control over the relative orientation of the chromophores, thus placing the naphthalimide in close proximity to a metal centre.[71] Complexes exhibit hypochromism and a red shift in the MLCT band when DNA is present, and cause DNA cleavage under irradiation in aerated solution.

In more recent work, "3d-metal scorpionates" incorporating 1,8-naphthalimide chromophores have been developed and are shown to exhibit moderately high affinity for *ct*-DNA.[50] As well as this, the Co(II) and Cu(II) derivatives have been found to induce DNA cleavage and to exhibit significantly higher cytotoxicity against HeLa cervical cancer cells when exposed to UV radiation.

Finally, two series of naphthalimide based Ru(II)-arene complexes showed that the presence of the intercalating naphthalimide moiety enhanced the cytotoxicity of the unit with cancer cells.[72] Findings reported that the intercalation mechanism of the naphthalimide unit within DNA along with the binding of the Ru(II)-arene unit with proteins led to the increased in anti-cancer selectivity for the complexes over model healthy cells, as well as cells with cis-platin acquired drug resistance.

1.4.4 Other uses of 1,8-naphthalimides

1,8-Naphthalimide derivatives can also be used as selective fluorescence sensors, for example in biochemistry and environmental research. It has been seen that using 1,8-naphthalimide units in fluorescent probes for detecting metal ions offers significant advantages over traditional detection methods, due to their increased sensitivity, simplicity and response time.[73,74] An example of this is provided by Wang *et al.*[75] who synthesised a naphthalimide-rhodamine B derivative which was suitable for use as a fluorescence turn-on chemodosimeter for Sn^{4+}. Chemodosimeters detect an analyte *via* a highly selective chemical reaction between a dosimeter molecule and target analyte.[76] In this case, the ring opening reaction of rhodamine and a fluorescence resonance energy transfer process caused a marked colour change and an enhancement in fluorescence in the presence of Sn^{4+}, Cu^{2+} and Cr^{3+}. As well as this, the structure has been useful as a fluorescent probe for Sn^{4+} in biological systems and can behave as an aid to investigate the physiological functions of tin or pathogenesis in the human body.

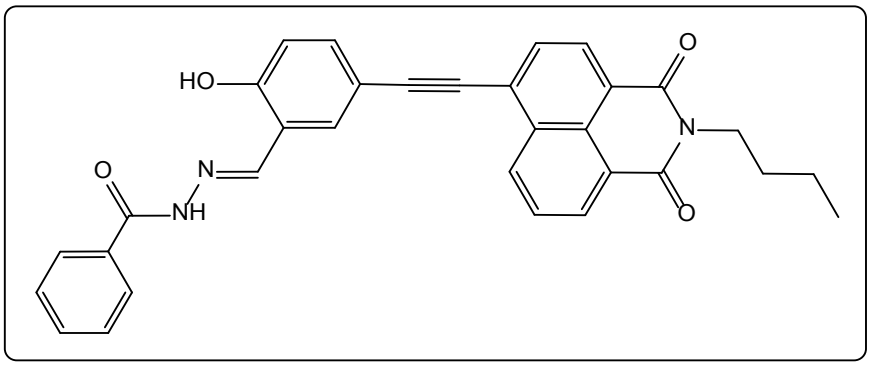

Figure 1.15:Fluorescence sensor for Zn^{2+} detection

The fluorescent sensing of Zn^{2+} is also biologically relevant due to the ions involvement in Alzheimer's disease, epilepsy, ischemic stroke and infantile diarrhoea.[73,77,74] A novel 1,8-naphthalimide compound has been designed for the sensitive turn-on fluorescence detection of Zn^{2+} in aqueous media and intracellular fluid (Figure 1.15).[78] The compound was selective for the Zn^{2+} in comparison to other metals, and a 13-fold increase in fluorescence was seen in the presence of the ion. A similar turn-on fluorescence sensor for Zn^{2+} has been developed that exhibits nucleus envelope penetrability in *in situ* imaging of HeLa and HepG2 cells.[79] In other recent work, Lui *et al.* have synthesised a 4-amino-1,8-naphthalimide-PeT-based fluorescent sensor.[80] The compound incorporated glutamic acid and iminodiacetic acid functionalities (Figure 1.16), the latter of which acts as a receptor for the highly selective detection of Zn^{2+}. A characteristic emission band was seen for the fluorescent probe at ~550 nm and was effectively utilised to image Zn^{2+} in living cells.

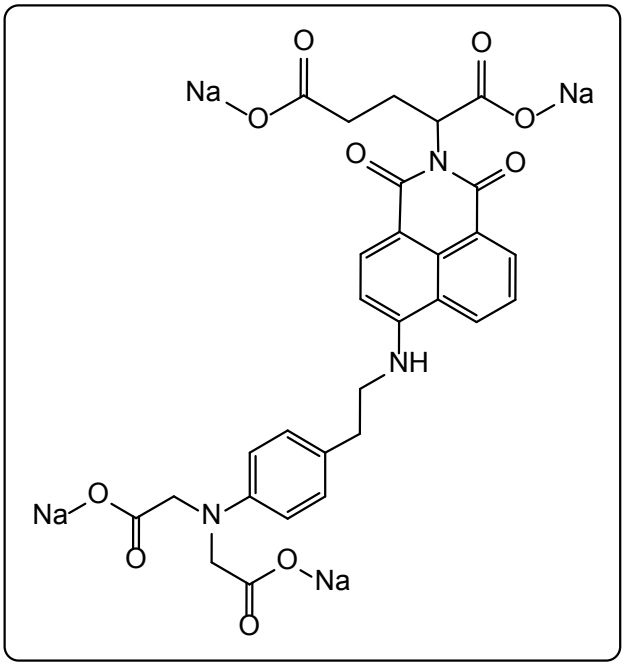

Figure 1.16:Fluorescence sensor for Zn^{2+} detection by Lui et al.

Silver ions have also been investigated in a similar way due to their ability to deactivate sulfhydryl enzymes and bind with amine, carboxyl and imidazole groups of several metabolites. Xu *et al.* have developed a naphthalimide based fluorescent probe (Figure 1.17) that contained a new receptor and acted as a turn-on fluorescence sensor with outstanding selectivity towards Ag^{+} in comparison to other metal ions.[81] A sensor for the live cell imaging of copper has also been developed, incorporating a tetrathia-azacrown into a naphthalimide-based structure.[82]

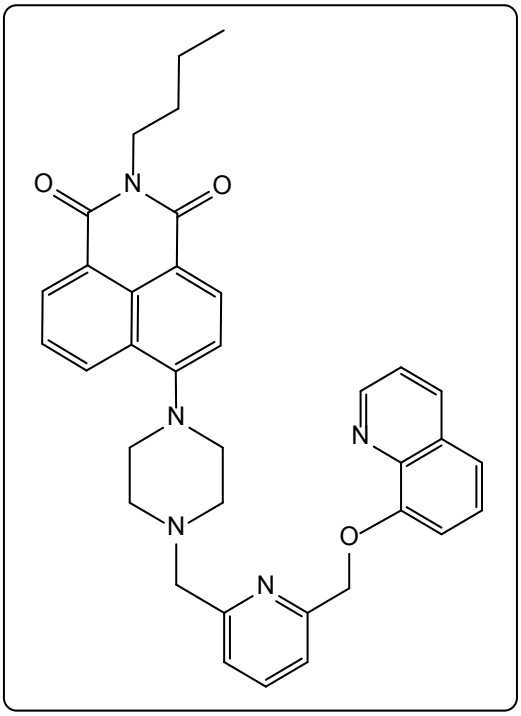

Figure 1.17:Fluorescence probe for Ag^+ by Xu et al.

As well as the sensing of metals, 1,8-naphthalimide derivatives can be used for the sensing of simple molecules, for example nitrous oxide (NO). This is important because it acts as a messenger in cardiovascular and nervous systems, and is also utilised in human immune responses. An example of fluorescent NO sensing comes from Hu *et al.* who synthesised a new copper(II) complex with a naphthalimide-containing ligand.[83] The complex demonstrated an approximate 8-fold increase in fluorescence where the detection limit of NO was 1nM in aqueous solution. The probe was shown to be specific for NO over other species such as ClO^-, NO_2^-, NO_3^-, H_2O_2, and $^1O_2$, all of which are biologically relevant reactive species. Other biologically important species include phosphates, due to their role in cellular ATP hydrolysis, DNA and RNA polymerization, and many enzyme controlled reactions. For this reason a zinc(II) complex incorporating 1,8-naphthalimide with two dipicolylamino arms has been developed as a novel fluorescence sensor to monitor intracellular phosphate.[84]

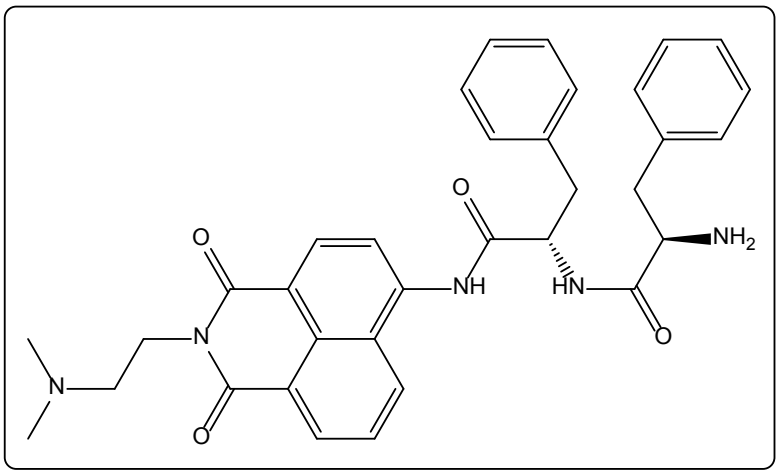

Figure 1.18: Lysosome specific, pH sensitive 'off-on' fluorescent probe[85]

A 1,8-naphthalimide-derived probe has also been developed for H_2S detection in bovine serum and live cell imaging, as well as having the ability to detect intracellular H_2S in lysosomes.[86] In related work, a pH sensitive 'off-on' fluorescent probe has been developed for lysosome imaging (Figure 1.18).[85] The probe was shown to have advantageous specificity for lysosomes over other organelles, and was based on a 4-acylated 1,8-naphthalimide fluorophore. In addition, the compound displayed intrinsic high signal to noise ratio in cell imaging, broad Stokes' shift and practical fluorescence quantum yield.

1 J. R. Lakowicz, *Principles of Fluorescence Spectroscopy*, Springer, Singapore, 3rd edn., 2006.

2 S. Ploem, *Fluorescent and Luminescent Probes for Biological Activity: A Practical Guide to Technology for Quantitative Real-Time Analysis*, Elsevier, 2nd edn., 1999.

3 G. F. Imbush, *Luminescence Spectroscopy*, Academic Press, London, 1st edn., 1978.

4 M. P. Coogan and S. J. A. Pope, *The Chemistry of Molecular Imaging*, John Wiley & Sons, Inc., New Jersey, 1st edn., 2015.

5 A. Periasamy, *Methods in Cellular Imaging*, Oxford University Press, New York, 2001.

6 C. N. Banwell and E. M. McCash, *Fundamentals in Molecular Spectroscopy*, McGraw Hill, UK., 4th edn., 1994.

7 P. Atkins and J. de Paula, *Physical Chemistry*, Oxford University Press, Oxford, 8th edn., 2006.

8 V. Balzani, P. Ceroni and A. Juris, *Photochemistry and Photophysics*, WILEY-VCH Verlag GmbH, Weinheim, 2014.

9 J. A. Broussard, B. Rappaz, D. J. Webb and C. M. Brown, *Nat. Protoc.*, 2013, **8**, 265–281.

10 W. S. Li Dangjuan and L. Jinjun, *Int. Conf. Thin Film Phys. Appl.*, 2010, **7995**, 799531–799534.

11 D. L. Pavia and G. M. Lampman, *Introduction to Spectroscopy*, Brooks/Cole, Belmont, 4th edn., 2009.

12 J. Hoyland, *Fluorescent and Luminescent Probes for Biological Activity - A practical guide to technology for quantitative real-time analysis*, Academic Press, 2nd edn., 1999.

13 S. Barlow, S. A. Odom, K. Lancaster, Y. A. Getmanenko, R. Mason, V. Coropceanu, J.-L. Brédas and S. R. Marder, *J. Phys. Chem. B*, 2010, **114**, 14397–14407.

14 X. Z. Dong Chen, J. Zhang and Y. Wang, *Supramol. Struct. Mater.*, 2015, **36**, 484–488.

15 B. J. Saiki, P. Gogoi, S. Sharmah and S. K. Dolui, *Polym. Int.*, 2015, **64**, 437–445.

16 D. W. G. Haridas Kar, F. Laquai and S. Ghodh, *Nanoscale*, 2015, **7**, 6729–6736.

17 Z. Liu, W. He and Z. Guo, *Chem. Soc. Rev.*, 2013, **42**, 1568–1600.

18 T. Kalai, E. Hideg, F. Ayaydin and K. Hideg, *Photochem. Photobiol. Sci.*, 2013, **12**, 432–438.

19 V. B. Bojinov, N. I. Georgiev and P. Bosch, *J. Fluoresc.*, 2009, **19**, 127–139.

20 M. Kumar, N. Kumar and V. Bhalla, *Chem. Commun.*, 2013, **49**, 877–879.

21 *Spectrochim. Acta Part A Mol. Biomol. Spectrosc.*, 2013, **105**, 57–61.

22 T. Gunnlaugsson, C. McCoy, R. Morrow, C. Phelan and F. Stomeo, *Arkivoc*, 2003, **7**, 216–228.

23 E. Kimura and S. Aoki, *BioMetals*, 2001, **14**, 191–204.

24 M. H. Lee, J. S. Kim and J. L. Sessler, *Chem. Soc. Rev.*, 2015, **44**, 4185–4191.

25 H. Woo, Y. You, T. Kim, G.-J. Jhon and W. Nam, *J. Mater. Chem.*, 2012, **22**, 17100–17112.

26 N. G. Connelly, T. Damhus, R. M. Hartshorn and A. T. Hutton, *Nomenclature of Inorganic Chemistry. IUPAC Recommendations 2005.*, Royal Society of Chemistry, Cambridge, 2005.

27 K. Bowman-James, *Acc. Chem. Res.*, 2005, **38**, 671–678.

28 D. M. P. Mingos, *Essentials of Inorganic Chemistry*, Oxford University Press, New York, 2nd edn., 2007.

29 D. F. Shriver, P. Atkins, T. L. Overton, J. P. Rourke, M. T. Weller and F. A. Armstrong, *Inorganic Chemistry*, Oxford University Press, Oxford, 4th edn., 2006.

30 A. K. Bridson, *Inorganic Spectroscopic Methods*, Oxford University Press, New

York, 1998.

31 N. F. Curtis, *J. Chem. Soc.*, 1964, 2644–2650.

32 J. Beutel, H. L. Kundel and R. L. Van Metter, *Handbook of Medical Imaging, Volume I: Physics and Psychophysics*, The Society of Photo-Optical Instrumentation Engineers, USA, 2000.

33 C. J. Jones and J. R. Thornback, *Medicinal Applications of Coordination Chemistry*, The Royal Society of Chemistry, 2007.

34 E. Toth, *Comptes Rendus Chim.*, 2010, **13**, 700–714.

35 Z. H. Cho, J. P. Jones and M. Singh, *Foundations of Medical Imaging*, Wiley, 1993.

36 V. Fernández-Moreira, F. L. Thorp-Greenwood and M. P. Coogan, *Chem. Commun.*, 2010, **46**, 186–202.

37 F. L. Thorp-Greenwood, *Organometallics*, 2012, **31**, 5686–5692.

38 F. L. Thorp-Greenwood, R. G. Balasingham and M. P. Coogan, *J. Organomet. Chem.*, 2012, **714**, 12–21.

39 T. Terai and T. Nagano, *Curr. Opin. Chem. Biol.*, 2008, **12**, 515–521.

40 R. Yuste, *Nat. Methods*, 2005, **2**, 902–904.

41 M. Chalfie, Y. Tu, G. Euskirchen, W. W. Ward and C. Prasherf, *Science (80-.).*, 1994, **263**, 802–804.

42 M. Muller, *An Introduction to Fluorescence Microscopy*, The International Society for Optical Engineering, 2006.

43 S. W. Paddock, *Confocal Microscopy: Methods and Protocols*, Humana Press Inc., 1999.

44 A. Yildiz, J. N. Forkey, S. A. McKinney, T. Ha, Y. E. Goldman and P. R. Selvin, *Science (80-.).*, 2003, **300**, 2061–2065.

45 D. A. Agard, Y. Hiraoka, P. Shaw and J. W. Sedat, *Methods Cell Biol.*, 1989, **30**, 353–77.

46 Photonics - School of Physics - Trinity College Dublin, http://www.tcd.ie/Physics/research/themes/photonics/nanophotonics/plasmon.php, (accessed 21 September 2017).

47 L. Schermelleh, R. Heintzmann and H. Leonhardt, *J. Cell Biol.*, 2010, **190**, 165–75.

48 E. Betzig, S. W. Hell and W. E. Moerner, *Nobel Media 2014.*, .

49 R. Tandon, V. Luxami, H. Kaur, N. Tandon and K. Paul, *Chem. Rec.*, 2017, **17**, 1–39.

50 S. Banerjee, E. B. Veale, C. M. Phelan, S. A. Murphy, G. M. Tocci, L. J. Gillespie, D. O. Frimannsson, J. M. Kelly, T. Gunnlaugsson, J. Kluza, D. Hochhauser, J. A. Hartley, M. Lee, F. Darro, R. Kiss, R. J. Diamond, R. J. McRipley, R. J. Page and J. L. Gross, *Chem. Soc. Rev.*, 2013, **42**, 1601–1618.

51 R. Stolarski, *Fibres Text. East. Eur.*, 2002, **71**, 91.95.

52 M. Brana and A. Ramos, *Curr. Med. Chem. Agents*, 2001, **1**, 237–255.

53 M. Brana, J. M. Castellano, C. M. Roldan, A. Santos, D. Vazquez and A. Jimenez, *Cancer Chemother. Pharmacol.*, 1980, **4**, 61–66.

54 M. J. Waring, A. González, A. Jiménez and D. Vázquez, *Nucleic Acids Res.*, 1979, **7**, 217–230.

55 R. M. Stone, E. Mazzola, D. Neuberg, S. L. Allen, A. Pigneux, R. K. Stuart, M. Wetzler, D. Rizzieri, H. P. Erba, L. Damon, J.-H. Jang, M. S. Tallman, K. Warzocha, T. Masszi, M. A. Sekeres, M. Egyed, H.-A. Horst, D. Selleslag, S. R. Solomon, P. Venugopal, A. S. Lundberg and B. Powell, *J. Clin. Oncol.*, 2015, **33**, 1252–1257.

56 K. A. Stevenson, S. F. Yen, N. C. Yang, D. W. Boykin and W. D. Wilson, *J. Med. Chem.*, 1984, **27**, 1677–1682.

57 K. Wang, Wang. Y., X. Yan, H. Chen, G. Ma, P. Zhang, J. Li, X. Li and J. Zhang, *Bioorg. Med. Chem. Lett.*, 2012, **22**, 937–941.

58 R. K. Y. Zee-Cheng and C. C. Cheng, *J. Med. Chem.*, 1985, **28**, 1216–1222.

59 M. F. Braña, J. M. Castellano, M. Morán, F. Emling, M. Kluge, E. Schlick, G. Klebe and N. Walker, *Arzneimittelforschung.*, 1995, **45**, 1311–8.

60 M. F. Braña, J. M. Castellano, M. Morán, M. J. Pérez de Vega, C. R. Romerdahl, X. D. Qian, P. Bousquet, F. Emling, E. Schlick and G. Keilhauer, *Anticancer. Drug Des.*, 1993, **8**, 257–68.

61 P. F. Bousquet, M. F. Braña, D. Conlon, K. M. Fitzgerald, D. Perron, C. Cocchiaro, R. Miller, M. Moran, J. George, X. D. Qian, G. Keilhauer and C. A. Romerdahl, *Cancer Res.*, 1995, **55**, 1176–80.

62 C. Bailly, M. Braña and M. J. Waring, *Eur. J. Biochem.*, 1996, **240**, 195–208.

63 R. J. McRipley, P. E. Burns-Horwitz, P. M. Czerniak, R. J. Diamond, M. A. Diamond, J. L. Miller, R. J. Page, D. L. Dexter, S. F. Chen, J. H. Sun, C. H. Behrens, S. P. Seitz and J. L. Gross, *Cancer Res.*, 1994, **54**, 159–64.

64 R. J. Cherney, S. G. Swartz, A. D. Patten, E. Akamike, J.-H. Sun, R. F. Kaltenbach, S. P. Seitz, C. H. Behrens, Z. Getahun, G. L. Trainor, M. Vavala, M. R. Kirshenbaum, L. M. Papp, M. P. Stafford, P. M. Czerniak, R. J. Diamond, R. J. McRipley, R. J. Page and J. L. Gross, *Bioorg. Med. Chem. Lett.*, 1997, **7**, 163–168.

65 E. B. Veale and T. Gunnlaugsson, *J. Org. Chem.*, 2010, **75**, 5513–5525.

66 K. Suzuki, H. Nagasawa, Y. Uto, Y. Sugimoto, K. Noguchi, M. Wakida, K. Wierzba, T. Terada, T. Asao, Y. Yamada, K. Kitazato and H. Hori, *Bioorg. Med. Chem.*, 2005, **13**, 4014–4021.

67 J. Reedijk, *Eur. J. Inorg. Chem.*, 2009, **2009**, 1303–1312.

68 N. J. Farrer, L. Salassa and P. J. Sadler, *Dalton Trans.*, 2009, **48**, 10690–10701.

69 José M. Pérez, Isabel López-Solera, Eva I. Montero, Miguel F. Braña, Carlos Alonso, and Simon P. Robinson and Carmen Navarro-Ranninger, *J Med. Chem.*, 1999, **42**, 5482–5486.

70 C. P. Bagowski, Y. You, H. Scheffler, D. H. Vlecken, D. J. Schmitz, I. Ott, L. I. Partecke, C. D. Heidecke, M. M. Lerch, C. P. Bagowski, M. Y. Geng, Y. J. Cai and J. Ding, *Dalton Trans.*, 2009, **99**, 10799–10805.

71 Gary J. Ryan, and Susan Quinn and T. Gunnlaugsson, *Inorg Chem*, 2008, **47**, 401–403.

72 K. J. Kilpin, C. M. Clavel, F. Edafe and P. J. Dyson, *Organometallics*, 2012, **31**, 7031–7039.

73 A. . Ivanov, I. . Nazimov and L. . Baratova, *J. Chromatogr. A*, 2000, **870**, 433–442.

74 G. Chen, L. Zhang and J. Wang, *Talanta*, 2004, **64**, 1018–1023.

75 Q. Wang, C. Li, Y. Zou, H. Wang, T. Yi and C. Huang, *Org. Biomol. Chem.*, 2012, **10**, 6740–1520.

76 H. Wen-jun and W. Wen-hui, *Imaging Sci. Photochem.*, 2011, **29**, 321–335.

77 K. Amarnath, V. Amarnath, K. Amarnath, H. L. Valentine and W. M. Valentine, *Talanta*, 2003, **60**, 1229–1238.

78 *Tetrahedron Lett.*, 2013, **54**, 3353–3358.

79 C. Zhang, Z. Liu, Y. Li, W. He, X. Gao and Z. Guo, *Chem. Commun.*, 2013, **49**, 11430–11432.

80 D.-Y. Liu, J. Qi, X.-Y. Liu, H.-R. He, J.-T. Chen and G.-M. Yang, *Inorg. Chem. Commun.*, 2014, **43**, 173–178.

81 L. Xu, Y. Xu, W. Zhu, C. Yang, L. Han and X. Qian, *Dalton Trans.*, 2012, **41**, 7212–7217.

82 C. Satriano, G. T. Sfrazzetto, M. E. Amato, F. P. Ballistreri, A. Copani, M. L. Giuffrida, G. Grasso, A. Pappalardo, E. Rizzarelli, G. A. Tomaselli and R. M. Toscano, *Chem. Commun.*, 2013, **49**, 5565–5567.

83 X. Hu, X. Zhang, H. Song, C. He, Y. Bao, Q. Tang and C. Duan, *Tetrahedron*, 2012, **68**, 8371–8375.

84 J. F. Zhang, S. Kim, J. H. Han, S.-J. Lee, T. Pradhan, Q. Y. Cao, S. J. Lee, C. Kang and J. S. Kim, *Org. Lett.*, 2011, **13**, 5294–5297.

85 L. Chen, J. Li, Z. Liu, Z. Ma, W. Zhang, L. Du, W. Xu, H. Fang and M. Li, *RSC Adv.*, 2013, **3**, 13412–13416.

86 T. Liu, Z. Xu, D. R. Spring and J. Cui, *Org. Lett.*, 2013, **15**, 2310–2313.

Chapter 2 - Trackable Fluorophore-Labelled Gold(I)-NHC Conjugates for Cell Imaging Applications

2.1 Introduction

2.1.1 Chemical Properties of Gold

Gold as a metal has been encountered since early civilisation, when it was associated with power, beauty and the cultural elite.[1] Initially, the understanding of the chemistry of gold was limited to its concentration, recovery and purification. However, over time, gold chemistry has advanced to become an extremely important branch of science with applications in various fields.[2] Gold has only one naturally occurring isotope, and is the most electronegative of all metals.[3] Gold's most commonly studied species are of oxidation state +1. However +3, 0 and -1 are also known.[1]

Gold(I) has an electronic configuration of $5d^{10}6s^{0}$, where 10 electrons in a closed set of 5*d* orbitals explains the relative stability of these compounds.[1] The post-lanthanide position of gold means a large number of protons are contained in its atomic nuclei and a very high effective nuclear charge is observed. For this reason, electrons are treated with a relativistic approach, as their movement reaches velocities approaching the speed of light. This effect (particularly for *s* electrons) causes the orbital radius to be contracted and the distance from the nucleus to be reduced, thus giving rise to a number of properties: i) the colour of gold arising from a transition from the filled 5*d* band to the Fermi level (2.4 eV); ii) shorter covalent bond lengths involving gold atoms; and iii) the closed 5*d* shell is no longer chemically inert and can interact with other gold atoms in molecules or clusters.

2.1.2 Au(I) Coordination Chemistry and Ligand Design

The chemistry of Au(I) compounds is by far the most studied and numerous mononuclear, dinuclear and polynuclear derivatives have been reported with interesting photochemical and photophysical properties.[4] Due to the small difference in energy between the *s* and *d* orbitals; linear, two-coordinate complexes dominate.[1] Trigonal three-coordination and tetrahedral four-coordination complexes have also been reported, but to a far lesser extent.[5] Au(I) is a soft cation, thus has a high affinity for sulfur, phosphine, arsenic, alkynyl and selenium donors;[3,6] numerous Au(I) complexes exist with such ligands.

Au(I) forms kinetically stable complexes due to its d^{10} configuration. However, ligand exchange is a major contributing factor in the biological activity and behaviour of Au(I) complexes. For example, solution calorimetry studies of a [AuCl(L)] (L = phosphine or phosphite) system showed that the electronic parameters of the ligand dominates. In this case, bond dissociation enthalpies for tertiary phosphines were estimated at 58-65±5 kcal mol^{-1}.[7] As well as this, factors such as protein binding, excretion pathways, and toxicity can be modulated by tuning the amphiphilic nature of Au(I) bound ligands.[8,9]

2.1.3 N-Heterocyclic Carbenes

Carbenes are an interesting class of carbon-containing compounds comprising a divalent carbon atom with a six-electron valence shell.[10] For this reason, free carbenes were normally very reactive and traditionally used as highly reactive transient intermediates, for example in cyclopropanation. Despite this, free carbenes have been stabilised using favourable interactions with phosphorus and silicon substituents,[11] well as through incorporation into a nitrogen heterocycle.[12] N-heterocyclic carbenes (NHCs) were first isolated and characterised in 1991, and have since developed into an extremely powerful group of compounds for organic and inorganic chemistry.[10] In this context, synthesis of the first isolable NHC, 1,3-di(adamantyl)imidazole-2-ylidene (IAd) (Figure 2.1), led to a significant increase in the experimental and theoretical studies with a vast library of novel NHCs being developed. Specifically, NHCs have been found to be excellent ligands for transition metals, and thus have found multiple applications, for example as catalysts.[10] In addition, these carbenes are currently recognised as a useful alternative to tackle the limitations associated with phosphine ligands in organometallics and catalysis.[13,14]

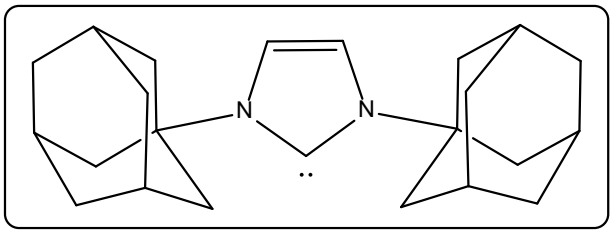

Figure 2.1: IAd

The broad definition of an NHC is a heterocyclic species containing a carbene carbon and at least one nitrogen atom within the ring structure.[15,16] They are also known as Arduengo carbenes, and form Fischer-type complexes with transition metals.[16] The carbene centre shows a remarkable level of stability due to the electronic and steric effects of the structural features. NHCs containing bulky substituents adjacent to the carbene atom increase the kinetic stability by sterically disfavouring dimerization (the Wanzlick equilibrium).[10] In addition, the steric impact of the N-substituents is affected by minor alterations to the NHC architecture, thus giving rise to huge changes of the electronic donor properties of the carbene groups with relation to a coordinated metal.[17,18] They have also been described as amongst the most powerful neutral organic bases, where their strength is comparable to DBU and pentacyclic vinamidines.[19,20]

The electronic stabilization provided by the nitrogen atoms is also a factor in explaining the stability of NHCs. NHCs such as IAd have a singlet-ground state electronic configuration with the HOMO and the LUMO best described as a formally sp^2-hybridised lone pair and an unoccupied *p*-orbital at the C^2 carbon.[10] The adjacent σ-electron withdrawing orbital and π-electron donating nitrogen atoms stabilise this arrangement both inductively and mesomerically. In addition, the cyclic nature of NHCs give rise to a bent, sp^2-like arrangement for the carbene carbon, further favouring the singlet state. The ground state structure described is supported by the C-N bond lengths that are observed in IAd (1.37 Å), which fall between those of its corresponding C^2-saturated analogue and imidazolium salt. This suggests that the C^2-nitrogen bonds possess partial double bond character.

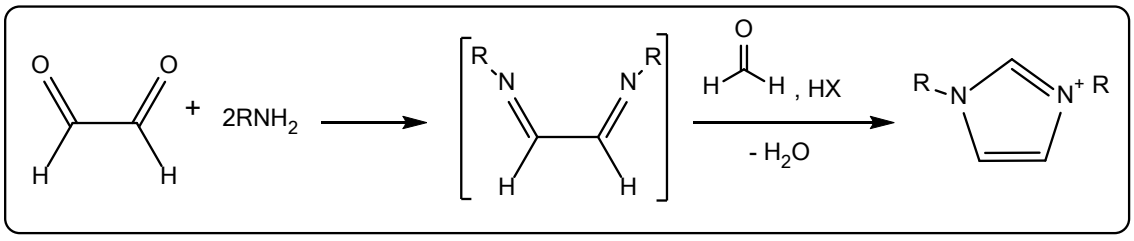

Scheme 2.1: Preparation of imidazolium precursors[16]

The main method of generating NHCs is through imidazolylidenes and imidazolidinylidenes, while other methods exist, but are rarely employed. In this vein, there are various routes available to prepare imidazolium precursors (Scheme 2.1).[21]

Perhaps the most simple is a one-pot synthesis, that utilises a primary amine and formaldehyde.[22] The corresponding Schiff base is formed via coupling between the amine and glyoxal under acidic conditions, followed by condensation with formaldehyde to form the imidazolium salt (Scheme 2.1). For more sterically demanding syntheses, Glorius *et al*. provide an alternative approach using silver triflate and chloromethyl pivalate. For unsymmetrical imidazolium salts, an alternative route has been developed involving the stepwise alkylation of an imidazolium anion generated from the reaction of imidazole with potassium.[21]

As discussed above, NHCs form a range of organometallic complexes with a wide variety of metals. It is generally accepted that NHCs bind strongly to metals via σ-bonding, while the back bonding can usually be considered to be negligible.[16] This is not observed, however, for Group 11 metals, where the π-back bonding component becomes significant.[23] NHCs have been compared to phosphines in metal complexes, where both act as monodentate two-electron donor ligands.[16] For example, NHCs have been shown to be more electron donating than most basic phosphines when studied with a variety of nickel(0) complexes.[24] NHCs have also formed metal complexes with alkali metals. For example, the 4,5-dimethyl-1,3-diisopropylimidazolium salt is deprotonated with lithium, sodium and potassium hexamethyldisilazide forming the corresponding carbene alkali metal complexes.[25] In addition, complexes have been formed with alkaline earth metals[26], group 13 metals[27], rare earth metals[15,28], and transition metals.[29] In contrast, the carbene chemistry of complexes with groups 14, 15 and 16 metals is extremely underdeveloped.[16]

2.1.4 Therapeutic Activity of Gold

The use of gold-based compounds in medicinal chemistry is referred to as chrysotherapy.[30–32] The most common variety of Au(I) coordination complexes used in a clinical setting are those incorporating thiolate or phosphine ligands.[5] Amongst the most widely utilised are auranofin, sodium aurothiomalate (Figure 2.2), and sodium aurothioglucose, all of which have been applied for the treatment of inflammatory autoimmune conditions such as rheumatoid arthritis.[33,34] Auranofin is also under

investigation as a treatment to reduce the viral reservoir of HIV that lies latent in the body's T-cells.[35]

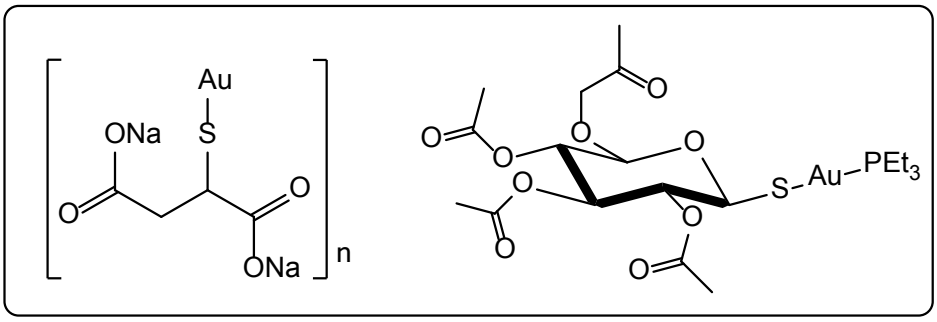

Figure 2.2: Sodium aurothiomalate (left) and auranofin (right)

The mechanism of biological action of such clinical treatments is extremely difficult to unravel,[36,37] although it is thought to be related to the inhibition of cathepsin B activity *via* targeting of lysosomal cysteine proteases.[38,39] Another hypothesis is that Au(I) complexes deactivate singlet O_2 through the inhibition of the enzyme thioredoxin reductase (TrxR), thus interrupting oxidative stress regulation in cells.[39,40–42] As well as being involved in many other metabolic pathways, it is the antioxidant capability of TrxR that is thought to be associated with protecting cells from oxidative stress.[43] In addition, elevated levels of TrxR have been reported in a range of cancer cell lines. Furthermore, recent work has observed the inhibition of the selenium-glutathione peroxidase enzyme, highlighting the thio- and selenophilic nature of Au(I).[44,45] As well as focused studies on developing treatments for rheumatoid arthritis, a variety of Au(I) complexes have been assessed in terms of their anti-tumour properties.[46,47]

In summary, mechanistic studies to date define three major classes of gold compounds according to their mode of action with biological targets:[5] i) prodrugs that are able to coordinate tightly to biomolecules' side chains; ii) 'big cations' capable of crossing membranes and binding non-covalently to biomolecules; and iii) compounds that react with biomolecules through redox chemistry to cause oxidative damage.

2.1.5 Au(I) Complexes as Anti-Cancer Agents

As previously introduced, gold compounds are an important class of metallodrugs with great scope for cancer treatment.[5] Over the last two decades, there have been several

reports suggesting that a variety of Au(I) complexes possess relevant antiproliterative properties *in vitro* against selected human tumour cell lines.

Preliminary research into the mode of action of Au(I) compounds for anti-cancer applications focused on DNA and RNA targets, as these biomolecules are considered to be important targets for similar platinum based drugs. However, weak interactions were observed between anti-arthritic gold(I) drugs and DNA, suggesting that different cellular processes may be involved in their cytotoxic mechanism.[48] Alternatively, relevant alterations observed on mitochondrial functions are observed following Au(I) complex treatment, which can be explained by the action of Au(I) compounds on TrxR.[5] In relation to this, expression levels of the cytosolic thioredoxin isoform Trx1 are increased in several human carcinomas,[49,50] and linked to tumour aggressiveness, and to inhibition of apoptosis.[51,52] For these reasons, much research focuses on the thioredoxin system as a potential target for new anti-cancer drugs. Auranofin acts as a specific inhibitor of both cytosolic[53] and mitochondrial TrxR[54–56] due to its reaction with thiol and/or selenol groups. As well as other structural analogues, it is also found to induce, in the presence of Ca^{2+} ions, mitochondrial swelling and mitochondrial membrane potential decrease, and stimulation of respiration which results in the overall release of cytochrome C into the cytoplasm.[8,55] The process described is, importantly, involved in the formation of apoptosomes and therefore the induction of apoptosis.

In this context, the ability of auranofin to inhibit TrxR and induce apoptosis has been confirmed in cis-platin resistant human ovarian cancer cells.[57] In addition, structural analogues of auranofin have been shown to display significant cytotoxicity against B16 melanoma and P388 leukemia cell lines.[58] The importance of nature of the ancillary tertiary phosphine was a key conclusion in this work. Some were found to induce additional potency to the complex, for example for a given thiolate ligand, triethyl derivatives were generally more cytotoxic than triphenyl. In addition, Tiekink summarised a number of studies evaluating the cytotoxicity of a large range of Au(I) complexes.[37] This work assessed the structure-property relationships with tetrahedral Au(I) complexes. Examples from this work include complexes with charged and/or bidentate thiols, chiral phosphines and thiols labelled with biologically active groups. In addition, gold phosphine compounds incorporating a variable number of coordinating

phosphorus atoms were seen to show increased cytotoxic potency in murine tumour cell lines as the number of gold-coordinated phosphorus atoms increases.[59,60]

There are also numerous examples of Au(I)-NHC complexes with anti-tumour applications. For examples of these, see Section 2.1.7.

2.1.6 Luminescent Monometallic Au(I) Complexes and Fluorescence Bioimaging

The development of organometallic Au(I) compounds has allowed investigations into luminescent complexes to be carried out, where photophysical properties are dictated by the nature of the coordinated ligand.[6] There are no ligand field excited states available due to the 5d frontier orbitals being full. However, low energy metal centred transitions (5*d*-6*s*/6*p* at ca. 250 nm) are accessible.[61] The ability of Au(I) to be both oxidising and reducing means LMCT transitions can also occur, most commonly with π-acceptor ligands such as phosphines. In addition, coordinatively unsaturated Au(I) complexes are able to aggregate through metallophilic interactions, which perturbs excited states with ligand-centred and/or CT character, as well as introduce new excited states due to aurophilic interactions.[6]

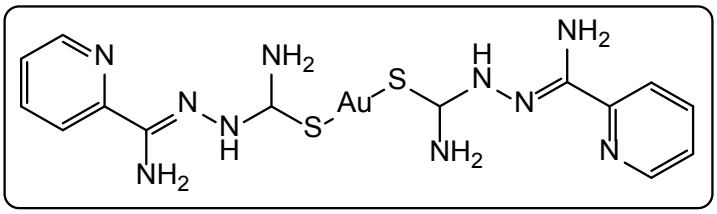

Figure 2.3: Example of luminescent Au(I) complex[62]

An example of this is provided by Castineiras *et al.,* who generated supramolecular Au(I) architectures based on 2-pyridineformamide thiosemicarbazone ligands (Figure 2.3), resulting in a luminescent species whose absorption spectra were dominated by ligand centred n-π^* transitions *ca.* 392 nm.[62] Corresponding solid-state emission peaks were assigned to ligand-centred fluorescence in all cases, which were perturbed to different degrees by the presence of Au(I) and the presence of any weak Au···Au interactions. Related compounds with thiocarbamoyl-pyrazoline ligands also showed absorption at 300-350 nm attributed to a LMCT transition (Figure 2.4).[63] This series of cytotoxic

mercapto-pteridine ligands also show overlapping ligand-centred and S-to-Au LMCT transitions, as well as displaying visible luminescence assigned to the fluorophore. A simple heteroleptic species, $[Au(PPh_3)(C_5H_5N)]^+$, was first reported by Schmidbaur in 2004.[64] Following this, related species based on $[Au(Py)_2]^+$ (Py = 4-subsituted pyridine) showed solid-state luminescence properties which were highly dependant upon the nature of the intermolecular Au(I)···Au(I) interactions.[65] In addition, naphthalimide based ligands have been studied and form a variety of complexes of the type $[Au(PR_3)(L)]^+$.[66,67] The compounds showed metal-perturbed ligand-centred fluorescence in all cases, as suggested by literature precedent.

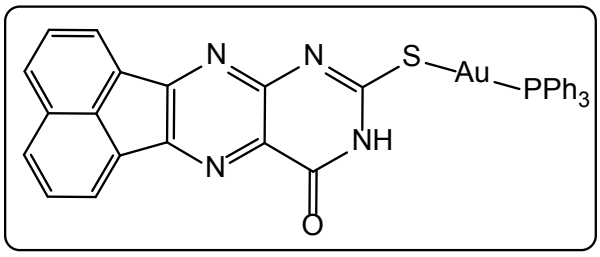

Figure 2.4:Example of luminescent Au(I) complex[63]

Due to the difficulties associated with understanding the biological action of Au(I) drugs, cellular imaging techniques have been commonly employed to elucidate the cellular uptake and intracellular distribution of Au(I) complexes.[6] This is still a challenging area of research, and can be embodied into two strategies: i) the functionalisation of Au(I) compounds with fluorescent labels compatible with CFM; and ii) the use of analytical techniques that allow elemental isotopic composition to be mapped. Unfortunately, the latter of the two is associated with destructive methods with low resolution, such as ICP-MS and SR-XRF. An example of the former identifies alkyne-coordinated Au(I) complexes which selectively target TrxR.[67] In addition, fluorescent alkynyl-functionalised anthraquinone ligands and their associated mono- and dimetallic Au(I) complexes have been applied to cellular imaging studies (Figure 2.5).[68] In this research, CFM showed good cellular uptake in MCF cells for all complexes (> 80 %).

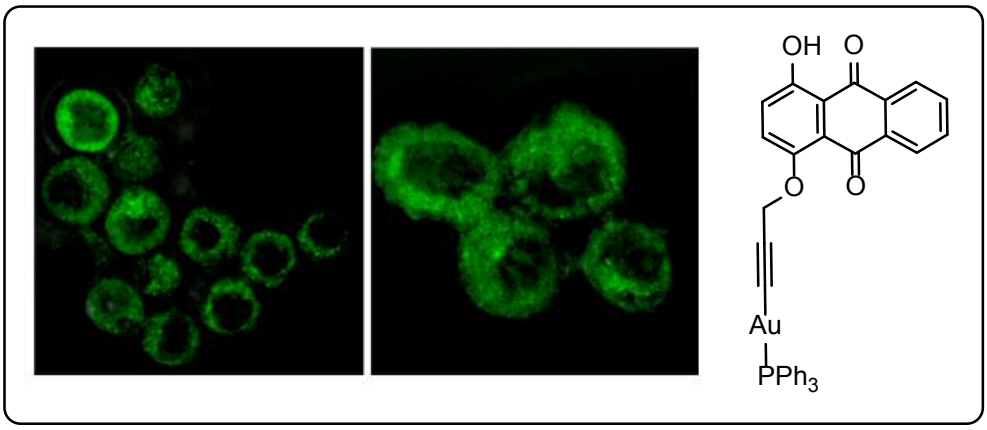

Figure 2.5: Examples of CFM images of MCF-7 cells. Cells incubated with anthraquinone species by Balasingham et al.[68]

The Ott group also presented linear Au(I) complexes incorporating an ancillary phosphine and a thiolated fluorophoric ligand of the form [Au(PR_3)(S-Nap))] (S-Nap = 4-mercapto-1,8-naphthalic anhydride or N-(N',N'-dimethylaminoethyl)-1,8-naphthalimide-4-sulfide).[69] CFM of MCF-7 cells showed localisation in cell nuclei, with supporting cytotoxicity studies giving IC_{50} values of 1.1-3.7 µM, comparable with those of auranofin (1.1 µM) and cisplatin (2.0 µM). It is also noteworthy that the free 1,8-naphthalimide ligands showed cytotoxicity, with IC_{50} values of 1.9-4.6 µM.

Au(I) complexes incorporating NHCs have also been applied to cellular imaging studies. For examples of these, see Section 2.1.7.

2.1.7 Au(I)-NHC Complexes

As well as extensive investigation of Au(I) complexes incorporating phosphine and thiolate ligands, a variety of research has been carried out into complexes incorporating NHCs.[70] Au(I)-NHCs have been known for over a quarter of a century, where initial synthetic methods used oxidative addition reactions. However, alternative methods were discovered after isolation by Burini *et al.* in 1989 (Figure 2.6).[71] Over the past decade, the use of NHCs as ligands for Au(I) have developed rapidly, and applications have been found to include antimitochondrial, anti-tumour,[72,73] antimicrobial,[74] and catalytic activity.[75]

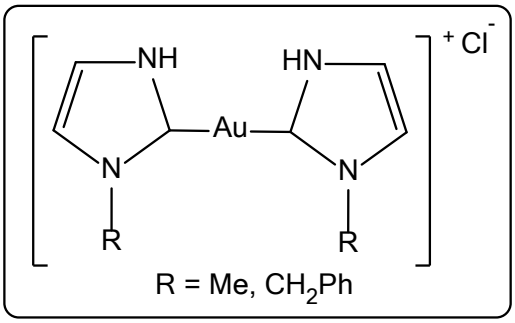

Figure 2.6: Example of complex by Burini et al.[71]

There are several methods that have been adopted to synthesise Au(I)-NHC compounds:[70] i) cleavage of electron rich olefins; ii) transfer of carbene from group 6 carbonyl complexes; iii) reaction of azolium salts of NHCs with a Au(I) source; iv) protonation or alkylation of gold azolyl compounds; and v) transmetallation between Ag(I)-NHCs and Au(I) pre-cursors. For the last of these examples, [Au(tht)Cl] (tht = tetrahydrothiophene) has been commonly employed as a reagent in the transmetallation step.

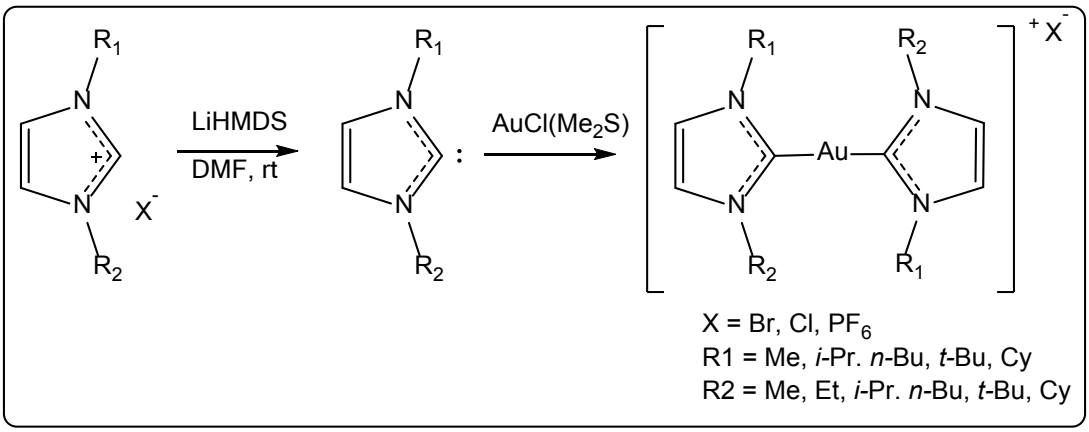

Scheme 2.2:Synthesis and structure of complexes by Baker et al. showing anti-mitochondrial activity[76]

The biological activity of Au(I)-NHC complexes is an extremely important application, where pioneering research by the groups of Baker and Berners-Price have found NHCs to be a viable alternative to more common phosphine ligands.[77,78] Steric control and electronic influences can be relatively easily controlled by tuning the nature of the precursor imidazolium salt. Lipophilicity of the complexes can also be controlled in this way, which is a significant consideration for biological applications. For example, NHC complexes have been shown to exhibit anti-tumour activity via TrxR inhibition,[79] where

more focused studies have suggested that mitochondria are targeted. Similarly, homoleptic cationic Au(I) complexes of the nature $[Au(NHC)_2]^+$ have been investigated as anti-mitochondrial agents (Scheme 2.2).[76] In this case, the lipophilicity was controlled by the alkyl group on the ligand, where the most lipophilic species gave rise to the greatest mitochondrial swelling and permeability. Fine-tuning of the ligand architecture was also applied in research by Hickley *et al.,* who designed lipophilic, cationic Au(I)-NHC complexes that selectively induce apoptosis in cancer cells and show selective targeting of mitochondrial selenoproteins, such as TrxR.[80] In addition, a complex of the form $[Au(NHC)_2]^+$ (NHC = bis-(N-methyl-N´(2-hydroxy-2-phenyl)ethyl)-imidazole-2-ylidine)) was found to be the most active anti-tumour compound in a range of Ag(I)- and Au(I)-NHCs.[81] In particular, the lipophilic, cationic compound exhibited lower IC_{50} values than its Ag(I) counterpart (1.0 and 2.6 µM on MCF-7 and ZR-75-1 breast cancer cells, respectively), thus suggesting the importance of gold for the increased anti-tumour activity. In the same study, it was found that the activity is attributed to the upregulation on p53 and $p21^{WAF1/Cip1}$ expression, dependant on the transcription factor Sp1. In other research, Visbal *et al.* found that lung and pancreatic cancer cells were more sensitive to acridine-based Au(I)-NHC compounds than their analogous Ag(I) compounds, where apoptosis was found to be the main cell death pathway (Figure 2.7).[82] Fluorescence cell microscopy found that complexes were mainly localised in the lysosomes and showed some nuclear and nucleolar staining. It is also noteworthy that the emission wavelengths of the compounds lay in the range of 470 to 530 nm.[82,83]

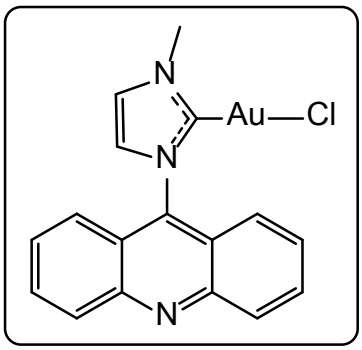

Figure 2.7: Example of complex from Visbal et al.[82]

Bis-chelated bidentate phosphine and NHC Au(I) complexes have also been shown to selectively induce apoptosis in MDA-MB-468 human breast adenocarcinoma cells rather than in human normal breast cells.[84] In this case, it was found that apoptosis was

induced via the mitochondrial pathway by inhibition of both Trx and TrxR. Another phosphine gold compound, μ-[1,2-bis(diphenylphosphino) ethane] *bis*[(1-thio-β-D-glucopyranosato-S)gold(I)], displayed IC_{50} values between 4-11 μM towards a selection of cisplatin-sensitive cell lines,[85] as well as similar cytotoxicity in cis-platin resistant cell lines.[86]

As discussed above, Au(I)-NHC complexes have also found use for cell imaging applications. An aforementioned range of dimetallic, water-soluble, cyclophane-bridged Au(I)-NHC complexes showed good uptake with RAW264.8 cells, with lysosomal localisation and mild toxicity (IC_{50} = 52 μM).[76] In addition, fluorescent Au(I) complexes incorporating anthracenyl NHC ligands have been observed to lead to oxidation of the thioredoxin system, as well as enabling visualisation of cellular distribution due to the anthracene fluorophore.[87] This specific example demonstrates that Au(I) complexes have dual opportunities to act as both cellular imaging and therapeutic agents. In related work, attachment of coumarin fluorophores to the NHC ligand framework of a series of Au(I) complexes showed TrxR inhibition, as well as nuclear compartment targeting studied by CFM.[88]

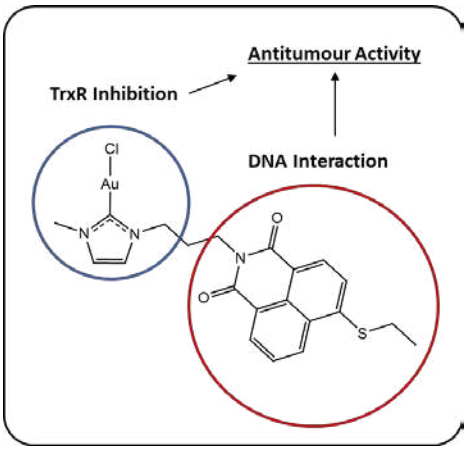

Figure 2.8: Example of Au(I)-NHC-naphthalimide complex showing antitumour activity[89]

Naphthalimide moieties have also been incorporated into Au(I)-NHC complexes to add an element of DNA binding, as they are well known to intercalate (Figure 2.8).[89] In this case, cytotoxic activity in MCF-7 cells was observed, as well as strong effects on cell metabolism, including respiration, cell independence and extracellular acidification. It is worth noting that the photophysical properties include λ_{max} = 252 and 345 nm in water

(235 and 336 in DCM) from UV-vis measurements, and luminescence investigations found λ_{em} = 395 or 450 (365 and 282 in DCM). In addition, effective inhibition of TrxR was confirmed as the most probable factor for cytotoxicity. The addition of the Au(I)-NHC partial structure resulted in enhanced interaction with DNA; therefore, it was concluded that the conjugation with naphthalimides may provide a method for design of bioorganic anti-cancer agents with multiple modes of action. In this vein, the combination of TrxR inhibition (redox-metabolism) with DNA intercalation (DNA-metabolism) is of particular interest as both mechanisms are associated with cancer research but are not directly linked to one another. In broader terms, this research was extremely important due to the ability of naphthalimide groups to act as active drugs in their own right. The addition of an organometallic Au(I)-NHC, whose chemical biology has been studied intensively, could allow scientists to modify the properties of existing bioactive agents or work towards drug targeting.

2.2 Aims

Gold-based compounds have been successfully utilised for medicinal purposes.[30–32] Most commonly, gold has been applied for the treatment of autoimmune conditions such as rheumatoid arthritis. However gold has also been utilised for anti-cancer applications.[33,34] A detailed understanding of the mechanisms of biological action informs the rational design of new therapeutics, but unravelling the biological action of such species is challenging.[36,37] One such technique involves the functionalisation of Au(I) complexes with fluorescent labels compatible with confocal fluorescence microscopy.

This project aimed to develop the synthetic protocol of a range of NHC-functionalised naphthalimide ligands that are suitable for coordination to Au(I). Once synthesised, all ligands and complexes would be spectroscopically and analytically characterised. It was an aim to investigate the species in terms of their biocompatibility and cytotoxicity against MCF-7 cells. It was thought that the tunable nature of the naphthalimide moiety would give rise to excellent control over the physical and photophysical properties of the final compounds. Therefore, the broad aim was to develop a range of imaging agents with potential therapeutic action.

2.3 Results and Discussion

2.3.1 Synthesis of Ligands and Complexes

The ligands were synthesised in three steps from commercially available 4-chloro-naphthalic anhydride (Scheme 2.3).[90] Firstly, the R1 group, comprising ethoxyethanol, propyl, benzyl, octyl, methoxyethyl or glycine ethyl ester was added at the diimide position to give **Cl$^{1-6}$** respectively. In this step, ethanol was used as a solvent and the reagents were heated at reflux under nitrogen for 24 hours. In the case of **Cl^{6}**, the amine was in the form of a hydrochloride salt; hence an excess of triethylamine was added in this reaction step.

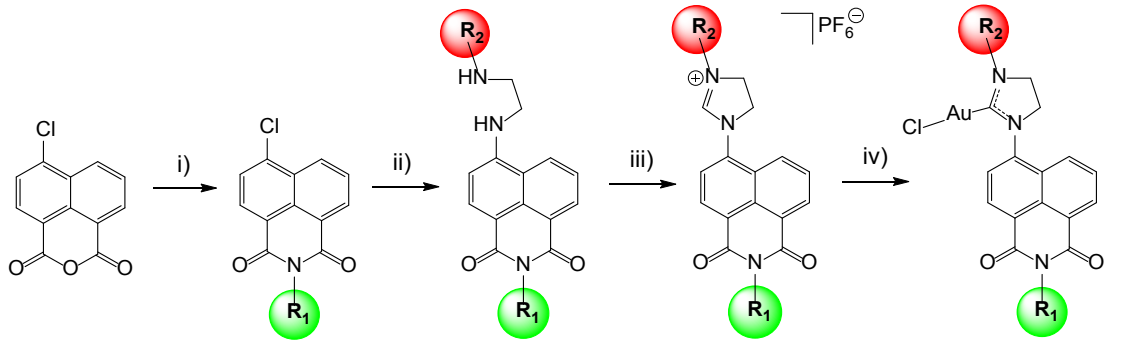

Cl^{1} - R1 = $(CH_2)_2O(CH_2)_2OH$
Cl^{2} - R1 = $Bn(CH_2)_2CH_3$
Cl^{3} - R1 = $(CH_2)_7CH_3$
Cl^{4} - R1 = $(CH_2)_2OCH_3$
Cl^{5} - R1 = $CH_2CHOOCH_2CH_3$
Cl^{6} - R1 = $CH_2CHOOCH_2CH_3$

L^{1} - R1 = $(CH_2)_2O(CH_2)_2OH$; R2 = Et
L^{2} - R1 = $(CH_2)_2O(CH_2)_2OH$; R2 = Ph
L^{3} - R1 = $(CH_2)_2CH_3$; R2 = Et
L^{4} - R1 = $(CH_2)_2CH_3$; R2 = Ph
L^{5} - R1 = Bn; R2 = Et
L^{6} - R1 = Bn; R2 = Ph

L^{7} - R1 = $(CH_2)_7CH_3$; R2 = Et
L^{8} - R1 = $(CH_2)_7CH_3$; R2 = Ph
L^{9} - R1 = $(CH_2)_2OCH_3$; R2 = Ph
L^{10} - R1 = $CH_2CHOOCH_2CH_3$; R2 = Ph

Scheme 2.3: Synthesis of ligands and complexes. i) R_1-NH_2, EtOH, reflux, ii) R_2-$NHCH_2CH_2NH_2$, DMSO, 100 °C, iii) NH_4PF_6, $HC(OEt)_3$, 100 °C and iv) [AuCl(tht)], CH_3OH, reflux

Secondly, **Cl$^{1-6}$** were then reacted with either N-ethylethylenediamine or N-phenylethylenediamine in DMSO to give the proligands **Pro$^{1-10}$**. In this step, R2 (ethyl or phenyl) was introduced *via* an S_NAr mechanism.[91] During this step, any unreacted amines were washed away with water. In the case where R2 is an ethyl substituent, it is noteworthy that preferential reaction at the less hindered primary amine was observed in all but one case (see Section 2.3.2), to give the desired products in good yields.

Subsequent ring closure using triethylorthoformate (both as reagent and solvent) in the presence of ammonium hexafluorophosphate yielded the cationic dihydroimidazolium based ligands $\mathbf{L^{1\text{-}10}}$ as their hexafluorophosphate salts, which were all shown to be soluble in acetone. During this step excess triethylorthoformate, as well as any soluble intermediates, were removed using diethyl ether and subsequent drying *in vacuo*. It is worth noting that during the course of this work, a literature report showed that imidazole can react with a 4-bromo-1,8-naphthalimide derivative to give an unsaturated system that can subsequently act as an NHC donor to Ir(III).[92]

The corresponding gold complexes were prepared using [AuCl(tht)] (tht = tetrahydrothiophene) as the Au(I) source and reacting with the dihydroimidazolium ligands in methanol, in the presence of a base, potassium *tert*-butoxide. Due to the light sensitivity of Au(I) compounds, tin foil was used to eliminate any light during the reaction. Intermediates and/or side products were removed by precipitation with the minimum of dichloromethane and diethyl ether.

2.3.2 Further Attempted Syntheses

An example was observed where preferential reaction at the less hindered amine to form the proligand did not occur. Instead, a mixture of products was formed upon the attempted S_NAr addition of *N*-ethylethylenediamine, where R1 was a glycine ethyl ester. Despite a number of repeated attempts, the mixture was consistently observed and was attributed to two isomeric forms of the product, shown in Figure 2.9.

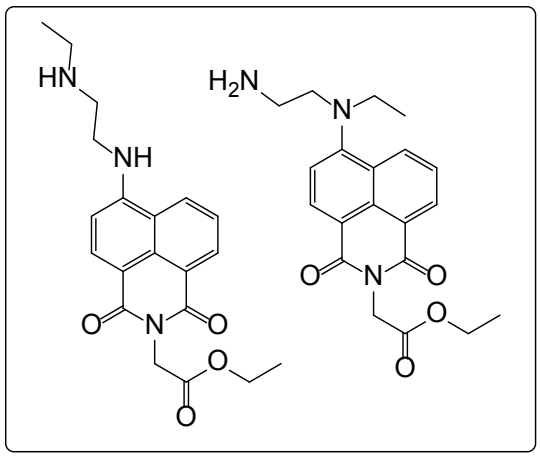

Figure 2.9:Mixture of products formed upon attempted S_NAr

This was confirmed by the ^{1}H NMR spectrum, which showed multiple additional peaks in the aromatic region, as well as two singlets corresponding to the protons adjacent to the imine nitrogen in glycine ethyl ester (Figure 2.10). Uniquely, this amine reactivity was only observed for the ethyl ester protected glycine ligand variant.

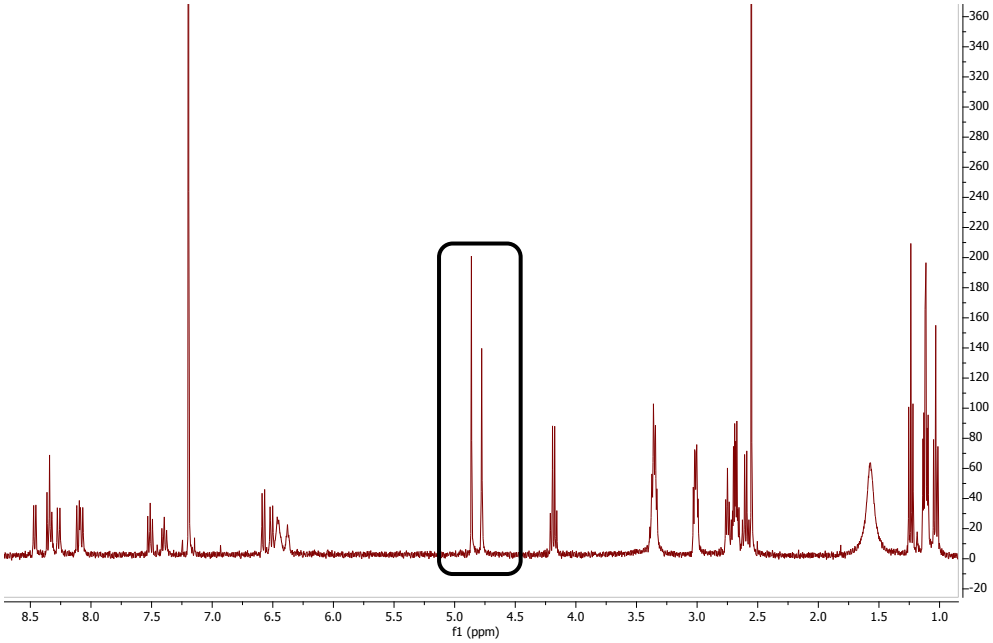

Figure 2.10: ^{1}H NMR spectrum for product mixture shown in Figure 2.9

Using ethylethylene diamine as a reagent for the second step in Scheme 2.3 was also unsuccessful when R1 was a methoxyethyl moiety. In this case, the spectroscopic characterisation, including ^{1}H NMR and mass spectrometry, was unclear and inconclusive. In addition, [AuCl(**L^{5}**)] could not be synthesised in sufficient quantities to allow unequivocal characterisation, despite several repeated attempts. It is currently unclear why this was the case and warrants further investigation.

2.3.3 Spectroscopic Characterisation

Pro$^{1\text{-}10}$ showed good solubility in a range of organic solvents, allowing characterisation in the solution state *via* ^{1}H NMR spectroscopy. In all cases, ^{1}H NMR spectra for **Pro$^{1\text{-}10}$** provided confirmation of substitution at the 4-position of the naphthalimide ring. In most cases a characteristic N*H* resonance was noted at *ca*. 6-6.5 ppm as a broad triplet,

which was assigned to the naphthalimide bound amine. For example, the ^{1}H NMR spectra of **Pro^{3}** is shown in Figure 2.11. In addition to the N*H* peak, two upfield triplets are observed associated with the presence of two terminal CH_3 groups.

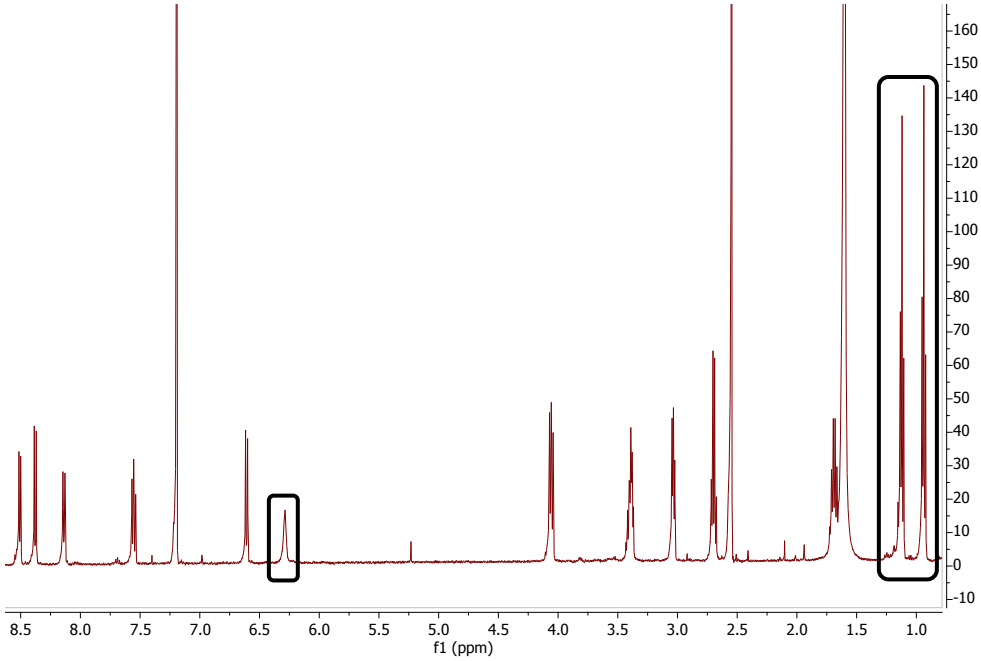

Figure 2.11: ^{1}H NMR spectrum of Pro^{3}

Upon cyclisation to form **L$^{1\text{-}10}$**, the corresponding ^{1}H NMR spectra show subtle changes in the chemical shifts of the dihydroimidazolium ethyl backbone; in most cases these were observed as two triplets at *ca*. 4.5-4.0 ppm. The N*H* resonance at 6.0-6.5 ppm had also disappeared, consistent with cyclisation. In addition, formation of **L$^{1\text{-}10}$** gives rise to an additional downfield singlet at 9-9.5 ppm corresponding to the carbene C*H* (Figure 2.12), consistent with literature examples.[93] Due to their charged nature as a PF_6^- salt, **L$^{1\text{-}10}$** all showed good solubility in acetone, allowing characterization in the solution state using ^{1}H, ^{13}C{^{1}H}, HRMS, UV-vis and luminescence spectroscopy, as well as IR in the solid state. IR spectra of **L$^{1\text{-}10}$** showed ν(C=O) at *ca*. 1650 cm^{-1} and confirmed absorbances consistent with the formation of the salts with $\nu(PF_6^-)$ *ca*. 830 cm^{-1}.

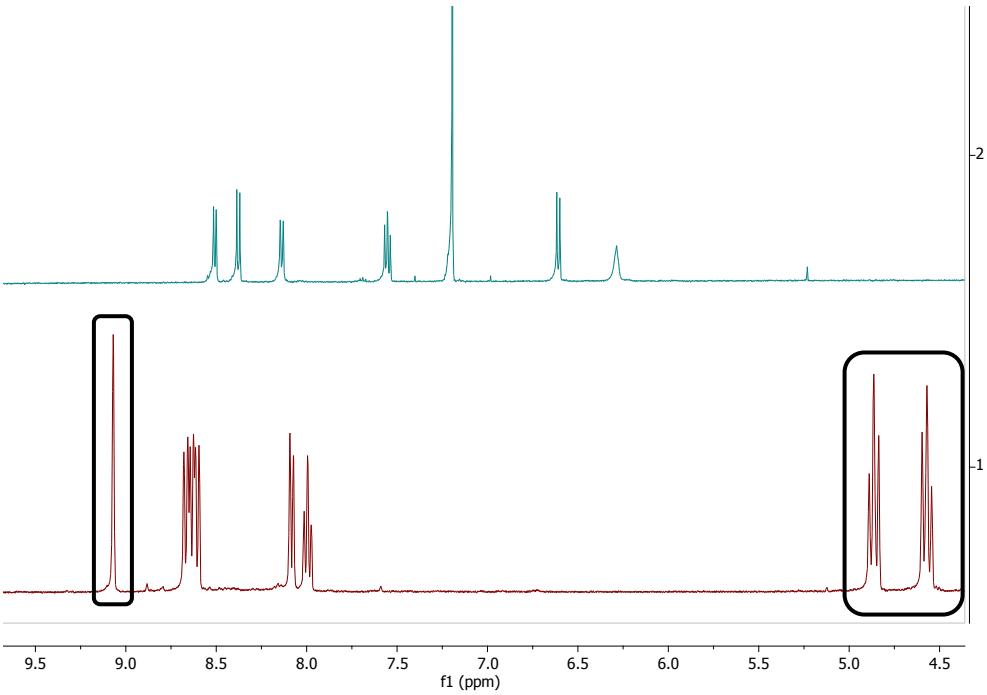

Figure 2.12: ^{1}H NMR spectrum comparison of Pro^{3} (top) and L^{3} (bottom)

In all cases, the proposed molecular formula for the target ligands was supported by HMRS (ES^{+}), each showing the expected $[M]^{+}$ peak, as well as $[M + NH_3]^{+}$ in the case of **L^{10}** (Figure 2.13).

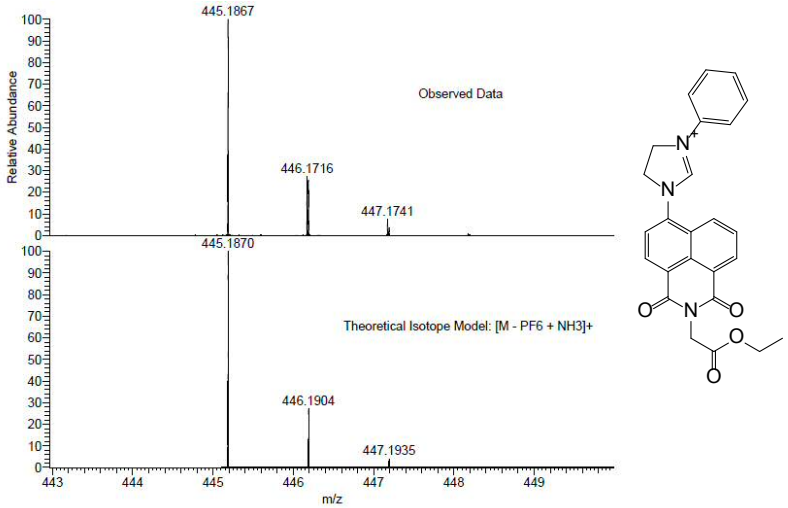

Figure 2.13: HRMS of L^{10}

The gold complexes were also characterised by a range of spectroscopic and analytical techniques. ^{1}H NMR spectra provided evidence of coordination to Au(I) through changes in the resonances associated with the coordinated NHC unit. For example, in [AuCl(**L^{1}**)] the ethyl backbone of the NHC ligand resolves to give two doublet of doublets between

3.99-3.86 ppm. This implies a greater rigidity in the NHC backbone and represents an upfield shift relative to **L^{1}**. In addition, the ^{1}H NMR spectrum of each of the complexes displays the removal of the singlet at 9-9.5 ppm associated with the loss of the C*H* proton upon coordination to Au(I).

In all cases, $^{13}C\{^{1}H\}$ NMR spectra revealed resonances that correlated with the presence of the different R1 and R2 groups. In addition, two carbonyl resonances (consistent with the unsymmetrical nature of the naphthalimide unit) *ca.* 162-165 ppm were observed together with a further downfield signal *ca*. 192-195 ppm. This latter observation was assigned to the coordinated carbene carbon and is thus diagnostic of the formation of the complex and consistent with the proposed coordination mode of these ligands with Au(I). An example of these observations is provided by [AuCl(**L^{7}**)], shown in Figure 2.14.

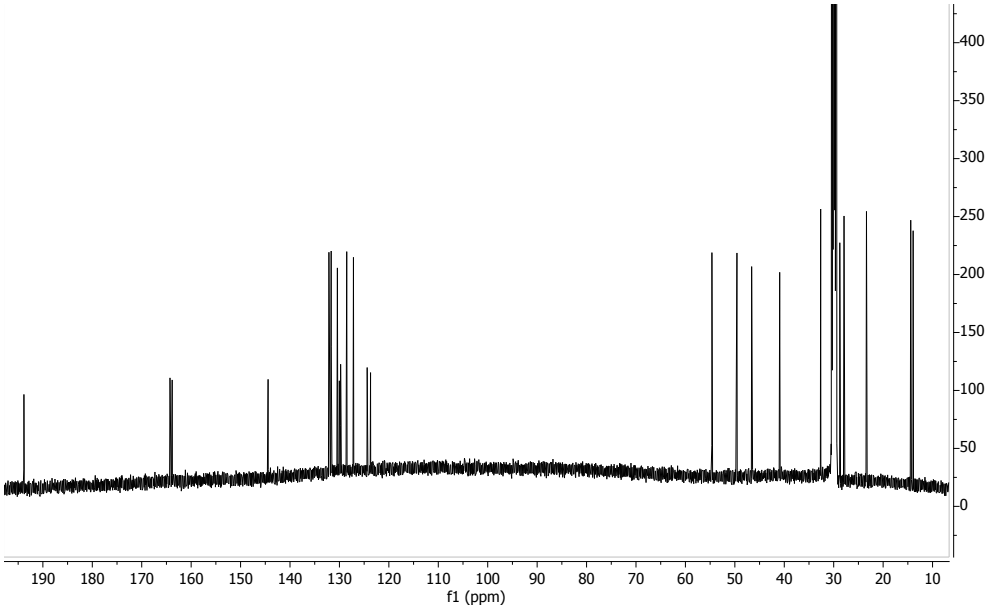

Figure 2.14: $^{13}C\{^{1}H\}$ NMR of [AuCl(L^{7})]

HRMS data were obtained for the neutral gold complexes, often correlating with the formation of a cationic complex fragment through loss of a chloride ligand, or addition of a cationic moiety such as Na^{+} or NH_4^{+}. All spectra were consistent with retention of the Au-NHC unit. Similarly to the ligands, IR spectra were primarily obtained to confirm the presence of the ligand *via* ν(C=O) *ca*. 1600-1650 cm^{-1}.

2.3.4 X-ray Crystallographic Structural Studies

In addition to solution state characterisation, confirmation of the solid-state structures was provided through X-ray crystallographic studies on one ligand and one complex, $\mathbf{L^3}$ and [AuCl($\mathbf{L^3}$)]. Crystals suitable for X-ray diffraction were obtained by room temperature vapour diffusion of diethyl ether into concentrated acetone ($\mathbf{L^3}$) or acetonitrile ([AuCl($\mathbf{L^3}$)]) solutions. Data collection, refinement and structure solution was conducted by Dr Peter Horton at the UK National Crystallography Service, Southampton. Data collection parameters are shown in Table 2.1, together with supporting bond length and bond angle data in Table 2.2. The resultant structures of $\mathbf{L^3}$ and [AuCl($\mathbf{L^3}$)] are shown in Figure 2.15.

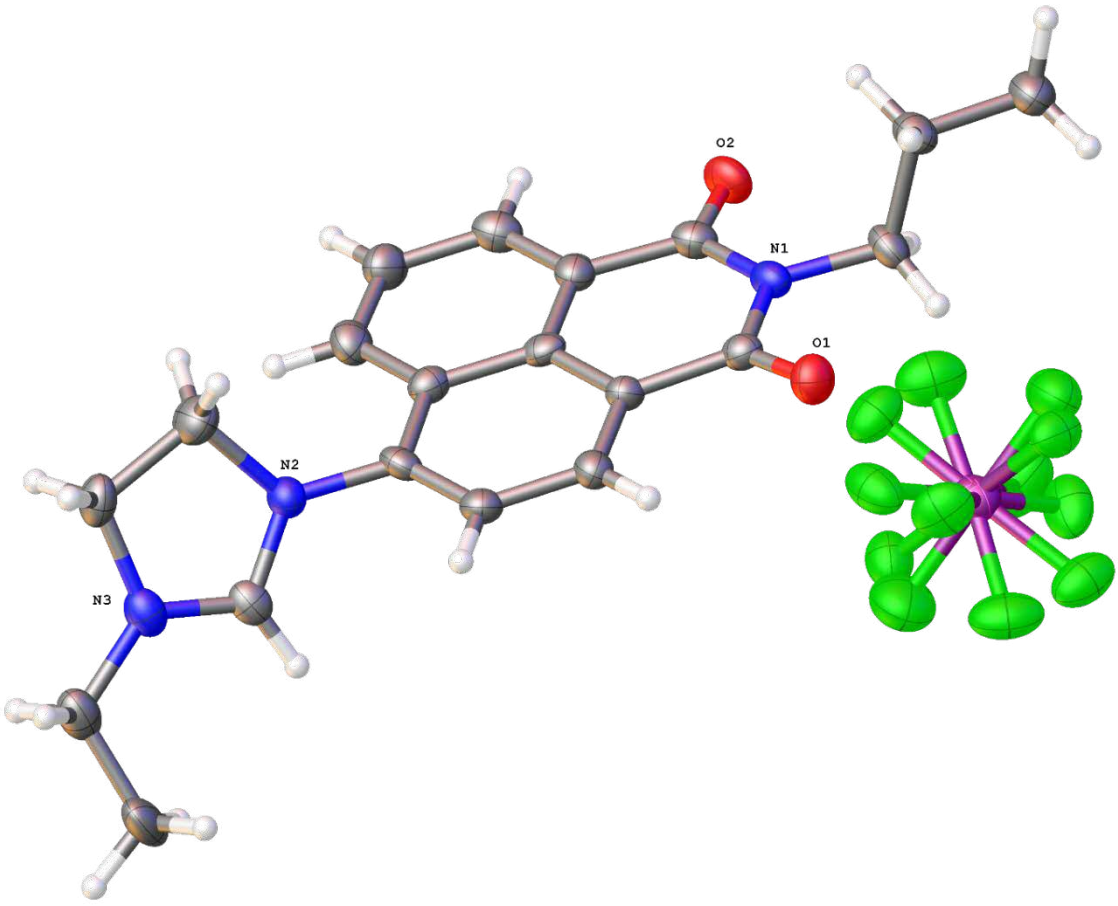

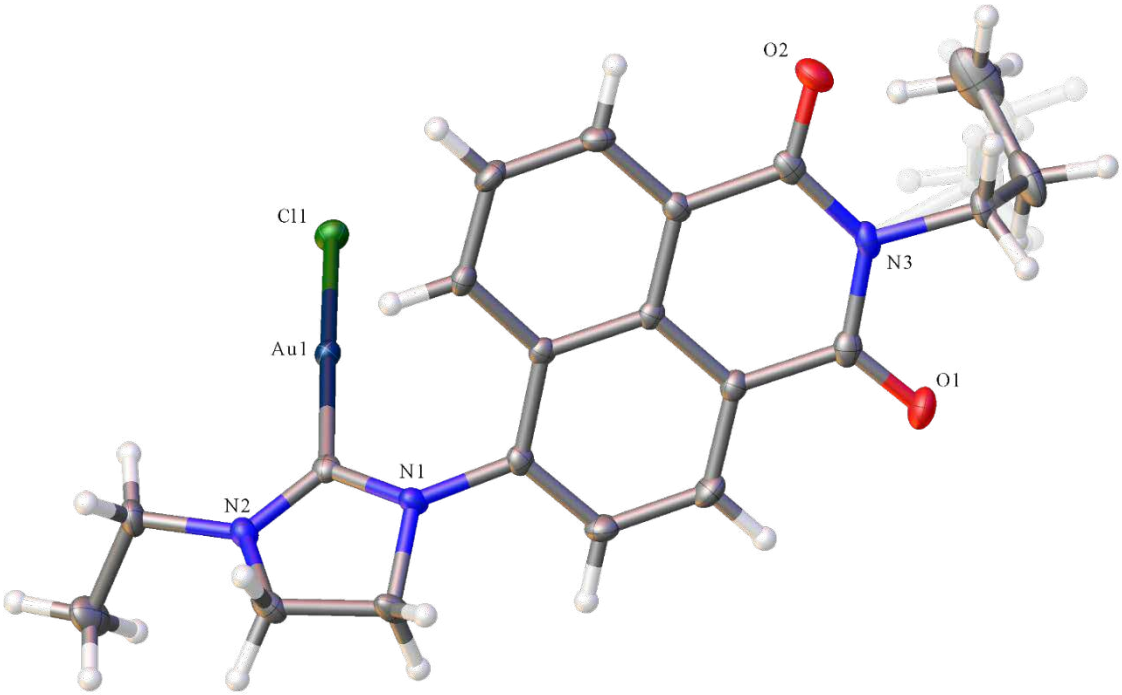

Figure 2.15: Structural representation of L^3 (top) and [AuCl(L^3)] (bottom)

Sample	**L³**	Sample	[AuCl(L³)]
Empirical formula	$C_{20}H_{22}F_6N_3O_2P$	Formula	$C_{20}H_{21}AuClN_3O_2$
Formula weight	481.37	$D_{calc.}$/ g cm^{-3}	1.924
Temperature	100(2) K	μ/mm^{-1}	7.659
Wavelength	0.71073 Å	Formula Weight	567.81
Crystal system	Monoclinic	Colour	light yellow
Space group	$P2_1/n$	Shape	plate
Unit cell dimensions	a = 15.6423(13) Å	Size/mm^3	0.150×0.080×0.020
	b = 8.2135(6) Å	T/K	100(2)
	c = 16.7365(13) Å α = 90° β = 104.089(9)° γ = 90°	Crystal System	triclinic
Volume	2085.6(3) Å^3	Space Group	P-1
Z	4	a/Å	9.1088(4)
Density (calculated)	1.533 Mg / m^3	b/Å	10.0395(5)
Absorption coefficient	0.208 mm^{-1}	c/Å	12.2613(5)
F(000)	992	α/°	67.610(4)
Crystal	Needle; Orange	β/°	72.865(4)
Crystal size	0.110 × 0.020 × 0.010 mm^3	γ/°	76.132(4)
θ range for data collection	2.509 – 25.025°	V/Å^3	980.36(8)
Index ranges	$-18 \le h \le 18$, $-9 \le k \le 9$, $-19 \le l \le 19$	Z	2
Reflections collected	16606	Z'	1
Independent reflections	3671 [R_{int} = 0.0750]	Wavelength/Å	0.71075
Completeness to θ = 25.025°	99.9 %	Radiation type	MoK
Absorption correction	Semi–empirical from equivalents	Θ_{min}/°	2.217
Max. and min. transmission	1.00000 and 0.75532	Θ_{max}/°	27.521
Refinement method	Full-matrix least-squares on F^2	Measured Refl.	4483
Data / restraints / parameters	3671 / 111 / 355	Independent Refl.	4483
Goodness-of-fit on F^2	1.112	Reflections Used	4327

Final *R* indices [$F^2 > 2\sigma(F^2)$]	*R1* = 0.0931, *wR2* = 0.2376	R_{int}	.
R indices (all data)	*R1* = 0.1327, *wR2* = 0.2586	Parameters	247
Largest diff. peak and hole	0.995 and −0.350 e Å^{-3}	Restraints	222
		Largest Peak	4.851
		Deepest Hole	-3.221
		GooF	1.196
		wR_2 (all data)	0.1323
		wR_2	0.1315
		R_1 (all data)	0.0494
		R_1	0.0481

Table 2.1: Data collection parameters for the X-ray structures

These structures revealed the anticipated formulations for the ligand and complex, and demonstrate retention of the NHC ethyl backbone, as well as the addition of a Au-Cl unit. As expected, the C-N bond lengths in the NHC are extended upon coordination to Au(I) (Table 2.2). In addition, C-N bond lengths in the NHC unit are shorter than those in the naphthalimide unit, and both are comparable to previous literature examples.[10]

Ligand Bond	*Length (Å)*	Complex Bond	*Length (Å)*
N3-C16	1.295(7)	N2-C1	1.366(11)
N2-C16	1.322(7)	N1-C1	1.331(11)
C16-H16	0.9500	C1-Au	1.983 (8)
		Au-Cl	2.299(2)

Table 2.2: Key bond lengths for L[3]

2.3.5 Photophysical Properties

The photophysical properties of **L$^{1\text{-}10}$** and **[AuCl(L$^{1\text{-}10}$)]** were investigated *via* UV-vis., steady state luminescence, luminescence lifetimes and quantum yields, measured in aerated solutions of acetone in each case. The solution state absorption properties of the ligands are shown in Figure 2.16. The photophysical properties are summarised in Table 2.3.

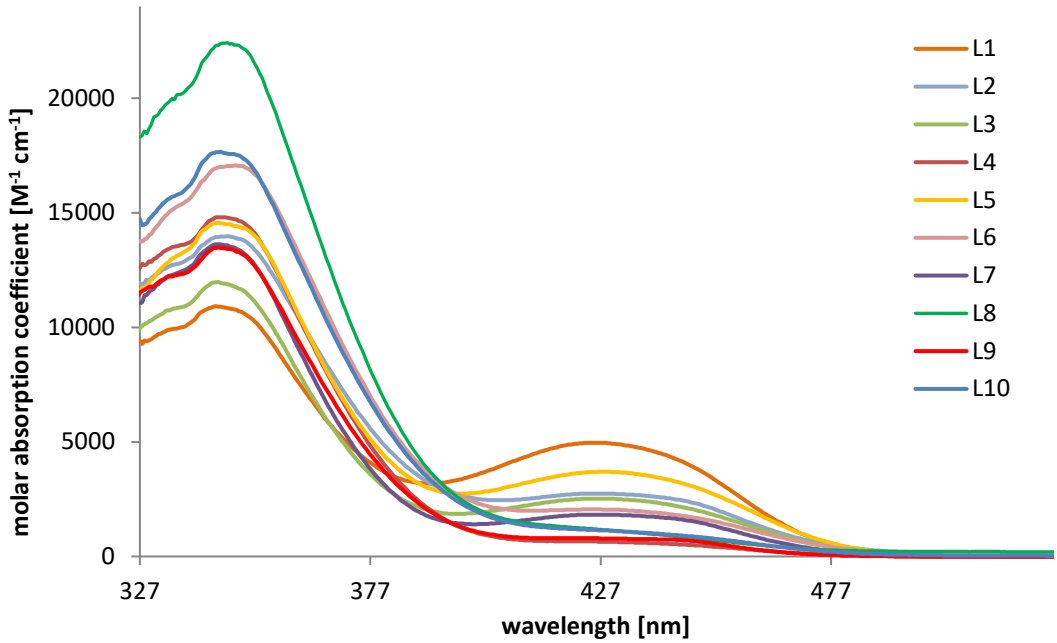

Figure 2.16: A comparison of the absorption spectra for the ligands

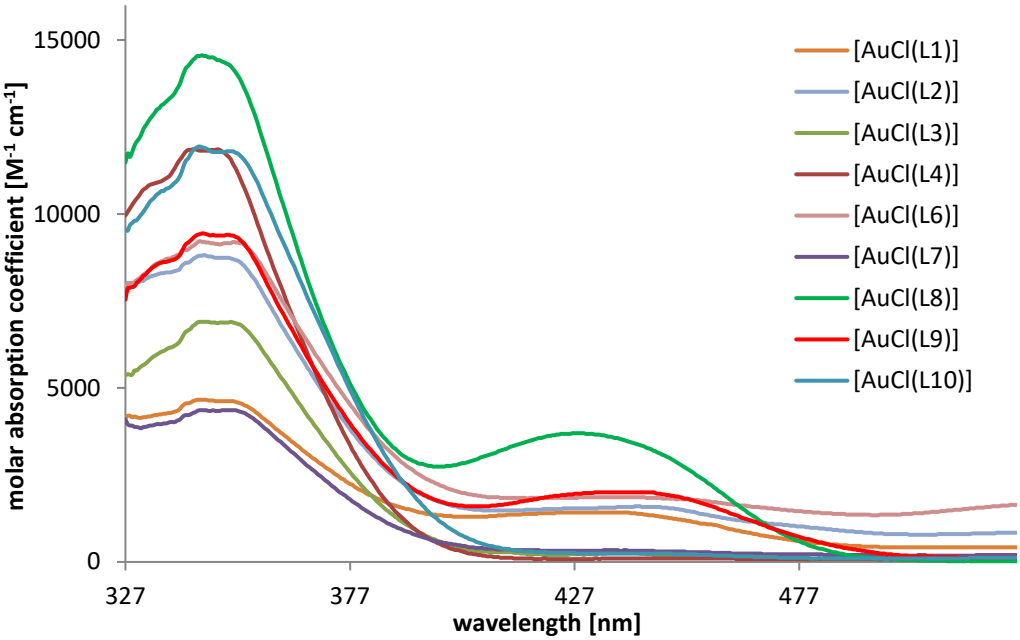

Figure 2.17: UV-vis spectra of Au(I) complexes

Compound	λ_{abs}[a] / nm	λ_{em}[b] / nm	τ_{obs} / ns	QY
L[1]	344, 426	504	7.3 (80%), 2.4 (20%)	4%
L[2]	342, 429	507	8.7	28%
L[3]	344, 426	502	9.1	4%
L[4]	344, 351, 432	503	7.2	4%
L[5]	344, 428	502	8.4	31%
L[6]	343, 435	504	8.8	17%
L[7]	344, 427	501	4.7	5%
L[8]	345, 433	503	9.0 (92%), 2.6 (8%)	12%
L[9]	344, 423	502	8.4	4%
L[10]	345, 432	505	7.8 (91%), 4.0 (9%)	3%
[AuCl(**L[1]**)]	344, 351, 436	507	7.8 (45%), 0.9 (55%)	2%
[AuCl(**L[2]**)]	349, 433	487	7.2 (78%), 2.8 (22%)	9%
[AuCl(**L[3]**)]	345, 351, 439	500	1.1 (76%), 0.2 (24%)	1%
[AuCl(**L[4]**)]	354, 352	504	6.9 (33%), 0.06 (67%)	1%
[AuCl(**L[6]**)]	343, 436	503	8.3 (82%), 2.6 (18%)	2%
[AuCl(**L[7]**)]	345, 351, 439	499	4.3 (9%), 1.0 (91%)	1%
[AuCl(**L[8]**)]	344, 351, 441	504	0.4 (21%), 0.01 (79%)	11%
[AuCl(**L[9]**)]	344, 350, 443	508	7.8 (89%), 0.6 (11%)	1%
[AuCl(**L[10]**)]	344, 351, 444	500	7.3 (68%), 0.1 (32%	1%

Table 2.3:Photophysical properties of ligands and complexes; [a] measurements obtained in aerated 10^{-5} M acetone solutions; [b] λ_{ex} = 405 nm; [c] $[Ru(bpy)_3](PF_6)_2$ as reference of 0.016 in aerated MeCN

The absorption spectra of the ligands were characterised by shorter wavelength peaks (<300 nm) which are assigned to $\pi \rightarrow \pi^*$ transitions associated with the naphthalimide chromophore and phenyl substituents. Between 300-450 nm the spectra also revealed weaker features which are assigned to a combination of different $n \rightarrow \pi^*$ transitions including an intramolecular charge transfer (ICT) that arises from the N donor to imide transition. It is notable that the wavelength position of the ICT band appears relatively insensitive, firstly to the nature of the imide (R1) substituent, and secondly, the R2 group on the dihydroimidazolium group. In the cases of **L[3]**, **L[4]**, **L[7]** and **L[10]**, the ICT band is hypochromically shifted and almost diminished upon coordination to form the Au(I) complexes. A clear example of this is shown in Figure 2.18, which compares **L[4]** with [AuCl(**L[4]**)]. When compared to other 4-amino-substituted 1,8-naphthalimides,[94,95] the intensity of the ICT bands in these ligands is relatively diminished and hypsochromically shifted. This is attributed to the cationic nature of the dihydroimidazolium moiety, which may modulate the overall donor ability of the nitrogen atom at the 4-position of the naphthalimide.

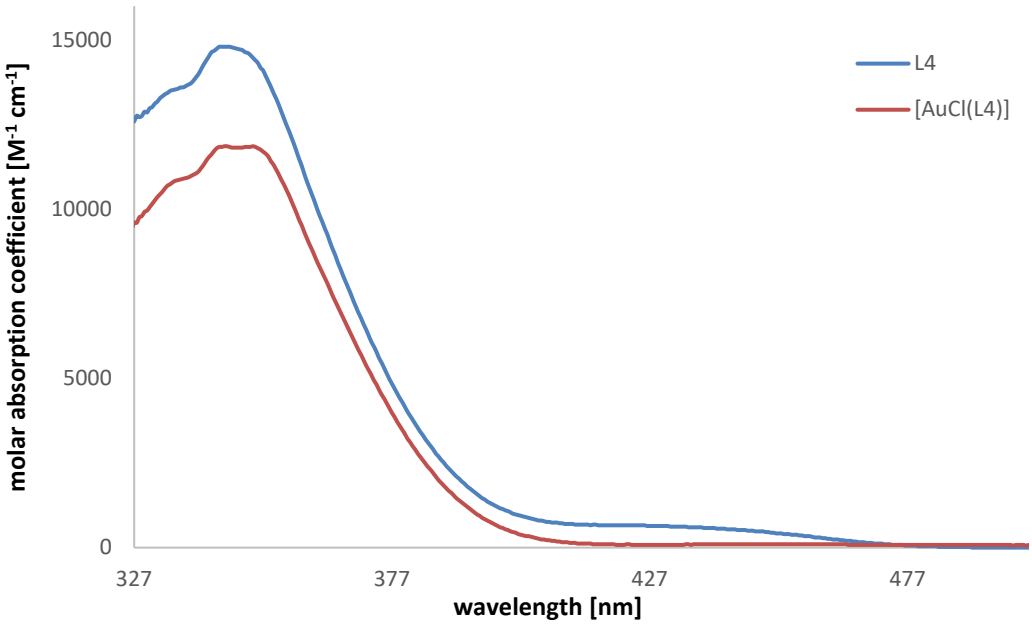

Figure 2.18: Comparative absorption profiles of L^4 and [AuCl(L^4)]

The absorption spectra of the complexes were dominated by the ligand-centred transitions highlighted above, with minor perturbations to the $\pi \rightarrow \pi^*$ region of the spectra due to the coordination of the AuCl unit. However, in the cases of [AuCl(**L**^{3})], [AuCl(**L**^{4})], [AuCl(**L**^{7})] and [AuCl(**L**^{10})], the ICT band is hypochromically shifted, as previously mentioned.

Luminescence spectra were also obtained on all ligands and complexes using aerated acetone solutions (Table 2.3). Using an excitation wavelength of 405 nm the ligands revealed a broad emission peak ranging from 501 to 507 nm, as well as a shoulder at 420-470 nm (Figure 2.19), which is in most cases associated with the presence of a phenyl substituent at R2. A wavelength of 405 nm was chosen due to its compatibility with both microscopy instruments and the ICT emitting state. Upon coordination, it can be seen that the intensity of the lower wavelength peak has increased in the majority of cases (Figure 2.20). This is in agreement with the observed lifetime values, which suggest two emitting states due to their data best fitting a double exponential algorithm for each of the complexes. In the case of [AuCl(**L**^{7})], the aforementioned peak is of a higher intensity than that at 499 nm. In addition, the broad emission peak is relatively unaffected by coordination, and ranges from 499 to 508 nm for the complexes, in

agreement with previous reports.[82] However, in the case of [AuCl(**L²**)], the peak is hypsochromically shifted upon coordination to 487 nm.

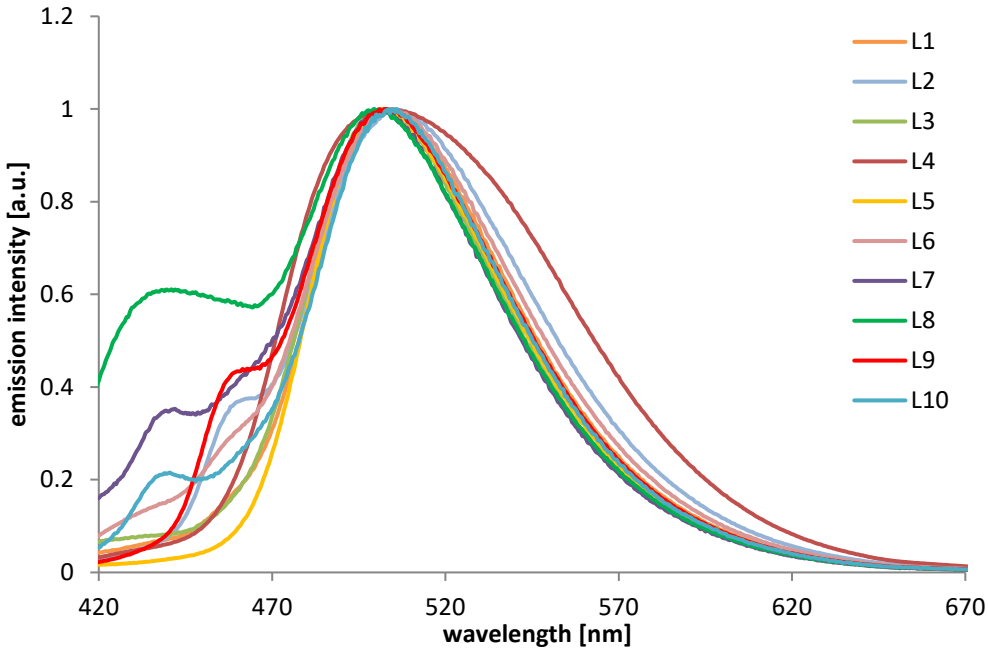

Figure 2.19: Emission spectra of the ligands

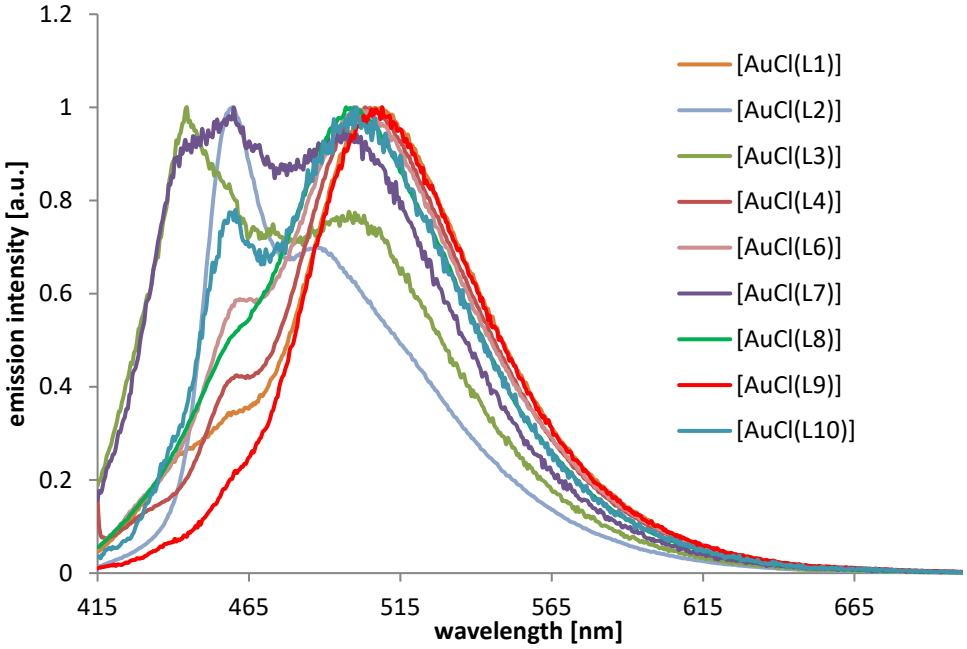

Figure 2.20: Emission spectra of the complexes

The aerated, solution state quantum yields were also obtained together with the luminescence lifetimes (Table 2.3). Luminescence lifetimes ranged from 4.7 to 9.0 ns for the ligands, and 0.1 to 8.3 ns for the complexes; all are indicative of fluorescence. The

lifetime data for the ligands best fit a single exponential decay, thus indicating single component emission, except for in the cases of **L^{1}**, **L^{8}** and **L^{10}**. As previously mentioned, each of the complexes exhibits a dual component emission. Quantum yields ranged from 4 to 31 % for the ligands and 1 to 11 % for the complexes, where both are generally consistent with previous examples.[6,39]

2.3.6 Cytotoxicity studies

Cytotoxicity assessments, using the MTT assay, were obtained for both series of ligands and complexes (Table 2.4). Data were recorded for four cancer cell lines: LOVO, A549, PC3 and MCF7, the latter for correlation with imaging studies.

Compound	LOVO	A549	PC3	MCF7
L^{1}	30.07(3.19)	33.62(5.09)	56.40(3.08)	68.35(3.95)
L^{2}	73.36(2.36)	>100	98.1(3.91)	66.83(2.85)
L^{3}	42.75(8.66)	56.83(4.06)	71.27(2.89)	61.21(3.02)
L^{4}	51.81(5.34)	75.68(1.10)	72.82(3.03)	56.38(2.84)
L^{5}	7.27(1.19)	47.10(0.55)	8.58(0.03)	7.12(0.36)
L^{6}	>100	>100	>100	>100
L^{7}	5.22(2.49)	53.95(1.41)	42.00(5.69)	9.98(4.77)
L^{8}	>100	>100	>100	33.23(5.84)
L^{9}	>100	91.02(3.70)	77.42(3.39)	58.86(6.42)
L^{10}	>100	>100	>100	>100
[AuCl(**L^{1}**)]	68.94(2.29)	>100	>100	84.21(11.38)
[AuCl(**L^{2}**)]	91.64(3.20)	>100	>100	62.88(5.58)
[AuCl(**L^{3}**)]	>100	>100	>100	48.58(10.58)
[AuCl(**L^{4}**)]	41.54(2.88)	>100	>100	27.79(11.89)
[AuCl(**L^{6}**)]	49.10(7.97)	>100	>100	46.21(13.01)
[AuCl(**L^{7}**)]	50.92(6.20)	>100	46.63(0.71)	41.75(9.34)
[AuCl(**L^{8}**)]	40.99(11.08)	>100	>100	4.82(0.77)
[AuCl(**L^{9}**)]	17.08(6.58)	>100	>100	76.99(11.58)
[AuCl(**L^{10}**)]	52.14(1.81)	>100	>100	83.94(5.88)

Table 2.4: Cytotoxicity data for ligands and complexes with a variety of cell lines

For the ligands, **L^{6}** and **L^{10}** were the least toxic with IC50 values >100 μM for each cell type. In contrast, closely related **L^{5}** was the most toxic with strong activity against LOVO, PC3 and MCF7s. From the pairs of ligands, it appeared that the ethyl variants (R1 = Et) were generally more toxic than the phenyl analogues. Most of the complexes were

inactive against A549 and PC3 cell lines and the data revealed a general trend where the majority of complexes were less toxic than their corresponding ligands for the LOVO, A549 and PC3 cell lines. An example of an exception to this observation is [AuCl(**L^{9}**)], which showed significant potency against the LOVO cell line (IC50 = 17.08 μM). This general trend was not observed for the MCF7 cell line, where cytotoxicity was enhanced in comparison to the ligand in the cases of [AuCl(**L^{2}**)], [AuCl(**L^{3}**)], [AuCl(**L^{4}**)], [AuCl(**L^{6}**)], [AuCl(**L^{8}**)] and [AuCl(**L^{10}**)]. The most noteworthy example of this observation was that [AuCl(**L^{8}**)], which showed significant and selective potency against MCF7 (IC50 = 4.82 μM) which was comparable with cisplatin.[5] In addition, within the series of complexes it was generally the phenyl variants (R1 = Ph) that demonstrated the greater antiproliferative activity for a given cell line.

The MCF7 data were of most interest to us as this was the cell line to be used in the confocal fluorescence microscopy studies. One ligand/complex pairing was selected to allow comparison of their imaging potential. Thus, **L^{3}** and [AuCl(**L^{3}**)] were chosen for imaging studies as they possessed intermediate lipophilicity and both showed only moderate toxicity to MCF7s.

2.3.7 Bioimaging Studies

Confocal fluorescence microscopy was performed using MCF7 cells. MCF-7 cells were grown on circular glass coverslips for 5-7 days in RPMI-1640 medium, supplemented with 5% foetal calf serum (heat inactivated) and 100 U/ml penicillin/streptomycin solution, until around 70-90% confluent. For experiments, culture medium was replaced with 1 ml fresh RPMI-1640 and cells were incubated with the following concentrations of commercially-derived (all from Molecular Probes) or in-house fluorescent compounds: 200 nM TMRE (stains mitochondria), 1:1000 dilution of LipidTOX red (stains lipid droplets), 1:5000 dilution of LysoTracker red (stains lysosomes), 5 uM of the Golgi Apparatus Marker, 1 uM of ERTracker red (stains endoplasmic reticulum) and 100 ug/ml of **L^{3}** and [AuCl(**L^{3}**)]. All compounds were incubated for 30 minutes at 37 °C, then washed in warmed PBS before imaging. In all cases, an excitation wavelength of 405 nm was used together with dual detection wavelengths suitable for both the probe (**L^{3}** and [AuCl(**L^{3}**)]) and the co-localisation agents.

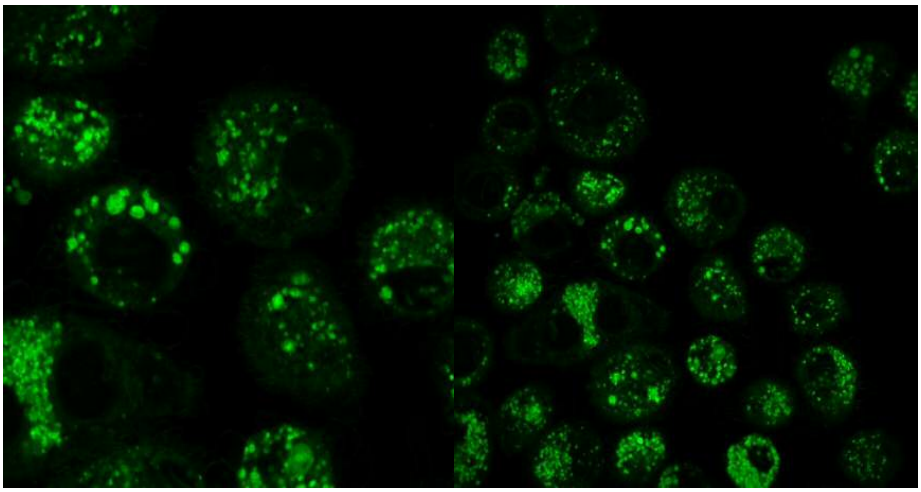

Figure 2.21: Preliminary CFM images of L^3 with MCF-7 cells

For **L^3** uptake into the cells was very fast and very bright images were obtained (Figure 2.21). For [AuCl(**L^3**)], the speed of uptake was similar and images were less bright, yet satisfactory. In both cases, preliminary studies found that there were many areas of the cell that appeared to be stained: mitochondria; nuclear membranes; Golgi apparatus; endoplasmic reticulum and lysosomes. Co-localisation was observed to some extent with LysoTracker Red. However none was observed for the mitochondria. At this stage, further studies with alternate concentrations were carried out due to the non-distinct nature of the localisation. It is thought that lysosomal staining might indicate that cells were incubated with too much of the probes.

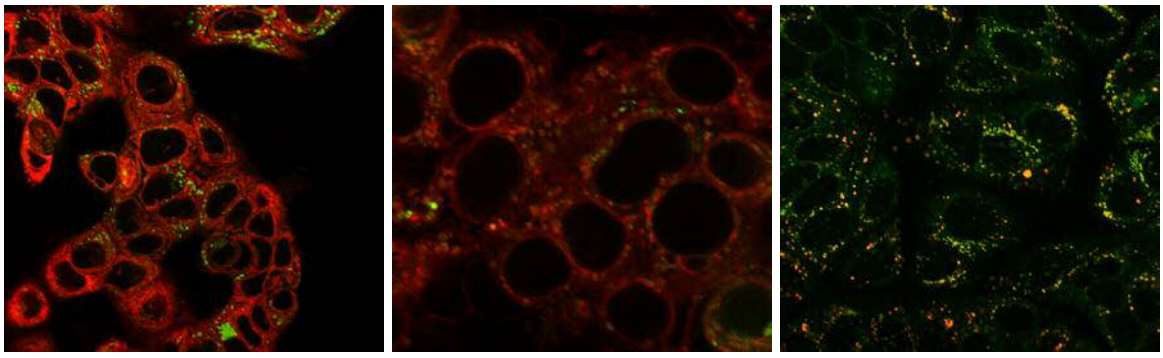

Figure 2.22: CFM images of L^3 with MCF-7 cells; representative images of colocalisation studies with (from left to right) an ER stain, Golgi stain and lysosomal stain

.

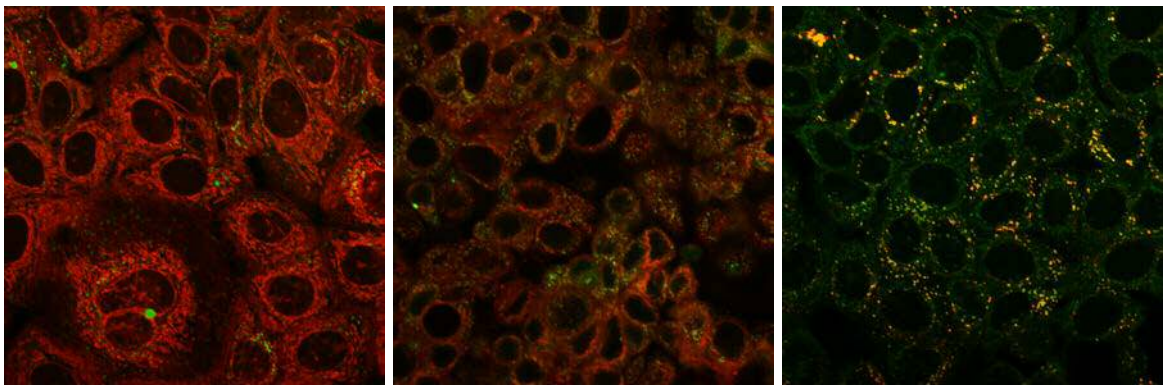

Figure 2.23:CFM images of [AuCl(L^3)] with MCF-7 cells; representative images of colocalisation studies with (from left to right) an ER stain, Golgi stain and lysosomal stain

In consecutive studies, more distinct localisation was observed for both the ligand and the complex at a 10 ng/ml concentration (1:10000 dilution when compared to initial studies). In this case, colocalisation with Lysotracker Red was exclusively confirmed, as can be seen in Figures 2.22 and 2.23. Lysosomes and their roles have been of interest in the context of cancer for decades.[96] For example, one literature example showed lysosomal localisation of acridine-based Au(I) compounds that were seen to be cytotoxic towards lung and pancreatic cancer cells.[82] In addition, studies have demonstrated that mammary gland cell death during involution (the natural degradation of mammary tissues after lactation ceases) involves lysosomal activity.[97,98] Involution is a commonly used model of breast tissue cell death, a large area of research in breast cancer studies. These studies highlight lysosomes as an important target for breast cancer therapies that could induce cell death. Overall, the imaging studies presented clear evidence of the biocompatible utility of **L^3** and [AuCl(**L^3**)] towards cell imaging using confocal fluorescence microscopy.

2.4 Conclusions

This chapter has described the synthetic development and spectroscopic analysis of a series of NHC-functionalised 1,8-naphthalimide fluorophores, generating ten new ligands that were successfully utilised for Au(I) coordination chemistry, with the exception of $\mathbf{L^5}$. Confirmation of the solid-state structures was provided through X-ray crystallographic studies on one ligand and one complex, $\mathbf{L^3}$ and [AuCl($\mathbf{L^3}$)], where an expected linear coordination mode was observed in the latter case. The optical properties of the fluorophores were dictated by ligand-centred transitions that provide visible absorption and emission characteristics, the latter associated with lifetimes up to *ca.* 9 ns and quantum yields between 1 and 31%. Cytotoxicity assessments revealed that all compounds were the most toxic to LOVO and MCF-7 cell lines, where the majority of cases for MCF-7 cells showed the complexes had enhanced cytotoxicity when compared to the corresponding ligands. A noteworthy example of this was for [AuCl($\mathbf{L^8}$)], whose IC_{50} value was comparable to that of cisplatin (IC_{50} = 4.8 and 5.3 μM, respectively). Cellular imaging studies were conducted on MCF-7 cells for one pair of fluorophores, $\mathbf{L^3}$ and [AuCl($\mathbf{L^3}$)]. Both showed good uptake and bright staining. However preliminary studies showed that localisation was not specific to a particular group of organelles. Upon a reduction in concentration of the ligand and complex, lysosomal colocalisation was confirmed in both cases *via* the use of LysoTracker Red. As lysosomes have been shown to be an important target for breast cancer therapies that could induce cell death, the observed colocalistion is of particular significance in cancer research.

The photophysical properties of 1,8-naphthalimides are further explored in Chapter 5, where they are designed for an electrochemical biosensing application.

2.5 Experimental

2.5.1 General Experimental Considerations

All reagents and solvents were commercially available and were used without further purification if not stated otherwise. Petroleum ether refers to the 40-60 °C fraction. For the measurement of ^{1}H and ^{13}C NMR spectra a Bruker Fourier^{300} (250, 300 MHz), 400 UltraShield^{TM} (400 MHz) or Ascend^{TM}500 (500 MHz) was used. The obtained chemical shifts δ are reported in ppm and are referenced to the residual solvent signal. Spin-spin coupling constants *J* are given in Hz.

Low-resolution mass spectra were obtained by the staff at Cardiff University. High-resolution mass spectra were carried out at the EPSRC National Mass Spectrometry Facility at Swansea University. High resolution mass spectral (HRMS) data were obtained on a Waters MALDI-TOF mx at Cardiff University or on a Thermo Scientific LTQ Orbitrap XL by the EPSRC UK National Mass Spectrometry Facility at Swansea University. IR spectra were obtained from a Shimadzu IR-Affinity-1S FTIR. UV-Vis studies were performed on a Jasco V-570 spectrophotometer as acetone solutions (2.5 or 5×10^{-5} M). Photophysical data were obtained on a JobinYvon–Horiba Fluorolog spectrometer fitted with a JY TBX picosecond photodetection module as acetone solutions. Emission spectra were uncorrected and excitation spectra were instrument corrected. The pulsed source was a Nano-LED configured for 459 nm output operating at 1 MHz. Luminescence lifetime profiles were obtained using the JobinYvon–Horiba FluoroHub single photon counting module and the data fits yielded the lifetime values using the provided DAS6 deconvolution software. Quantum yield measurements were obtained on aerated acetone solutions of the complexes using $[Ru(bpy)_3](PF_6)_2$ in aerated MeCN as a standard ($\Phi = 0.016$). [23]

2.5.2 X-ray Diffraction

For both samples, Single plate-shaped crystals were recrystallised from ether. A suitable crystal was selected and mounted on a MITIGEN holder in perfluoroether oil on a Rigaku FRE+ equipped with VHF Varimax confocal mirrors and an AFC12 goniometer and HyPix

6000 detector diffractometer. The crystal was kept at T = 100(2) K during data collection. Using **Olex2**,[99] the structure was solved with the **ShelXT**[100] structure solution program, using the Intrinsic Phasing solution method. The model was refined with version 2014/7 of **ShelXL**[101] using Least Squares minimisation. All non-hydrogen atoms were refined anisotropically. Hydrogen atom positions were calculated geometrically and refined using the riding model.

2.5.3 Ligand Synthesis

Ethoxyethanol

Synthesis of Cl[1 94]

4-chloro-1,8-naphthalic anhydride (2.5 g, 10.8 mmol) and 2-(2-aminoethoxy)ethanol (2.15 ml, 21.6 mmol) were heated at reflux in EtOH for 24 hours under a nitrogen atmosphere. The solution was cooled to room temperature at stored at -20 °C for 24 hours. The resulting precipitate was filtered to yield **Cl**[1] as an orange solid. ^{1}H NMR (400 MHz, $CDCl_3$) δ_H 8.61 (d, 1H, $^3J_{HH}$ = 7.3 Hz), 8.55 (d, 1H, $^3J_{HH}$ = 8.5 Hz), 8.45 (d, 1H, $^3J_{HH}$ = 7.9 Hz), 7.81 (d, 1H, $^3J_{HH}$ = 7.9 Hz), 7.76 (d, 1H, $^3J_{HH}$ =7.9 Hz), 4.48 (t, 2H, $^3J_{HH}$ = 5.6 Hz), 3.79 (t, 2H, $^3J_{HH}$ = 5.6 Hz), 3.66-3.58 (m, 4H) ppm. IR (solid. V_{max})/cm^{-1}: 3455, 2869, 1700, 1651, 1588, 1574, 1505, 1370, 1341, 1235, 1119, 104, 1022, 558, 855, 780, 750, 729, 667. HRMS ES- found *m/z* 320.0687, calculated *m/z* 320.0684 for $[C_{16}H_{14}ClNO_4H]^+$.

Synthesis of Pro[1]

Cl[1] (502 mg, 1.6 mmol) and N-ethylethylenediamine (0.64 ml, 6.3 mmol) were heated for 48 hours at 100 °C in DMSO under a nitrogen atmosphere. The solution was cooled and water (15 ml) added. The solution was neutralised using 1 M HCl and then extracted into DCM. The organic phase was washed with water, dried over $MgSO_4$, and the solvent removed to yield **Pro**[1] as an orange solid (yield: 125 mg, 22%). ^{1}H NMR (400 MHz, $CDCl_3$): δ_H 8.51 (d, 1H, $^3J_{HH}$ = 7.2 Hz), 8.30 (d, 1H, $^3J_{HH}$ = 8.4 Hz), 8.09 (d, 1H, $^3J_{HH}$ = 8.5 Hz), 7.48 (app. t, 1H, $^3J_{HH}$ = 7.7 Hz), 6.51 (d, 1H, $^3J_{HH}$ = 8.4 Hz), 6.35 (br. t, 1H), 4.36 (t, 2H, $^3J_{HH}$ = 5.2 Hz), 3.81 (t, 2H, $^3J_{HH}$ = 8.1 Hz), 3.70-3.60 (m, 4H), 3.35 (t, 2H, $^3J_{HH}$ = 5.8 Hz), 3.02 (t, 2H, $^3J_{HH}$ = 5.8 Hz), 2.69 (q, 2H, $^3J_{HH}$ = 7.1 Hz), 1.13 (t, 3H, $^3J_{HH}$ = 7.1 Hz). HRMS found *m/z* 372.1919, calcd *m/z* 372.1918 for $[C_{20}H_{26}N_3O_4]^+$.

Synthesis of L^1

Pro^1 (100 mg, 0.27 mmol) and NH_4PF_6 (49 mg, 0.30 mmol) were heated at 100 °C in $HC(OEt)_3$ for 3 hrs under a nitrogen atmosphere. The solution was cooled and the solvent decanted to leave an orange coloured oil. Et_2O (2 x 10 ml) was then added and slowly decanted and the remaining oil dried *in vacuo* to yield **L^1** as an orange oil (77 mg, 54%). ^{1}H NMR (300 MHz, $(CD_3)_2CO$): δ_H 8.97 (s, 1H), 8.59 (dd, 1H, J_{HH} = 8.5, 3.4 Hz), 8.55 – 8.46 (m, 2H), 8.00 (dd, 1H, J_{HH} = 7.5, 2.3 Hz), 7.95 – 7.86 (m, 1H), 4.80 (t, 2H, $^3J_{HH}$ = 9.9 Hz), 4.50 (t, 2H, $^3J_{HH}$ = 10.5 Hz), 4.24 (t, 2H, $^3J_{HH}$ = 6.2 Hz), 3.90 (q, 2H, $^3J_{HH}$ = 7.3 Hz), 3.73 – 3.66 (m, 2H), 3.58 – 3.52 (m, 2H), 2.03 – 1.99 (m, 2H), 1.47 (t, 3H, $^3J_{HH}$ = 7.3 Hz). $^{13}C\{^1H\}$ NMR (101 MHz, $(CD_3)_2CO$): δ_C 158.15, 138.59, 131.65, 130.78, 128.74, 128.43, 127.07, 124.09, 123.39, 72.43, 70.15, 69.62, 67.34, 61.06, 53.04, 49.31, 44.12, 39.24, 39.12, 14.61, 12.00. UV/Vis ($(CH_3)_2CO$): λ_{max} / nm (ε / $M^{-1}cm^{-1}$) = 426 (4960), 344 (10920). HRMS found *m/z* 382.1752, calcd *m/z* 382.1761 for $[C_{21}H_{24}N_3O_4]^+$. IR (solid) ν / cm^{-1}: 2978, 2947, 2875, 1697, 1651, 1581, 1503, 1462, 1450, 1346, 1157, 1123, 1090, 1057, 825, 783, 754, 739, 556, 422, 405, 392.

Synthesis of Pro^2

As for **Pro^1**, but using **Cl^1** (502 mg, 1.6 mmol) and N-phenylethylenediamine (0.82 ml, 6.2 mmol). The product **Pro^2** was isolated as a yellow solid (yield: 260 mg, 66 %). ^{1}H NMR (400 MHz, $CDCl_3$): δ_H 8.37 (d, 1H, $^3J_{HH}$ = 7.3 Hz), 8.28 (d, 1H, $^3J_{HH}$ = 8.7 Hz), 8.09 (d, 1H, $^3J_{HH}$ = 8.3 Hz), 7.44 (app. t, 1H, $^3J_{HH}$ = 7.4 Hz), 7.30 (t, 2H, $^3J_{HH}$ = 7.6 Hz), 7.01 – 6.93 (m, 2H), 6.54 (d, 1H, $^3J_{HH}$ = 8.3 Hz), 6.11 (s, 1H), 4.38 (t, 2H, $^3J_{HH}$ = 4.9 Hz), 3.87 (t, 2H, $^3J_{HH}$ = 4.7 Hz), 3.77 – 3.62 (overlapping m, 8H).

Synthesis of L^2

As for **L^1**, but using **Pro^2** (198 mg, 0.47 mmol) and NH_4PF_6 (82 mg, 0.52 mmol). The product **L^2** was yielded as a yellow powder (yield: 129 mg, 64 %). ^{1}H NMR (400 MHz, $(CD_3)_2CO$): δ_H 9.85 (s, 1H), 8.85 (d, 1H, $^3J_{HH}$ = 8.5 Hz), 8.77 – 8.62 (m, 2H), 8.30 (d, 1H, $^3J_{HH}$ = 7.8 Hz), 8.06 (dd, 1H, J_{HH} = 15.5, 7.9 Hz), 7.72 (d, 2H, $^3J_{HH}$ = 7.7 Hz), 7.63 (d, 2H, $^3J_{HH}$ = 7.5 Hz), 7.56 – 7.43 (m, 1H), 5.23 – 4.98 (m, 4H), 4.37 (t, 2H, $^3J_{HH}$ = 6.2 Hz), 3.89 – 3.71 (overlapping m, 6H). $^{13}C\{^1H\}$ NMR (101 MHz, $(CD_3)_2CO$): δ_C 164.16, 163.68, 157.17, 138.78, 137.02, 132.68, 131.59, 130.92, 130.54, 129.88, 129.68, 129.57, 128.87, 128.02,

125.92, 124.93, 124.27, 119.78, 73.32, 71.03, 68.20, 61.92, 54.57, 50.84, 40.16. UV/Vis ($(CH_3)_2CO$): λ_{max} / nm (ε / $M^{-1}cm^{-1}$) 429 (1000), 342 (9700). HRMS ES^- found *m/z* 430.1756, calcd *m/z* 430.1761 for $[C_{25}H_{24}N_3O_4]^+$. IR (solid) ν / cm^{-1}: 3010, 2932, 2810, 1699, 1654, 1626, 1581, 1492, 1379, 1348, 1269, 1234, 1142, 1128, 1097, 1057, 829, 785, 754, 736, 689, 556, 410.

<u>*Propyl*</u>

Synthesis of Cl²

4-Chloro-1,8-naphthalic anhydride (3 g, 12.9 mmol) and propylamine (1.9 ml, 25.8 mmol) were heated at reflux in EtOH for 24 hours under a nitrogen atmosphere. The solution was cooled to room temperature and stored at -20 °C for 24 hours. The resulting precipitate was filtered to yield **Cl²** as a bright yellow solid (2.74 g, 78 %). ^{1}H NMR (400 MHz, $CDCl_3$): δ_H 8.59 (d, 1H, $^3J_{HH}$ = 7.3 Hz), 8.53 (d, 1H, $^3J_{HH}$ = 8.5 Hz), 8.42 (d, 1H, $^3J_{HH}$ = 7.9 Hz), 7.82-7.73 (m, 2H), 4.08 (t, 2H, $^3J_{HH}$ = 7.6 Hz), 1.70 (app. sext., 2H, $^3J_{HH}$ = 7.5 Hz), 0.95 (t, 3H, $^3J_{HH}$ = 7.4 Hz) ppm.

Synthesis of Pro³

As for **Pro¹**, but using **Cl²** (491 mg, 1.8 mmol) and *N*-ethylethylenediamine (0.76 ml, 7.2 mmol). The product was obtained as an orange solid **Pro³** (573 mg, 98 %). ^{1}H NMR (500 MHz, $CDCl_3$): δ_H 8.51 (d, 1H, $^3J_{HH}$ = 7.3 Hz), 8.38 (d, 1H, $^3J_{HH}$ = 8.4 Hz), 8.14 (d, 1H, $^3J_{HH}$ = 8.4 Hz), 7.55 (app. t, 1H, $^3J_{HH}$ = 8.2 Hz), 6.61 (d, 1H, $^3J_{HH}$ = 8.4 Hz), 6.29 (br. t, 1H), 4.08 – 4.03 (m, 2H), 3.41 – 3.36 (m, 2H), 3.06 – 3.01 (m, 2H), 2.69 (q, 2H, $^3J_{HH}$ = 7.1 Hz), 1.69 (q, 2H, $^3J_{HH}$ = 7.5 Hz), 1.12 (t, 3H, $^3J_{HH}$ = 5.1 Hz), 0.94 (t, 3H, $^3J_{HH}$ = 7.4 Hz) ppm. HRMS found *m/z* 326.1866, calcd *m/z* 326.1863 for $[C_{29}H_{24}N_3O_2]^+$.

Synthesis of L³

As for **L¹**, but using **Pro³** (346 mg, 1.1 mmol) and NH_4PF_6 (190 mg, 1.2 mmol). The product **L³** was obtained as an orange oil (254 mg, 50 %). ^{1}H NMR (400 MHz, $(CD_3)_2CO$): δ_H 8.94 (s, 1H), 8.58-8.47 (m, 3H), 7.97 (d, 1H, $^3J_{HH}$ = 7.8 Hz) 7.88 (app. t, 1H, $^3J_{HH}$ = 7.9 Hz), 4.65 (t, 2H, $^3J_{HH}$ = 10.0 Hz), 4.45 (t, 2H, $^3J_{HH}$ = 11.1 Hz), 3.82 (q, 2H, $^3J_{HH}$ = 7.3 Hz), 1.66-1.52 (m, 2H), 1.07-0.96 (m, 3H), 0.85 (t, 3H, $^3J_{HH}$ = 7.5 Hz) ppm. $^{13}C\{^1H\}$ NMR (101 MHz, $(CD_3)_2CO$): δ_C 164.03, 163.54, 158.98, 139.33, 132.40, 131.53, 129.79, 129.56, 129.29, 127.90,

125.02, 124.20, 124.17, 53.90, 50.14, 44.96, 42.42, 21.91, 12.85, 11.69. UV/Vis ($(CH_3)_2CO$): λ_{max} / nm (ε / $M^{-1}cm^{-1}$) = 426 (2520), 344 (11980). HRMS found *m/z* 336.1709, calcd *m/z* 336.1707 for $[C_{20}H_{22}N_3O_2]^+$. IR (solid) ν / cm^{-1}: 3381, 3089, 2968, 1697, 1651, 1591, 1514, 1443, 1429, 1408, 1389, 1350, 1269, 1234, 1201, 1155, 1086, 1069, 962, 891, 876, 825, 789, 760, 738, 556, 463, 434, 409.

Synthesis of Pro[4]

As for **Pro[1]**, but using **Cl[2]** (767 mg, 2.8 mmol) and N-phenylethylenediamine (1.5 ml, 11.2 mmol). The product **Pro[4]** was yielded as an orange solid (yield: 1.00 g, 97 %). ^{1}H NMR (400 MHz, $(CD_3)_2CO$): δ_H 8.42 (d, 1H, $^3J_{HH}$ = 8.5 Hz), 8.35 (d, 1H, $^3J_{HH}$ = 7.2 Hz), 8.21 (d, 1H, $^3J_{HH}$ = 8.5 Hz), 7.52 (app. t, 1H, $^3J_{HH}$ = 8.2 Hz), 6.98 (app. t, 2H, $^3J_{HH}$ = 8.2 Hz), 6.76 (d, 1H, $^3J_{HH}$ = 8.5 Hz), 6.58 (d, 2H, $^3J_{HH}$ = 8.0 Hz), 6.48 (br. t, 1H), 5.15 (br. t, 1H, N*H*), 3.93 (t, 2H, $^3J_{HH}$ = 7.5 Hz), 3.62 (t, 2H, $^3J_{HH}$ = 5.8 Hz), 3.47 (t, 2H, $^3J_{HH}$ = 6.0 Hz), 1.58 (q, 2H, $^3J_{HH}$ = 7.5 Hz), 0.81 (t, 3H, $^3J_{HH}$ = 7.5 Hz).

Synthesis of L[4]

As for **L[1]**, but using **Pro[4]** (750 mg, 2.0 mmol) and NH_4PF_6 (360 mg, 2.2 mmol). The product **L[4]** was obtained as a yellow solid (yield: 860 mg, 81 %). ^{1}H NMR (400 MHz, $(CD_3)_2CO$): δ_H 9.87 (s, 1H), 8.86 (d, 2H, $^3J_{HH}$ = 8.5 Hz), 8.71 (overlapping d, 2H), 8.31 (d, 1H, $^3J_{HH}$ = 7.8 Hz), 8.06 (app. t, 1H, $^3J_{HH}$ = 7.9 Hz), 7.73 (d, 2H, $^3J_{HH}$ = 7.6 Hz), 7.62 (app. t, 2H, $^3J_{HH}$ = 7.5 Hz), 7.50 (app. t, 1H, $^3J_{HH}$ = 7.4 Hz), 5.17-5.08 (m, 4H), 4.12 (t, 2H, $^3J_{HH}$ = 7.5 Hz), 1.78 (q, 2H, $^3J_{HH}$ = 7.5 Hz), 1.00 (t, 3H, $^3J_{HH}$ = 7.4 Hz) ppm. $^{13}C\{^1H\}$ NMR (101 MHz, $(CD_3)_2CO$): δ_C 164.07, 163.58, 157.18, 138.69, 137.04, 132.60, 131.48, 130.94, 130.78, 129.91, 129.55, 128.89, 128.04, 125.94, 125.11, 124.42, 119.80, 119.59, 119.27, 54.60, 50.86, 42.51, 21.95, 11.70. UV/Vis ($(CH_3)_2CO$): λ_{max} / nm (ε / $M^{-1}cm^{-1}$) = 432 (620), 351 (14320), 344 (0.599). HRMS found *m/z* 384.1700, calcd *m/z* 384.1707 for $[C_{24}H_{22}N_3O_2]^+$. IR (solid) ν / cm^{-1}: 2974, 1699, 1651, 1626, 1585, 1494, 1391, 1364, 1350, 1271, 1236, 1072, 8423, 829, 787, 758, 689, 557, 469, 434.

<u>*Benzyl*</u>

Synthesis of Cl[3]

4-Chloro-1-8-naphthalic anhydride (1.00 g, 4.3 mmol) and benzylamine (1 ml, 9.2 mmol) were heated at reflux in EtOH for 24 hours under a nitrogen atmosphere. The solution was cooled to room temperature and stored at -20 °C for 24 hours. The resulting precipitate was filtered to yield **Cl^3** as a bright yellow solid (1.2 g 88.0 %). ^{1}H NMR (500 MHz, $CDCl_3$): δ_H 8.61 (d, 1H, $^3J_{HH}$ = 7.3 Hz), 8.53 (d, 1H, $^3J_{HH}$ = 8.5 Hz), 8.45 (d, 1H, $^3J_{HH}$ = 7.8 Hz), 7.77 (dd, 2H, J_{HH} = 17.4, 8.2 Hz), 7.49 (d, 2H, $^3J_{HH}$ = 7.6 Hz), 7.26 (app. t, 1H, $^3J_{HH}$ = 7.4 Hz), 7.23 – 7.16 (m, 2H), 5.32 (s, 2H).

Synthesis of Pro^5

As for **Pro^1**, but using **Cl^3** (500 mg, 1.6 mmol) and *N*-ethylethylenediamine (0.65 ml, 6.2 mmol). The product **Pro^5** was obtained as an orange solid (574 mg, 94 %). ^{1}H NMR (300 MHz, $CDCl_3$) δ 8.41 (d, 1H, *J* = 7.3 Hz), 8.29 (d, 1H, *J* = 8.4 Hz), 7.97 (d, 1H, *J* = 8.3 Hz), 7.52 – 7.37 (m, 3H), 7.25 – 7.10 (m, 3H), 6.48 (d, 1H, *J* = 8.4 Hz), 6.25 (br. t, 1H), 5.28 (s, 2H), 3.27 (dd, 2H, *J* = 10.3, 5.0 Hz), 2.97 (t, 2H, *J* = 5.7 Hz), 2.65 (q, 2H, *J* = 7.1 Hz), 1.09 (t, 3H, *J* = 7.1 Hz).

Synthesis of L^5

As for L^1, but using **Pro^5** (LG361) (389 mg, 1.0 mmol) and ammonium hexafluorophosphate (187 mg, 1.15 mmol). The product **L^5** was obtained as an orange oil (371 mg, 67%). ^{1}H NMR (300 MHz, Acetone) δ 9.00 (s, 1H), 8.63 (d, 1H, *J* = 8.5 Hz), 8.54 (overlapping d. 2H), 8.01 (d, 1H, *J* = 7.8 Hz), 7.94 (t, 1H, *J* = 7.9 Hz), 7.44 (d, 2H, *J* = 7.3 Hz), 7.33 – 7.20 (m, 3H), 5.25 (s, 2H), 4.82 (t, 2H, *J* = 10.4 Hz), 4.53 (t, 2H, *J* = 10.5 Hz), 3.94 (q, 2H, *J* = 7.2 Hz), 1.52 (t, 3H, *J* = 7.4 Hz). ^{13}C{^{1}H} NMR (126 MHz, $(CD_3)_2CO$): δ_C 163.26, 162.75, 158.03, 138.67, 137.52, 131.84, 130.96, 128.95, 128.49, 128.31, 128.23, 127.24, 127.03, 124.11, 123.14, 123.07, 53.00, 49.27, 44.12, 43.23, 35.19, 23.58, 20.56, 11.97. UV/Vis ($(CH_3)_2CO$): λ_{max} / nm (ε / $M^{-1}cm^{-1}$): 428 (3700), 344 (14560). HRMS found *m/z* 384.1718, calcd *m/z* 384.1712 for $[C_{24}H_{22}N_3O_2]^+$. IR (solid) ν / cm^{-1}: 2372, 2341, 1699, 1651, 1582, 1549, 1497, 1454, 1423, 1381, 1346, 1290, 1234, 1182, 1155, 1072, 1028, 970, 876, 827, 783, 754, 734, 702, 665, 613, 583, 556, 469, 407.

Synthesis of Pro^6

As for **Pro^1**, but using **Cl^3** NS103 (513 mg, mmol) and N-phenylethylenediamine (0.83ml, mmol) were heated in DMSO (6 ml) at reflux under nitrogen for 48 hours. The product

was cooled giving an orange precipitate. Water (6 ml) was added to form yellow precipitate. The reaction solution was neutralised with hydrochloric acid (3 ml, 0.1 M) and filtered to give a yellow product. Product re-precipitated using dichloromethane and Et_2O and filtered to give yellow product **Pro^6** (yield: 551 mg, 87 %). ^{1}H NMR (400 MHz, $CDCl_3$): δ_H 8.51 (d, 1H, $^3J_{HH}$ = 6.6 Hz), 8.41 (d, 1H, $^3J_{HH}$ = 8.3 Hz), 7.88 (d, 1H, $^3J_{HH}$ = 8.3 Hz), 7.56 (d, 2H, $^3J_{HH}$ = 7.1 Hz), 7.54 – 7.48 (m, 1H), 7.30 (app. t, 2H, $^3J_{HH}$ = 7.3 Hz), 7.23 (d, 3H, $^3J_{HH}$ = 7.4 Hz), 6.81 (app. t, 1H, $^3J_{HH}$ = 7.4 Hz), 6.76 (d, 2H, $^3J_{HH}$ = 7.6 Hz), 6.66 (d, 1H, $^3J_{HH}$ = 8.4 Hz), 5.57 (br. t, 1H), 5.35 (s, 2H), 3.61 (overlapping s, 4H).

Synthesis of L^6

As for **L^1**, but using **Pro^6** (346 mg, 0.87 mmol) and NH_4PF_6 (156 mg, 0.97 mmol). The product **L^6** was obtained as a yellow powder (yield: 322 mg, 85 %). ^{1}H NMR (400 MHz, $(CD_3)_2CO$): δ_H 9.87 (s, 1H), 8.86 (d, 1H, $^3J_{HH}$ = 8.5 Hz), 8.74 – 8.68 (m, 2H), 8.30 (d, 1H, $^3J_{HH}$ = 7.6 Hz), 8.06 (app. t, 1H, $^3J_{HH}$ = 7.7 Hz), 7.72 (d, 2H, $^3J_{HH}$ = 8.4 Hz), 7.62 (app. t, 2H, $^3J_{HH}$ = 8.2 Hz), 7.48 (d, 3H, $^3J_{HH}$ = 6.7 Hz), 7.36 – 7.24 (m, 3H), 5.35 (s, 2H), 5.15 – 5.09 (m, 4H). $^{13}C\{^1H\}$ NMR (101 MHz, $(CD_3)_2CO$): δ_C 164.16, 163.67, 157.20, 138.91, 138.41, 137.02, 132.89, 131.78, 130.94, 130.15, 129.96, 129.82, 129.62, 129.22, 129.16, 128.90, 128.17, 128.07, 125.94, 125.18, 124.95, 124.29, 119.77, 54.59, 50.85, 44.18. UV/Vis ($(CH_3)_2CO$): λ_{max} / nm (ε / $M^{-1}cm^{-1}$) 435 (400), 343 (5700). HRMS found *m/z* 432.1701, calcd *m/z* 432.1707 for $[C_{28}H_{22}N_3O_2]^+$. IR (solid) ν / cm^{-1}: 1699, 1655, 1637, 1589, 1495, 1452, 1387, 1350, 1337, 1290, 1277, 1232, 1182, 959, 881, 839, 825, 791, 756, 748, 700, 689, 557, 472.

<u>*Octanyl*</u>

Synthesis of Cl^4

4-Chloro-1,8-naphthalic anhydride (3 g, 12.9 mmol) and octylamine (4.26 ml, 25.8 mmol) were heated at reflux in EtOH for 24 hours under a nitrogen atmosphere. The solution was cooled to room temperature and stored at -20 °C for 24 hours and the resulting precipitate filtered. The crude product was dissolved in DCM (30 ml) and washed with 0.1 M HCl (30 ml), followed by H_2O (30 ml) and brine (30 ml). The collected organic phase was dried over $MgSO_4$, and the solvent removed to yield **Cl^4** as a yellow solid (3.78 g, 85 %). ^{1}H NMR (400 MHz, $CDCl_3$): δ_H 8.60 (d, 1H, $^3J_{HH}$ = 7.3 Hz), 8.53 (d, 1H, $^3J_{HH}$ = 8.5 Hz),

8.45 (d, 1H, $^3J_{HH}$ = 7.9 Hz), 7.82-7.75 (m, 2H), 4.11-4.05 (m, 2H), 1.69-1.50 (m, 2H), 1.47-1.12 (overlapping m, 10H), 0.80 (t, 3H, $^3J_{HH}$ = 6.7 Hz).

Synthesis of Pro^7

As for **Pro**^{1}, but using **Cl**^{4} (600 mg, 1.7 mmol) and *N*-ethylethylenediamine (0.71 ml, 7.0 mmol). The product was obtained **Pro**^{7} as an orange solid (582 mg, 84 %). ^{1}H NMR (400 MHz, $CDCl_3$): δ_H 8.60 (d, 1H, $^3J_{HH}$ = 6.5 Hz), 8.37 (d, 1H, $^3J_{HH}$ = 8.4 Hz), 8.15 (d, 1H, $^3J_{HH}$ = 8.2 Hz), 7.55 (app. t, 1H, $^3J_{HH}$ = 7.6 Hz), 6.59 (d, 1H, $^3J_{HH}$ = 8.4 Hz), 6.32 (br. t, 1H), 4.07 (t, 2H, $^3J_{HH}$ = 7.6 Hz), 3.40 (q, 2H, $^3J_{HH}$ = 4.9 Hz), 3.05 (t, 2H, $^3J_{HH}$ = 5.4 Hz), 2.71 (q, 2H, $^3J_{HH}$ = 7.1 Hz), 1.66 (m, 2H), 1.40-1.11 (overlapping m, 13H), 0.78 (t, 3H, $^3J_{HH}$ = 7.0 Hz). HRMS found *m/z* 396.2644, calcd *m/z* 396.2646 for $[C_{24}H_{34}N_3O_2]^+$.

Synthesis of L^7

As for **L**^{1}, but using **Pro**^{7} (476 mg, 1.2 mmol) and NH_4PF_6 (217 mg, 1.3 mmol). The product **L**^{7} was obtained as a yellow solid (496 mg, 74 %). ^{1}H NMR (500 MHz, $(CD_3)_2CO$): δ_H 9.06 (s, 1H), 8.69 – 8.58 (m, 3H), 8.08 (d, 1H, $^3J_{HH}$ = 7.8 Hz), 7.99 (dd, 1H, J_{HH} = 8.5, 7.3 Hz), 4.86 (t, 2H, $^3J_{HH}$ = 10.0 Hz), 4.57 (t, 2H, $^3J_{HH}$ = 11.0 Hz), 4.13 – 4.09 (m, 2H), 3.95 (q, 2H, $^3J_{HH}$ = 7.2 Hz), 2.87 (d, 3H, $^3J_{HH}$ = 15.7 Hz), 1.70 (dt, 2H, $^3J_{HH}$ = 15.0, 7.5 Hz), 1.51 (t, 2H, $^3J_{HH}$ = 7.3 Hz), 1.33 – 1.24 (m, 8H), 0.87 (t, 3H, $^3J_{HH}$ = 6.9 Hz) ppm. ^{13}C{^{1}H} NMR (101 MHz, $(CD_3)_2CO$): δ_H 163.95, 163.45, 158.88, 139.29, 132.38, 131.50, 129.72 (two overlapping environments), 129.53, 129.29, 127.86, 124.99, 124.13, 53.88, 50.13, 44.96, 40.90, 32.51, 30.00, 29.91, 28.62, 27.75, 23.26, 14.33, 12.82. UV/Vis ($(CH_3)_2CO$): λ_{max} / nm (ε / $M^{-1}cm^{-1}$) = 427 (1820), 344 (13620). HRMS found *m/z* 406.2482, calcd *m/z* 406.2489 for $[C_{25}H_{32}N_3O_2]^+$. IR (solid) ν / cm^{-1}: 2959, 2924, 2855, 1703, 1651, 1589, 1508, 1391, 1354, 1254, 1232, 1155, 1093, 827, 785, 754, 555, 416.

Synthesis of Pro^8

As for **Pro**^{1}, but using **Cl**^{4} (503 mg, 1.4 mmol) and N-phenylethylenediamine (0.76 ml, 5.8 mmol. The product **Pro**^{8} was isolated as a yellow solid (yield: 601 mg, 65 %). ^{1}H NMR (400 MHz, $CDCl_3$): δ_H 8.55 (d, 1H, $^3J_{HH}$ = 6.6 Hz), 8.43 (d, 1H, $^3J_{HH}$ = 8.4 Hz), 8.03 (d, 1H, $^3J_{HH}$ = 8.5 Hz), 7.61 – 7.55 (m, 1H), 7.25 – 7.19 (m, 2H), 6.83 (app. t, 1H, $^3J_{HH}$ = 7.4 Hz), 6.78 (d, 2H, $^3J_{HH}$ = 8.5 Hz), 6.72 (d, 1H, $^3J_{HH}$ = 8.4 Hz), 5.70 (br. s, 1H), 4.17 – 4.09 (m, 2H),

3.65 (t, 4H, $^3J_{HH}$ = 4.3 Hz), 1.72 (dd, 2H, J_{HH} = 15.2, 7.3 Hz), 1.46 – 1.20 (m, 10H), 0.86 (t, 3H, $^3J_{HH}$ = 6.8 Hz).

Synthesis of L[8]

As for **L[1]**, but using **Pro[8]** (497 mg, 1.1 mmol) and NH_4PF_6 (200 mg, 1.2 mmol). The product **L[8]** was obtained as a yellow solid (yield: 274 mg, 54 %). ^{1}H NMR (400 MHz, $(CD_3)_2CO$): δ_H 9.85 (s, 1H), 8.84 (d, 1H, $^3J_{HH}$ = 8.6 Hz), 8.70 (dd, 2H, $^3J_{HH}$ = 7.6, 2.6 Hz), 8.29 (d, 1H, $^3J_{HH}$ = 7.8 Hz), 8.08 – 8.03 (m, 1H), 7.72 (d, 2H, $^3J_{HH}$ = 7.7 Hz), 7.62 (app. t, 2H, $^3J_{HH}$ = 8.0 Hz), 7.49 (app. t, 1H, $^3J_{HH}$ = 7.4 Hz), 5.18 – 5.07 (m, 4H), 4.14 (t, 2H, $^3J_{HH}$ = 7.2 Hz), 1.77 – 1.66 (m, 2H), 1.45 – 1.24 (m, 10H), 0.87 (t, 3H, $^3J_{HH}$ = 6.9 Hz). $^{13}C\{^1H\}$ NMR (101 MHz, $(CD_3)_2CO$): δ_C 164.01, 163.52, 157.13, 138.68, 137.02, 132.58, 131.47, 130.91, 129.83, 129.56, 128.86, 128.00, 125.92, 125.03, 124.35, 119.79, 54.56, 50.83, 40.98, 32.54, 30.47, 30.28, 30.08, 29.94, 28.65, 27.77, 23.29, 14.34. UV/Vis ($(CH_3)_2CO$): λ_{max} / nm (ε / $M^{-1}cm^{-1}$) 433 (200), 345 (7200). HRMS found *m/z* 454.2478, calcd *m/z* 454.2489 for $[C_{29}H_{32}N_3O_2]^+$. IR (solid) ν / cm^{-1}: 2922, 2850, 1708, 1697, 1653, 1536, 1589, 1492, 1390, 1352, 1267, 1232, 1095, 831, 785, 754, 734, 686, 557, 464, 405.

<u>*Methoxyethylamine*</u>

Synthesis of Cl[5]

4-chloro-1,8-naphthalic anhydride (2 g, 8.9 mmol) and 2-methoxyethylamine (1.53 ml, 17.8 mmol) were heated at reflux in EtOH (40 ml) for 24 hours under a nitrogen atmosphere. The solution was cooled and the product precipitated and filtered to yield **Cl[5]** as a yellow solid. ^{1}H NMR (400 MHz, $CDCl_3$) δ_H 8.61 (d, 1H, $^3J_{HH}$ = 7.3 Hz), 8.55 (d, 1H, $^3J_{HH}$ = 8.5 Hz), 8.46 (d, 1H, $^3J_{HH}$ = 7.9 Hz) 7.82-7.74 (m, 2H), 4.39 (t, 2H, $^3J_{HH}$ = 5.8 Hz), 3.68 (t, 2H, $^3J_{HH}$ = 5.8 Hz), 3.32 (s, 3H) ppm. HRMS found *m/z* 290.0579, calculated *m/z* 290.0578 for $[C_{15}H_{12}ClNO_3 + H]^+$.

Synthesis of Pro[9]

As for **Pro[1]**, but using **Cl[5]** (754 mg, 2.6 mmol) and N-phenylethylenediamine (1.36 ml, 10.4 mmol). The product **Pro[9]** was yielded as a light orange solid (776 mg, 77%). ^{1}H NMR (400 MHz, $CDCl_3$) δ_H 8.49 (d, 1H, $^3J_{HH}$ = 7.4 Hz), 8.39 (d, 1H, $^3J_{HH}$ = 8.4 Hz), 7.94 (d, 1H, $^3J_{HH}$ = 9.3 Hz), 7.51 (t, 1H), 7.16 (s, 1H), 6.75 (t, 1H, $^3J_{HH}$ = 7.8 Hz), 6.70 – 6.64 (m, 1H), 5.59 (s,

1H), 4.36 (t, 1H, $^3J_{HH}$ = 6.0 Hz), 3.67 (t, 1H, $^3J_{HH}$ = 5.9 Hz), 3.59 (d, 1H, $^3J_{HH}$ = 6.1 Hz) ppm. HRMS found *m/z* 390.1812, calculated *m/z* 390.1812 for $[C_{23}H_{23}N_3O_3 + H]^+$.

Synthesis of L[9]

As for **L[1]**, but using **Pro[9]** (442 mg, 1.3 mmol) and ammonium hexafluorophosphate (234 mg, 1.4 mmol). The product **L[9]** was yielded as an orange solid (319 mg, 45%). ^{1}H NMR (500 MHz, Acetone) δ 9.84 (s, 1H), 8.85 (dd, 1H, $^3J_{HH}$ = 8.5, 1.0 Hz), 8.72 – 8.67 (m, 2H), 8.29 (d, 1H, $^3J_{HH}$ = 7.8 Hz), 8.05 (dd, 1H, $^3J_{HH}$ = 8.5, 7.3 Hz), 7.75 – 7.70 (m, 2H), 7.62 (dd, 2H, $^3J_{HH}$ = 8.5, 7.6 Hz,), 7.49 (t, 1H, $^3J_{HH}$ = 7.4 Hz), 5.17 – 5.05 (m, 4H), 4.36 (t, 2H, $^3J_{HH}$ = 6.2 Hz), 3.67 (t, 2H, $^3J_{HH}$ = 6.2 Hz), 3.32 (s, 3H). ^{13}C NMR (101 MHz, Acetone) δ 164.09, 163.60, 157.17, 138.79, 137.03, 132.69, 131.59, 130.93, 129.90, 129.68, 129.58, 128.90, 128.05, 125.95, 124.95, 124.28, 119.82, 69.70, 58.63, 54.59, 50.87, 39.87. UV/Vis ($(CH_3)_2CO$) : λ_{max}/nm (ε/M^{-1} cm^{-1}) = 423 (800), 344 (13480). HRMS found *m/z* 400.1658, calculated *m/z* 400.1656 for $[C_{24}H_{22}N_3O_3]^+$. IR (solid. V_{max})/cm^{-1}: 3107, 2983, 2951, 1699, 1655, 1628, 1585, 1514, 1479, 1450, 1406, 1393, 1375, 1269, 1236, 1182, 1105, 1056, 954, 825, 786, 756, 736, 688, 557, 468.

<u>*Glycine ethyl ester*</u>

Synthesis of Cl[6]

4-chloro-1,8-naphthalic anhydride (1 g, 4.3 mmol), glycine ethyl ester hydrochloride (1.2 g, 8.6 mmol) and triethylamine (3 ml, 40 mmol) were heated at reflux in ethanol (30 ml) under nitrogen for 24 hours. The solution was cooled and the resulting precipitate filtered and dried in *vacuo* to give **Cl[6]** as an orange solid (1.0 g, 73 %). ^{1}H NMR (400 MHz, $CDCl_3$) δ_H 8.63 (d, 1H, $^3J_{HH}$ = 7.3 Hz), 8.57 (d, 1H, $^3J_{HH}$ = 8.5 Hz), 8.45 (d, 1H, $^3J_{HH}$ = 7.9 Hz), 7.82 (d, 1H, $^3J_{HH}$ = 7.9 Hz), 7.78 (d, 1H, $^3J_{HH}$ = 7.8 Hz), 4.86 (s, 2H), 4.18 (q, 2H, $^3J_{HH}$ =7.1 Hz), 1.23 (t, 3H, $^3J_{HH}$ =7.1 Hz). IR (solid. V_{max})/cm^{-1}: 3055, 2984, 1748, 1705, 1667, 1620, 1591, 1574, 1397, 1375, 1352, 1339, 1317, 1265, 1236, 1206, 1181, 1128, 1051, 1020, 980, 941, 853, 783, 731, 700, 662.

Synthesis of Pro[10]

As for **Pro[1]**, but using **Cl[6]** (354 mg, 1.1mmol) and N-phenylethylenediamine (0.58 ml, 4.5 mmol). The product **Pro[10]** was yielded as an orange solid (86.2%). ^{1}H NMR (400 MHz,

$CDCl_3$) δ_H 8.17-8.08 (m, 2H), 7.95 (d, 1H, $^3J_{HH}$ = 8.5 Hz), 7.24-7.12 (m, 2H), 6.70 (d, 3H, $^3J_{HH}$ = 7.8 Hz), 6.41 (d, 1H, $^3J_{HH}$ = 8.5 Hz), 6.08 (s, 1H), 4.86 (s, 2H), 4.06 (q, 2H, $^3J_{HH}$ = 7.2 Hz), 3. 49 (s, 4H), 1.18 (t, 3H, $^3J_{HH}$ = 7.2 Hz) ppm. HRMS found *m/z* 418.1761, calculated *m/z* 418.1761 for $[C_{24}H_{23}N_3O_4 + H]^+$.

Synthesis of L[10]

As for **L[1]**, but using **Pro[10]** LG228 (318 mg, 0.76 mmol) and ammonium hexafluorophosphate (137 mg, 0.84 mmol). The product **L[10]** was yielded as an orange solid (403 mg, 93 %). ^{1}H NMR (500 MHz, Acetone) δ_H 9.87 (s, 1H), 8.93 (d, 1H, $^3J_{HH}$ = 8.5 Hz), 8.72 (t, 2H, $^3J_{HH}$ = 7.9 Hz), 8.34 (d, 1H, $^3J_{HH}$ = 7.8 Hz), 8.10 (t, 1H, $^3J_{HH}$ = 7.4 Hz), 7.75 (d, 2H, $^3J_{HH}$ = 7.8Hz), 7.64 (t, 2H, $^3J_{HH}$ = 7.5 Hz), 7.51 (t, 1H, $^3J_{HH}$ = 7.4 Hz), 5.22-5.08 (m, 4H), 4.91 (s, 1H), 4.25 (q, 2H, $^3J_{HH}$ = 7.2 Hz), 1.29 (t, 3H, $^3J_{HH}$ = 7.1 Hz). ^{13}C NMR (101 MHz, Acetone) δ 168.65, 163.76, 163.26, 157.16, 139.27, 137.00, 133.00, 132.00, 130.92, 130.25, 129.86, 129.67, 128.92, 128.15, 126.02, 124.24, 123.62, 119.84, 62.06, 54.56, 50.88, 42.05, 30.28, 30.09, 14.45. UV/Vis ($(CH_3)_2CO$) : λ_{max}/nm (ε/ M^{-1} cm^{-1}) = 432 (1080), 345 (17760). HRMS found *m/z* 428.1607, calculated *m/z* 428.1605 for $[C_{25}H_{22}N_3O_4]^+$, found *m/z* 445.1867, calculated *m/z* 445.1870 for $[C_{25}H_{22}N_3O_4 + NH_3]^+$. IR (solid. V_{max})/cm^{-1}: 2978, 1753, 1705, 1659, 1633, 1589, 1404, 1379, 1323, 1275, 1215, 1180, 829, 791, 760, 688, 665, 557, 497, 462, 457, 403.

2.5.4 Complex Synthesis

Ethoxyethanol

Synthesis of [AuCl(L[1])]

L[1] (81 mg, 0.15 mmol), KO^{t}Bu (17 mg, 0.15 mmol) and [AuCl(tht)] (49 mg, 0.15 mmol) were dissolved in CH_3OH and then heated to reflux, under nitrogen, overnight in the absence of light. The solution was cooled, and then concentrated *in vacuo*, and then Et_2O added dropwise to induce precipitation. **[AuCl(L[1])]** was yielded as a grey coloured solid (yield: 76 mg, 81 %). ^{1}H NMR (400 MHz, $CDCl_3$): δ_H 8.68 – 8.59 (m, 2H), 8.25 (d, 1H, $^3J_{HH}$ = 8.7 Hz), 7.83 (d, 2H, $^3J_{HH}$ = 7.8 Hz), 4.46 (q, 2H, $^3J_{HH}$ = 4.6 Hz), 4.04-3.81 (m, 5H), 3.73 – 3.63 (m, 2H), 3.56 (s, 1H), 3.47 (q, 2H, $^3J_{HH}$ = 6.8 Hz) 1.42 (t, 2H, $^3J_{HH}$ = 7.3 Hz), 0.84 (br. t, 3H). ^{13}C{^{1}H} NMR (126 MHz, $CDCl_3$): δ_C 193.85, 163.89, 163.68, 132.27, 131.62,

129.05, 128.49, 128.00, 127.97, 126.22, 122.97, 72.38, 70.35, 70.00, 68.47, 66.76, 62.00, 53.72, 48.66, 46.28, 39.86, 39.44, 15.29, 13.75. UV/Vis ($(CH_3)_2CO$): λ_{max} / nm (ε / $M^{-1}cm^{-1}$) 436 (1420), 351 (4620), 344 (4660). HRMS found *m/z* 636.0918, calcd *m/z* 636.0935 for $[C_{21}H_{23}AuClN_3O_4 + Na]^+$. IR (solid) ν / cm^{-1}: 2899, 2666, 2360, 1695, 1653, 1582, 1537, 1510, 1477, 1427, 1379, 1348, 1341, 1265, 1230, 1105, 1043, 835, 785, 737, 669, 600, 581, 556, 455, 444, 436, 428, 420, 409.

Synthesis of [AuCl(L^2)]

As for **[AuCl(L^1)]**, but using **L^2** (68 mg, 0.16 mmol), [AuCl(tht)] (51 mg, 0.16 mmol) and KO^{t}Bu (18 mg, 0.16 mmol). The product **[AuCl(L^2)]** was obtained as a grey solid (yield: 88 mg, 84 %). ^{1}H NMR (500 MHz, CD_3CN): δ_H 8.66 – 8.59 (m, 2H), 8.01 (d, 1H, $^3J_{HH}$ = 7.9 Hz), 7.94 (app. t, 1H, $^3J_{HH}$ = 7.9 Hz), 7.82 (d, 2H, $^3J_{HH}$ = 7.9 Hz), 7.53 (d, 2H, $^3J_{HH}$ = 7.8 Hz), 7.43 (d, 2H, $^3J_{HH}$ = 7.6 Hz), 4.39 – 4.21 (m, 4H), 3.81 – 3.49 (overlapping m, 8H). $^{13}C\{^1H\}$ NMR (126 MHz, $CDCl_3$): δ_C 192.74, 163.83, 163.63, 132.24, 131.47, 131.42, 129.73, 128.95, 128.15, 128.07, 126.46, 123.38, 123.25, 116.48, 113.91, 72.42, 70.36, 70.01, 68.48, 66.76, 66.00, 62.00, 53.70, 52.29, 52.24, 39.94, 15.41, 15.28. UV/Vis ($(CH_3)_2CO$): λ_{max} / nm (ε / $M^{-1}cm^{-1}$) 433 (900), 349 (8700). HRMS found *m/z* 643.1608, calcd *m/z* 643.1614 for $[C_{25}H_{23}AuN_3O_4 + NH_3]^+$. IR (solid) ν / cm^{-1}: 2990, 2880, 1705, 1659, 1593, 1487, 1437, 1408, 1381, 1346, 1337, 1321, 1288, 1234, 1188, 1121, 1049, 887, 843, 789, 756, 692, 559, 482, 451, 438, 426, 419, 405.

<u>*Propyl*</u>

Synthesis of [AuCl(L^3)]

As for **[AuCl(L^1)]**, but using **L^3** (80 mg, 0.17 mmol), KO^{t}Bu (19 mg, 0.17 mmol) and [AuCl(tht)] (53 mg, 0.17 mmol). The product **[AuCl(L^3)]** was obtained as an off-white solid (yield: 40 mg, 45 %). ^{1}H NMR (500 MHz, $CDCl_3$): δ_H 8.55 (dd, 1H, J_{HH} = 7.3, 1.0 Hz), 8.52 (d, 1H, $^3J_{HH}$ = 7.7 Hz), 8.21 (d, 1H, $^3J_{HH}$ = 8.4 Hz), 7.76 (d, 1H, $^3J_{HH}$ = 7.7 Hz), 7.71 (t, 1H, $^3J_{HH}$ = 7.3 Hz), 4.10 (m, 4H), 3.93 (t, 2H, $^3J_{HH}$ = 9.3 Hz), 3.83 (s, 2H), 1.76-1.67 (m, 2H), 1.29 (t, 3H, $^3J_{HH}$ = 7.2 Hz), 0.96 (t, 3H, $^3J_{HH}$ = 7.4 Hz) ppm. $^{13}C\{^1H\}$ NMR (126 MHz, $CDCl_3$): δ_C 193.48, 163.87, 163.40, 142.86, 131.92, 131.29, 129.37, 129.03, 128.44, 127.91, 126.27, 123.52, 123.10, 53.78, 48.72, 46.22, 42.23, 21.50, 13.66, 11.66. UV/Vis ($(CH_3)_2CO$): λ_{max} / nm (ε / $M^{-1}cm^{-1}$) 439 (280), 351 (6900), 345 (6900). HRMS found *m/z* 602.0682, calcd

m/z 602.0682 for $[C_{20}H_{21}N_3O_2AuCl + Cl]^+$. IR (solid) ν / cm^{-1}: 2959, 2882, 2357, 1691, 1651, 1585, 1520, 1470, 1423, 1383, 1362, 1344, 1333, 1267, 1234, 1190, 1065, 907, 833, 789, 644, 557, 482, 405, 382, 359, 334, 324, 318, 312, 301, 293, 284, 276, 257, 231, 220, 214.

Synthesis of [AuCl(L^4)]

As for **[AuCl(L^1)]**, but using **L^4** (98 mg, 0.17 mmol), KO^{t}Bu (19 mg, 0.17 mmol) and [AuCl(tht)] (53 mg, 0.17 mmol). The product **[AuCl(L^4)]** was obtained as a grey solid (yield: 86 mg, 85 %). ^{1}H NMR (500 MHz, $CDCl_3$): δ_H 8.56 (d, 1H, $^3J_{HH}$ = 7.3 Hz), 8.50 (d, 1H, $^3J_{HH}$ = 7.7 Hz), 8.25 (d, 1H, $^3J_{HH}$ = 8.4 Hz), 7.83 (d, 1H, $^3J_{HH}$ = 7.7 Hz), 7.73 – 7.69 (m, 1H), 7.65 (d, 2H, $^3J_{HH}$ = 7.2 Hz), 7.31 (m, 3H), 4.40 (br. t, 2H), 4.15 – 4.09 (m, 4H), 1.78-1.69 (m, 2H), 0.98 (t, 3H, $^3J_{HH}$ = 7.4 Hz) ppm. ^{13}C NMR (126 MHz, $CDCl_3$): δ_C 192.25, 163.80, 163.34, 142.56, 140.00, 131.80, 131.28, 129.60, 129.23, 128.81, 128.01, 127.93, 127.89, 126.41, 123.51, 123.40, 123.22, 53.78, 52.49, 42.30, 21.53, 11.70. UV/Vis ($(CH_3)_2CO$): λ_{max} / nm (ε / $M^{-1}cm^{-1}$) 352 (11760), 345 (11860). HRMS found *m/z* 597.1551, calcd *m/z* 597.1559 for $[C_{24}H_{21}N_3O_2AuCl – HCl + NH_4]^+$. IR (solid) ν / cm^{-1}: 2967, 2955, 2873, 1703, 1655, 1622, 1591, 1506, 1475, 1433, 1389, 1354, 1340, 1286, 1276, 1238, 1068, 1018, 958, 908, 858, 785, 764, 754, 692, 673, 588, 546.

<u>*Benzyl*</u>

Synthesis of [AuCl(L^6)]

As for **[AuCl(L^1)]**, but using **L^5** (62 mg, 0.16 mmol), [AuCl(tht)] (57 mg, 0.16 mmol) and KO^{t}Bu (17 mg, 0.16 mmol). The product **[AuCl(L^6)]** was obtained as a grey solid. (yield: 49 mg, 49 %). ^{1}H NMR (400 MHz, $CDCl_3$): δ_H 8.67 (d, 1H, $^3J_{HH}$ = 6.2 Hz,), 8.62 (d, 1H, $^3J_{HH}$ = 7.7 Hz), 8.32 (d, 2H, $^3J_{HH}$ = 7.7 Hz), 7.91 (d, 1H, $^3J_{HH}$ = 7.8 Hz), 7.86 – 7.76 (m, 1H), 7.73 (d, 2H, $^3J_{HH}$ = 8.0 Hz), 7.54 (d, 2H, $^3J_{HH}$ = 7.1 Hz), 7.47 – 7.30 (m, 5H), 5.42 (s, 2H), 4.48 (s, 2H), 1.25 (s, 2H). ^{13}C{^{1}H} NMR (126 MHz, $CDCl_3$): δ_C 192.51, 164.75, 164.16, 163.82, 163.32, 149.44, 142.67, 139.94, 137.97, 137.19, 134.42, 132.20, 131.57, 131.54, 130.31, 129.63, 128.99, 128.94, 128.64, 128.47, 128.05, 127.68, 127.37, 126.42, 125.09, 125.03, 123.29, 122.67, 121.61, 120.90, 110.83, 104.00, 54.61, 54.52, 53.88, 53.83, 53.71, 52.32, 50.12, 45.35, 43.89, 43.45, 40.19, 25.69. UV/Vis ($(CH_3)_2CO$): λ_{max} / nm (ε / $M^{-1}cm^{-1}$) 436 (700), 343 (1600). HRMS found *m/z* 645.1549, calcd *m/z* 645.1559 for $[C_{28}H_{20}AuN_3O_2 +$

$NH_4]^+$. IR (solid) ν / cm^{-1}: 2961, 2914, 2845, 1703, 1682, 1655, 1580, 1522, 1508, 1472, 1454, 1425, 1402, 1383, 1312, 1260, 1236, 1177, 1136, 1069, 1016, 964, 845, 799, 785, 737, 704, 692, 617, 594, 583, 557, 544, 500, 480, 459, 436, 428, 417.

Octanyl

Synthesis of [AuCl(L^7)]

As for **[AuCl(L^1)]**, but using **L^7** (86 mg, 0.16 mmol), KO^{t}Bu (18 mg, 0.16 mmol) and [AuCl(tht)] (50 mg, 0.16 mmol). The product **[AuCl(L^7)]** was obtained as a grey solid (yield: 68 mg, 68 %). ^{1}H NMR (400 MHz, $(CD_3)_2CO$): δ_H 9.39 (d, 2H, $^3J_{HH}$ = 7.5 Hz), 9.33 (d, 1H, $^3J_{HH}$ = 7.6 Hz, 3H), 8.80 (d, 1H, $^3J_{HH}$ = 8.7 Hz), 8.71 (app. t, 1H, $^3J_{HH}$ = 7.5 Hz), 5.18 (br. s, 2H), 5.03 – 4.89 (m, 4H), 4.72 (dd, 2H, J_{HH} = 13.8, 6.6 Hz), 2.57 – 2.47 (m, 2H), 2.16 (dd, 13H, J_{HH} = 27.8, 22.6 Hz), 1.66 (t, 3H, $^3J_{HH}$ = 5.6 Hz). $^{13}C\{^1H\}$ NMR (126 MHz, $(CD_3)_2CO$): δ_C 193.83, 164.27, 163.83, 144.41, 132.10, 131.65, 130.39, 130.00, 129.73, 128.50, 127.14, 124.36, 123.68, 54.59, 49.52, 46.55, 40.87, 32.58, 30.24, 30.08, 28.71, 27.85, 23.31, 14.35, 13.86. UV/Vis ($(CH_3)_2CO$): λ_{max} / nm (ε / $M^{-1}cm^{-1}$) 439 (340), 351 (4360), 345 (4360). HRMS found *m/z* 660.1678, calcd *m/z* 660.1663 for $[C_{25}H_{31}AuClN_3O_2 + Na]^+$. IR (solid) ν / cm^{-1}: 3341, 2920, 2854, 2110, 1703, 1657, 1585, 1531, 1470, 1429, 1391, 1350, 1275, 1234, 1096, 856, 729, 478.

Synthesis of [AuCl(L^8)]

As for **[AuCl(L^1)]**, but using **L^8** (70 mg, 0.16 mmol), [AuCl(tht)] (50 mg,0.16 mmol) and KO^{t}Bu (17 mg, 0.16 mmol). The product **[AuCl(L^8)]** was obtained as a grey coloured solid (yield: 31 mg, 79 %). ^{1}H NMR (500 MHz, CD_3CN): δ_H 8.63 (d, 2H, $^3J_{HH}$ = 7.4 Hz,), 8.57 (d, 1H, $^3J_{HH}$ = 8.6 Hz,), 8.00 (d, 1H, $^3J_{HH}$ = 7.2 Hz), 7.93 (app. t, 1H, $^3J_{HH}$ = 7.8 Hz), 7.82 (d, 2H, $^3J_{HH}$ = 7.8 Hz), 7.52 (app. t, 2H, $^3J_{HH}$ = 7.4 Hz), 7.42 (app. t, 1H, $^3J_{HH}$ = 7.1 Hz), 4.45 (br. t, 2H), 4.32 (br. t, 2H), 4.10 (t, 2H, $^3J_{HH}$ = 7.5 Hz), 2.81 (dd, 2H, J_{HH} = 13.8, 6.8 Hz), 1.44 – 1.22 (m, 10H), 0.88 (t, 3H, $^3J_{HH}$ = 6.0 Hz). $^{13}C\{^1H\}$ NMR (126 MHz, $CDCl_3$): δ_C 192.80, 163.80, 163.31, 142.42, 139.95, 131.98, 131.34, 129.71, 129.40, 128.62, 128.13, 128.11, 128.04, 126.41, 123.68, 123.50, 123.25, 66.00, 53.70, 52.27, 40.86, 31.99, 29.51, 29.39, 28.27, 27.33, 22.80, 15.42, 14.24. UV/Vis ($(CH_3)_2CO$): λ_{max} / nm (ε / $M^{-1}cm^{-1}$) 441 (3380), 351 (14160), 344 (14560). HRMS found *m/z* 650.2071, calcd *m/z* 650.2076 for $[C_{29}H_{31}AuN_3O_2 - Cl]^+$. IR (solid) ν / cm^{-1}: 3059, 2949, 2918, 2851, 1703, 1655, 1620, 1589,

1502, 1477, 1438, 1404, 1392, 1357, 1340, 1321, 1288, 1234, 1176, 1097, 1074, 1045, 1024, 858, 785, 754, 692, 671, 651, 613, 584, 559, 543, 482, 410.

Methoxyethylamine

Synthesis of [AuCl(L^9)]

As for **[AuCl(L^1)]**, but using **L^9** LG217 (85 mg, 0.15 mmol), KO^{t}Bu (18 mg, 00.16 mmol), and LG216 (50 mg, 0.16 mmol). The product **[AuCl(L^9)]** was yielded as a light grey solid (85 mg, 86 %). ^{1}H NMR (500 MHz, Acetone-d_6) δ 8.62 – 8.48 (m, 3H), 8.04 (d, 1H, $^3J_{HH}$ = 7.7 Hz), 7.85 (d, 2H, $^3J_{HH}$ = 8.5 Hz), 7.78 (d, 1H, $^3J_{HH}$ = 7.4 Hz), 7.42 – 7.35 (m, 2H), 7.28 (d, 1H, $^3J_{HH}$ = 7.3 Hz), 4.61-4.45 (br m, 4H), 4.25 (t, 2H, $^3J_{HH}$ = 6.4 Hz), 3.56 (t, 2H, $^3J_{HH}$ = 6.4 Hz), 3.31 (s, 3H). ^{13}C NMR (126 MHz, $CDCl_3$) δ 198.63, 197.24, 193.10, 135.21, 132.25, 131.55, 129.77, 129.55, 128.66, 128.19, 128.11, 126.42, 123.47, 123.17, 122.68, 69.72, 66.00, 59.02, 58.94, 53.65, 52.18, 52.16, 39.68, 15.42. UV/Vis ($(CH_3)_2CO$) : λ_{max}/nm (ε/ M^{-1} cm^{-1}) 443 (2000), 350 (9400), 344 (9440). HRMS found *m/z* 654.0807, calculated *m/z* 654.0829 for $[C_{24}H_{21}AuClN_3O_3 + Na]^+$. IR (solid. Vmax)/cm-1: 3310, 2957, 2870, 2198, 2032, 1703, 1657, 1591, 1504, 1487, 1474, 1427, 1404, 1381, 1331, 1290, 1238, 1184, 1115, 1059, 1018, 1001, 758, 765, 756, 739, 692, 671, 652, 590, 577, 536, 482, 428, 417, 401.

Glycine ethyl ester

Synthesis of [AuCl(L^{10})]

As for **[AuCl(L^1)]**, but using **L^{10}** LG238 (89 mg, 0.16 mmol), KO^{t}Bu (18 mg, 0.16 mmol) and LG36 (50 mg, 0.16 mmol). The product **[AuCl(L^{10})]** was yielded as a grey solid (82 mg, 79%). ^{1}H NMR (400 MHz, $CDCl_3$) δ 8.59 (d, 1H, *J* = 7.2 Hz), 8.51 (d, 1H, *J* = 7.7 Hz,), 8.40 (d, 1H, *J* = 8.5 Hz), 7.91 (d, 1H, *J* = 7.7 Hz), 7.74 – 7.69 (m, 1H), 7.69 – 7.64 (m, 2H), 7.35 – 7.31 (m, 3H), 4.99 (s, 2H), 4.36 (br. s, 4H), 4.27 (q, 2H, *J* = 7.1 Hz), 1.32 (t, 3H, *J* = 7.1 Hz). ^{13}C NMR (126 MHz, $CDCl_3$) δ 192.11, 168.12, 163.50, 163.00, 143.11, 139.94, 132.23, 131.70, 129.58, 129.54, 129.35, 128.04, 128.00, 127.93, 126.47, 123.47, 122.88, 122.53, 61.82, 53.83, 52.61, 41.73, 14.35. UV/Vis ($(CH_3)_2CO$) : λ_{max}/nm (ε/ M^{-1} cm^{-1}) 444 (240), 351 (11800), 344 (11920). LRMS (ES+) found m/z 683.9; calculated 683.9 for $[C_{25}H_{21}AuClN_3O_4 + Na]^+$. HRMS found *m/z* 641.1445, calculated *m/z* 641.1458 for

$[C_{25}H_{21}AuClN_3O_4 - HCl + NH_4]^+$. IR (solid. Vmax)/cm-1: 2991, 2163, 2001, 1749, 1705, 1659, 1591, 1506, 1476, 1427, 1404, 1386, 1348, 1329, 1287, 1238, 1213, 1182, 1163, 1126, 1032, 980, 953, 787, 758, 691, 669, 650, 588, 563, 482, 455, 417, 409, 403.

1 M. Concepcion Gimeno, *Modern Supramolecular Gold Chemistry: Gold-Metal Interactions and Applications*, Wiley VCH, 2008.

2 H. Schmidbaur and P. J. Sadler, *Appl. Organomet. Chem.*, 2000, **14**, 171–171.

3 N. Greenwood and A. Earnshaw, *Chemistry of the Elements; Copper, Silver and Gold*, Butterworth-Heinemann Ltd, 1997, vol. 1.

4 N. J. Long and C. K. Williams, *Angew. Chemie Int. Ed.*, 2003, **42**, 2586–2617.

5 S. Nobili, E. Mini, I. Landini, C. Gabbiani, A. Casini and L. Messori, *Med. Res. Rev.*, 2010, **30**, 550–580.

6 E. E. Langdon-Jones, S. J. A. Pope, H. J. Mottram, M. P. Coogan, S. J. A. Pope, S. Can, D. H. Vlecken, W. S. Sheldrick, S. Wolfl, I. Ott, C. P. Bagowski, C.-W. Kan, K. S.-Y. Leung and W.-Y. Wong, *Chem. Commun.*, 2014, **50**, 10343.

7 G. C. Fortman and S. P. Nolan, *Organometallics*, 2010, **29**, 4579–4583.

8 M. J. McKeage, L. Maharaj and S. J. Berners-Price, *Coord. Chem. Rev.*, 2002, **232**, 127–135.

9 G. D. Hoke, G. F. Rush, G. E. Bossard, J. V. McArdle, B. D. Jensen and C. K. Mirabelli, *J. Biol. Chem.*, 1988, **262**, 11203–11210.

10 M. N. Hopkinson, C. Richter, M. Schedler and F. Glorius, *Nature*, 2014, **510**, 485–496.

11 A. Igau, H. Gruetzmacher, A. Baceiredo and G. Bertrand, *J. Am. Chem. Soc.*, 1988, **110**, 6463–6466.

12 A. J. Arduengo, R. L. Harlow and M. Kline, *J. Am. Chem. Soc.*, 1991, **113**, 361–363.

13 W. A. Herrmann, M. Elison, J. Fischer, C. Köcher and G. R. J. Artus, *Angew. Chemie Int. Ed. English*, 1995, **34**, 2371–2374.

14 D. Enders and T. Balensiefer, *Acc. Chem. Res.*, 2004, **37**, 534–541.

15 D. Bourissou, O. Guerret, F. P. Gabbaï and G. Bertrand, *Chem. Rev.*, 2000, **100**, 39–92.

16 P. de Frémont, N. Marion and S. P. Nolan, *Coord. Chem. Rev.*, 2009, **253**, 862–892.

17 E. Despagnet-Ayoub and R. H. Grubbs, *J. Am. Chem. Soc.*, 2004, **126**, 10198–10199.

18 F. E. Hahn and M. C. Jahnke, *Angew. Chemie Int. Ed.*, 2008, **47**, 3122–3172.

19 I. Kaljurand, T. Rodima, I. Leito, I. A. Koppel and R. Schwesinger, *J. Org. Chem.*,

2000, **65**, 6202–6208.

20 R. Schwesinger, M. Missfeldt, K. Peters and H. G. von Schnering, *Angew. Chemie - Int. Ed.*, 1987, **26**, 1165.

21 W. A. Herrmann, *Angew. Chemie Int. Ed.*, 2002, **41**, 1290–1309.

22 A. A. Gridnev and I. M. Mihaltseva, *Synth. Commun.*, 1994, **24**, 1547–1555.

23 X. Hu, Y. Tang, P. Gantzel and K. Meyer, *Organometallics*, 2003, **22**, 612–614.

24 R. Dorta, E. D. Stevens, N. M. Scott, C. Costabile, L. Cavallo, C. D. Hoff and S. P. Nolan, *J. Am. Chem. Soc.*, 2005, **127**, 2485–2495.

25 R. W. Alder, M. E. Blake, C. Borlotti, S. Bufali, C. P. Butts, E. Linehan, J. M. Oliva, A. G. Orpen and M. J. Quayle, *Chem. Commun.*, 1999, **3**, 241–242.

26 W. A. Herrmann, O. Runte and G. R. J. Artus, *J. Organomet. Chem.*, 1995, **501**, C1–C4.

27 A. J. Arduengo, H. V. Rasika Dias, J. C. Calabrese and F. Davidson, *J. Am. Chem. Soc.*, 1992, **114**, 9424–9425.

28 P. L. Arnold and S. T. Liddle, *Chem. Commun.*, 2006, **38**, 3959–3971.

29 H. Braband, T. I. Kuckmann and U. Abram, *J. Organomet. Chem.*, 2005, **690**, 5421–5429.

30 G. J. Higby, *Gold Bull*, 1982, **15**, 130–140.

31 C. F. Shaw III, *Chem. Rev.*, 1999, **99**, 2589–2600.

32 P. J. Sadler, *Struct. Bond.*, 1976, **29**, 171–219.

33 W. F. Kean, F. Forestier, Y. Kassam, W. W. Buchanan and P. J. Rooney, *Semin. Arthritis Rheum*, 1985, **14**, 180–186.

34 K. D. Mjos and C. Orvig, *Chem. Rev.*, 2014, **114**, 4540–4563.

35 S. J. Berners-Price, A. Filipovska, A. Myers, R. Tarrien, R. Levine, R. Scott, W. T. Self, C. Severini, E. Hansell, G. Lau, J. Langille, M. Olsen, L. Qin, R. Skerlj, R. S. Y. Wong, Z. Santucci and J. H. McKerrow, *Metallomics*, 2011, **3**, 863.

36 A. J. Lewis and D. T. Walz, *Prog. Med. Chem.*, 1982, **19**, 1–58.

37 E. R. T. Tiekink, *Crit. Rev. Oncol. Hematol.*, 2002, **42**, 225–248.

38 S. S. Gunatilleke and A. M. Barrios, *J. Med. Chem.*, 2006, **49**, 3933–3937.

39 E. E. Langdon-Jones, D. Lloyd, A. J. Hayes, S. D. Wainwright, H. J. Mottram, S. J. Coles, P. N. Horton and S. J. A. Pope, *Inorg. Chem.*, 2015, **54**, 6606–6615.

40 B. A. Stanley, V. Sivakumaran, S. Shi, I. McDonald, D. Lloyd, W. H. Watson, M. A. Aon and N. Paolocci, *J. Biol. Chem.*, 2011, **286**, 33669–33677.

41 C. F. Williams, N. Yarlett and M. A. Aon, *Mol. Biochem. Parasitol.*, 2014, **196**, 45–52.

42 T. V. Serebryanskaya, A. S. Lyakhov, L. S. Ivashkevich, J. Schur, C. Frias, A. Prokop and I. Ott, *Dalt. Trans.*, 2015, **44**, 1161–1169.

43 K. Becker, S. Gromer, R. H. Schirmer and S. Muller, *Eur. J. Biochem.*, 2000, **267**, 6118–6125.

44 J. R. Roberts and C. F. Shaw, *Biochem. Pharmacol.*, 1998, **55**, 1291–1299.

45 J. Chaudiere and A. L. Tappel, *J. Inorg. Biochem.*, 1984, **20**, 313–325.

46 P. J. Sadler and Z. Guo, *Pure Appl. Chem.*, 1998, **70**, 863–871.

47 O. M. Ni Dhubhghaill and P. J. Sadler, *Gold Complexes in Cancer Chemotherapy*, Weinheim, VCH, 1993.

48 C. K. Mirabelli, C. M. Sung, J. P. Zimmerman, D. T. Hill, S. Mong and S. T. Crooke, *Biochem. Pharmacol.*, 1986, **35**, 1427–1433.

49 L. Engman, M. McNaughton, M. Gajewska, S. Kumar, A. Birmingham and G. Powis, *Anticancer Drugs*, 2006, **17**, 539–544.

50 P. Nguyen, R. T. Awwad, D. D. Smart, D. R. Spitz and D. Guis, *Cancer Lett*, 2006, **236**, 164–174.

51 T. M. Grogan, C. Fenoglio-Prieser, R. Zeheb, W. Bellamy, Y. Frutiger, G. Vela, E. Stemmerman, J. Macdonald, L. Richter, A. Gallegos and G. Powis, *Hum. Pathol.*, 2000, **31**, 475–481.

52 J. Raffel, A. K. Bhattacharyya, A. Gallegos, H. Cui, J. G. Einspahr, D. S. Alberts and G. Powis, *J. Lab. Clin. Med.*, 2002, **142**, 46–51.

53 S. Gromer, L. D. Arscott, C. H. Williams, R. H. Schirmer and K. Becker, *J. Biol. Chem.*, 1998, **273**, 20096–20101.

54 M. P. Rigobello, L. Messori, G. Marcon, M. Agostina Cinellu, M. Bragadin, A. Folda, G. Scutari and A. Bindoli, *J. Inorg. Biochem.*, 2004, **98**, 1634–1641.

55 M. P. Rigobello, G. Scutari, R. Boscolo and A. Bindoli, *Br. J. Pharmacol.*, 2002, **136**, 1162–1168.

56 Y. Omata, M. Folan, M. Shaw, R. L. Messer, P. E. Lockwood, D. Hobbs, S. Bouillaguet, H. Sano, J. B. Lewis and J. C. Wataha, *Toxicol. Vitr.*, 2006, **20**, 882–890.

57 C. Marzano, V. Gandin, A. Folda, G. Scutari, A. Bindoli and M. P. Rigobello, *Free Radic Biol Med*, 2007, **42**, 872–881.

58 C. K. Mirabelli, R. K. Johnson, D. T. Hill, L. F. Faucette, G. R. Girard, G. Y. Kuo, C. M. Sung and S. T. Crooke, *J. Med. Chem.*, 1986, **29**, 218–223.

59 M. J. McKeage, P. Papathanasiou, G. Salem, A. Sjaarda, G. F. Swiegers, P. Waring and S. B. Wild, *Met. Based. Drugs*, 1998, **5**, 217–23.

60 P. Papathanasiou, G. Salem, P. Waring and A. C. Willis, *J Chem Soc Dalt. Trans*, 1997, **19**, 3435–3443.

61 A. Vogler and H. Kunkely, *Coord. Chem. Rev.*, 2001, **219**, 489–507.

62 A. Castiñeiras, N. Fernández-Hermida, R. Fernández-Rodríguez and I. García-Santos, *Cryst. Growth Des.*, 2012, **12**, 1432–1442.

63 L. A. Mullice, H. J. Mottram, A. J. Hallett and S. J. A. Pope, *Eur. J. Inorg. Chem.*, 2012, **2012**, 3054–3060.

64 S. E. Thwaite, A. Schier and H. Schmidbaur, *Inorg. Chim. Acta.*, 2004, **357**, 1549–1557.

65 J. C. Y. Lin, S. S. Tang, C. S. Vasam, W. C. You, T. W. Ho, C. H. Huang, B. J. Sun, C. Y. Huang, C. S. Lee, W. S. Hwang, A. H. H. Chang and I. J. B. Lin, *Inorg. Chem.*, 2008, **47**, 2543–2551.

66 L. A. Mullice, F. L. Thorp-Greenwood, R. H. Laye, M. P. Coogan, B. M. Kariuki, S. J. A. Pope, G. Accorsi, F. Barigelletti, C. S. Lee, W. S. Hwang, A. H. H. Chang and I. J. B. Lin, *Dalt. Trans.*, 2009, **360**, 6836.

67 A. Meyer, C. P. Bagowski, M. Kokoschka, M. Stefanopoulou, H. Alborzinia, S. Can, D. H. Vlecken, W. S. Sheldrick, S. Wölfl and I. Ott, *Angew. Chemie Int. Ed.*, 2012, **51**, 8895–8899.

68 R. G. Balasingham, C. F. Williams, H. J. Mottram, M. P. Coogan and S. J. A. Pope, *Organometallics*, 2012, **31**, 5835–5843.

69 C. P. Bagowski, Y. You, H. Scheffler, D. H. Vlecken, D. J. Schmitz, I. Ott, L. I. Partecke, C. D. Heidecke, M. M. Lerch, C. P. Bagowski, M. Y. Geng, Y. J. Cai and J. Ding, *Dalt. Trans.*, 2009, **99**, 10799–10805.

70 I. J. Lin and C. S. Vasam, *Can. J. Chem.*, 2005, **83**, 812–825.

71 F. Bonati, A. Burini, B. R. Pietroni and B. Bovio, *J. Organomet. Chem.*, 1989, **375**, 147–160.

72 P. J. Barnard, M. V. Baker, B. W. Skelton, A. H. While and S. J. Berners-Price, *J. Inorg. Biochem.*, 2003, **96**, 99.

73 P. J. Barnard, M. V. Baker, S. J. Berners-Price and D. A. Day, *J. Inorg. Biochem.*,

2004, **98**, 1642–1647.

74 İ. Özdemir, A. Denizci, H. T. Öztürk and B. Çetinkaya, *Appl. Organomet. Chem.*, 2004, **18**, 318–322.

75 S. K. Schneider, W. A. Herrmann and E. Herdtweck, *Zeitschrift für Anorg. und Allg. Chemie*, 2003, **629**, 2363–2370.

76 M. V. Baker, P. J. Barnard, S. J. Berners-Price, S. K. Brayshaw, J. L. Hickey, B. W. Skelton and A. H. White, *Dalt. Trans.*, 2006, **0**, 3708–3715.

77 P. J. Barnard, M. V. Baker, S. J. Berners-Price, B. W. Skelton, A. H. White, A. J. P. White, D. J. Williams, A. H. White, B. W. Skelton and S. T. Crooke, *Dalt. Trans.*, 2004, **327**, 1038–1047.

78 M. V. Baker, P. J. Barnard, S. J. Berners-Price, S. K. Brayshaw, J. L. Hickey, B. W. Skelton and A. H. White, *J. Organomet. Chem.*, 2005, **690**, 5625–5635.

79 R. Rubbiani, E. Schuh, A. Meyer, J. Lemke, J. Wimberg, N. Metzler-Nolte, F. Meyer, F. Mohr, I. Ott, A. Casini, A. Prokop, S. Wölfl and I. Ott, *Medchemcomm*, 2013, **4**, 942–948.

80 J. L. Hickey, R. A. Ruhayel, P. J. Barnard, M. V. Baker, S. J. Berners-Price and A. Filipovska, *J. Am. Chem. Soc.*, 2008, **130**, 12570–12571.

81 C. Saturnino, I. Barone, D. Iacopetta, A. Mariconda, M. S. Sinicropi, C. Rosano, A. Campana, S. Catalano, P. Longo and S. Andò, *Future Med. Chem.*, 2016, **8**, 2213–2229.

82 R. Visbal, V. Fernández-Moreira, I. Marzo, A. Laguna, M. C. Gimeno, B. M. Stoltz, J. E. Bercaw, K. I. Goldberg, M. H. de Jager, G. M. M. Groothuis, M. Picquet, A. Casini, A. Melnick, P. Huang, A. Wiestner and K. N. Bhalla, *Dalt. Trans.*, 2016, **45**, 15026–15033.

83 M. C. Gimeno, A. Laguna and R. Visbal, *Organometallics*, 2012, **31**, 7146–7157.

84 J. L. Hickey, R. A. Ruhayel, P. J. Barnard, M. V. Baker, S. J. Berners-Price and A. Filipovska, *J. Am. Chem. Soc.*, 2008, **130**, 12570–12571.

85 C. K. Mirabelli, B. D. Jensen, M. R. Mattern, C. M. Sung, S. M. Mong, D. T. Hill, S. W. Dean, P. S. Schein, R. K. Johnson and S. T. Crooke, *Anticancer Drug Des.*, 1986, **1**, 223–234.

86 P. J. Sadler and R. E. Sue, *Met. Based. Drugs*, 1994, 107–144.

87 A. Citta, E. Schuh, F. Mohr, A. Folda, M. L. Massimino, A. Bindoli, A. Casini and M. P. Rigobello, *Metallomics*, 2013, **5**, 1006–1015.

88 B. Bertrand, A. de Almeida, E. P. M. van der Burgt, M. Picquet, A. Citta, A. Folda, M. P. Rigobello, P. Le Gendre, E. Bodio and A. Casini, *Eur. J. Inorg. Chem.*, 2014, **27**, 4523–4528.

89 A. Meyer, L. Oehninger, Y. Geldmacher, H. Alborzinia, S. Wölfl, W. S. Sheldrick and I. Ott, *ChemMedChem*, 2014, **9**, 1794–1800.

90 K. N. de Oliveira, P. Costa, J. R. Santin, L. Mazzambani, C. Bürger, C. Mora, R. J. Nunes and M. M. de Souza, *Bioorg. Med. Chem.*, 2011, **19**, 4295–4306.

91 R. Stolarski, *Fibres Text. East. Eur.*, 2002, **71**, 91.95.

92 P.-H. Lanoë, J. Chan, G. Gontard, F. Monti, N. Armaroli, A. Barbieri and H. Amouri, *Eur. J. Inorg. Chem.*, 2016, **2016**, 1631–1634.

93 A. Vellé, A. Cebollada, R. Macías, M. Iglesias, M. Gil-Moles and P. J. Sanz Miguel, *ACS Omega*, 2017, **2**, 1392–1399.

94 E. E. Langdon-Jones, N. O. Symonds, S. E. Yates, A. J. Hayes, D. Lloyd, R. Williams, S. J. Coles, P. N. Horton and S. J. A. Pope, *Inorg. Chem.*, 2014, **53**, 3788–3797.

95 S. Banerjee, E. B. Veale, C. M. Phelan, S. A. Murphy, G. M. Tocci, L. J. Gillespie, D. O. Frimannsson, J. M. Kelly, T. Gunnlaugsson, J. Kluza, D. Hochhauser, J. A. Hartley, M. Lee, F. Darro, R. Kiss, R. J. Diamond, R. J. McRipley, R. J. Page and J. L. Gross, *Chem. Soc. Rev.*, 2013, **42**, 1601–1618.

96 A. C. Allison, *J. Clin. Pathol. Suppl. (R. Coll. Pathol).*, 1974, **7**, 43–50.

97 E. Anton, D. Brandes and S. Barnard, *Anat. Rec.*, 1969, **164**, 231–251.

98 R. Halaby, *Breast Cancer Res.*, 2001, **1**, 4.

99 O. V. Dolomanov, L. J. Bourhis, R. J. Gildea, J. A. K. Howard, H. Puschmann, S. K., W. L., P. G. and S. R., *J. Appl. Crystallogr.*, 2009, **42**, 339–341.

100 G. M. Sheldrick, *Acta. Cryst.*, 2015, **71**, 3–8.

101 G. M. Sheldrick, *Acta. Cryst.*, 2015, **A71**, 3–8.

Chapter 3 - Fluorophore-Labelled Substituted Phosphinites and Aminophosphine Ligands and their Gold(I) Complexes: Syntheses, Photophysics and X-Ray Structure

3.1 Introduction

3.1.1 Phosphines

The chemistry of phosphorus has for some time been of invaluable importance due to its potential for use in an extreme breadth of applications, from consumer industry to biological and medicinal applications.[1] For these reasons, it accounts for a major branch of chemistry in today's society. The ground state valence electronic configuration of phosphorus is $3s^2$, $3p_x^1$, $3p_y^1$, $3p_z^1$, which allows its involvement in ambivalent bonding (tri- and pentavalent), as well as access to a range of different bonding modes. The pyramidal geometry for trivalent phosphorus atoms is of particular significance. Stable trivalent tricoordinate compounds are formed with a variety of other elements, for example hydrogen, carbon, nitrogen, oxygen, sulphur and halogens and are a class of P(III) compounds related to the parent compound, PH_3.[1]

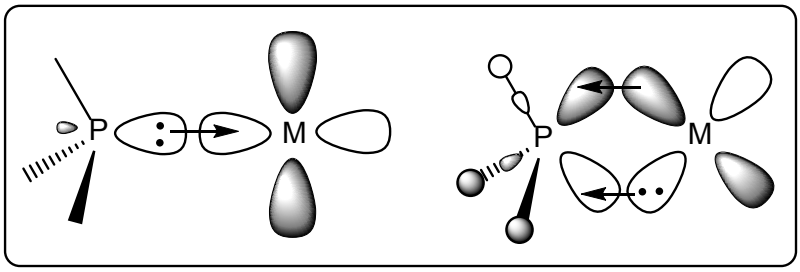

Figure 3.1: Orbital interactions and bonding of PR_3 donors with d-block metals. Left: σ bonding. Right: π backbonding

Primary, secondary and tertiary phosphines are classified according one (PH_2R), two (PHR_2) or three (PR_3) R group substituents, respectively. Phosphines and their corresponding applications make up an extensive proportion of phosphorus chemistry, for example showing promising potential in semiconductor industries.[2,3] In addition, their contribution to the development, understanding and utility of organometallic chemistry is of particular importance due to numerous catalytic applications.[1]

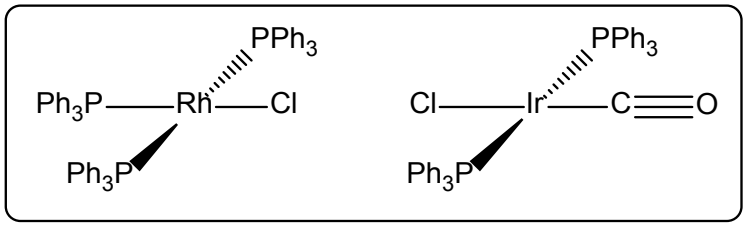

Figure 3.2: Wilkinson's catalyst (left) and Vaska's complex (right)

In organometallic chemistry, phosphine ligands are classed as σ-donors, with relatively weak π-acceptor character, where the donating and accepting properties vary according to the nature of the substituents on the phosphorus atom (Figure 3.1).[4,5] Phosphorus has been involved in many well documented organometallic literature examples, for example Wilkinson's catalyst ([$RhCl(PPh_3)$]), Vaska's complex ([$IrCl(CO)(PPh_3)_2$]) (Figure 3.2) and Kagan's phosphine [$Fe(CpPPh_2)\{1,2\text{-}Cp(PPh_2)(C^*HMe(NMe_2))\}$].[6,7] In more recent work, ferrocenyl ligands containing phosphine moieties have been utilised as homogenous enantioselective hydrogenation catalysts.[8] In addition, water soluble phosphines have been shown to have biomedical applications, for example Katti *et al.* reported a wide range of phosphine ligands and complexes,[9] which also found uses in asymmetric hydrogenation and hydrovinylation reactions.[10,11]

3.1.2 Aminophosphines

Aminophosphines (also referred to as phosphanamines, phosphazanes or phosphinous amides) are classed as a tricoordinate P(III) centre bound to a tricoordinate N(III) centre.[1] Michaelis discovered the first example of an aminophosphine in 1903.[12] Due to the possibility of manipulation on both the phosphorus and the nitrogen atom, aminophosphines are hugely important in organometallic chemistry.[13] However, there are currently no examples of aminophosphine metal complexes where both the nitrogen and the phosphorus coordinate to the metal. Structural variety of aminophosphines is also important, where cyclic, cage, polymeric and supramolecular P-N networks have been described.[14–16] It is also worth noting that P-unsubstituted phosphinous amides H_2PNR_2 are extremely rare, with the exception of the documented compounds $H_2PN(SiMe_3)_2$[17] and $H_2PN(CF_3)_2$.[18,19] In terms of their reactivity, the presence of a lone pair on the adjacent nitrogen atom increases the nucleophilicity of the phosphorus, but

the extent of this is not comparable to the alpha effect observed for N-N and N-O nucleophiles.[20] It is thought that the increase in nucleophilicity is due to the repulsive interaction between the N and P lone pairs, thus raising the energy to cause higher levels of basicity and nucleophilicity.[21]

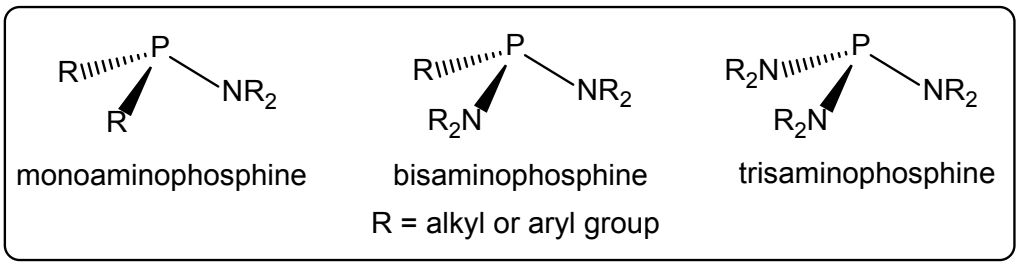

Figure 3.3: Structural representation of aminophosphines

Synthesis of aminophosphines involves the creation of one, two or three P-N bonds around a trivalent phosphorus centre, as shown in Figure 3.3. There are three main synthetic methods: condensation, scrambling and transamination, where the condensation route is the most widely used.[1] This reaction usually involves a phosphorus(III) halide (most commonly phosphorus trichloride) and a primary or secondary amine.[22–29] The synthesis is considered to be of relative ease for three main reasons: i) cost, availability and reactive nature of starting materials; ii) the common byproduct, amine hydrochloride, is relatively easy to separate from the product; and iii) suitable reaction conditions can be chosen in order to exert control over product formation. Reaction conditions that can be altered accordingly include temperature, time, solvent, mole ratio, mode of addition of the reagents and presence of a hydrogen chloride scavenger.[1] Reaction temperatures have been found to range from -40 to 100 °C, and aliphatic amino groups react more readily than aromatic and heteroaromatic moieties due to enhanced nucleophilicity.[13] Information on the breadth of this synthetic method is shown in Figure 3.4, where Grignard reactions are typically used to form P-Ph bonds.[1] A scrambling reaction between a tris(amino)phosphine and phosphorus trichloride is another synthetic possibility, and usually leads to the formation of amino(chloro)phosphines, $(R_2N)_xPCl_{3-x}$ (x= 1, 2).[30,31] An additional variation of a scrambling reaction, known as transamination, is observed when a tris(amino)phosphine is treated with a primary or secondary amine. Although this synthetic method is reasonably well understood, desired products only form when the

product amine is a volatile compound. For this reason, transamination has been used for the synthesis of tris(dimethylamino)phosphine and tris(diethylamino)phosphine.[32,33]

Alternatively, aminophosphines can be prepared by exploiting the high affinity between silicon and halogen atoms. In this case, reactions between halophosphines and *N*-(trimethylsilyl)anilines, *N*-(trimethylsilyl)amides or *N*-(trimethylsilyl)ureas and thioureas have been carried out, where the P-N bond and a halosilane are formed *in situ*.[34–37] Despite being thermally stable, the majority of aminophosphines exhibit sensitivity to air oxidation; hence they require a dry and inert atmosphere for their preparation, handing and storage. This routinely requires the use of Schlenk techniques, inert atmosphere manipulations and vacuum line techniques for safe handling.[38,39]

^{31}P NMR spectroscopy is an extremely important technique when identifying organophosphorus compounds, specifically aminophosphines, as reaction products.[40] Here, the chemical shift values are dependent upon a number of characteristics associated with the central phosphorus atom: i) nature; ii) electronegativity; iii) sterics; iv) π-bonding effects or the phosphorus substituents and v) bond angles. For example, upon replacement of a chloro group with an amino group, the chemical shift values are shifted upfield due to shielding.[1] With reference to NMR, it is also worth noting that low temperature ^{1}H NMR (-65 °C) has detected hindered rotation around the P-N bond for tetrasubstituted phosphorus amides.[41] In this work, different environments were observed for two Me_3Si groups in the compound $Ph_2PN(SiMe_3)_2$, where the activation energy for rotation was 10.2 kcal mol^{-1}.[42]

Despite the sensitivity of P(III)-N bonds, aminophosphines are involved in a wide variety of applications, for example as essential materials for day-to-day life.[1] In this vein, $P(NMe_2)_3$ has been found to catalyse the production of polyethers from the reaction between thiodiglycol and triethylene glycol, where shorter reaction times and improved product yields are observed in comparison to traditional methods. Aminophosphines have also found applications as both inorganic heterocycles[43] and synthons.[44] They have also been found to possess antimicrobial activity.[45] In addition, gallium phosphide (GaP) thin film depositions using trimethyl gallium and $P(NMe_2)_3$ have been indicated to be suitable for use in optoelectronic materials.[46]

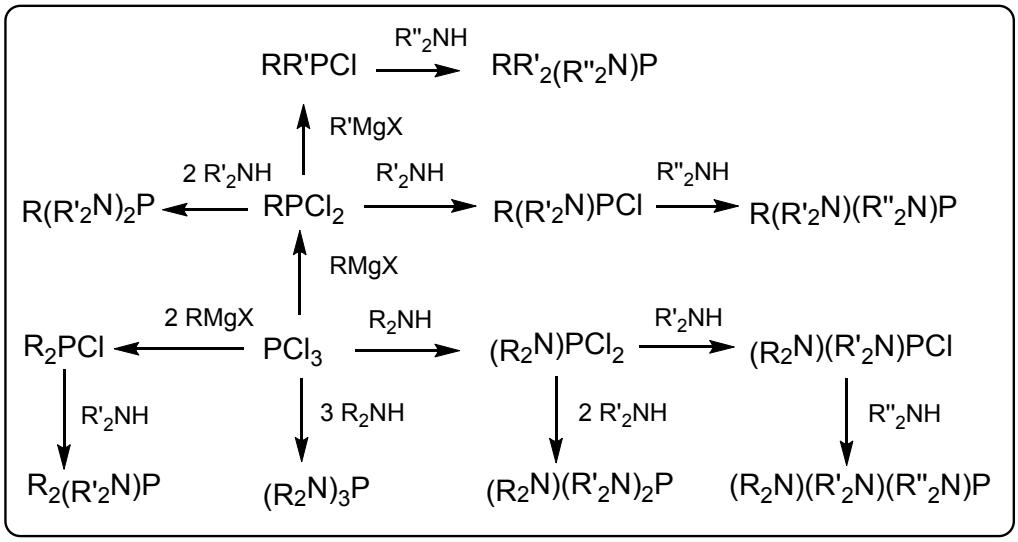

Figure 3.4: Condensation reactions for formation of aminophosphines[1]

In comparison to phosphines, the coordination chemistry of aminophosphines is under explored. However, it is commonly seen that upon the synthesis of a novel aminophosphine, the preparation of the corresponding metal complex is explored.[47] In particular, a significant contribution to this developing area of research has been made by Woollins and coworkers, amongst others.[48–51] This has given rise to a huge breadth of exploration of organometallic aminophosphine complexes.

For monodentate aminophosphine ligands, the cone created by the phosphorus ligand is a significant factor when it comes to investigating the steric crowding around a central metal atom, and is referred to as the Tolman cone angle.[52] Variation of this angle thus dictates the coordination number of the complex, and therefore is reflected in the potential catalytic activity of the final complex. For this reason, catalytic activity can be tuned depending on the nature of the substituent on the nitrogen atom of the aminophosphine. For bidentate ligands, the catalytic activity of a metal complex can be partly determined by the bite angle.[53,54] As mentioned above, despite the possibility to exploit the donor capabilities of both the nitrogen and the phosphorus atom, there are to date no examples of metals being bound *via* the nitrogen centre. It is thought that this is due to the nitrogen lone pair's involvement in negative hyperconjugation with phosphorus orbitals. In addition, most of the literature displays the soft nature of aminophosphine ligands where they coordinate with soft metal centres, for example

Cu(I), Mo(0), Ru(I), Ru(II), Ir(I) and Au(I). Work by Dixon *et al*. demonstrated that the electronic properties of a metal complex can be drastically altered when appropriate changes to the P substituent on an aminophosphine are made.[55] A variety of [Ru(terpyridine)(bipyridine)L]$^{2+}$ (L = aminophosphine, phosphine or phosphite) were prepared and their electronic properties investigated using cyclic voltammetry , UV-vis and luminescence spectroscopy, all of which demonstrated appreciable differences. In addition, these complexes showed luminescence at 77 K in an alcoholic matrix and lifetimes originating from ^{3}MLCT states (3.5 – 5.5 μs).

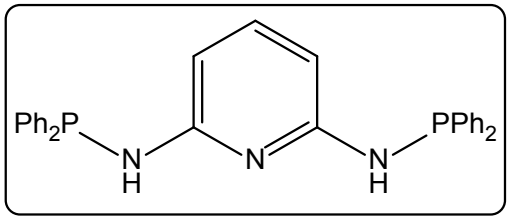

Figure 3.5: N,N-bis(diphenylphosphino)-2,6-diaminopyridine (PNP)

The most explored application of organometallic compounds containing an aminophosphine ligand is catalysis, particularly of organic reactions.[13] For example, the ligand N,N-bis(diphenylphosphino)-2,6-diaminopyridine (PNP), shown in Figure 3.5, has been used in the preparation of complexes of the type [M(PNP)]Cl·L (M = Ni, L = H_2O; M = Pd, L = EtOH, M = Pt) and mer-[M(NPN)$(CO)_3$]·2THF (M = Cr, Mo, W). These complexes have been used as catalysts in the hydrogenation of styrene to ethylbenzene.[56] It is also well established that the oxidative addition step of the Suzuki-Miyaura reaction is accelerated by the use of electron rich phosphanes, making aminophosphines ideal candidates due to their strong σ-donor ligand ability.[13] Chiral aminophosphines have also been found to be useful catalysts for enantioselective allylic alkylation reactions.[57] In addition, Gilbertson *et al.* developed a range of iridium complexes based on enantio-enriched aminophosphine ligands, which were found to catalyse the asymmetric hydrogenation reactions of C=C and C=O bonds.[58] Other reaction types include asymmetric 1,4-addition to enones[59] and asymmetric hydrosilylation.[60]

3.1.3 Fluorescent Phosphines

In Chapter 2, new ligand architectures were developed that are able to impart fluorescence properties upon a coordination complex. Aminophosphines present a class of compounds that are extremely under-explored in this area. However Zhang and co-workers reported a series of papers in the early 2000s that described the Au(I) coordination chemistry of anthracene-based aminophosphine ligands together with their fluorescence properties.[61–63] In the most recent of these works, Zhang developed a range of novel gold(I) η^2-arene complexes with arm-closing configurations and hence weak fluorescence emission (structured profile between 400 and 450 nm) attributed to charge transfer from the anthracene unit to the Au^+ ion. When these complexes were reacted with one equivalent of triphenylphosphine in dichloromethane, an arm-opening configuration was formed and a stronger emission was observed.[63] Research into fluorescent phosphine-based ligands is also relatively under-developed. One example comes from Higham, who developed a range of Bodipy-tagged systems with desirable photophysical properties common to the Bodipy scaffold (λ_{em} = 526 – 532)[64], and have been successfully applied to cell imaging studies (Figure 3.6)[65]. In other work, it was seen that the Au(I) complexes of Bodipy-phosphine dyads have been investigated in gold-catalysed alkyne transformations.[66]

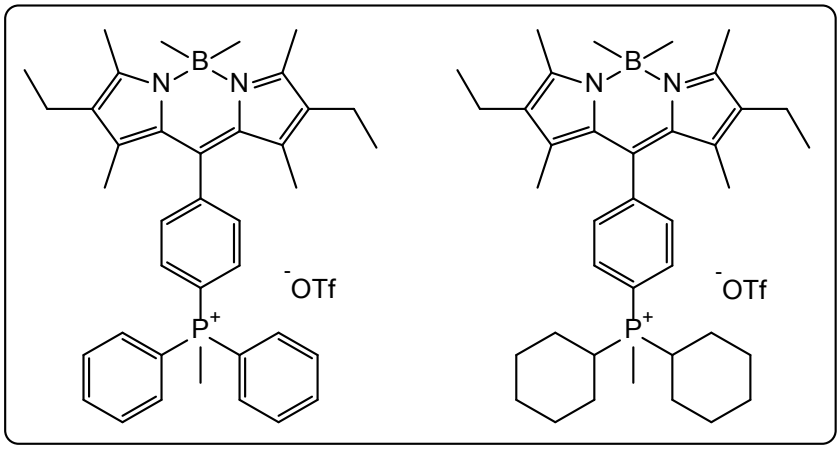

Figure 3.6: BODIPY derivatives for imaging of mitochondrial dysfunction in cancer and heart cells[65]

In recent work, Gabbai has demonstrated that a fluorescein-functionalised tertiary phosphine can be used as a "sensor" for Au(III) ions by modulating photoinduced electron transfer between the phosphorus atom and fluorophore.[67] Other examples of fluorophore-functionalised phosphines have attempted to manipulate the reactivity of phosphorus in the detection of reactive oxygen species (ROS).[68–71] Similar approaches utilising aminophosphine architectures have not been widely reported.

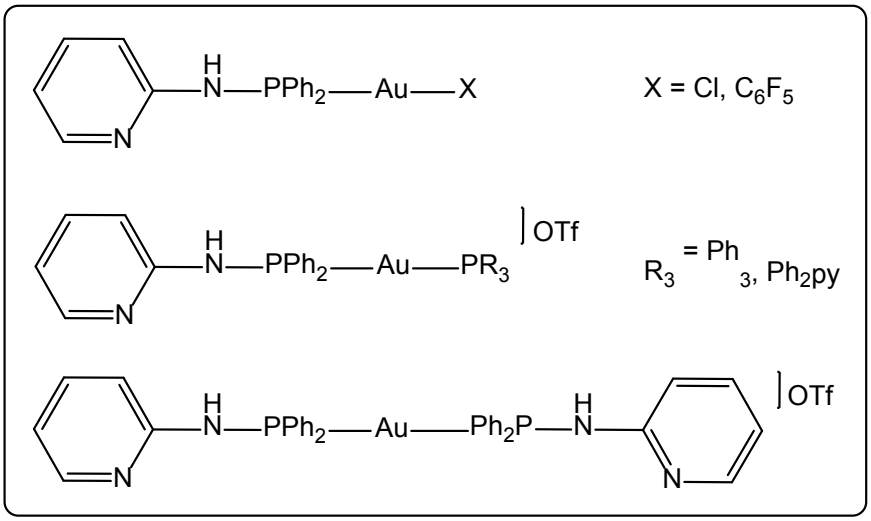

Figure 3.7: Anti-bacterial aminophosphine Au(I) complexes[72]

Aminophosphine complexes of Au(I) and Ag(I) have also been reported, and have shown anti-bacterial activity against Gram-negative *Salmonella enterica* serovar *typhimurium* and *Echerrichia coli* and Gram-positive *Listeria monocytogenes* and *Staphylococcus aureus* (Figure 3.7).[72] The bacterial assays showed effectiveness of all novel Au(I) compounds, comparable to reference antibiotics.

3.1.4 Phosphinites

In addition to aminophosphines, phosphinites (R_2POR) comprise an important family of ligands for organometallic chemistry. Although transition metal complexes incorporating tertiary phosphines and phosphites have a more developed history, phosphinites and phosphonites ($RP(OR)_2$) have recently received increased levels of attention.[73] Phosphinites differ from phosphines, phosphonites and phosphites in the number of P-C and P-O bonds (Figure 3.8). Electronic and steric parameters rank

phosphinites between phosphines and phosphonites bearing the same substituents. The nature of these parameters can in part be measured by studying the Tolman cone angle,[52] which decreases from 132° (phosphine) to 109° for R=Et, and from 118° to 107° for R=Me, with intermediate values predicted for the phosphinite and phosphonite.[52,74,75] When compared to other organophosphorus ligands, additional benefits are observed due to the tunable nature of the donor-acceptor ability and ligand topology of phosphinites.[76] For example, the π-acceptor ability of the ligands is predicted to decrease in the order $P(OR)_3 > RP(OR)_2 > R_2P(OR) > R_3P$, especially for small R groups where steric effects are negligible. The electronegativity of OR groups lowers the energy of the empty 3d orbitals of phosphorus, thus enhancing the π-acceptor properties. As OR groups stabilise the σ-donor orbitals, σ-bonding tendencies should reverse the order of the series, where R_3P ligands are the best.[73] However, when steric and metal-ligand combination effects are considered, a complex picture emerges and generalizations can become somewhat unreliable. For this reason, explicit consideration of the aforementioned factors and comparison of closely related compounds must be explored before planning applications, for example in homogenous catalysis.[73]

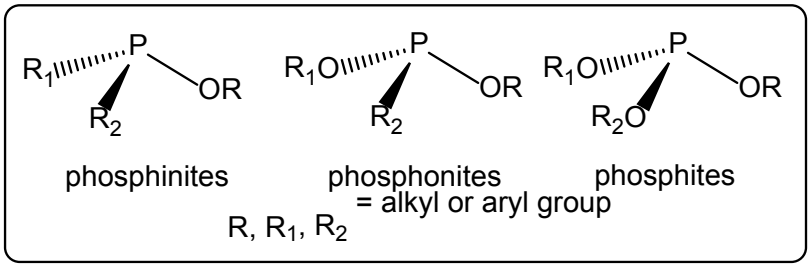

Figure 3.8: Structures of some P-O containing compounds

When compared to phosphine ligands, the synthesis of phosphinite ligands relatively simple, and most commonly involves mixing ROH and R'R''PCl with a base such as Et_3N or DMAP.[76] This method was recently utilised by Diez-Gonzalez *et al*., who synthesised a range of phosphonites and phosphinite ligands for Cu(I) complexes suitable for Click azide-alkyne cycloaddition catalysis.[77] The synthesis, structures and ^{31}P NMR shifts are displayed in Figure 3.9. In addition, stronger bases such as NaH or *n*-BuLi can be required when a sterically crowded phosphorus centre is present. In a less common synthetic method, a Grignard reagent is reacted with methoxy chlorophosphines[78] or substituted

aryls are lithiated and treated with aminodichlorophosphine in the first step, followed by methanolysis.[79]

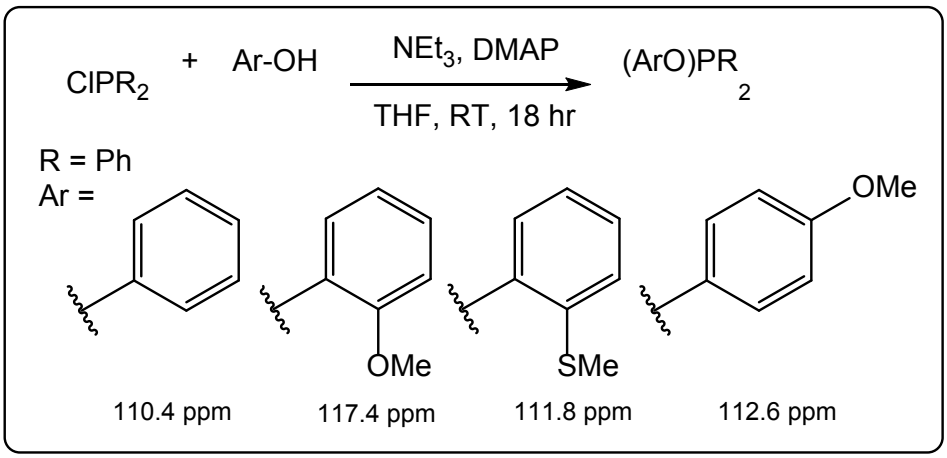

Figure 3.9: Synthesis, structures and ^{31}P NMR shifts of compounds by Diez-Gonzalez et al.[77]

The simplicity of synthesis of phosphinite ligands, as well as the low cost of starting materials means they have found application in transition metal catalysis, sometimes being used as attractive surrogates for previously investigated phosphines.[76] For example, (*t*-Bu)$_2$PO(*n*-Pr) was used to replace the more expensive but sterically similar phosphine ligand Ad$_2$P(*n*-Bu) (Ad = 1-adamantyl) in the palladium catalysed reductive carbonylation of aryl bromides, where catalytic activity was not compromised.[80] One of the earliest examples of phosphinite ligands in catalysis involved the use of diphenylphosphinite derived from (S,S)-trans-1,2-cyclohexanediol in the Rh(I)-catalysed asymmetric hydrogenation of alkenes.[81] Phosphinites have been found to be less susceptible to hydrolysis when compared to phosphites and phosphonites. However, π-acceptor capability is still maintained, which leads to advantages for catalytic activity.[76] For example, DuPont employed phosphites as supporting ligands for the nickel-catalysed hydrocyanation of butadiene and 4-pentenenitrile, but other organophosphorus compounds were sought as alternatives due to their tendency to be hydrolysed by adventitious water.[82] In relation to this, Pringle *et al.* discovered that phospha-adamantane-based phosphonites were very effective for the desired hydrocyanation reaction and stable to air and moisture.[83] A large number of chiral phosphinite ligands have also been developed due to the ready availability of chiral alcohols, including carbohydrates.[73,84–86] Optically active bidentate ligands with phosphine and phosphonate moieties have also been developed, but they require more

difficult synthetic protocols.[87] In addition to this, aminophosphine phosphinites have been developed as chiral precatalysts and used in asymmetric catalysis.[88]

Phosphinites have also been used to construct catalytically active metallacyclic compounds of two discrete classes: monometallacyclic phosphinite complexes and phosphinite-based pincer complexes.[76] One article describes the synthesis of a tetranuclear gold(I) metallacycle containing bridging thiolate ligands and a phosphinous acid/phosphinite ligand combination, the latter of which gives rise to additional bridging through strong hydrogen bonding.[89] Organic transformations such as the Mitsunobu reacton and the Arbuzov reaction have also employed phosphinites.[90,91] Notable metal catalysed transformations that have utilised phosphinite ligands include hydrogenation, transfer hydrogenation, Suzuki-Miyaura coupling, Mizoroki-Heck coupling, hydroformylation and allylation.[76,92]

3.2 Aims

This chapter describes the development of the synthesis of of a range of novel, fluorescent aminophosphine and phosphinite ligands and their corresponding Au(I) complexes. The desired compounds incorporate naphthyl (**L1**), pyrenyl (**L2**) and anthraquinone (**L3** and **L4**) chromophores into their structures. It was thought that the ligands would react with [AuCl(tht)] (tht = tetrahydrothiophene) to give monometallic complexes of the form [AuCl(**L**)], as well as the possibility of a dimetallic complex [Au_2Cl_2(**L**)]. Another aim was to design a synthetic protocol for phosphinite compounds incorporating anthracene (**L5**) and pyrene (**L6**), and for their Au(I) chemistry to be investigated. Among other techniques, ^{31}P NMR spectroscopy would be utilised to confirm formation of products.

The difference in photophysical properties between ligands and complexes would also be important due to the presence of a range of fluorophores within the chapter. Solid state X-ray crystallographic data would also be obtained to consider the coordination geometry of the resulting Au(I) compounds, as well as to study interactions between different moieties comprising the complexes. In addition, supporting TD-DFT calculations would be computed to assist and inform the assignments of the electronic transitions noted from experimental observations.

3.3 Results and Discussion

3.3.1 Synthesis of Ligands and Complexes

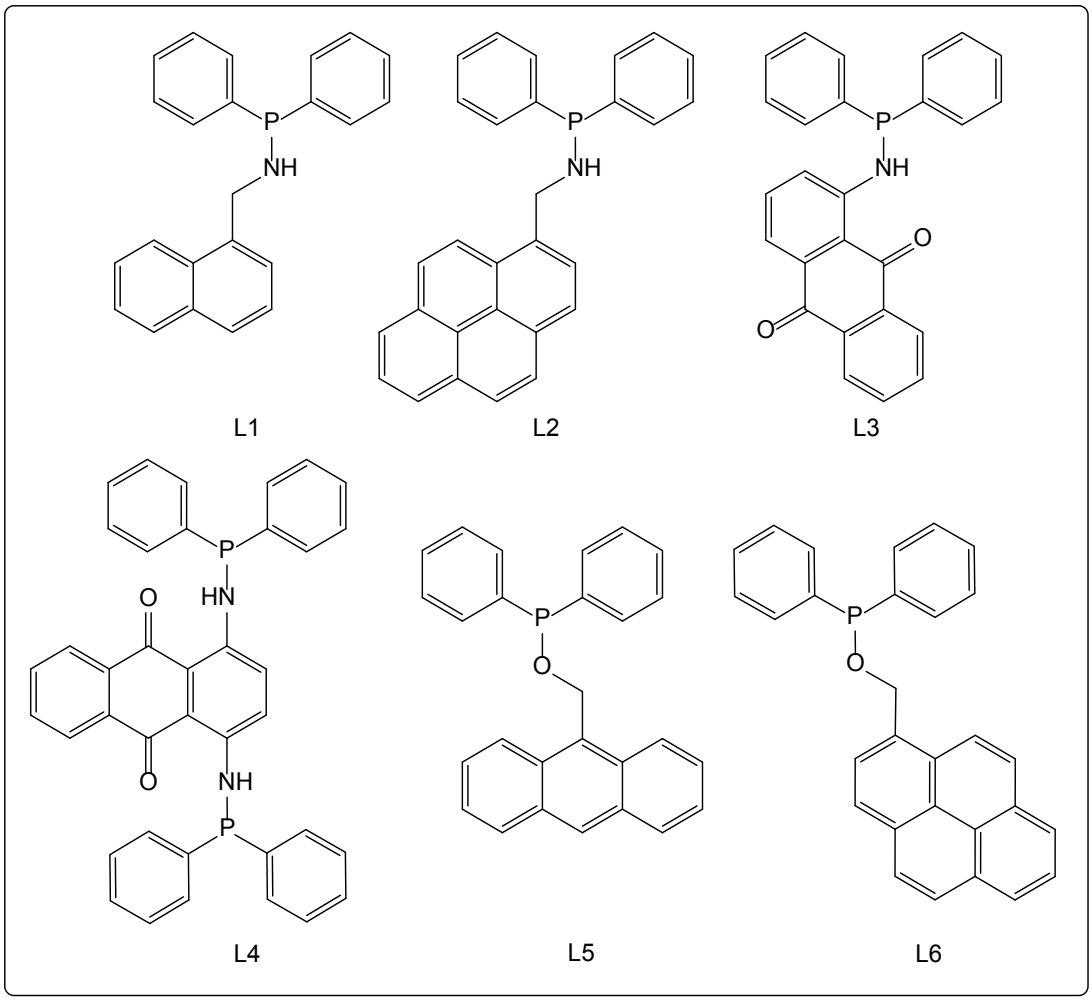

Figure 3.10: Structures of the isolated ligands

The aminophosphine ligands were synthesised in a single step from chlorodiphenylphosphine (Ph_2PCl) and the relevant primary amine (1-naphthalenemethylamine, 1-pyrenemethylamine, 1-aminoanthraquinone). The phosphine was added dropwise to a stirred degassed dichloromethane solution of the amine and triethylamine at 0 °C. **L1** and **L2** were isolated as colourless and yellow oils, respectively, while the anthraquinone derivative **L3** was obtained as a dark orange solid and **L4** as a dark pink solid. The formation of **L3** is noteworthy as the aryl amine of 1-aminoanthraquinone is far less basic than the other amines and is delocalised into the strongly electron withdrawing anthraquinone ring. As the only disubstituted ligand, **L4** is also of particular interest as it gives rise to the potential of coordination to two Au(I)

atoms. All ligands were treated as air-sensitive materials and were stored under inert atmosphere. The corresponding gold(I) complexes were synthesised by stirring [AuCl(tht)] (where tht = tetrahydrothiophene) with the ligand in deoxygenated dichloromethane to yield monometallic complexes of the form [AuCl(**L**)], as well as a dimetallic complex [$AuCl_2$(**L4**)$_2$]. Due to the light sensitivity of Au(I) compounds, tin foil was used to eliminate any light during the reaction.

The substituted phosphinites were also synthesised in a single step process from chlorodiphenylphosphine and the relevant methanol derivative (9-anthracenemethanol and 1-pyrenemethanol). The methanol derivative and 4-dimethylaminopyridine (DMAP) were dissolved in dry and degassed tetrahydrofuran (THF). Following this, triethylamine was added as well as chlorodiphenylphosphine. **L5** and **L6** were both isolated as pale yellow oils. Similarly to the aminophosphines, both ligands were treated as air-sensitive in their storage. Despite repeated attempts, the corresponding Au(I) complexes for these ligands were unable to be synthesised successfully. This was sopported by the observation of starting material and what is thought to be an oxidised ligand peak in the ^{31}P NMR.

3.3.2 Spectroscopic Characterisation

Multinuclear NMR spectroscopy was used to confirm the proposed structures of the ligands. In the first instance, ^{31}P NMR data (Table 3.1) gave immediate indication of the formation of the target aminophosphine. For structurally related **L1** and **L2**, which incorporate a methylamine unit, this value is approximately +42 ppm, which is comparable to reports on chemical shift values for monoaminophosphine type species (+40 to +70 ppm).[93–96] For **L3** and **L4** the ^{31}P chemical shift value appeared at a significantly upfield value +26.11 and +26.30 ppm suggesting that the phosphorus nucleus is more shielded in the aminoanthraquinone derivative. This value is consistent with the report of Woollins which describes the reactivity of an arylamine with Ph_2PCl to give a corresponding aminophosphine with ^{31}P NMR resonance at approximately +27 ppm.[97] In addition, the ^{31}P NMR chemical shifts of **L5** and **L6** (+113.74 and +114.03, respectively) are comparable to a previously reported derivative,

benzyldiphenylphosphinite (118.1 ppm),[98] as well as to other related analogues by Diez-Gonzalez *et al.*[77]

Compound	^{31}P NMR δ / ppm	($\delta_{complex}$ - δ_{ligand}) / ppm
L1	+42.19	
L2	+42.12	
L3	+26.11	
L4	+26.30	
L5	+113.74	
L6	+114.03	
[AuCl(**L1**)]	+64.58	+22.39
[AuCl(**L2**)]	+64.72	+22.60
[AuCl(**L3**)]	+55.77	+29.66
[Au_2Cl_2(**L4**)]	+56.63	+30.33

Table 3.1: ^{31}P NMR chemical shift values for the ligands and complexes

In the ^{1}H NMR spectra of **L1** and **L2**, the N*H* resonance gave rise to a complex multiplet around 2.3 ppm due to both $^{3}J_{HH}$ and $^{2}J_{HP}$ coupling. The methylene resonances for **L1** and **L2** were observed at 4.44 and 4.67 ppm, respectively. In **L3** the N*H* resonance appeared much further downfield at *ca*. 10.3 ppm, due to the strongly electron withdrawing anthraquinone unit, and is a doublet, which is attributed to H-P coupling ($^{2}J_{HP}$ = 7.3 Hz). **L4** displays a similar downfield peak at 11.13 ppm, which integrates to two protons in this case. These values are consistent with previous work on substituted aminoanthraquinones which often show such resonances at chemical shifts above 9 ppm.[99] In addition, the methylene resonances for **L5** and **L6** were observed at 5.68 and 5.39 respectively, where each is a doublet due to ^{3}J coupling to the phosphorus atom.

For **L3**, the ^{13}C NMR spectrum revealed the two carbonyl carbons at 186.38 and 183.52 ppm due to the unsymmetrical nature of the anthraquinone moiety. In contrast, **L4** shows a single carbonyl carbon resonance at 184.83 ppm due to its symmetrical nature. In **L1** and **L2**, the methylene carbon resonance was a doublet ($^{2}J_{CP}$ ~ 16 Hz) *ca*. 48 ppm,

again consistent with the formation of the aminophosphine. High resolution mass spectrometry (HRMS) was obtained for each ligand, where $[M+H]^+$ or $[M]^+$ was observed in each case, thus confirming the proposed formulation. IR spectra of the ligands allowed identification of ν(N-H) and in the case of **L3** and **L4**, ν(C=O) stretching frequencies. In the cases of **L5** and **L6**, ν(C-O) stretching frequencies were observed.

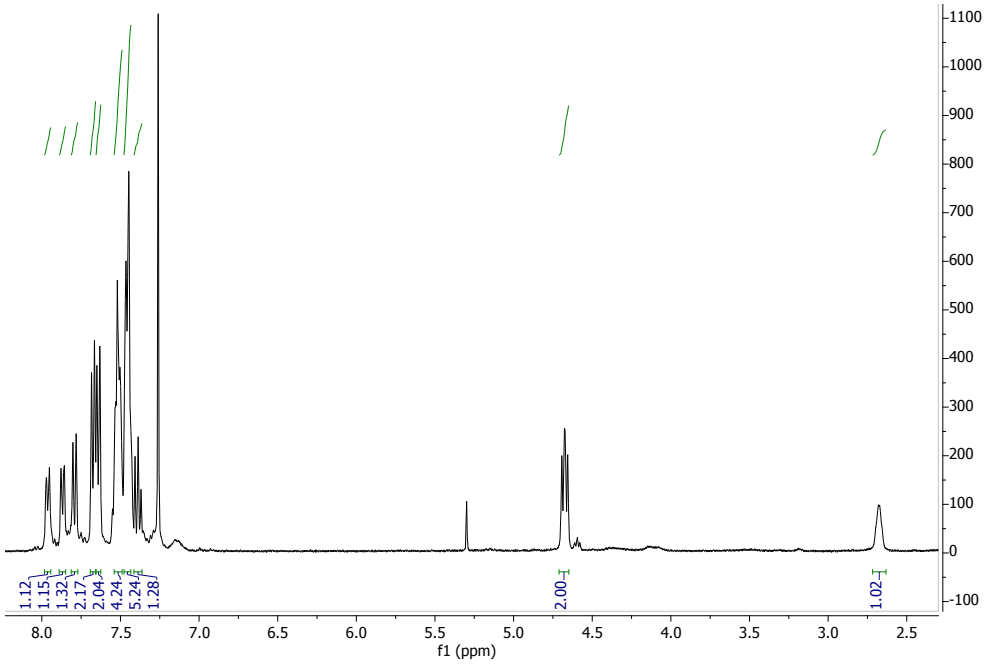

*Figure 3.11: ^{1}H NMR spectrum of [AuCl(**L1**)]*

The Au(I) complexes were similarly characterised by an array of techniques. Firstly, ^{31}P NMR spectra (Table 3.1) revealed significant downfield shifts (up to around +30 ppm) for each of the complexes relative to the free ligands consistent with coordination to Au(I). As with the corresponding ligands, the phosphorus resonances for [AuCl(**L1**)] and [AuCl(**L2**)] are very similar (*ca*. +65 ppm), while [AuCl(**L3**)] appeared at +55.77 ppm and $[Au_2Cl_2$(**L4**)] at +56.63. ^{1}H NMR spectra show retention of the fluorophore labelled aminophosphine in each case (with the appropriate number of aromatic resonances), and for [AuCl(**L1**)] (Figure 3.11) and [AuCl(**L2**)] the methylene resonances were shifted downfield by around +0.2 ppm upon formation of the complexes. These spectra also show the N*H* resonance again confirming the integrity of the aminophosphine upon coordination to Au(I). For [AuCl(**L3**)] and $[Au_2Cl_2$(**L4**)], the ^{13}C NMR spectrum showed a subtle shift in the carbonyl carbon resonances of the anthraquinone unit (two for [AuCl(**L3**)] and one for $[Au_2Cl_2$(**L4**)]), while for [AuCl(**L1**)] and [AuCl(**L2**)] the methylene

carbon was again around 48 ppm. HRMS data showed $[M-H]^-$ or $[M-Cl]^+$ for each of the complexes supporting their successful formation. An example for [AuCl(**L2**)] is shown in Figure 3.12.

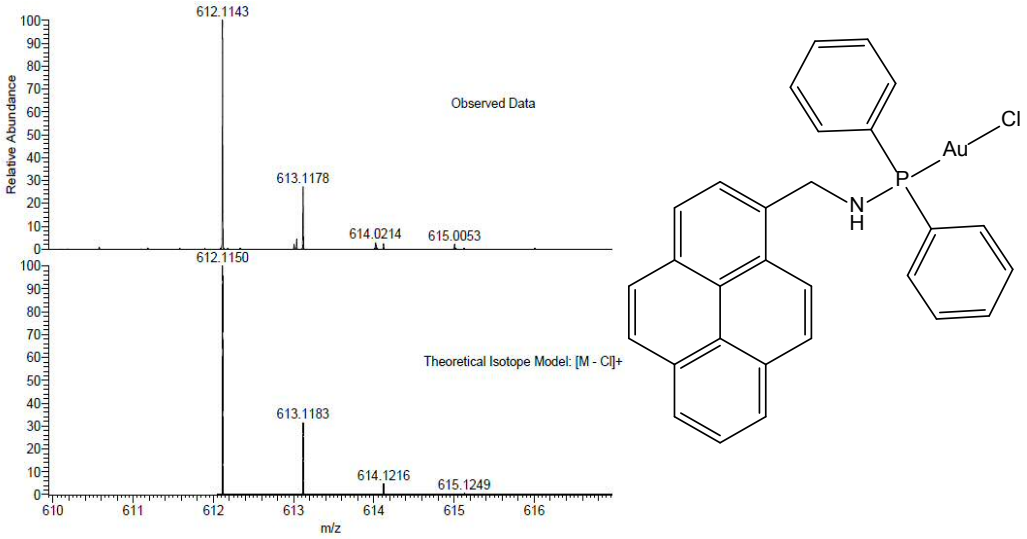

Figure 3.12: HRMS of [AuCl(L2)]

3.3.3 X-ray Crystallography

In addition to solution state characterisation, confirmation of the solid-state structures was provided through X-ray crystallographic studies on one complex, [AuCl(**L3**)]. Crystals suitable for X-ray diffraction were obtained by room temperature vapour diffusion of diethyl ether into a concentrated acetonitrile solution of [AuCl(**L3**)]. Data collection, refinement and structure solution was conducted by Dr Peter Horton at the UK National Crystallography Service, Southampton. Data collection parameters are shown in Table 3.2, together with selected bond length and bond angle data in Table 3.3. The resultant structures of [AuCl(**L3**)] are shown in Figure 3.13.

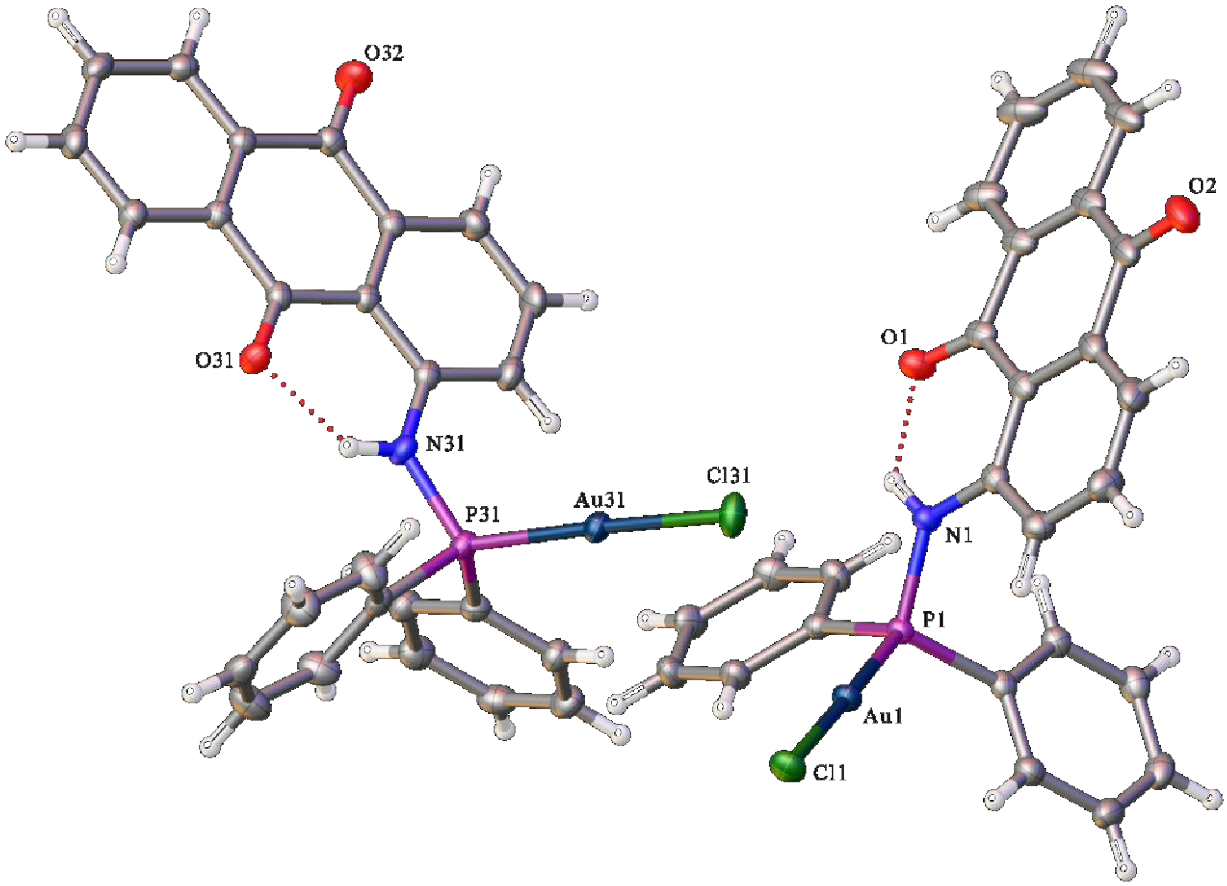

Figure 3.13:Crystal structure of [AuCl(L3)]. Ellipsoid drawn at 50% probability

The X-ray crystal structure for [AuCl(**L3**)] confirms the suggested formulation in the solid state (Figure 3.13). Within the structure there are two independent molecules within the asymmetric unit. The structure reveals the integrity of the anthraquinone functionalised aminophosphine and its coordination to Au(I). The complex adopts an approximately linear coordination geometry at Au(I) with ∠P-Au-Cl in the range 176.75(2)-178.38(2). The Au-P and Au-Cl bond lengths are around 2.22 Å and 2.29 Å, respectively. The geometry around the nitrogen atom is approximately trigonal planar rather than pyramidal as noted in the X-ray structures of other aminophosphines.[100] The P-N distances are *ca*. 1.67 Å. While these can be regarded as relatively short when compared to other aminophosphines,[13] the distinction here is that the ligand is coordinated; Woollins has previously reported a Pt(II) complex of a bis-aminophosphine with a comparable reported P-N distance of 1.6843(19) Å.[49] The structure also reveals an intramolecular hydrogen bonding interaction of 2.9 Å between the N-H and C=O

groups of the anthraquinone. The influence of this, together with the relatively planarised nitrogen, is to orient the P-N bond in the plane of the anthraquinone.

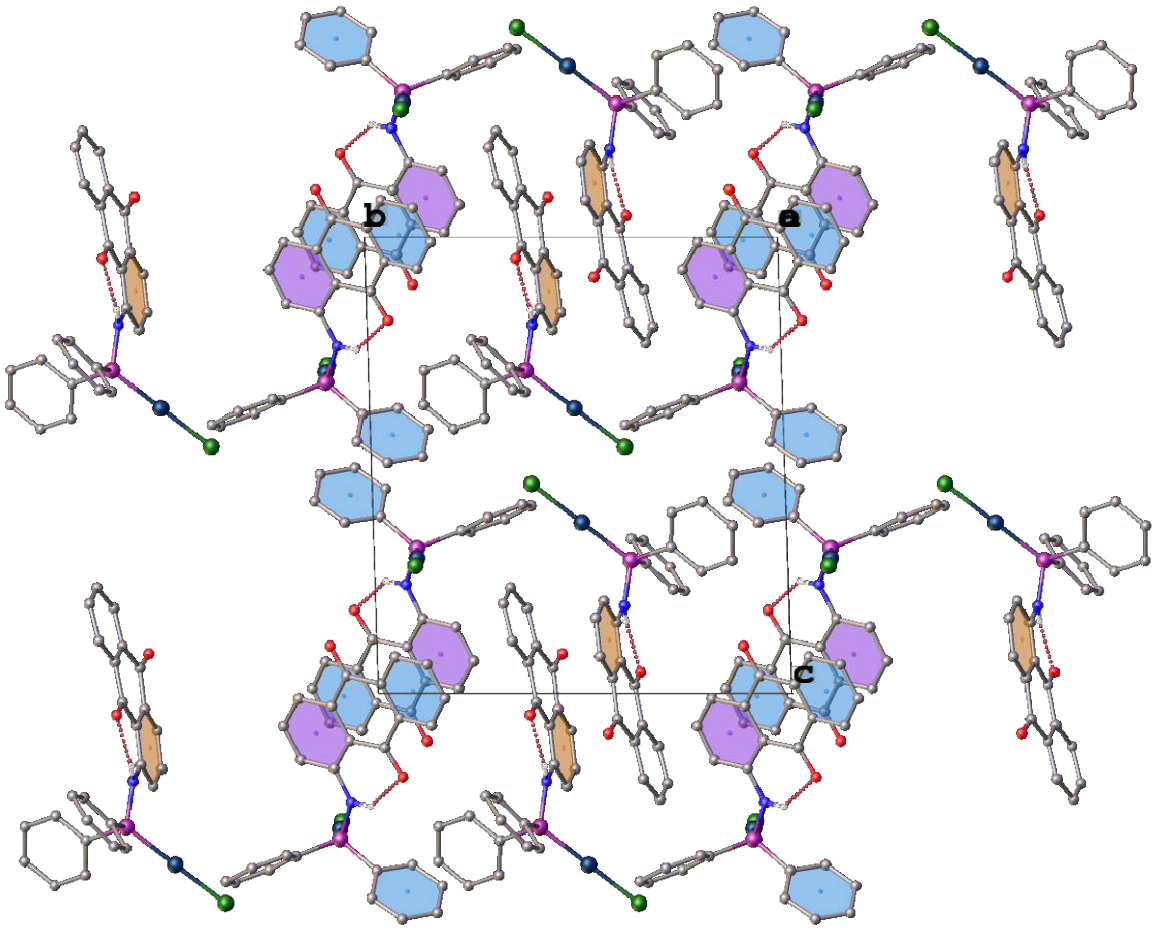

Figure 3.14: Packing diagram for [AuCl(L3)]

Sample	[AuCl(**L^3**)]
Empirical formula	$C_{26}H_{18}AuClNO_2P$
Formula weight	639.80
Temperature	100(2) K
Wavelength	0.71073 Å
Crystal system	Triclinic
Space group	*P*−1
Unit cell dimensions	9.23605(10) Å, α = 90.9323(9)°
	14.82932(17) Å, β = 101.3732(9)°
	16.64944(19) Å, γ = 94.2899(9)°
Volume	2228.21(4) Å^3
Z	4
Density (calculated)	1.907 g / cm^{-3}
Absorption coefficient	6.819 mm^{-1}
Crystal	Block; orange
Crystal size	0.167×0.059×0.050 mm^3
θ range for data collection	2.497 − 27.483°
Reflections collected	60900
Independent reflections	10204 [R_{int} = 0.0335]
Absorption correction	Semi−empirical from equivalents
Data / restraints / parameters	9595 / 0 / 577
Goodness-of-fit on F^2	1.032
Final R indices [F^2 > 2σ(F^2)]	*R1* = 0.0176, *wR2* = 0.0391
R indices (all data)	*R1* = 0.0197, *wR2* = 0.0399
Largest diff. peak and hole	0.74 and −0.506 e Å^{-3}

Table 3.2:Data collection parameters for the X-ray structures

The packing arrangement displayed in Figure 3.14 revealed a number of intermolecular π-π interactions for [AuCl(**L3**)] that exist between phenyl rings of the anthraquinone unit, and the phenyl rings of the diphenylphosphine moiety. From the packing arrangements, the angles between the two planes involved in these interactions are

0.000, 0.664 and 3.656 °, the centroid-centroid distances are 3.559, 3.615, 3.702, 3.819, 3.823 and 3.939 Å, and the shift distances are 0.961, 1.258, 1.484, 1.486 and 2.263 Å. The closest interactions are between the anthraquinone units of neighbouring complex units. There are no aurophilic interactions revealed by this structure, presumably due to the large steric requirements of the aminophosphine ligand.

Selected bond lengths (Å)			
Au(1)-Cl(1)	2.2874(5)	Au(31)-Cl(31)	2.2900(6)
Au(1)-P(1)	2.2225(6)	Au(31)-P(31)	2.2224(6)
P(1)-N(1)	1.6774(19)	P(31)-N(31)	1.6851(19)
Selected bond angles (Å)			
P(1)-Au(1)-Cl(1)	178.38(2)	P(31)-Au(31)-Cl(31)	176.75(2)
N(1)-P(1)-Au(1)	116.88(7)	N(31)-P(31)-Au(31)	117.38(7)

Table 3.3:Selected bond lengths and bond angles for [AuCl(L3)]

The steric properties of **L3** have also been assessed from the crystal data by use of the SambVca 2 program[101] for determination of buried volume (%Vbur) and the method of Mingos[102] for deriving crystallographic cone angles. The %Vbur values for the two independent molecules in the unit cell are 32.0 and 32.9 respectively, with attendant cone angles of 163° and 169°. These relatively large values reflect the absence of any steric hindrance at the metal (as is typical for a linear L-Au-Cl complex) with the largest values being associated with the complex where both phenyl rings are orthogonal with M-P-C-C torsion angles of 13.3° and 9.9°.

3.3.4 Photophysical Properties

The photophysical properties of all the ligands and complexes were investigated *via* UV-vis., steady state luminescence and luminescence lifetimes, measured in aerated solutions of acetonitrile in all cases, excluding **L5** and **L6** where measurements were carried out in aerated solutions of chloroform. For the complexes, quantum yields were also obtained. This was not carried out for any of the ligands due to instability in solution

for extended time periods. A summary of the photophysical properties are shown in Table 3.4.

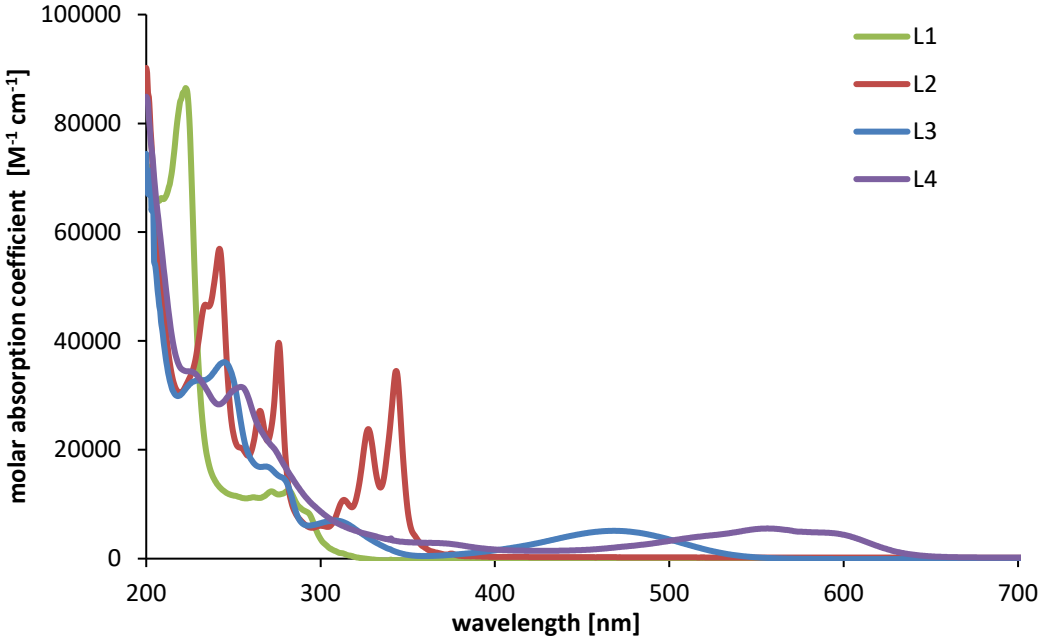

Figure 3.15: UV-vis spectra of L1-L4

The absorption spectra for the ligands are dominated by $\pi \rightarrow \pi^*$ absorbances associated with the various aromatic units (Figures 3.15 and 3.16). The phenyl substitutents contribute at the higher energies (<260 nm), while the naphthyl, pyrenyl, anthracenyl and anthraquinone chromophores gave absorbances at progressively longer wavelengths. For **L2 and L6**, the spectra revealed a vibronically structured appearance at 300-375 nm, consistent with the various pyrene centred $\pi \rightarrow \pi^*$ transitions. Similarly, **L5** showed a vibronically structured appearance at 330-385 nm.

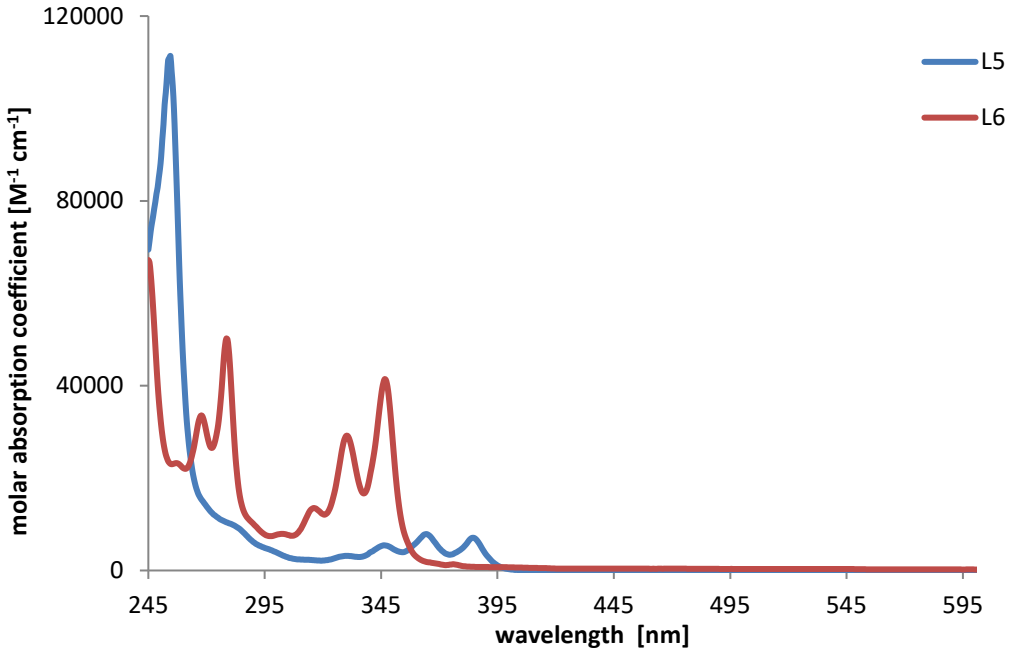

Figure 3.16: UV-vis spectra of L5 & L6

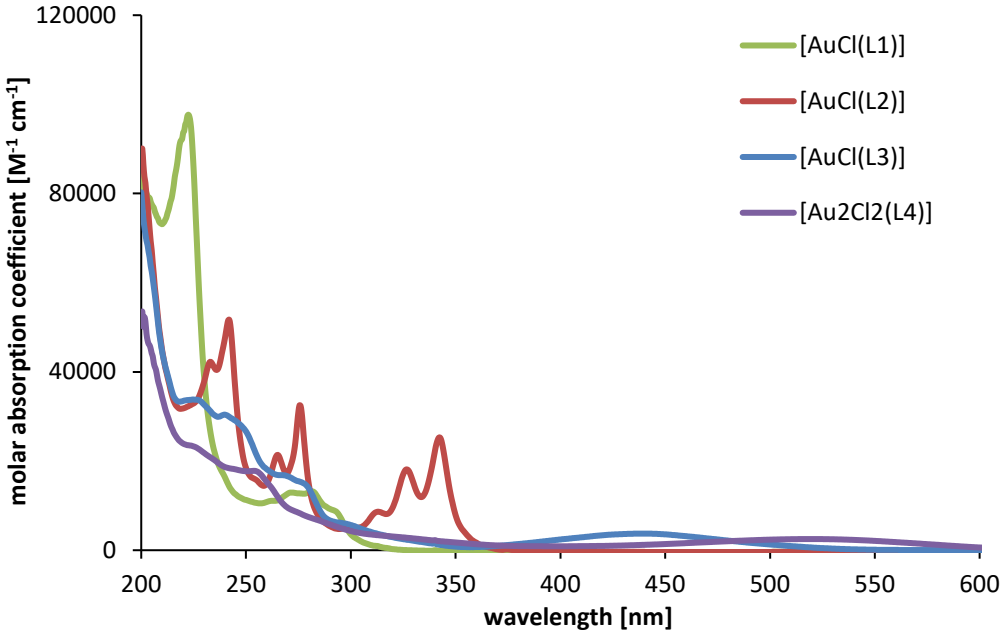

Figure 3.17: UV-vis spectra of the complexes

In the case of the anthraquinone derivatives, **L[3]** and **L[4]**, a lowest energy broad absorption band appeared at 470 nm (ε ~ 5000 $M^{-1}cm^{-1}$) and 600 nm (ε ~ 5000 $M^{-1}cm^{-1}$) respectively. Amine-substituted anthraquinone derivatives are known to possess N-to-quinone transitions that can be described as ICT[103] due to the donor-acceptor character of the chromophore. The precise positioning of the ICT band can depend upon the nature and

position of the substitutent on the anthraquinone core. Therefore the 470 nm and 600 nm bands are also ascribed to an ICT-type transition, but one that may involve participation from the bonded P atom in the donor component.

For the Au(I) complexes the UV-vis. spectra were dominated by the ligand-centred transitions discussed above (Figure 3.17), with minor perturbations observed as a consequence of coordination to Au(I). The cases of [AuCl(**L3**)] and [Au_2Cl_2(**L4**)] are most noteworthy, both with a hypsochromic shift of the ICT visible band. The shift is consistent with a reduction in the donor ability of the nitrogen donor at anthraquinone, and rationalised by the attachment of the gold atom to the anthraquinone unit through the P-N bond.

Compound	λ_{abs} / nm[a]	λ_{em} / nm	τ_{obs} / ns[b]	ϕ [c]
L1	293, 282, 272, 262, 223	339	6.5	-[d]
L2	375, 344, 328, 314, 300, 276, 266, 242, 235 sh	398, 478	8.0	-[d]
L3	470, 309, 279, 269, 245, 228 sh	571	1.0	-[d]
L4	600, 555, 371, 255, 224	630	1.5	-[d]
L5	385, 365, 347, 330, 283 sh, 255	418, 442	1.5	-[d]
L6	376, 347, 331, 316, 302, 279, 268, 257	397 sh, 417	4.5	-[d]
[AuCl(**L1**)]	291, 282, 272, 223	339	3.9	8 %
[AuCl(**L2**)]	375, 343, 327, 313, 300, 276, 266, 242, 233	377, 397, 417	14.9	17 %
[AuCl(**L3**)]	442, 298, 270, 241, 224	574	1.0	2 %
[Au_2Cl_2(**L4**)]	523, 325, 282, 254, 224	603	1.3	2%

Table 3.4:Absorption and emission data for the complexes [a] measurements obtained in MeCN solutions (with the exception of L5 and L6: $CHCl_3$); [b] using λ_{ex} 295 nm.; [c] for quantum yield measurements using $[Ru(bpy)_3](PF_6)_2$ as reference of 0.016 in aerated MeCN;[d] not determined due to air-sensitivity in solution.

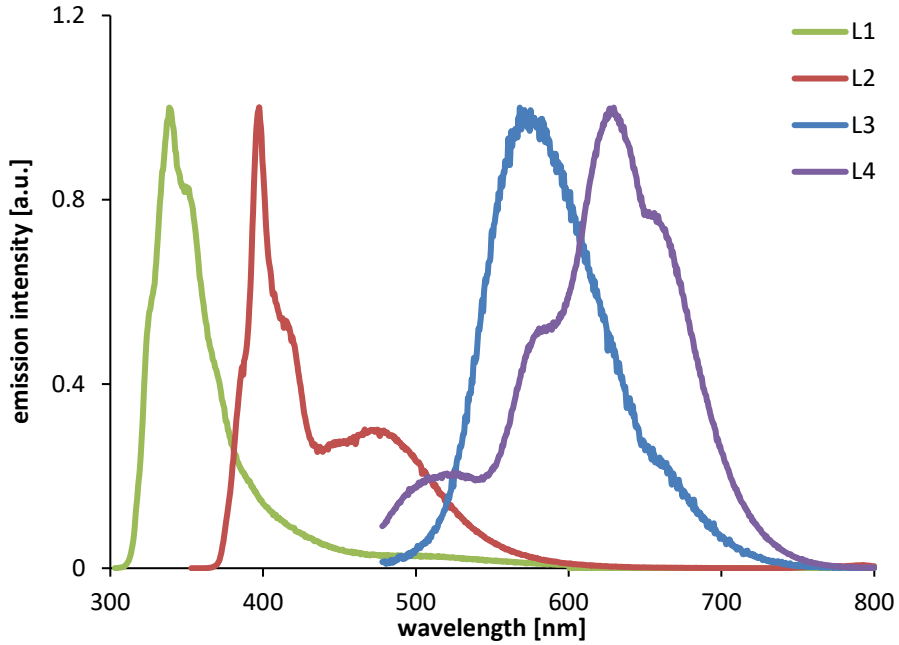

Figure 3.18: Emission profiles of L1-4

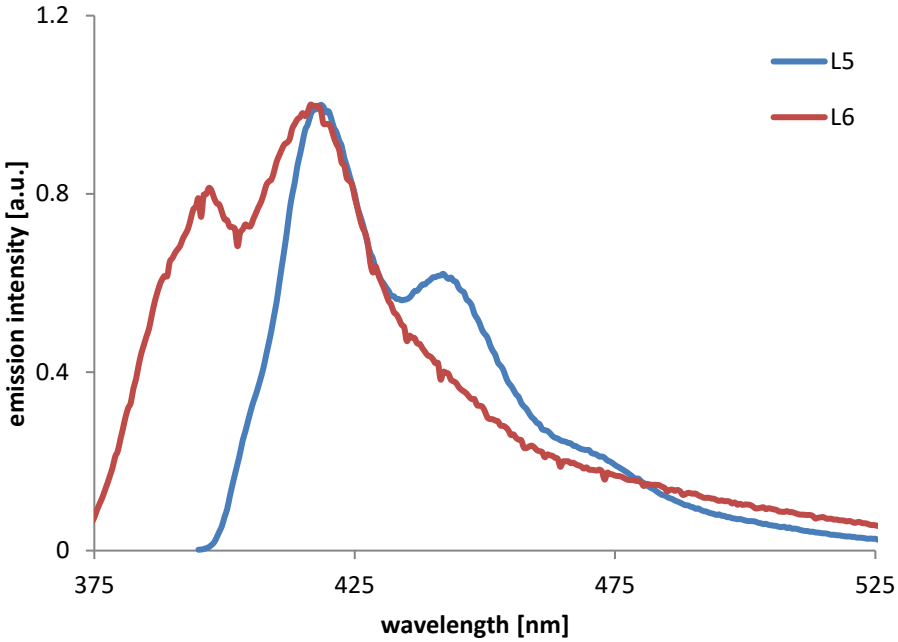

Figure 3.19: Emission profiles of L5 and L6

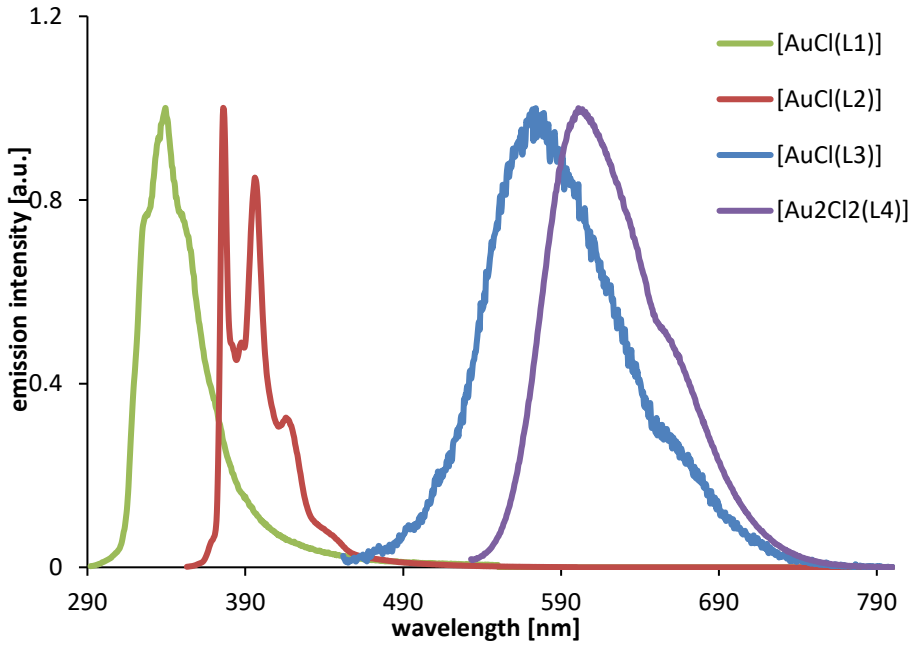

Figure 3.20: Emission profiles for the complexes

Each of the ligands was shown to be fluorescent in solution, with emission wavelengths (Table 3.4) and profiles (Figures 3.18 and 3.19) consistent with the presence of the fluorophore; the emission energy decreased across the series **L1** (naphthyl) > **L2** (pyrenyl) > **L3** (anthraquinone) > **L4** (anthraquinone). For **L5** and **L6**, similar emission energies were observed, with emission intensity maxima at *ca.* 417 nm in both cases. In the case of **L2**, the emission profile was composed of both structured monomer-type (350-425 nm) and a broader feature at 475 nm which was attributed to excimer-type emission. For **L3**, the visible emission peak at *ca.* 575 nm was broad and structure-less in appearance which is consistent with an emitting state of ICT character localised on the aminoanthraquinone group. By comparison of **L3** and **L4**, it can be seen that movement from a mono-substituted anthraquinone moiety to a disubstituted causes a bathochromic shift in the visible emission peak, which is consistent with literature examples.[104,105]

Time-resolved measurements (λ_{ex} = 295 nm) revealed observed lifetimes that were consistent with fluorescence emission in all cases (Table 3.4). The corresponding measurements on the complexes, using excitation wavelengths that correlate with the ligand-based absorption bands, revealed that the characteristic ligand-based fluorescence was retained upon complexation to Au(I) (Figure 3.20). For [AuCl(**L2**)] the

appearance of the emission profile was highly structured with no evidence of excimer-type emission. The emission spectra of **L2** and [AuCl(**L2**)] were obtained using the same concentration solutions (2.5×10^{-5} M), and therefore suggests that the presence of the coordinated {AuCl} unit may inhibit π-π stacking (the excimer band in **L2** may be due to intramolecular interactions between the pyrene and phenyl groups within the ligand). [AuCl(**L3**)] and [Au_2Cl_2(**L4**)] again showed visible region ICT-based fluorescence bands with small shifts attributed to metal-based perturbation upon Au(I) coordination. It is noteworthy that formation of the complexes led to variations in the recorded lifetimes, and in the case of [AuCl(**L2**)] an extension to *ca*. 15 ns. This may indicate that the quenching of the pyrene fluorophore is inhibited by coordination to Au(I). In all cases the observed lifetimes suggest a ligand-centred emission which is fluorescent in nature. Quantum yields were also obtained for the complexes using aerated solvent and determined to be 8%, 17%, 2% and 2% for [AuCl(**L1-3**)] and [Au_2Cl_2(**L4**)], respectively.

3.3.5 Density Functional Theory Studies

Supporting TD-DFT calculations of **L3** and [AuCl(**L3**)] were computed to assist and inform the assignments of the electronic transitions noted from experimental observations. These calculations were performed by Dr Benjamin Ward. Long-range corrected functionals such as CAM-B3LYP[106] are often required to give an adequate description of excited states with a significant charge-transfer component.[107] In this case however, all the TD-DFT analyses (*vide infra*) gave excitation energies that were significantly higher in energy than those observed experimentally. After several functionals were screened, the M06 functional gave good agreement between experiment and theory,[108] and was therefore used throughout. The SDD basis set,[109] along with associated effective core potentials, was used for the Au atom, as is common practice for heavy transition metals; Dunning's correlation-consistent double-ζ basis set cc-pVDZ gave good results with reasonable computational cost,[110] although the cc-pV(D+d)Z basis set was used for the third period elements, since this gives improved d-polarization compared to the original formulations,[111] and is likely to be beneficial in coordination complexes bearing P and Cl donors.

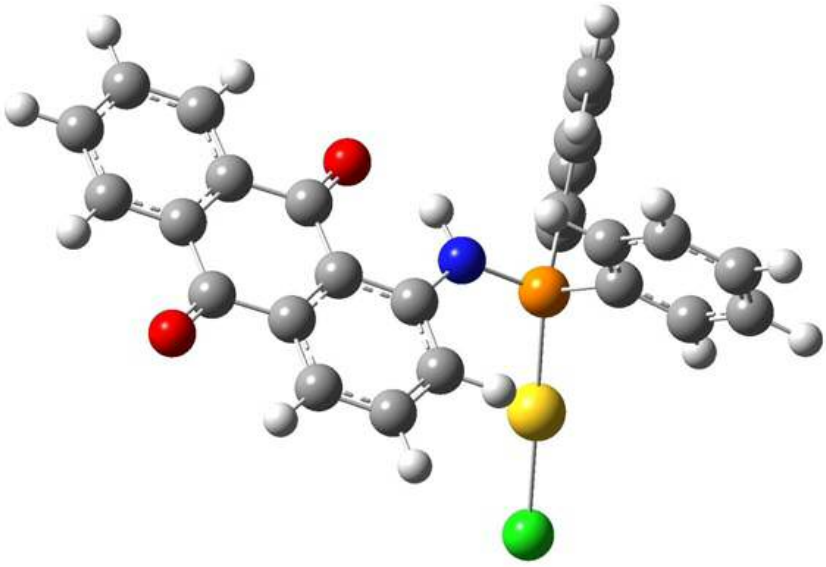

Figure 3.21:Calculated structure of [AuCl(L3)] [M06 – SDD/cc-pV(D+d)Z/cc-pVDZ][112]

The calculated structure of [AuCl(**L3**)] is shown in Figure 3.21, and is in good agreement with that obtained from X-ray data. The Au-donor distances (see Table 3.3) are slightly overestimated in the calculated structure (Au–Cl: calculated = 2.356 Å, experimental = 2.2874(5) Å and 2.2900(6) Å; Au–P: calculated = 2.296 Å, experimental = 2.2225(6) Å and 2.2224(6) Å), whilst those within the ligand manifold are more accurately reproduced (e.g. P–N: calculated = 1.698 Å, experimental = 1.6774(19) Å and 1.6851(19) Å). The trigonal planar (sp^2-hybridized) amine is well replicated by the calculations (sum of angles subtended at N: calculated = 358.2°, experimental = 360.0° for both independent molecules in the asymmetric unit). The modest differences in bond distance are not thought to be significant in light of crystal packing forces and temperature effects (X-ray data were collected at 100 K), and other properties pertaining to this complex were well-reproduced (*vide infra*).

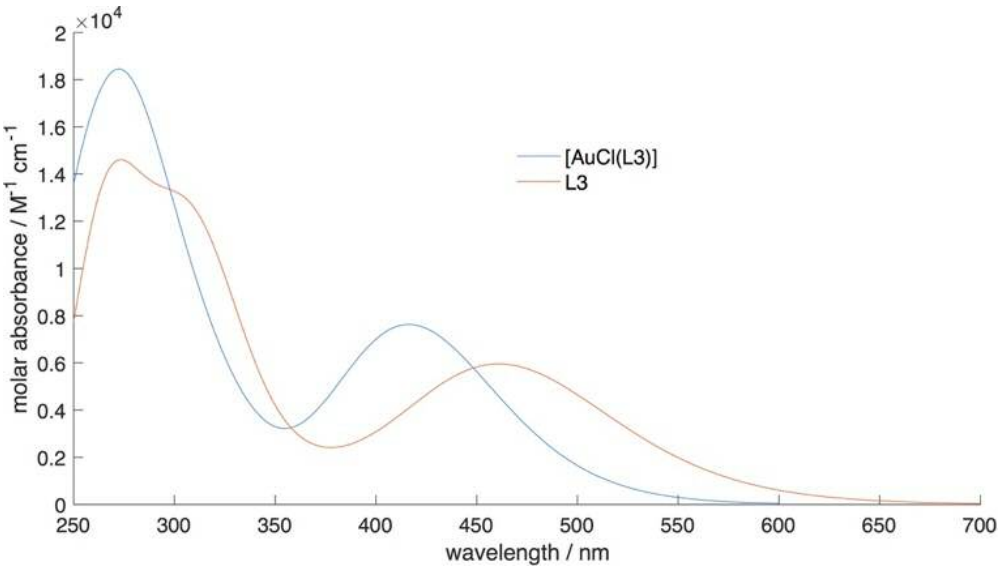

Figure 3.22:Simulated UV-vis absorption spectra of L3 and [AuCl(L3)] [M06 – SDD/cc-pV(D+d)Z/cc-pVDZ][112]

The ^{31}P NMR shielding tensors were calculated to validate the observed experimental values; this is especially relevant since there are few literature examples of this molecular fragment to give a reliable expected chemical shift range. As noted by Pellegrinet,[113,114] the accuracy of such calculations can be improved by ensuring that a suitable reference molecule is chosen and calculated at the same level of theory. Given the structure of **L3** (*i.e.* bearing two phenyl groups), PPh_3 was used, and for which the experimental chemical shift is well established (–6 ppm). These calculations allowed the ^{31}P NMR chemical shifts (Table 3.1) of **L3** and [AuCl(**L3**)] to be estimated as +26.8 and +49.9 ppm respectively, in good agreement with the experimental values of +26.1 and +55.8 ppm.

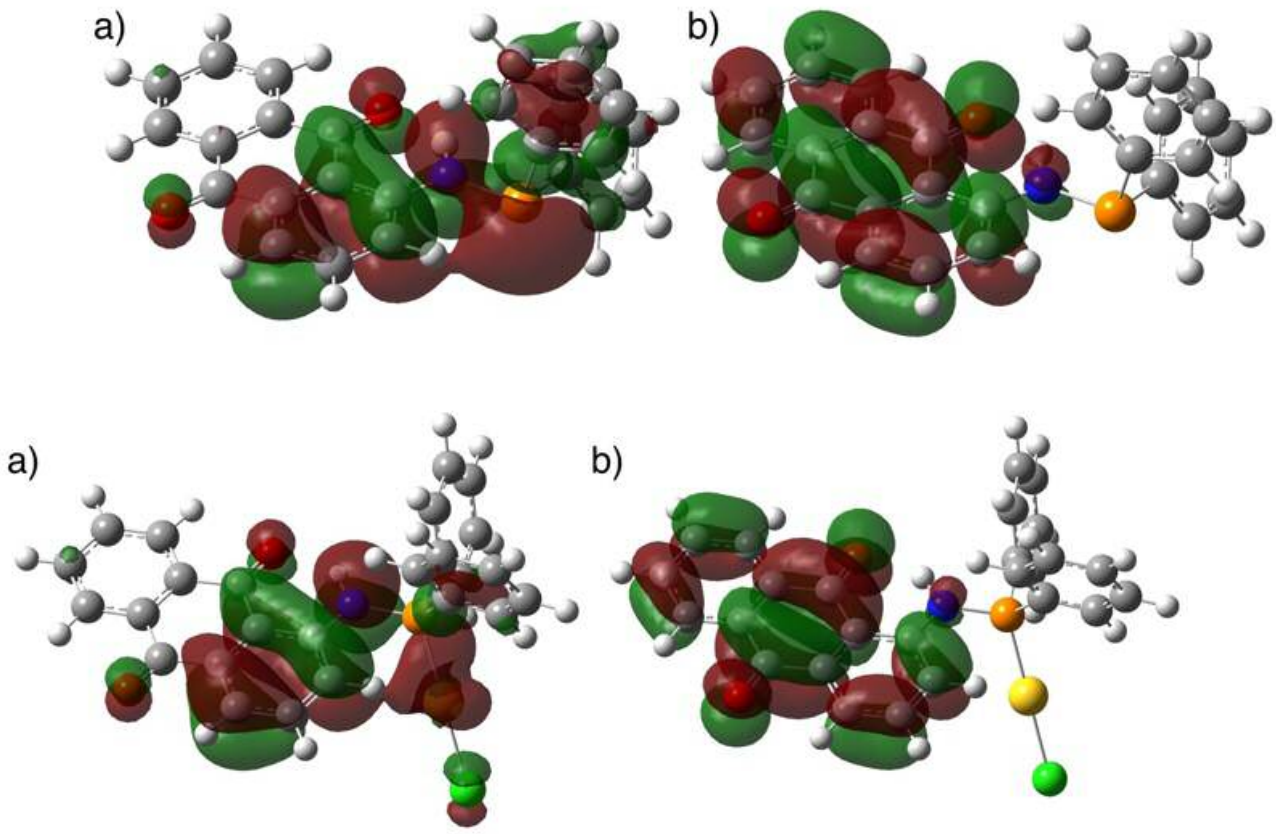

Figure 3.23:Top: Calculated a) HOMO and b) LUMO of L3 [M06 – SDD/cc-pV(D+d)Z/cc-pVDZ]. Bottom: Calculated a) HOMO and b) LUMO of [AuCl(L3)] [M06 – SDD/cc-pV(D+d)Z/cc-pVDZ][112]

The underlying electronic basis of the observed differences in the absorption spectra for L3 and its Au(I) complex was also investigated. Simulated spectra, derived from the TD-DFT data, are shown in Figure 3.22, and represent a good agreement with those obtained experimentally. The principal area of interest is the low energy band between 400 and 500 nm, which undergoes a significant blue-shift upon coordination to the Au(I) centre, as observed in the experimental data. As expected, the low energy bands correspond primarily to HOMO-LUMO transitions in both **L3** and [AuCl(**L3**)] (Figure 3.22), and are dominated by significant π-π* character within the substituted anthraquinone. In addition, the HOMO of **L3** contains appreciable orbital coefficients based upon the phosphorus and nitrogen atoms, effectively the P and N lone pairs, which gives the low energy transition a combination of π-π*, *n*(P)-π*, and *n*(N)-π* character. The nitrogen orbital component is retained in the HOMO of [AuCl(**L3**)], but the phosphorus orbital character is somewhat altered, as expected, due to coordination of the phosphorus atom to the Au(I) centre; in [AuCl(**L3**)] this component is encompassed in the Au-P σ-bond and thus $\sigma_{Au\text{-}P}$-π* character may also contribute to the HOMO-LUMO transition

(Figure 3.23). Considering the energies of the orbitals involved, the energy of the LUMO is lowered very slightly upon Au coordination, from –2.83 eV in L3 to –2.98 eV in [AuCl(**L3**)], whereas the corresponding effect on the HOMO is much more pronounced, reducing the energy from –6.29 eV to –6.80 eV. Thus, in effect, the observed blue shift in the absorption spectra is predicted upon lowering of the HOMO upon coordination of the Au(I) ion.

3.4 Conclusions

This chapter has described the synthetic development and spectroscopic analysis of a series of aminophosphines and phosphinite fluorophores, generating six new ligands, where **L1-4** were utilised for Au(I) coordination chemistry.

Two fluorescent, functionalised phosphinites (**L5** and **L6**) have been synthesised from a corresponding methanol-functionalised fluorophore and chlorodiphenylphosphine, where fluorophores include anthracene and pyrene. In addition, four aminophosphines (**L1-4**) have been synthesised straightforwardly using an appropriate amino-derived fluorophore and chlorodiphenylphosphine. Examples in this chapter show that naphthyl, anthracenyl or anthraquinone fluorophores can be incorporated into aminophospine ligand structures in this way. The ligands **L1-L4** react with [AuCl(tht)] to give the expected Au(I) complexes *via* coordination through the phosphorus donor.

The resultant ^{31}P NMR spectra of the complexes show significant downfield shifts (+22 to +31 ppm) for the coordinated aminophosphines. An X-ray structure for the anthraquinone derivative, [AuCl(**L3**)], showed the expected linear coordination geometry at Au(I) and significant intermolecular packing interactions between neighbouring anthraquinone units. The complexes are luminescent with ligand-based emission dominating. In the series, [AuCl(**L3**)] shows visible emission at 574 nm which is attributed to ICT-type emitting state localised on the phosphino-amino-anthraquinone unit and is relatively similar to the free ligand. In contrast, the dimetallic complex, [Au_2Cl_2(**L4**)], displays a hypsochromically shifted emission wavelength when compared to the free ligand (630 nm and 603 nm, respectively).

Supporting TD-DFT calculations reliably reproduced the structural features of [AuCl(**L3**)] and support the notion that the emission is ICT in nature with coordination to Au(I) diminishing the phosphorus contribution to the HOMO. The adopted TD-DFT approaches can also reliably reproduce the excitation energies for the anthraquinone derivative and provide further validation via calculated ^{31}P NMR chemical shifts. Future work will explore and expand the coordination chemistry of fluorescent

aminophosphine and phosphinite ligands and investigate their viability in bioimaging and catalytic applications.

3.5 Experimental

3.5.1 General Experimental Considerations

All reagents and solvents were commercially available and were used without further purification if not stated otherwise. For the measurement of ^{1}H, ^{31}P, and ^{13}C NMR spectra a Bruker Fourier^{300} (300 MHz), Bruker AVANCE HD III equipped with a BFFO SmartProbe^{TM} (400 MHz) or Bruker AVANCE III HD with BBO Prodigy CryoProbe (500 MHz) was used. The obtained chemical shifts δ are reported in ppm and are referenced to the residual solvent signal. Spin-spin coupling constants *J* are given in Hz.

Low-resolution mass spectra were obtained by the staff at Cardiff University. High-resolution mass spectra were carried out at the EPSRC National Mass Spectrometry Facility at Swansea University. High resolution mass spectral (HRMS) data were obtained on a Waters MALDI-TOF mx at Cardiff University or on a Thermo Scientific LTQ Orbitrap XL by the EPSRC UK National Mass Spectrometry Facility at Swansea University. IR spectra were obtained from a Shimadzu IR-Affinity-1S FTIR. UV-Vis studies were performed on a Shimadzu UV-1800 spectrophotometer as MeCN solutions (2.5 or 5 × 10^{-5} M) or $CHCl_3$ solutions (2.5 or 5 × 10^{-5} M). Photophysical data were obtained on a JobinYvon–Horiba Fluorolog spectrometer fitted with a JY TBX picosecond photodetection module as MeCN/$CHCl_3$ solutions. Emission spectra were uncorrected. The pulsed source was a Nano-LED configured for 459 nm output operating at 1 MHz. Luminescence lifetime profiles were obtained using the JobinYvon–Horiba FluoroHub single photon counting module and the data fits yielded the lifetime values using the provided DAS6 deconvolution software. Quantum yield measurements were obtained on aerated MeCN solutions of the complexes using $[Ru(bpy)_3](PF_6)_2$ in aerated MeCN as a standard (Φ = 0.016).[115]

3.5.2 X-ray Diffraction

Single orange block-shaped crystals of [AuCl(**L3**)] were submitted. A suitable crystal (0.167 × 0.059×0.050) mm^3 was selected and mounted on a MITIGEN holder in perfluoroether oil on a Rigaku FRE+ equipped with HF Varimax confocal mirrors and an

AFC12 goniometer and HG Saturn 724+ detector diffractometer. The crystal was kept at *T* = 100(2) K during data collection. Using Olex2[116], the structure was solved with the Superflip[117] structure solution program, using the Charge Flipping solution method. The model was refined with version 2014/7 of ShelXL[118] using Least Squares minimisation. All non-hydrogen atoms were refined anisotropically. Hydrogen atom positions were calculated geometrically and refined using the riding model. The value of Z' is 2. This means that there are two independent molecules in the asymmetric unit.

3.5.3 Preparation of Aminophosphine Ligands and Complexes

Preparation of aminophosphine ligands

Synthesis of L1

1-Naphthalenemethylamine (0.17 ml, 1.4 mmol) and triethylamine (0.19 ml, 1.4 mmol) were dissolved in deaerated dichloromethane (10 ml) under a nitrogen atmosphere. Diphenylchlorophosphine (0.21 ml, 1.4 mmol) in dicloromethane (10ml) was added dropwise at 0 °C over 10 minutes. The resulting solution was stirred at room temperature for 2 hours. The solution was then washed with deaerated water (20 ml), dried over $MgSO_4$ and the solvent removed *in vacuo* to give L1 as a colourless oil (463 mg, 97 %). ^{1}H NMR (400 MHz, $CDCl_3$): δ_H 7.91 – 7.87 (m, 1H), 7.77 (dd, J_{HH} = 6.8, 2.8 Hz, 1H), 7.67 (d, $^{3}J_{HH}$ = 7.8 Hz, 1H), 7.43-7.34 (m, 7H), 7.34 – 7.24 (m, 7H), 4.44 (app. t, $^{3}J_{HH}$ = 6.7 Hz, 2H, C*H*$_2$), 2.25 – 2.16 (m, 1H, N*H*) ppm. ^{13}C{^{1}H} NMR (101 MHz, $CDCl_3$): δ_C 141.20 (d, J_{CP} = 12.5 Hz), 137.08 (d, J_{CP} = 8.1 Hz), 133.95, 132.33, 132.23, 131.68, 131.48, 128.98, 128.84, 128.79, 128.73, 128.45, 128.96, 128.39, 127.99, 126.20, 125.82, 125.75, 125.70, 125.57, 123.89, 123.32, 48.12 (d, J_{CP} = 16.3 Hz) ppm. ^{31}P{^{1}H} NMR (162 MHz, $CDCl_3$): δ_P +42.19 ppm. HRMS found *m/z* 342.1400, calcd *m/z* 342.1412 for $[C_{23}H_{20}NP]^{+}$. UV-vis. (MeCN) λ_{max} (ε / $dm^3mol^{-1}cm^{-1}$): 293 (8520), 282 (12520), 272 (12360), 262, (11280), 223 (86480) nm. IR (solid) ν / cm^{-1}: 3399, 3243, 3049, 1595, 1581, 1508, 1477, 1431, 1390, 1321, 1311, 1261, 1167, 1094, 1082, 1061, 1026, 997, 970, 910, 883, 858, 839, 794, 769, 740, 711, 634, 617, 594, 552, 521, 507, 488, 469, 444, 420, 413.

Synthesis of L2

As with L1, but using, 1-pyrenemethylamine (487 mg, 2.1 mmol), triethylamine (0.33 ml, 2.5 mmol), diphenylchlorophosphine (0.38 ml, 2.1 mmol) and dichloromethane (20 ml) to give L2 as a yellow oil (808 mg, 93 %). ^{1}H NMR (400 MHz, $CDCl_3$): δ_H 8.14 – 8.06 (m, 2H), 8.02 – 7.83 (m, 7H), 7.69 (dd, J_{HH} = 11.1, 7.6 Hz, 1H), 7.50 (app. t, J_{HH} = 7.9 Hz, 1H), 7.45 – 7.39 (m, 5H), 7.28 (d, $^{3}J_{HH}$ = 5.1 Hz, 2H), 7.18 – 7.13 (m, 1H), 4.67 (app. t, $^{3}J_{HH}$ = 6.6 Hz, 2H, CH_2), 2.34 – 2.26 (m, 1H, N*H*) ppm. ^{13}C{^{1}H} NMR (101 MHz, $CDCl_3$): δ_C 141.18 (d, J_{CP} = 12.5 Hz), 135.54 (d, J_{CP} = 7.1 Hz), 135.34 (d, J_{CP} = 7.1 Hz), 134.87 (d, J_{CP} = 8.0 Hz), 131.71, 131.52, 131.41, 130.89 (d, *J* = 7.9 Hz), 129.74, 128.98, 128.78, 128.75, 128.67, 128.59, 128.57, 128.44 (d, *J* = 6.2 Hz), 127.72, 127.56, 127.25, 126.69, 126.02, 125.24, 125.18, 125.13, 124.95, 124.87, 123.36, 48.26 (d, J_{CP} = 15.8 Hz) ppm. ^{31}P{^{1}H} NMR (202 MHz, $CHCl_3$): δ_P +42.12 ppm. HRMS found *m/z* 415.1484, calcd *m/z* 415.1490 for $[C_{29}H_{22}NP]^+$. UV-vis: (MeCN) λ_{max} (ε / dm^{3}mol^{-1}cm^{-1}): 375 (920), 344 (34480), 328 (23800), 314 (10800), 300 (6040), 276 (39680), 266 (27120), 242 (56960), 235 sh (46440) nm. IR (solid) ν / cm^{-1}: 3044, 2963, 2857, 1601, 1585, 1477, 1431, 1414, 1391, 1342, 1306, 1261, 1179, 1173, 1159, 1088, 1067, 1026, 997, 968, 912, 893, 841, 816, 739, 719, 692, 617,586, 555, 513, 419, 409, 401.

Synthesis of L3

As for L1, but using 1-aminoanthraquinone (1 g, 4.6 mmol), triethylamine (0.74 ml, 5.5 mmol), diphenylchlorophosphine (0.85 mmol, 4.6 mmol) and dichloromethane (30 ml) to give L3 as a dark orange solid (583 mg, 64 %). ^{1}H NMR (500 MHz, $CDCl_3$): δ_H 10.36 (d, $^{2}J_{HP}$ = 7.3 Hz, 1H, N*H*), 8.17 – 8.08 (m, 2H), 7.87 – 7.80 (m, 1H), 7.67 – 7.57 (m, 5H), 7.47-7.39 (m, 6H), 7.29-7.26 (m, 2H), 7.12 (s, 1H) ppm. ^{13}C{^{1}H} NMR (126 MHz, $CDCl_3$): δ_C 186.38 (C=O), 183.52 (C=O), 152.47, 152.33, 139.00, 138.92, 135.26, 135.24, 134.74, 134.61, 134.17, 133.62, 133.14, 131.47 (d, J_{CP} = 21.3 Hz), 129.65, 128.90 (d, J_{CP} = 7.1 Hz), 127.04 (d, J_{CP} = 16.9 Hz), 126.93, 123.27, 122.78, 122.55, 118.50, 117.40, 116.09, 116.07 ppm. ^{31}P{^{1}H} NMR (162 MHz, $CHCl_3$): δ_P +26.11 ppm. UV-vis. (MeCN) λ_{max} (ε / dm^{3}mol^{-1}cm^{-1}): 470 (4880), 309 (7880), 279 (16160), 269 (18120), 245 (36720), 228 sh (32720) nm. HRMS found *m/z* 408.1167, calcd *m/z* 408.1153 for $[C_{26}H_{19}N_2OP]^+$. IR (solid) ν /

cm^{-1}: 3167, 3051, 1668, 1630, 1593, 1570, 1431, 1396, 1346, 1300, 1253, 1231, 1169, 1092, 1070, 1040, 1018, 997, 912, 893, 831, 806, 775, 748, 735, 704, 692, 602, 546, 513, 476, 436, 420.

Synthesis of L4

As for L1, but using 1,4-diaminoanthraquinone (250 mg, 1.05 mmol), triethylamine (0.33 ml, 2.5 mmol) and diphenylchlorophosphine (0.38 ml, 2.1 mmol) and dichloromethane (15 ml) to give L4 as a dark pink solid (408 mg, 64 %). ^{1}H NMR (400 MHz, $CDCl_3$) δ 11.13 (d, $^{2}J_{HP}$ = 6.0 Hz, 2H, N*H*), 8.23 – 8.14 (m, 2H), 7.96 – 7.91 (m, 2H), 7.62 – 7.55 (m, 4H), 7.48 – 7.37 (m, 14H), 7.15 (d, J_{HH} = 2.9 Hz, 2H). $^{13}C\{^{1}H\}$ NMR (101 MHz, $CDCl_3$) δ 184.83 (C=O), 147.18, 147.00, 145.98, 139.27, 139.18, 139.10, 134.35, 134.25, 132.94, 132.88, 132.61, 131.40 (d, J_{CP} = 21.0 Hz), 131.32, 129.41, 128.70 (d, J_{CP} = 7.1 Hz), 128.46, 128.22, 126.55. $^{31}P\{^{1}H\}$ NMR (162 MHz, $CHCl_3$): δ_P +26.30 ppm. HRMS found *m/z* 607.1702, calcd *m/z* 607.1704 for $[C_{38}H_{29}N_2P_2O_2]^+$. UV-vis: (MeCN) λ_{max} (ε / $dm^3mol^{-1}cm^{-1}$): 600 (4400), 555 (5520), 371 (2800), 255 (31520), 224 (34440). IR (solid) ν / cm^{-1}: 3053, 1614, 1582, 1560, 1533, 1464, 1433, 1395, 1367, 1335, 1287, 1240, 1161, 1123, 1109, 1096, 1024, 972, 907, 883, 822, 797, 729, 691, 529, 509, 461, 419, 411.

Preparation of aminophosphine complexes

Synthesis of [AuCl(L1)]

L1 (111 mg, 0.32 mmol) and tetrahydrothiophenegold chloride (94 mg, 0.29 mmol) were added to degassed dichloromethane (20 ml) and the solution stirred at room temperature under nitrogen for 1.5 hours. The solvent was reduced *in vacuo* and hexane added dropwise. The mother liquor was decanted to leave [AuCl(L1)] as a grey solid (35 mg, 21 %). ^{1}H NMR (400 MHz, $CDCl_3$): δ_H 7.96 (d, $^{3}J_{HH}$ = 7.9 Hz, 1H), 7.87 (d, $^{3}J_{HH}$ = 8.4 Hz, 1H), 7.79 (d, $^{3}J_{HH}$ = 8.2 Hz, 1H), 7.67 (d, $^{3}J_{HH}$ = 7.5 Hz, 2H), 7.64 (d, $^{3}J_{HH}$ = 7.4 Hz, 2H), 7.54-7.48 (m, 4H), 7.48-7.42 (m, 5H), 7.42 – 7.36 (m, 1H), 4.71 – 4.64 (m, 2H), 2.71-2.63 (m, 1H, N*H*) ppm. $^{13}C\{^{1}H\}$ NMR (101 MHz, $CDCl_3$): δ_C 134.06, 132.70, 132.55, 132.38, 132.35, 131.80, 131.17, 129.30, 129.18, 129.09, 129.06, 126.84, 126.70, 126.21, 125.54, 123.41, 47.89 ppm. $^{31}P\{^{1}H\}$ NMR (162 MHz, $CDCl_3$): δ_P +64.58 ppm. UV-vis. (MeCN) λ_{max} (ε / dm^3mol^{-}

$^{1}cm^{-1}$): 291 (9080), 282 (13160), 272 (12920), 223 (97680) nm. HRMS found *m/z* 572.0629, calcd *m/z* 572.0609 for $[C_{23}H_{19}AuClNP]^{-}$. IR (solid) ν / cm^{-1}: 3248, 3207, 3049, 2359, 1595, 1576, 1555, 1508, 1499, 1476, 1460, 1435, 1395, 1379, 1306, 1265, 1248, 1180, 1167, 1105, 1063, 1041, 1026, 995, 962, 881, 854, 800, 789, 770, 745, 714, 691, 619.

Synthesis of [AuCl(L2)]

L2 (267 mg, 0.64 mmol) and tetrahydrothiophenegold chloride (187 mg, 0. 58 mmol) were added to degassed dichloromethane (20 ml) and the solution stirred at room temperature under nitrogen for 2 hours. The solvent was reduced *in vacuo* and diethyl ether added dropwise. The resultant precipitate was filtered and dried to yield [AuCl(L2)] as a pale yellow solid (50 mg, 13 %). ^{1}H NMR (500 MHz, $CDCl_3$): δ_H 8.15 – 8.10 (m, 3H), 8.05 (d, $^{3}J_{HH}$ = 9.2 Hz, 1H), 7.99 (d, $^{3}J_{HH}$ = 8.9 Hz, 1H), 7.95 (s, 1H), 7.87 (d, $^{3}J_{HH}$ = 7.7 Hz, 1H), 7.74 (dd, J_{HH} = 13.9, 7.1 Hz, 2H), 7.62 – 7.56 (m, 4H), 7.41 – 7.37 (dd, J_{HH} = 7.4, 1.8 Hz, 1H), 7.36 – 7.31 (m, 3H), 7.23 (app. t, J_{HH} = 7.2 Hz, 2H), 4.83 (dd, J_{HH} = 8.8, 6.4 Hz, 1H), 2.75 (br. s, 1H, N*H*) ppm. $^{13}C\{^{1}H\}$ NMR (101 MHz, $CDCl_3$): δ_C 134.25, 133.14, 132.69, 132.54, 132.33, 132.27, 131.41, 131.38, 130.83, 129.41, 129.29, 129.17, 128.89, 128.56, 128.03, 127.91, 127.87, 127.48, 127.15, 126.34, 125.74, 125.62, 124.97, 124.84, 124.80, 122.78, 122.66, 119.82, 48.21 ppm. $^{31}P\{^{1}H\}$ NMR (202 MHz, $CDCl_3$): δ_P +64.72 ppm. UV-vis. (MeCN) λ_{max} (ε / $dm^3mol^{-1}cm^{-1}$): 375 (200), 343 (25280), 327 (18120), 313 (8640), 300 (5080), 276 (32480), 266 (21240), 242 (51680), 233 (42280) nm. HRMS found *m/z* 612.1143, calcd *m/z* 612.1150 for $[C_{29}H_{22}AuNP]^{+}$. IR (solid) ν / cm^{-1}: 3379, 3036, 2363, 1605, 1587, 1553, 1504, 1499, 1477, 1435, 1418, 1395, 1375, 1304, 1240, 1180, 1169, 1130, 1101, 1067, 1049, 1022, 995, 961, 920, 903, 878, 843, 825, 820, 808, 746, 723, 710, 692, 619.

Synthesis of [AuCl(L3)]

L3 (130 mg, 0.32 mmol) and tetrahydrothiophenegold chloride (93 mg, 0.29 mmol) were added to degassed dichloromethane (15 ml) and the solution stirred at room temperature under nitrogen for 2 hours. The solvent was reduced *in vacuo* and diethyl ether added dropwise. The resultant precipitate was filtered and dried to give a crude solid. This was then purified by column chromatography

(silica) and eluted as the first fraction from 9:1 DCM:MeOH, to give [AuCl(L3)] as an orange solid (13 mg, 19 %). ^{1}H NMR (500 MHz, $CDCl_3$): δ_H 10.92 (d, $^{2}J_{HP}$ = 6.1 Hz, 1H, N*H*), 8.31 – 8.24 (m, 2H), 7.95 (d, $^{3}J_{HH}$ = 7.4 Hz, 1H), 7.89 – 7.83 (m, 4H), 7.80 (dd, J_{HH} = 5.9, 2.1 Hz, 2H), 7.67 (d, J_{HH} = 8.0 Hz, 1H), 7.64 – 7.60 (m, 3H), 7.60 – 7.55 (m, 4H) ppm. ^{13}C{^{1}H} NMR (126 MHz, $CDCl_3$): δ_C 187.47, 182.67, 146.60, 135.88, 134.70, 134.55, 134.45, 134.09, 133.20, 133.18, 133.16, 132.71, 132.65 (d, *J* = 16.1 Hz) 130.29, 129.83 (d, *J* = 12.7 Hz), 127.34, 122.84 (d, *J* = 13.8 Hz), 120.96, 117.96, 117.92 ppm. ^{31}P{^{1}H} NMR (162 MHz, $CDCl_3$): δ_P +55.77 ppm. HRMS found *m/z* 604.0791, calcd *m/z* 604.0735 for $[C_{26}H_{18}AuNO_2P]^+$. UV-vis. (MeCN) λ_{max} (ε / $dm^3mol^{-1}cm^{-1}$): 442 (3720), 298 (6040), 270 (16560), 241 (30240), 224 (33760) nm. IR (solid) ν / cm^{-1}: 3410, 3306, 3042, 2976, 2587, 2496, 2374, 1165, 1632, 1585, 1543, 1472, 1460, 1435, 1396, 1344,1265, 1298, 1233, 1171, 1159, 1105, 1042, 1022, 997, 829, 802, 777, 748, 735, 695, 640, 606.

Synthesis of *$[Au_2Cl_2$(**L4**)$]$*

L4 (50 mg, 008 mmol) and tetrahydrothiophenegold chloride (48 mg, 0.15 mmol) were added to degassed dichloromethane (8 ml) and the solution stirred at room temperature under nitrogen for 2 hours. The solvent was reduced *in vacuo* and diethyl ether added dropwise. The resultant precipitate was filtered and dried to give *$[Au_2Cl_2(L_4)]$* as a purple solid (31 mg, 35 %). ^{1}H NMR (500 MHz, $CDCl_3$) δ 11.24 (d, *J* = 6.1 Hz, 2H), 8.27 – 8.25 (m, 2H), 7.84 – 7.78 (m, 8H), 7.62 – 7.62-7.59 (m, 4H), 7.59 – 7.54 (m, 10H), 7.53 (s, 2H). ^{13}C{^{1}H} NMR (126 MHz, $CDCl_3$) δ 186.54 (C=O), 142.13, 135.41, 135.30, 134.54, 133.51, 133.34, 133.32, 132.67, 132.60 (d, J_{CP} = 16.1 Hz), 132.52, 130.70, 130.15, 129.91 (d, J_{CP} = 12.7 Hz), 129.78, 129.68, 127.26, 126.29, 126.18, 119.70. ^{31}P{^{1}H} NMR (202 MHz, $CDCl_3$) δ + 56.63. HRMS found *m/z* 1035.0640, calcd *m/z* 1035.0640 for $[C_{38}H_{28}Au_2N_2P_2Cl]^+$. UV-vis. (MeCN) λ_{max} (ε / $dm^3mol^{-1}cm^{-1}$): 523 (4240), 325 (4620), 282 (15640), 254 (31560), 224 (34440). IR (solid) ν / cm^{-1}: 3402, 2363, 2347, 1620, 1587, 1574, 1537, 1472, 1435, 1364, 1342, 1294, 1242, 1177, 1126, 1105, 1030, 984, 901, 880, 827, 797, 748, 729, 691, 528, 511, 438, 403.

3.5.4 Preparation of Substituted Phosphinite Ligands

Synthesis of L5

9-Anthracenemethanol (500 mg, 2.4 mmol) and 4-dimethylaminopyridine (DMAP) (59 mg, 0.48 mmol) were dissolved in dry & degassed THF (30 ml). Triethylamine was added (2.9 mmol, 0.40 ml) followed by diphenylchlorophosphine (2.6 mmol, 0.48 ml). The resulting solution was stirred at room temperature for two hours under a nitrogen atmosphere. The solvent was reduced *in vacuo* and 9:1 hexane:ethyl acetate (50 ml) was added. The resulting mixture was filtered through celite and alumina and the solvent removed *in vacuo* to give LG334 as a yellow oil. (866 mg, 92%). ^{1}H NMR (500 MHz, $CDCl_3$) δ 8.31 (s, 1H), 8.21 (d, *J* = 8.7 Hz, 1H), 8.16 (d, *J* = 8.7 Hz, 1H), 7.85 (d, *J* = 8.1 Hz, 2H), 7.69 – 7.60 (m, 1H), 7.41 – 7.30 (m, 8H), 7.25 – 7.13 (m, 5H), 5.68 (d, *J* = 8.0 Hz, 2H). ^{13}C{^{1}H} NMR (126 MHz, $CDCl_3$) δ 141.90, 141.76, 132.23, 132.20, 131.84, 131.76, 131.52, 131.41, 131.00, 130.90, 130.72, 130.55, 130.41, 129.38, 129.07, 129.05, 128.78, 128.53, 128.43, 128.35, 128.30, 126.74, 126.32, 125.15, 125.05, 124.52, 124.02. ^{31}P{^{1}H} NMR (202 MHz, $CDCl_3$) δ 113.74, 32.22 (minor oxidised product impurity). HRMS found *m/z* 393.1415, calculated *m/z* 393.1408 for $[C_{27}H_{22}OP]^{+}$. λ_{max} {ε/dm^3 mol^{-1} cm^{-1}}: 385 {7080), 365 {7880}, 347 {5440}, 330 {3920}, 283 (s) (9720}, 255 {111320}. IR (solid. V_{max})/cm^{-1}: 3051, 1720, 1665, 1655, 1624, 1602, 1582, 1526, 1472, 1435, 1371, 1341, 1308, 1259, 1180, 1157, 1128, 1111, 1093, 1053, 1026, 968, 887, 868, 845, 804, 770, 727, 690, 626, 602, 579, 554, 515.

Synthesis of L6

As for *L5*, but using 1-pyrenemethanol (250 mg, 1.1 mmol), DMAP (26 mg, 0.22 mmol), dry & degassed THF (20 ml), triethylamine (0.17 ml, 1.3 mmol) and diphenylchlorophosphine (0.22 ml, 1.2 mmol) to give LG335 as a pale yellow oil (407 mg, 91%). ^{1}H NMR (400 MHz, $CDCl_3$) δ 8.09 (d, *J* = 9.2 Hz, 1H), 7.96 (d, *J* = 7.6 Hz, 10H), 7.70 – 7.61 (m, 1H), 7.47 (dd, *J* = 7.9, 6.9 Hz, 1H), 7.43 – 7.35 (m, 4H), 7.23-7.16 (m, 2H), 5.39 (d, *J* = 8.9 Hz, 2H). ^{13}C{^{1}H} NMR (101 MHz, $CDCl_3$) δ 140.69, 140.51, 134.38, 134.31, 134.18, 134.11, 130.64, 130.24, 130.08, 129.62, 129.57, 129.36, 128.53, 128.25, 127.91, 127.46, 127.24, 127.18, 126.59, 126.32, 126.27, 125.69, 124.77, 124.48, 124.12, 123.70,

123.55, 123.42, 122.21. $^{31}P\{^{1}H\}$ NMR (162 MHz, $CDCl_3$) δ 114.03. HRMS found *m/z* 416.1335, calculated *m/z* 416.1330 for $[C_{29}H_{21}OP]^+$. λ_{max} {ε/dm^3 mol^{-1} cm^{-1}}: 376 {1360}, 347 {41400}, 331 {29160}, 316 {13520}, 302 {7920}, 279 {50200}, 268 {33520}, 257 {23340}. IR (solid. V_{max})/cm^{-1}: 3042, 1600, 1587, 1510, 1481, 1454, 1435, 1416, 1375, 1371, 1306, 1223, 1182, 1126, 1094, 1063, 1026, 991, 980, 843, 816, 739, 691, 610.

1 J. Gopalakrishnan, *Appl. Organomet. Chem.*, 2009, **23**, 291–318.

2 J. I. G. Cadogan, *Organophosphorus Reagents in Organic Synthesis*, Academic Press: New York, 1979.

3 D. V. Shenai, M. L. Timmons, R. L. DiCarlo and C. J. Marsman, *J. Cryst. Growth.*, 2004, **272**, 603–608.

4 G. Pacchioni and P. S. Bagus, *Inorg. Chem.*, 1992, **31**, 4391–4398.

5 F. A. Cotton, G. Wilkinson, C. Murillo and M. Y. Bochman, *Advanced Inorganic Chemistry 6th edn.*, John Wiley & Sons Inc: New York, 1999.

6 L. Vaska, *J. Am. Chem. Soc.*, 1968, **88**, 5325.

7 H. B. Kagan, N. Langlois and T. Dang, *J. Organomet. Chem.*, 1975, **90**, 353–365, 2007.

8 M. Lotz, F. Spindler, European Patent EP1756131, 2007.

9 Kattesh V. Katti, Hariprasad Gali, Charles J. Smith, and and Douglas E. Berning, *Acc. Chem. Res.* , 1998, **32**, 9–17.

10 A. Trifonova, J. S. Diesen, C. J. Chapman and P. G. Andersson, *Org. Lett.*, 2004, **6**, 3825–3827.

11 A. Grabulosa, G. Muller, J. I. Ordinas, A. Mezzetti, M. Maestro, M. Font-Bardia and X. Solans, *Organometallics*, 2005, **24**, 4961–4973.

12 A. Michaelis, *Ann. Chim.*, 1903, **326**, 129–258.

13 M. Alajarín, C. López-Leonardo and P. Llamas-Lorente, *Top Curr. Chem.*, 2005, **250**, 77–106.

14 M. Becke-Goehring and J. Schulze, *Chem. Ber.*, 1958, **91**, 1188–1195.

15 J. Goubeau and R. Pantzer, *Z. Anorg. Allg. Chem.*, 1972, **390**, 25–30.

16 R. B. King, N. D. Sadanani and P. M. Sundaram, *J. Chem. Soc. Chem. Commun.*, 1983, **8**, 447–448.

17 N. E and R. R, *Angew. Chemie Int. Ed.*, 1982, **21**, 62–63.

18 G. S. Harris, *J. Chem. Soc.*, 1965, **87**, 3092–3097.

19 A. B. Burg and J. Heners, *J. Am. Chem. Soc.*, 1965, **87**, 3092–3097.

20 H. R. Hudson, *The chemistry of organophosphorus compounds*, John Wiley & Sons Inc: New York, 1990.

21 R. D. Kroeshefsky and J. G. Verkade, *Inorg. Chem.*, 1975, **14**, 3090–3095.

22 G. Ewart, A. P. Lane, J. McKechnie and D. S. Payne, *J. Chem. Soc.*, 1964, **0**, 1543–1547.

23 A. P. Lane, D. A. Morton-Blake and D. S. Payne, *J. Chem. Soc. A*, 1967, **0**, 1492–1498.

24 T. Mohan, M. N. Sudheendra Rao and G. Aravamudan, *Tetrahedron Lett.*, 1989, **30**, 4871–4874.

25 R. B. King and P. M. Sundaram, *J. Org. Chem.*, 1984, **49**, 1784–1789.

26 R. P. K. Babu, S. S. Krishnamurthy and M. Nethaji, *Heteroat. Chem.*, 1991, **2**, 477–485.

27 J. F. Nixon, *J. Chem. Soc. A*, 1968, **0**, 2689–2692.

28 R. Jefferson, J. F. Nixon, T. M. Painter, R. Keat and L. Stobbs, *J. Chem. Soc. Dalton Trans.*, 1973, **0**, 1414–1419.

29 R. Keat, D. S. Rycroft and D. G. Thompson, *J. Chem. Soc. Dalton Trans.*, 1979, **0**, 1224–1230.

30 L. Maier, *Helv. Chim. Acta*, 1963, **46**, 2667–2676.

31 J. R. VanWazer and L. Maier, *J. Am. Chem. Soc.*, 1964, **86**, 811–814.

32 A. Tarassoli, R. C. Haltiwanger and A. D. Norman, *Inorg. Chem.*, 1982, **21**, 2684–2690.

33 L. A. Hussain, A. J. Elias and M. Rao, *Tetrahedron Lett.*, 1988, **29**, 5983–5986.

34 R. Contreras, J. M. Grevy, Z. García-Hernández, M. Göizado-Rodriguez and B. Wrackmeyer, *Heteroat. Chem.*, 2001, **12**, 542–550.

35 R. Vogt, P. G. Jones, R. Schmutzler and A. Kolbe, *Chem. Ber.*, 1991, **124**, 2705–2714.

36 P. Braunstein, C. Frison, X. Morise, R. D. Adams, S. J. Rettig, F. Speiser, A. Tiripicchio and F. Ugozzoli, *J. Chem. Soc. Dalton Trans.*, 2000, **90**, 2205–2214.

37 P. Bhattacharyya, A. M. Z. Slawin, M. B. Smith, D. J. Williams and J. D. Woollins, *J. Chem. Soc. Dalton Trans.*, 1996, **97**, 3647.

38 D. F. Shriver and M. A. Drezdzon, *The Manipulation of Air-sensitive Compounds, 2nd edn.*, John Wiley & Sons Inc: New York, 1986.

39 R. J. Errington, *Advanced Practical Inorganic and Metalorganic Chemistry*, Blackie Academic and Professional: London, 1997.

40 D. G. Gorenstein, *Phosphorus-31 NMR: Principles and Applications*, Academic Press: Orlando, FL., 1984.

41 A. H. Cowley, M. J. S. Dewar, W. R. Jackson and W. B. Jennings, *J. Am. Chem. Soc.*, 1970, **92**, 5206–5213.

42 H. Schmidbaur, S. Lauteschläger and F. H. Köhler, *J. Organomet. Chem.*, 1984, **271**, 173–180.

43 T. Torroba, *J. für Prakt. Chemie*, 1999, **341**, 99–113.

44 H. W. Roesky, J. Lucas, J. Noltemeyer and G. M. Sheldrick, *Chem. Ber.*, 1984, **117**, 1583–1590.

45 F. R. Hartley, *The Chemistry of Phosphorus Compounds. Vols 1-3*, John Wiley & Sons Inc: New York, 1994.

46 E. Graugnard, V. Chawla, D. Lorang and C. J. Summers., *Appl. Phys. Lett.*, 2006, **89**, 211102–211103.

47 Srinivasan Priya, Maravanji S. Balakrishna, and Joel T. Mague and S. M. Mobin, 2003, **42**, 1272–1281.

48 M. R. Zubiri, H. L. Milton, A. M. Z. Slawin and J. D. Woollins, *Poyhedron*, 2004, **23**, 865–868.

49 M. R. I. Zubiri, H. L. Milton, D. J. Cole-Hamilton, A. M. Z. Slawin and J. Derek Woollins, *Polyhedron*, 2004, **23**, 693–699.

50 S. M. Aucott, A. M. Z. Slawin and J. D. Woollins, *Polyhedron*, 2003, **22**, 361–368.

51 T. Appleby, S. M. Aucott, M. L. Clarke, A. M. Z. Slawin and J. D. Woollins, *Polyhedron*, 2002, **21**, 2639–2654.

52 C. A. Tolman, *Chem. Rev.*, 1977, **77**, 313–348.

53 P. Dierkes and P. W. N. M. van Leeuwen, *J. Chem. Soc. Dalton Trans.*, 1999, **0**, 1519–1530.

54 Z. Freixa, P. W. N. M. van Leeuwen, G. D. Batema, C. B. Dieleman, G. P. F. van Strijdonck, J. N. H. Reek, P. C. J. Kamer, J. Fraanje, K. Goubitz, P. W. N. . M. van Leeuwen, A. L. Spek and P. W. N. M. van Leeuwen, *Dalton Trans.*, 2003, **211**, 1890–1901.

55 I. M. Dixon, E. Lebon, G. Loustau, P. Sutra, L. Vendier, A. Igau, A. Juris and G. van Koten, *Dalton Trans.*, 2008, **30**, 5627.

56 W. Schirmer, U. Florke and H.-J. Haupt, *Zeitschrift für Anorg. und Allg. Chemie*, 1987, **545**, 83–97.

57 Fu-Yao Zhang, and Cheng-Chao Pai and A. S. C. Chan, 1998, **120**, 5808–5809.

58 G. Xu and S. R. Gilbertson, *Tetrahedron Lett.*, 2003, **44**, 953–955.

59 C. Blanc and F. Agbossou-Niedercorn, *Tetrahedron: Asymmetry*, 2004, **15**, 757–761.

60 H. Brunner and H. Weber, *Chem. Ber.*, 1985, **118**, 3380–3395.

61 Feng-Bo Xu, Lin-Hong Weng, A. Li-Juan Sun, Zheng-Zhi Zhang and Z.-F. Zhou, *Organometallics*, 2000, **19**, 2658–2660.

62 Feng-Bo Xu, Qing-Shan Li, Li-Zhu Wu, Xue-Bing Leng, Zu-Cheng Li, Xian-Shun Zeng, A. Yuan L. Chow and Zheng-Zhi Zhang, *Organometallics*, 2003, **22**, 633–640.

63 Qing-Shan Li, Chong-Qing Wan, Ru-Yi Zou, Feng-Bo Xu, Hai-Bin Song, A. Xiang-Jian Wan and Z.-Z. Zhang, *Inorg. Chem.*, 2006, **45**, 1888–1890.

64 L. H. Davies, B. Stewart, R. W. Harrington, W. Clegg and L. J. Higham, *Angew. Chemie*, 2012, **124**, 5005–5008.

65 S. Nigam, B. P. Burke, L. H. Davies, J. Domarkas, J. F. Wallis, P. G. Waddell, J. S. Waby, D. M. Benoit, A.-M. Seymour, C. Cawthorne, L. J. Higham and S. J. Archibald, *Chem. Commun.*, 2016, **52**, 7114–7117.

66 O. Halter, R. Vasiuta, I. Fernández and H. Plenio, *Chem. - A Eur. J.*, 2016, **22**, 18066–18072.

67 A. M. Christianson and F. P. Gabbaï, *Inorg. Chem.*, 2016, **55**, 5828–5835.

68 S. Yamaguchi, S. Akiyama and K. Tamao, *J. Organomet. Chem.*, 2002, **652**, 3–9.

69 K. T. S. Yamaguchi, S. Akiyama, *J. Organomet. Chem.*, 2002, **646**, 277–281.

70 T. Hatakeyama, S. Hashimoto and M. Nakamura, *Org. Lett.*, 2011, **13**, 2130–2133.

71 J. Wang, Q. Zhao, C. M. Lawson and G. M. Gray, *Opt. Commun.*, 2011, **284**, 3090–3094.

72 L. Ortego, J. Gonzalo-Asensio, A. Laguna, M. D. Villacampa and M. C. Gimeno, *J. Inorg. Biochem.*, 2015, **146**, 19–27.

73 T. V. B. Rajanbabu, in *Phosphorus(III) Ligands in Homogeneous Catalysis: Design and Synthesis*, John Wiley & Sons, Ltd, Chichester, UK, 2012, pp. 159–232.

74 C. A. Tolman, *J. Am. Chem. Soc.*, 1970, **92**, 2956–2965.

75 D. White and N. J. Coville, *Adv. Organomet. Chem.*, 1994, **36**, 95–158.

76 A. Adhikary and H. Guan, *ACS Catal.*, 2015, **5**, 6858–6873.

77 S. Lal, J. McNally, A. J. P. White and S. Díez-González, *Organometallics*, 2011, **30**, 6225–6232.

78 Y. Sato, S. I. Kawaguchi and A. Ogawa, *Chem. Commun.*, 2015, **51**, 10385–10388.

79 E. Drent, R. van Dijk, R. van Ginkel, B. van Oort and R. Pugh, *Chem. Commun.*,

2002, **9**, 964–965.

80 H. Neumann, R. Kadyrov, X. Wu and M. Beller, *Chem. Asian J.*, 2012, **7**, 2213–2216.

81 M. Tanaka and I. Ogata, *Chem. Commun.*, 1975, **18**, 735.

82 L. Bini, C. Muller and D. Vogt, *Chem. Commun.*, 2010, **46**, 8325–8334.

83 I. Mikhel, M. Garland, J. Hopewell, S. Mastroianni, C. McMullin, A. Orpen and P. Pringle, *Organometallics*, 2011, **30**, 974–985.

84 M. Dieguez, O. Pamies and C. Claver, *Chem. Rev.*, 2004, **104**, 3189–3215.

85 S. Castillon, C. Claver and Y. Diaz, *Chem. Soc. Rev.*, 2005, **34**, 702–713.

86 S. Woodward, M. Dieguez and O. Pamies, *Coord. Chem. Rev.*, 2010, **254**, 2007–2030.

87 H. Fernandez-Perez, P. Etayo, A. Panossian and A. Vidal-Ferran, *Chem. Rev.*, 2011, **111**, 2119–2176.

88 F. Agbossou-Niedercorn, *Coord. Chem. Rev.*, 2003, **242**, 145–158.

89 W. Hunks, M. Jennings and R. Puddephatt, *Inorg. Chem.*, 2000, **39**, 2699–2702.

90 J. A. M. van den Goorbergh and A. van der Gen, *Tetrahedron Lett.*, 1980, **21**, 3621–3624.

91 A. K. Bhattacharyya and G. Thyagarajan, *Chem. Rev.*, 1981, **81**, 415–430.

92 U. Işık, M. Aydemir, N. Meriç, F. Durap, C. Kayan, H. Temel and A. Baysal, *J. Mol. Catal. A Chem.*, 2013, **379**, 225–233.

93 A. D. Burrows, M. F. Mahon and M. T. Palmer, *Dalton Trans.*, 2000, 3615.

94 S. Naik, S. Kumar, J. T. Mague, M. S. Balakrishna, D. Ma, Z. Xie, L. Wang, K. D. John, B. L. Scott, J. D. Thompson, D. E. Morris and J. L. Kiplinger, *Dalton Trans.*, 2016, **45**, 18434–18437.

95 L. Baiget, A. S. Batsanov, P. W. Dyer, M. A. Fox, M. J. Hanton, J. A. K. Howard, P. K. Lane and S. A. Solomon, *Dalton Trans.*, 2008, **89**, 1043.

96 P. W. Dyer, J. Fawcett and M. J. Hanton, *J. Organomet. Chem.*, 2005, **690**, 5264–5281.

97 Q. Zhang, G. Hua, P. Bhattacharyya, A. M. Z. Slawin, J. Derek Woollins, A. V. Aerschot, A. De Bruyn, D. De Keukeleire, A. P. Uzerman, P. Herdewijn and R. H. Yu, *Dalton Trans.*, 2003, **582**, 3250–3257.

98 N. Z. and Douglas C. Neckers, *J. Org. Chem.*, 2000, **65**, 2145–2150.

99 J. E. Jones, B. M. Kariuki, B. D. Ward, S. J. A. Pope, T. J. Meyer, B. A. DeGraff, N.

Chattopadhyay, H. Pal, J. N. Alumasa, P. D. Roepe, D. G. I. Kingston, C. F. Williams and M. P. Coogan, *Dalton Trans.*, 2011, **40**, 3498.

100 D. Wester and G. J. Palenik, *J. Am. Chem. Soc.*, 1973, **95**, 6506–6506.

101 L. Falivene, R. Credendino, A. Poater, A. Petta, L. Serra, R. Oliva, V. Scarano and L. Cavallo, *Organometallics*, 2016, **35**, 2286–2293.

102 T. E. Muller and D. M. P. Mingos, *Transit. Met. Chem.*, 1995, **20**, 533–539.

103 E. E. Langdon-Jones and S. J. A. Pope, *Coord. Chem. Rev.*, 2014, **269**, 32–53.

104 P. Dahiya, M. Kumbhakar, T. Mukherjee and H. Pal, *J. Mol. Struct.*, 2006, **798**, 40–48.

105 T. Wang, H. Sun, T. Lu, K. C. Weerasinghe, D. Liu, W. Hu, X. Zhou, L. Wang, W. Li and L. Liu, *J. Mol. Struct.*, 2016, **1116**, 256–263.

106 T. Yanai, D. P. Tew and N. C. Handy, *Chem. Phys. Lett.*, 2004, **393**, 51–57.

107 A. Vlcek and S. Zalis, *Coord. Chem. Rev.*, 2007, **251**, 258.

108 Y. Zhao and D. G. Truhlar, *Theor. Chem. Acc.*, 2008, **120**, 215–241.

109 D. Andrae, U. Haubermann, M. Dolg, H. Stoll and H. Preub, *Theor. Chim. Acta.*, 1990, **77**, 123–141.

110 T. H. Dunning, *J. Chem. Phys.*, 1989, **90**, 1007–1023.

111 T. H. Dunning, K. A. Peterson and A. K. Wilson, *J. Chem. Phys.*, 2001, **114**, 9244–9253.

112 P. J. Stephens and N. Harada, *Chirality*, 2009, **22**, 229–233.

113 A. M. Sarotti and S. C. Pellegrinet, *J. Org. Chem.*, 2009, **74**, 7254–7260.

114 A. M. Sarotti and S. C. Pellegrinet, *J. Org. Chem.*, 2012, **77**, 6059–6065.

115 M. Frank, M. Nieger, F. Vögtle, P. Belser, A. von Zelewsky, L. De Cola, V. Balzani, F. Barigelletti and L. Flamigni, *Inorganica Chim. Acta*, 1996, **242**, 281–291.

116 O. V. Dolomanov, L. J. Bourhis, R. J. Gildea, J. A. K. Howard, H. Puschmann, S. K., W. L., P. G. and S. R., *J. Appl. Crystallogr.*, 2009, **42**, 339–341.

117 L. Palatinus, G. Chapuis, C. P., C. R. M., E. J., M. E. and F. T., *J. Appl. Crystallogr.*, 2007, **40**, 786–790.

118 G. M. Sheldrick, *Acta. Cryst.*, 2015, **71**, 3–8.

Chapter 4 - Rapid, Machine-Assisted Syntheses of Substituted Iridium(III)-Pyrazolate Complexes with Tuneable Luminescence

4.1 Introduction

4.1.1 Synthesis and Applications of Pyrazole and Pyrazolate

The synthesis of heterocyclic compounds is an extremely important area of research. In an already established field, the diversity, simplicity of scale up and sustainability of the synthetic protocol represent key factors in the future progress of the field.[1] Pyrazoles are characterized as five-membered heterocycles featuring two adjacent nitrogen atoms, with applications in materials, agrochemicals and pharmaceuticals, for example celecoxib, crizotinib, sildenafil and pyrazoxyfen (Figure 4.1).[2]

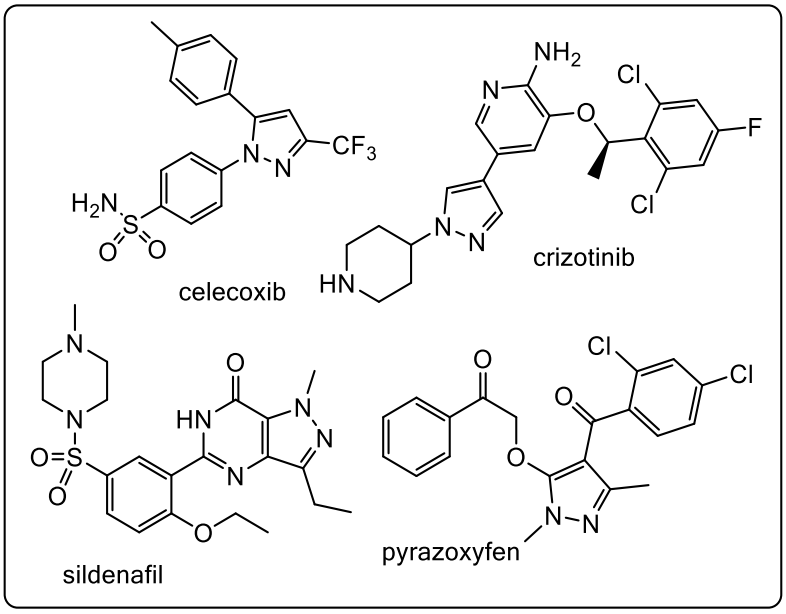

Figure 4.1: Structures of celecoxib, crizotinib, sildenafil and pyrazoxyfen[2]

Cyclo-condensation of hydrazines with 1,3-dicarbonyl compounds is the most common preparatory method for pyrazoles and pyrazolates at scale. This can either be carried out *via* cyclo-condensation with simple hydrazine followed by a non-selective alkylation of a tautomeric mixture, or by specific substitution of hydrazine followed by an electronically controlled regioselective cyclo-condensation. The latter of these synthetic methods is usually a more selective process and hence is more commonly used. However, because methods are associated with the preparation and storage of hydrazines on a large scale, there is a significant safety risk.[1]

Palladium-catalysed cross-coupling methods have been utilised for the synthesis of substituted hydrazines, where the scope for this technique has been recently increased by the development of specific ligands that assist a difficult reductive elimination step.[3] Due to this problematic step, a continuous flow approach has also been explored.[4] In addition, amine-redox chemistry has been employed and allows access to a wide range of substituted hydrazine centres. This synthetic technique involves oxidation through diazotization, followed by reduction of the N-N triple bond, usually with tin(II) chloride. An example of this is provided by Widlicka et al, who reported N-aryl pyrazoles prepared from anilines in a three-step telescoped approach, where a continuous flow set up was used to minimise accumulation of the highly energetic and potentially explosive diazonium salt and hydrazine intermediates to enable safe scale up.[5]

Due to the increased importance of green chemistry, there has recently been advances in the use of more sustainable reductants that can be washed away from the product through simple aqueous extraction. In this vein, methods utilising ascorbic acid or sodium sulfite acting as a reductant have been described.[6] In addition, a selection of di-, tri- and tetrasubstituted pyrazoles have been synthesised from α,β-unsaturated aldehydes and ketones via I_2-mediated oxidative C-N bond formation (Figure 4.2).[7]

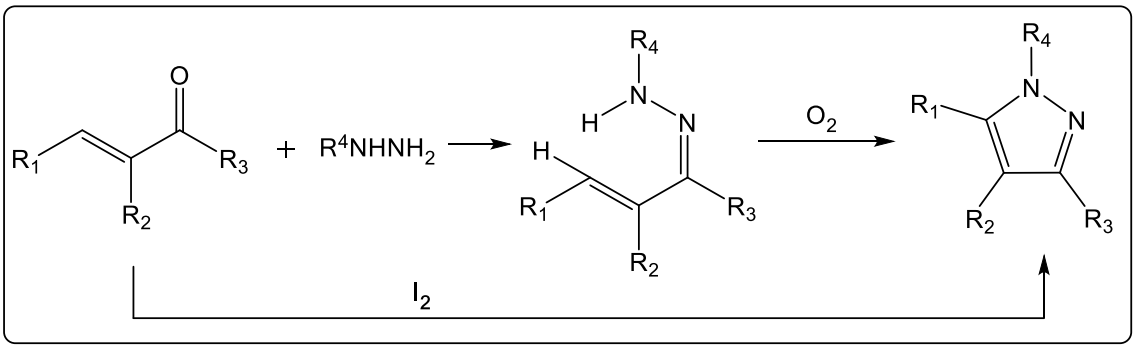

Figure 4.2: Oxidative bond formation with I_2[7]

Recent work describes the first example of an end-to-end, metal-free, multistep continuous flow process.[1] The process begins with an amine-redox cycle followed by hydrolysis of the hydrazine surrogate resulting in cyclo-condensation. The method involves by low levels of diazonium salt and hydrazine at all times, as well as the use of

vitamin C as the reductant. The authors demonstrated that the conditions and parameters were applicable to a broad range of amine and 1,3-dicarbonyl substituents.

4.1.2 Pyrazole and Pyrazolate as Ligands

Heterocyclic compounds with bidentate and tridentate ligand capabilities have been extensively reviewed. For example, compounds containing six membered rings such as 2,2'-bipyridine (bipy) and 1,10-phenanthroline (phen) have been the basis of many studies.[8] The vacant low-lying π* orbitals in the nucleus makes them excellent π-acceptors and hence they act as soft ligands for metal coordination. In contrast, the π-excessive five-membered nitrogen heterocycle, pyrazole, is a better π-donor and thus acts as a hard donor site. Anionic tripodal ligands, poly(pyrazolyl)borates, have found a range of applications in bioinorganic and organometallic chemistry since their discovery in 1966.[9] In more recent years, a wider range of pyrazole/pyrazolate-based chelating ligands have been utilised to create a range of coordination complexes, providing varying coordination geometry and nuclearity.[8] These ligands have a huge potential in terms of their coordination chemistry as they can range from mono- through to tetra-dentate, although in this chapter only bidentate applications will be discussed. In addition, the ease of synthesis is a beneficial factor in the design of new ligands, and allows electronic and steric control of the properties of the metal complexes.

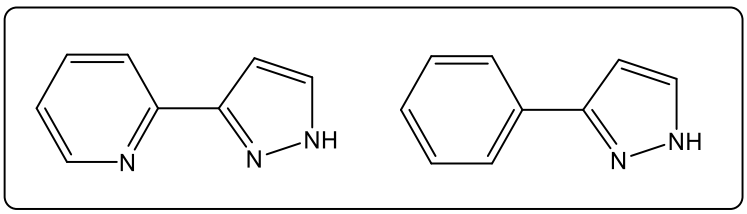

Figure 4.3: 3-(2-pyridyl)pyrazole and 3-(2-phenyl)pyrazole

Estevan *et al.* conducted research that explored the versatility and ability of stabilizing pyrazole and pyrazolate ligands. In this work, novel palladium(II) and (III) compounds were synthesized and structurally characterized, where one compound was the first paddlewheel dinuclear palladium(II) compound with pyrazolato bridging ligands described in the literature.[10]

4.1.3 Pyrazole and Pyrazolates as Ligands for Iridium(III)

Pyrazoles and pyrazolates have been utilized as ligands for Ir(III). An example of this is provided by Costa *et al.,* who incorporated a 3,5-dimethyl-1-phenylpyrazole ligand into an ionic iridium complex $[Ir(dmppz)_2(pbpy)][PF_6]$ (Hdmppz = 3,5-dimethyl-1-phenylpyrazole; pbpy = 6-phenyl-2,2'-bipyridine).[11] This ligand was used to exploit the wider band gap of phenylpyrazole based ligands when compared to their 2-phenylpyridine (ppy) based equivalents.[12,13] The complex was used to form a supramolecular cage, upon which a new light emitting electrochemical cell (LEEC) was based which showed extremely high stability of around 2000 h. Rh(I) and Ir(I) complexes incorporating bidentate chelate groups through one pyrazole nitrogen and a pyridine nitrogen atom have also been described, where the Ir(I) compounds act as modest catalysts for the hydrosilyation of phenylcetylene with triethylsilane at 60 °C.[14] In addition, Han *et al.* described DFT studies and photophysical properties of three novel heteroleptic iridium(III) complexes bearing two cyclometalated 2',6'-difluoro-2,3'-bipyridyl (dfpypy) chelates and one pyridyl pyrazolate ligand (Figure 4.4).[15] It was shown that the lowest energy absorption wavelength calculated is in agreement with the experimental value, where the lowest energy emissions are localised between 454 and 821 nm. A range of iridium(III) complexes with similar designs and photophysical properties have also been reported for use as highly efficient phosphorescent organic light emitting diodes (OLEDs) (Figure 4.4).[16]

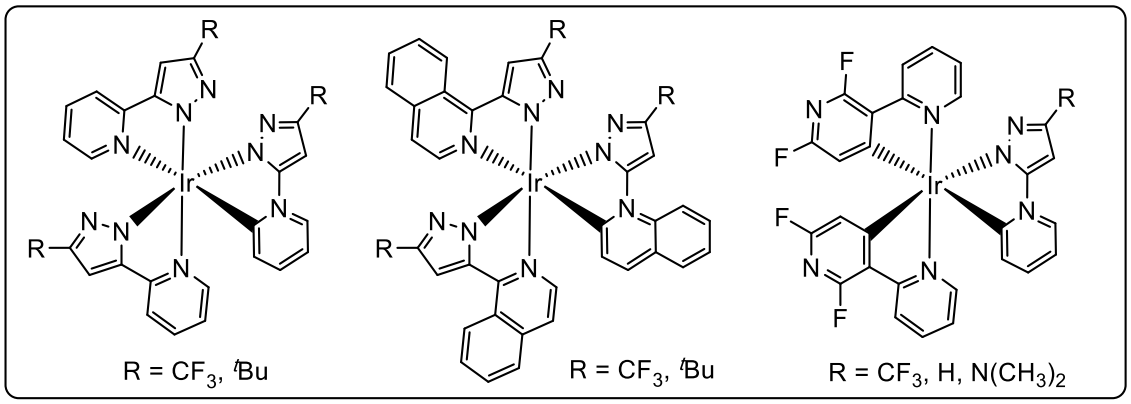

Figure 4.4: Examples of Ir(III) complexes containing pyrazole ligands[15,16]

As well as this, three multifunctional cationic Ir(III) complexes with aggregation-induced emission and piezochomic luminescence characteristics have been designed and synthesized.[17] Complexes contain cyclometalated dfppz (dfppz = 1-(2,4-difluorophenyl)1H-pyrazole) and varying ancillary ligands which are used to tune the photophysical properties. Absorption spectra exhibited spin allowed π-π* transitions, as well as triplet metal to ligand charge transfer (^{3}MLCT) and ligand-to-ligand charge transfer (^{1}LLCT). In addition, solution state emission spectra displayed a broad, featureless peak at 497 nm in MeCN. Finally, Davies *et al.* used 3-substituted phenylpyrazoles ligands to demonstrate that cyclometalated phenyls with substituents para to the iridium have a larger impact on the redox potentials and emission of complexes $[Ir(R\text{-}ppz)_2(bipy)]PF_6$ than those at the meta position.[18] In this case, emission wavelengths ranged from 504-615 nm depending on the nature of the substituent.

4.1.4 Luminescent, Cyclometalated Iridium(III) Complexes and their Applications

Currently, luminescent iridium(III) complexes are at the forefront of scientific interest in coordination complexes due to a number of specific properties: kinetic inertness, large Stokes' shifts, long luminescence lifetimes and high photostability.[19] The inherent stability of iridium(III) through kinetic inertness is due to its low-spin, d^6 configuration. This configuration means iridium(III) has a strong preference to cyclometalate and thus has the ability to form a number of complexes with a range of mono-, bi- or tri-dentate ligands.[20] In turn, emission profiles are representative of ^{3}MLCT[21], triplet intraligand charge transfer (^{3}ILCT)[22], triplet ligand to ligand charge transfer (^{3}LLCT)[23] and sigma bond

to ligand charge transfer (^{3}SBLCT).[24] As well as long lifetimes, the luminescent properties of iridium(III) often show high phosphorescence quantum yields, with tunable and environment sensitive emission properties.[25]

The highly efficient emission properties described exist for several reasons. Firstly, a large Δ is caused due to the presence of strong field cyclometalating ligands, such as ppy. In addition, the high oxidation state and the presence of 5d electrons gives rise to a large Δ, giving rise to efficient heavy atom assisted spin-orbit coupling (SOC).[26] As a consequence, long-lived triplet states are accessible via efficient intersystem crossing (ISC).[27] Singlet and triplet state mixing then allows Larporte forbidden phosphorescence relaxation. For example, Ir(III) complexes with phenylimidazo-phenanthroline ligands show strong orange-yellow phosphorescence (Ʈ = 0.2-100 μs, Φ = 1-50 %) centered between 540-600 nm. The excited states of the complexes possess a significant degree of charge transfer nature and hence have large Stokes' shifts (*ca.* 210nm) associated with a reduction in self-quenching.[25,26,28] In addition, synthesis and purification of the complexes with yields approaching theoretical can be performed with ease.[26a]

For the reasons outlined above, iridium(III) complexes are being employed for a range of varied applications, including sensing techniques, OLEDs[29], light-emitting electrochemical cells (OLECs)[30], photosensitisers in catalysis (including redox)[31], photocatalysts for water splitting,[32] cellular bioimaging[33], piezochromics[34], and as responsive materials for data recording[35] (for some examples, see Figure 4.5).

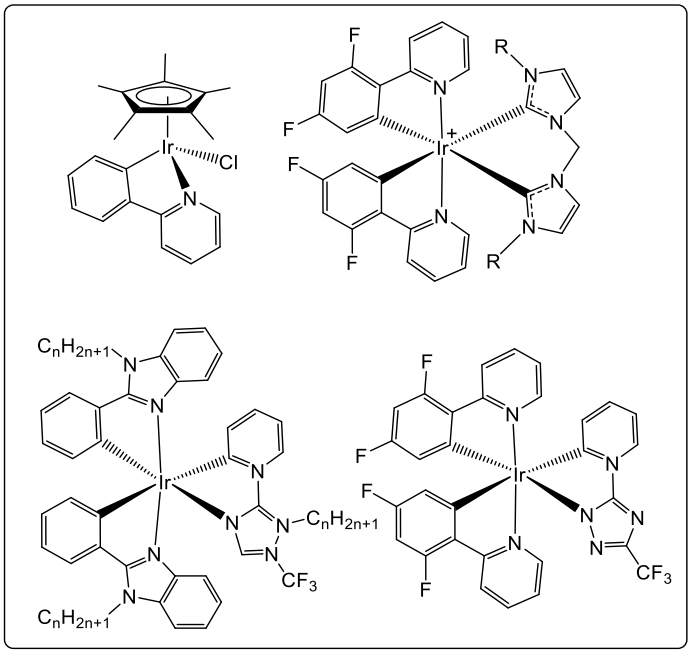

Figure 4.5: Examples of Ir(III) complexes for water splitting,[32] OLEC,[30] piezochromics[34] and OLED[29] applications

Cyclometalated iridium(III) complexes most widely investigated application is as OLEDs. An early example is provided by Lamansky *et al.* who reported complexes containing a range of CˆN ligands. By variation of the nature of the ligand, green to red phosphorescence and lifetimes less than 10 μs were observed, resulting in high performance OLEDs operating from the green to the red.[36] In a similar study, cyclometalated iridium(III) complexes based on CˆN ligands were shown to be suitable for use as red-emissive materials in OLEDs. Specifically, the OLED devices doped with $Ir(piq)_3$ (piq = 1-phenylisoquinoline) exhibited very high electroluminescence as well as distinctly saturated red emission, which was found to originate predominantly from ^{3}MLCT excited states with high quantum yields.[37] Another example is provided by Wong *et al*,[38] who demonstrated for the first time the synthesis of iridium phosphor complexes based on a diphenylaminofluorene framework for OLED applications. The complexes were shown to emit very strongly in the yellow to orange region, and had the potential for further structural modification for application variation. In addition, recent work has shown a yellow-emitting homoleptic iridium(III) complex constructed from a multifunctional spiro ligand.[39] The compound was applied as a highly efficient phosphorescent OLED, and almost equal energy levels when compared to the commercial phosphor iridium(III) bis(4-phenylthieno[3,2-c]pyridinato-N,$C^{2'}$)acetylacetonate (PO-01). As well as this, another commercially available complex,

bis[2-(4,6-difluorophenyl)pyridinato-C^2,N](picolinato)iridium(III) (FIrpic), has been shown to be effective as an addition to host materials to improve the efficiencies of blue phosphorescent OLEDs.[40] Four carbazolylphosphines and carbazolylphosphine oxide compounds were synthesised which, when incorporated with FIrpic, proved to be among the best performing FIrpic-based blue phosphorescent OLEDs without using any light extraction methods.[41]

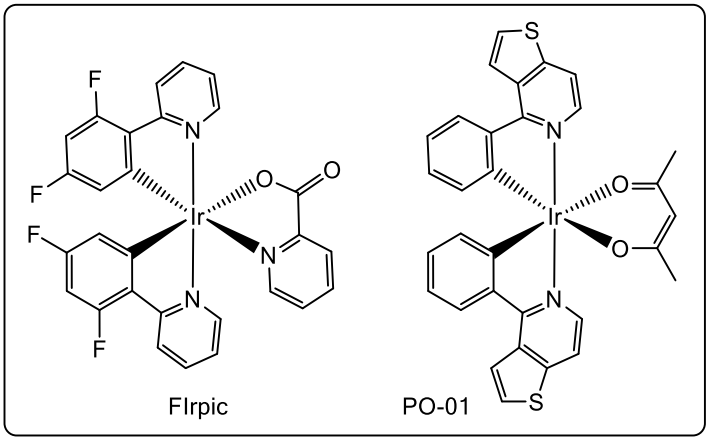

Figure 4.6: Examples of commercially available Ir(III) phosphors

In a similar vein, applications of iridium(III) as LEECs has been established and are now extensive. An LEEC is a solid-state device that has most of the advantages of OLEDs, as well as a few further benefits. An example of this is provided by Slinker *et al.*, who reported single layer devices incorporating $[Ir(ppy)_2\text{-}(dtb\text{-}bpy)]^+(PF6)^-$ (ppy: 2-phenylpyridine, dtb-bpy: 4,4'-di-tert-butyl-2,2'-dipyridyl).[42] The devices exhibited yellow electroluminescence with brightness that exceeds 300 cd/m^2 and a luminous power efficiency that exceeds 10 lm/W at just 3 V. In addition, cyclometalated iridium(III) complexes with methoxy- and methyl- substituted 2,3'-bipy and 4,4'-di-*tert*-butyl-2,2'-bipy were shown to exhibit blue-green emission with onsets around 450 nm and quantum yields above 40%.[43] When compared to previously published devices containing fluorine emitters the overall performance of these complexes was similar, with maximum luminescence above 1000 cd/m^2 and efficacy of 9.74 cd/A. Similarly, Fernandez-Hernandez et al reported blue emitting electrochemical cells containing triazole-based luminophores (Figure 4.7).[44]

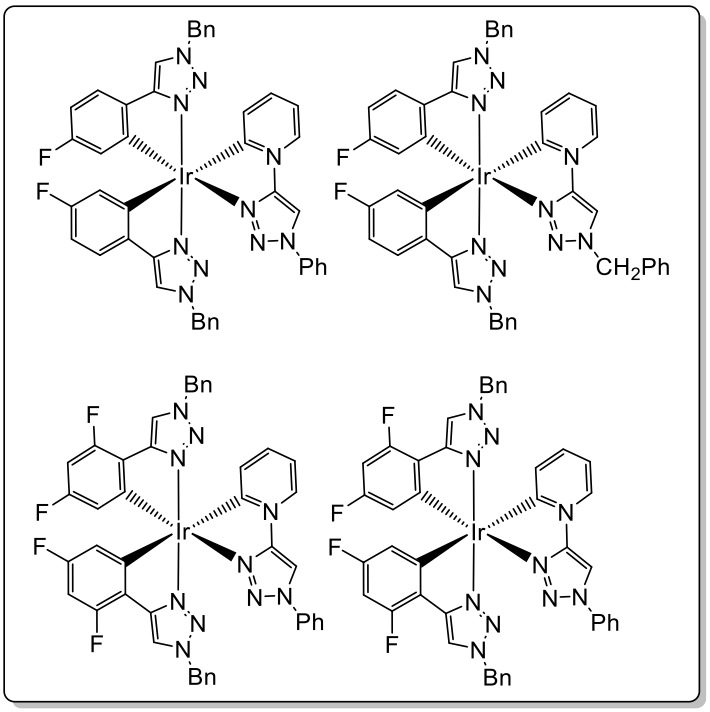

Figure 4.7: LEECs containing triazole-based lumophores[44]

There have been recent developments of Ir(III) diamine complexes as luminescent labels for biological applications.[45,46] A specific example comes from Lo *et al.* where a positively charged $[Ir(ppy)_2(dppz)]^+$ complex has been synthesised and proven to show luminescence and avid DNA binding.[47] As well as this, a highly selective chemosensor for homocysteine with emission enhancement based on the phosphorescent complex $Ir(pba)_2(acac)$ (Hpba = 4-(2-pyridyl)-benzaldehyde; acac = acetylacetone) that contains an aldehyde group has been presented.[48] Surface charge analysis and electrochemical measurement shows that a photoinduced electron transfer process for $[Ir(pba)_2(acac)]$-Cysteine might be responsible for the high specificity of $Ir(pba)_2(acac)$ toward homocysteine over cysteine. $[Ir(phq)_2(H_2O)_2)]$ (phq = 2-phenylquinoline) is a cell permeable cyclometalated complex that preferentially stains the cytoplasm of both live and dead cells with a bright luminescence, and hence has been developed as a phosphorescent probe (Figure 4.8).[49] Results indicate that the complex exhibits a high degree of selectivity for histidine over other amino acids, and the emission maximum falls on the boundary of the near-infrared optical window. In similar work $[Ir(ppy)_2(DMSO)_2]^+$ has been used as a luminescent agent for imaging live cell nuclei.[50] In recent work, Qui *et al.* reported two iridium(III) complexes with aggregation enhanced $^1O_2$ generation and bright phosphorescence for mitochondria-targeted two photon

photodynamic therapy (PDT) in monolayer cells and multicellular tumour spheroids (MCTSs).[51]

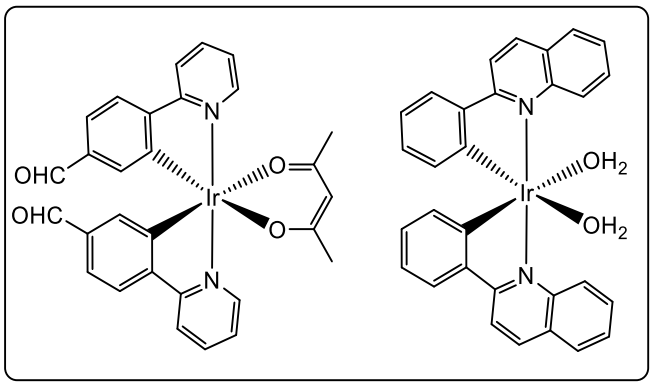

Figure 4.8: A chemosensor for homocysteine[48] and a cytoplasmic stain[49]

There have also been several reports of water soluble iridium complexes.[52,53,54] For example triazoles have been utilised by Zanarini *et al.* who synthesised a cationic iridium(III) complex comprising two ppy ligands and a neutral bidentate triazole-pyridine ligand, where the high solubility in water makes them highly advantageous in electrochemiluminescence.[55]

As well as the biological applications discussed, Ir(III) complexes can be used as ion probes. Complexes can be exploited as pH sensors when they contain an acidic or basic substituent, for example iridium(III) bis-terpyridine complexes reported by Licini and Williams.[56] Another example comes from Chi *et al*. where free nitrogen atoms cause a vast change in emission when in the presence of specific cations due to increased ^{3}MLCT character.[57] Anion sensors also exist and can be used to monitor by a specific colour change the cyanide anion, due to the cyanide anion breaking the conjugation in the molecule.[58]

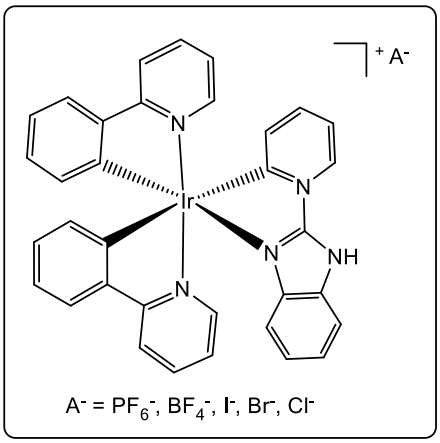

Figure 4.9: Complex used for data encryption and decryption[35]

In addition, smart luminescent materials that are responsive to external stimuli have received considerable interest, and are seen as promising candidates for data recording and security protection. Sun *et al.* reported iridium(III) complexes that simultaneously delivered mechanochromic, vapochromic and electrochomic phosphorescence (Figure 4.9).[35] Anionic counterion variation caused a change in emission colours from yellow to green due to hydrogen bond formation with an N-H moiety in the ligand. A data-recording device was constructed and data encryption and decryption via fluorescence lifetime imaging and time-gated luminescence imaging techniques were demonstrated.[35]

4.1.5 Machine-Assisted Synthesis

In recent years, an increase in the use of machine-assisted practice in the synthesis laboratory has begun to streamline the discovery and scale-up of organic molecules with biological activity, such as pharmaceuticals, agrochemicals, flavours and fragrances.[59] For example, a compact, reconfigurable manufacturing platform has been developed for the continuous flow synthesis and formulation of active pharmaceutical ingredients (Figure 4.10).[60] The system has the capacity to produce hundreds to thousands of oral or topical liquid doses of diphenhydramine hydrochloride, lidocaine hydrochloride, diazepam and fluoxetine hydrochloride, all of which met US Pharmacopeia standards. In addition, inductively heated mesofluidic devices have shown high performance in an array of reactions, including heterocyclic condensations, transfer hydrogenations,

pericyclic reactions, cross-couplings and oxidations, as well as for the preparation of pharmaceutical compounds.[61]

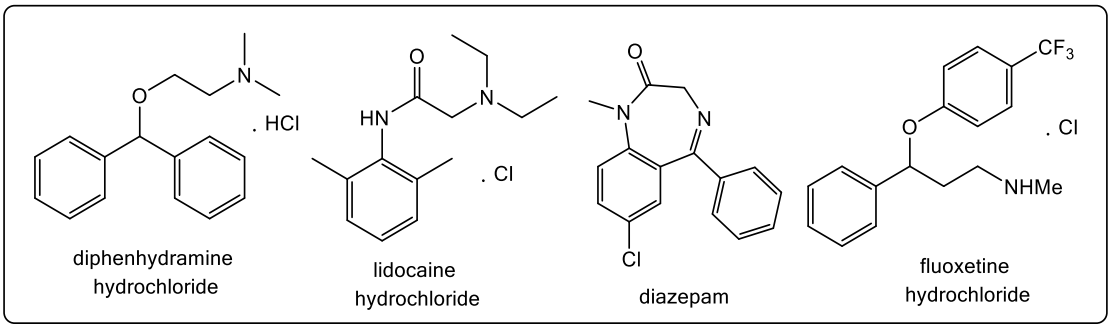

Figure 4.10: Examples of compounds synthesised using a machine-assisted approach[60]

The use of robotic microwaves with touchscreen user interfaces and continuous flow apparatus has led to systems that can operate unmanned in a 24/7 regime and deliver results and data to human operators. The recent addition of computer control, inline analytics[62] and optimising algorithms[63] has already afforded early examples of machines capable of the unassisted optimisation of chemical reactions. Further, the addition of automated biological assays into the machine-assisted discovery loop has now led to a closed-loop machine platform that is capable of optimising compound potency through iterative synthesis, characterisation and screening cycles.[64] Clearly these methods have the potential to be extremely powerful and greatly assist in the pursuit of new or improved material properties. However, the approach is highly multidisciplinary and requires significant proof-of-concept and machine testing studies to fully understand and develop the true capabilities of the method. To date, there have been few applications of these techniques to the area of inorganic synthesis including the preparation of metal complexes.[18, 65]

During the course of the work described in this chapter, Stephenson and co-workers reported a significant reduction in the reaction times for complex formation using a microwave method for the two-step synthesis of cyclometalated Ir(III) complexes in ethylene glycol.[66] In addition, Davies and co-workers have described microwave reaction conditions using ^{i}PrOH as solvent, which successfully gave cyclometalated Ir(III) dimer species.[18]

4.2 Aims

This chapter describes initial efforts towards a machine–assisted discovery platform, for the delivery of a series of pyrazolate-iridium complexes with tunable luminescent properties. Due to advances in the efficient, rapid and cost-effective synthesis of such species being rarely employed in the literature but highly desirable, a proof of concept model has been developed (Figure 4.11).

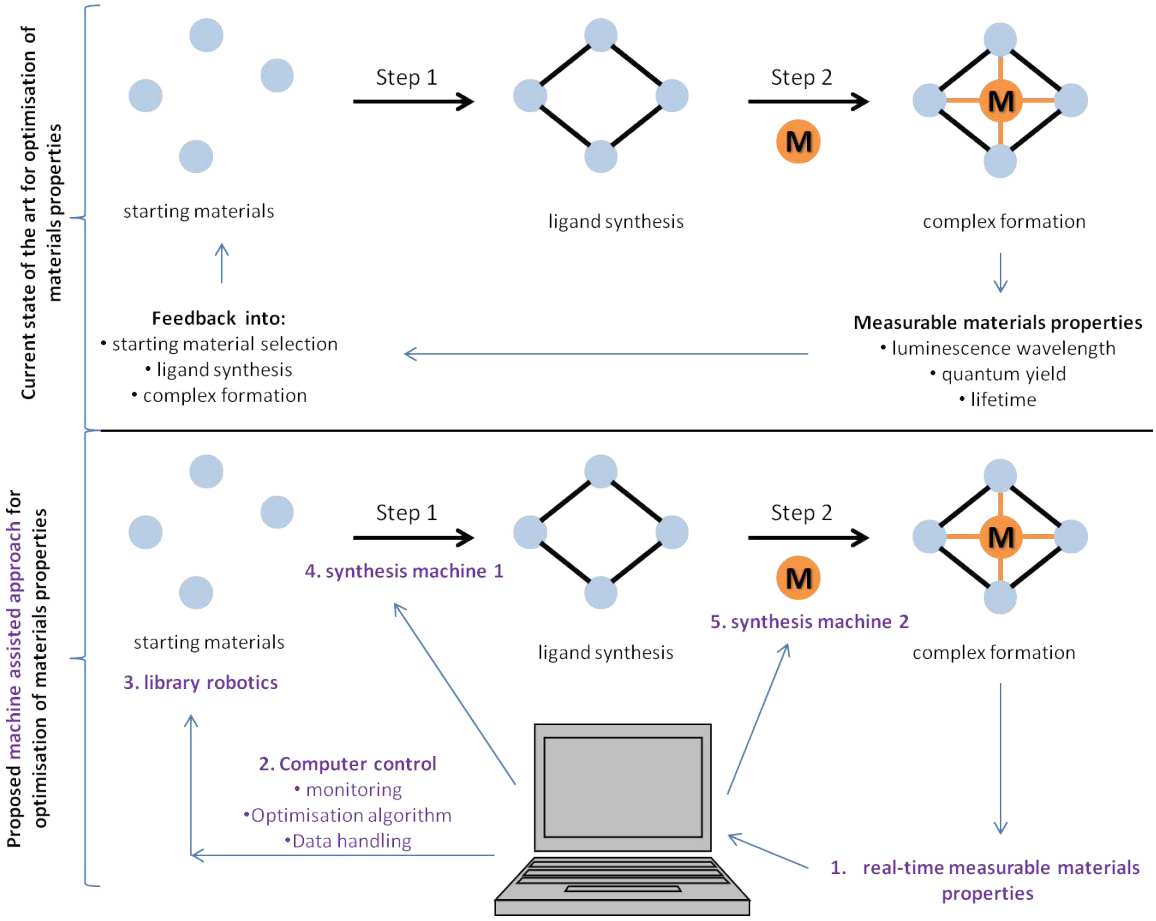

Figure 4.11: This work: proof of concept, chemistry model validation and development of synthesis machines 1 and 2

As well as the current state-of the art process for materials optimisation, it is thought that machine-assistance would consist of real-time characterisation of material properties with direct input of this data into a computer. The computer would offer multiple purposes, such as reaction or property optimisation through statistical analysis, data storage, and management and direction of the synthetic steps. For the computer to be able to interface with the synthetic reaction steps of the process, the reactions

should be carried out by a technique that can readily interface with computer control. This first-generation approach towards this goal consists of the demonstration of a modular flow/microwave hybrid approach to the synthesis of a novel series of ligands, demonstration of a microwave approach to the assembly of the complexes, and identification of suitable model chemical system with which to explore this concept.

This chapter extends the concepts discussed to synthesise a range of iridium complexes based on substituted 3,5-dimethyl-1-phenylpyrazole ligands. The characterisation and photophysical properties of the novel ligands and complexes would be investigated. In addition, theoretical studies have been conducted in order to support spectral data, along with electrochemistry investigations.

4.3 Results and Discussion

4.3.1 Synthesis of Ligands and Complexes

Please note: all ligand synthesis was carried out by Christiane Schotten.

Phenyl-pyrazoles were targeted as ligands with electron withdrawing, fluorine-containing phenyl substituents that would firstly permit facile C-H insertion/cyclometalation following initial coordination of the pyrazole nitrogen to an iridium centre. Secondly, the ligand should induce a strong element of electronic tuning to the iridium colour centre. A family of such fluorinated pyrazole-iridium complexes have not been reported. Enhancing the electron withdrawing capability of the coordinating phenyl unit is known to blue shift the emission wavelength of luminescent Ir(III) complexes.[67] The synthetic protocol is outlined in Scheme 4.1 and features the input of the appropriately fluorinated aniline(s) into the continuous flow apparatus for the ligand synthesis phase. This was followed by a two-step iridium ligation process in which both batch and microwave approaches were compared.

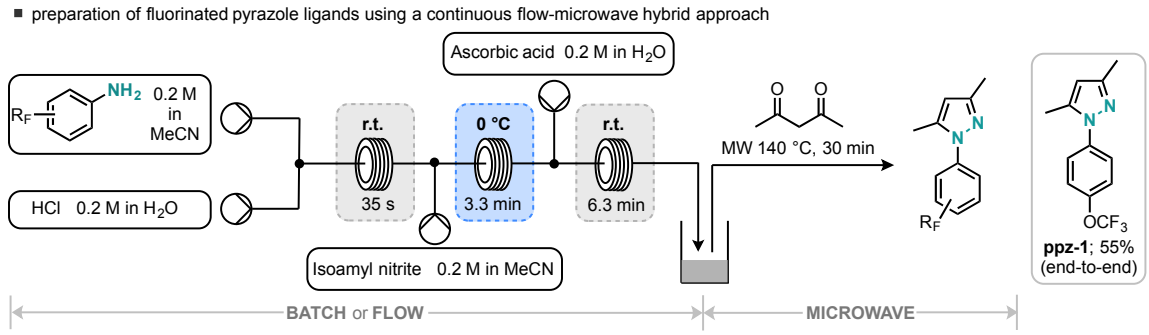

Scheme 4.1. Preparation of fluorinated pyrazole ligands using a continuous flow-microwave hybrid approach.

The substituted pyrazoles (ppz-1 to ppz-6) were synthesised from a selected aniline (4-(trifluoromethoxy)aniline, 3-(trifluoromethyl)aniline, 4-(trifluoromethyl)aniline, 4-(pentafluorothio)aniline, 3-(pentafluorothio)aniline, 4-fluoroaniline), which was firstly diazotised in the flow reactor (outlined in Scheme 4.2) by combination with a stream of HCl and isoamylnitrite, before combination with a further stream that delivered the

ascorbic acid for reduction to the oxamayl-hydrazide derivative. The formed hydrazine surrogate was then collected in a microwave vial before combining with acetylacetone and irradiation at 140 °C for 30 minutes.

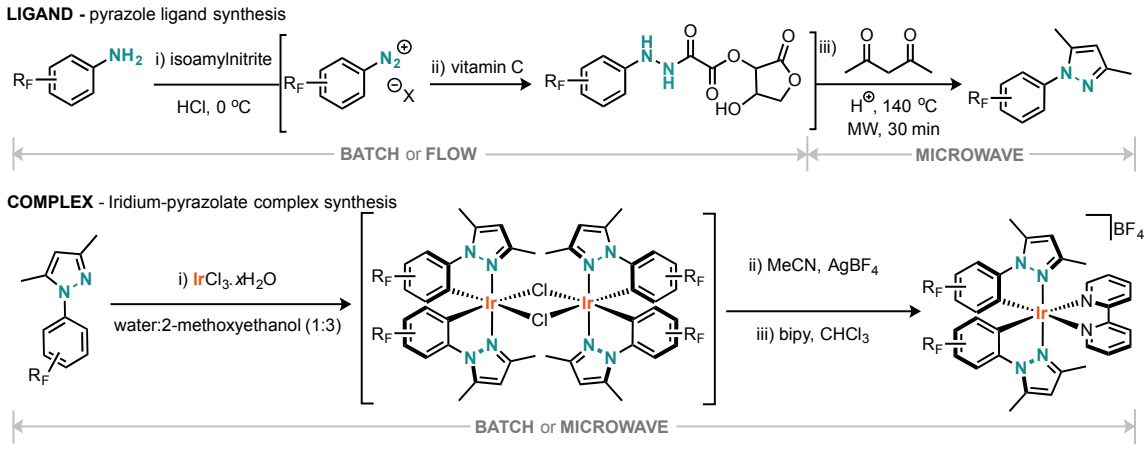

Scheme 4.2. Summary of the synthetic routes to the ligands and complexes.

The resultant product was purified by aqueous extraction and silica chromatography to furnish the fluorous substituted 3,5-dimethyl pyrazoles (ppz-X) in good-to-excellent yield. The utilised 'flow + microwave' setup is shown schematically in Scheme 4.2. It should be noted that whilst this chapter concerns the design and development of automatable machines, this chemistry can also be conducted more conventionally (batch) in a round-bottom-flask. For the latter approach, where unknown diazonium entities are being generated, small scale reactions are advisable due to potential for diazoniums to undergo uncontrollable energy release. Thus, the flow process for the generation and consumption of diazonium salts affords safety benefits as well as versatility and the potential for automation.

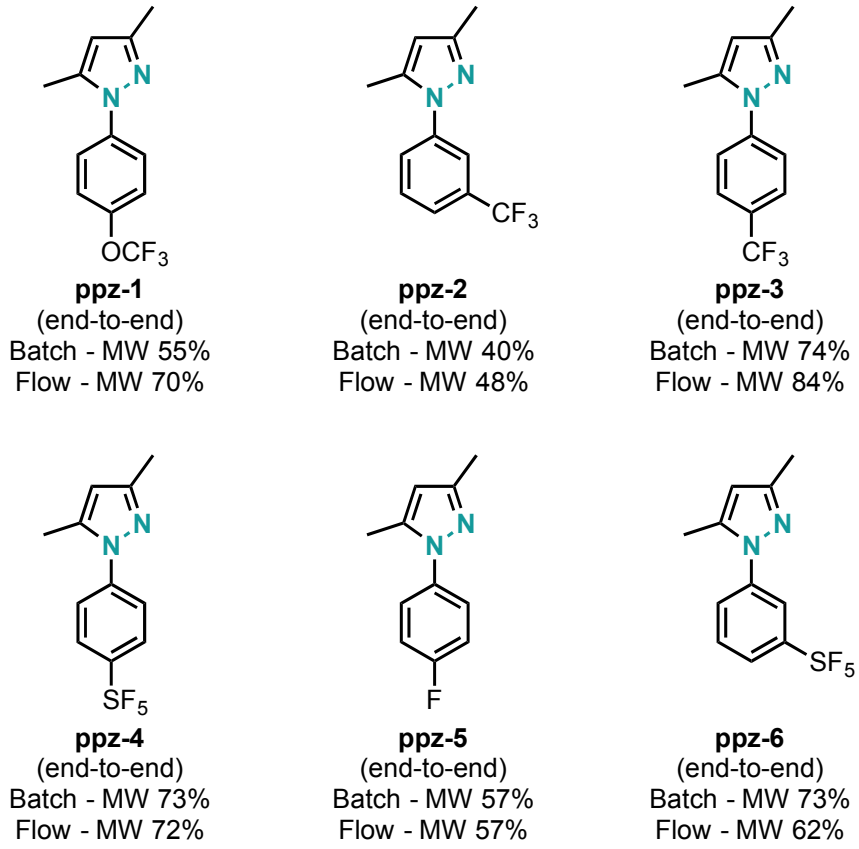

Figure 4.12: Structures and comparison of preparative yields of the ligands

These fluorinated pyrazoles were then successfully utilised as cyclometalating ligands with Ir(III), thus delivering six new complexes of the general form $[Ir(ppz)_2(bipy)]BF_4$. Firstly, the complexes were synthesised by applying well-known batch chemistry conditions[68] for the dimeric precursors $[(ppz)_2Ir(\mu\text{-}Cl)_2Ir(ppz)]$, where the reaction duration is 48 hours. Each $[(ppz)_2Ir(\mu\text{-}Cl)_2Ir(ppz)_2]$ compound was then reacted with $AgBF_4$ in MeCN (2 hrs) to give the corresponding bis-acetonitrile adduct $[Ir(ppz)_2(MeCN)_2]BF_4$ (Scheme 4.2), and subsequent reaction with 2,2′-bipyridine gave conversion (24 hrs) to the mixed-ligand target complexes $[Ir(ppz)_2(bipy)]BF_4$. The six complexes were isolated as pale green-brown powders. It is worth noting that, following formation of the $[(ppz)_2Ir(\mu\text{-}Cl)_2Ir(ppz)_2]$, the remaining experimental procedure described differs from traditional methods used for Ir(III) complex synthesis,[69] but has been shown to produce complexes in higher yields and without the need for purification *via* column chromatography in the majority of cases.

Following the regular batch chemistry, the usefulness of the machine-assisted approach for the iridium chemistry was assessed. Here the microwave approach was applied to each of the three steps: (i) $[(ppz)_2Ir(\mu\text{-}Cl)_2Ir(ppz)_2]$ from $IrCl_3$ in 2-methoxyethanol for 15 min at 180 °C; (ii) dimer cleavage to *cis*-$[Ir(ppz)_2(MeCN)_2]BF_4$ achieved in acetonitrile for 10 min at 120 °C; (iii) conversion to $[Ir(ppz)_2(bipy)]BF_4$ in chloroform for 15 min at 130 °C. Using this microwave-assisted approach, the target $[Ir(ppz)_2(bipy)]BF_4$ complexes were much more rapidly isolated with total reaction times of < 1 hr. The yields of the target complexes are respectable and directly comparable to conventional methods, where 74 hrs are required to isolate these species. However, the complexes are now obtainable within a day, including work-up procedures and purification *via* column chromatography (if required).

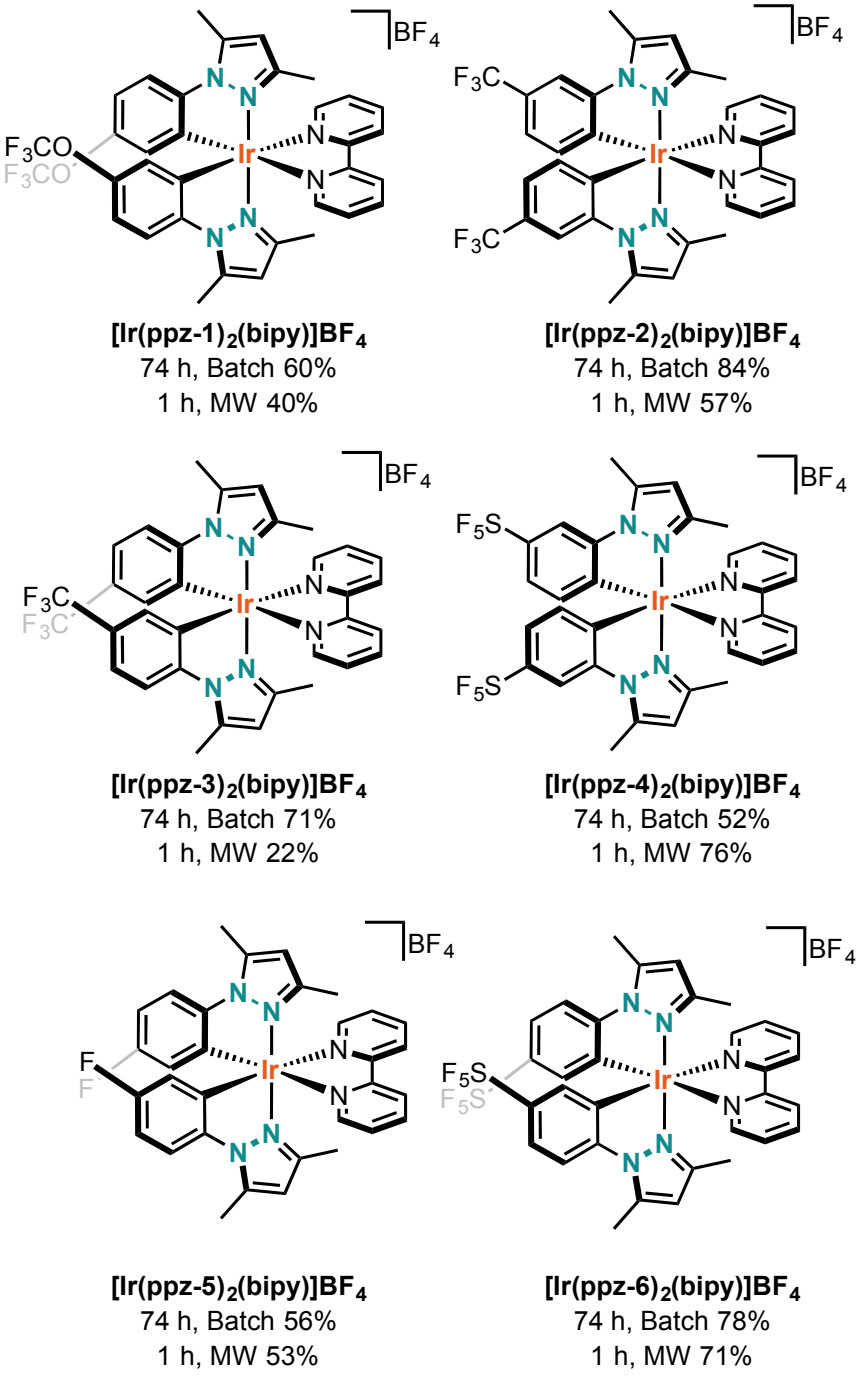

Figure 4.13:Structures, total reaction times and comparative yields (final step) of the complexes

4.3.2 Characterisation of the Ir(III) Complexes

The Ir(III) complexes were sufficiently soluble in a range of common organic solvents allowing characterization in the solution state using ^{1}H, $^{13}C\{^{1}H\}$, high resolution mass spectrometry, UV-vis., time-resolved transient absorption, luminescence spectroscopies

and cyclic voltammetry, as well as IR in the solid state. Supporting TD-DFT calculations were also used to assist and inform the assignments of the electronic transitions noted from experimental observations. Confirmation of the solid-state structures were provided through X-ray crystallographic studies on two examples.

As well as the protons associated with the pyrazole ligand, the ^{1}H NMR spectra of the complexes show additional peaks in the aromatic region corresponding to the additional 2,2′-bipyridine ligand. By comparison of ppz-5 and $[Ir(ppz\text{-}5)_2(bipy)]BF_4$, it can be seen that complex formation affects the shifts and multiplicities of the peaks associated with the ppz-5 ligand. The characteristic methyl groups (2.26 and 2.28 ppm in the ligand) have shifted to 2.85 and 1.57 ppm respectively in the complex, possibly due to the proximity to the cyclometalating nitrogen. In addition, the cyclometalating carbon means there is one less phenyl proton per pyrazole ligand observed for the complex and hence a doublet at 8.18 ppm is observed (Figure 4.15).

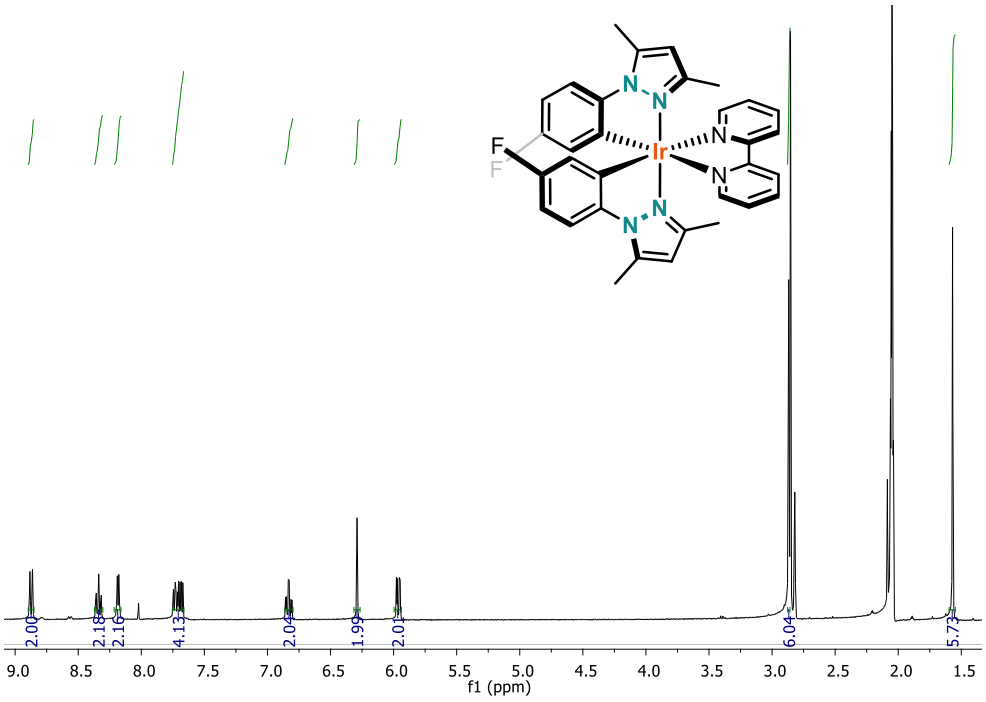

Figure 4.14: ^{1}H NMR spectrum of $[Ir(ppz\text{-}5)_2(bipy)]BF_4$

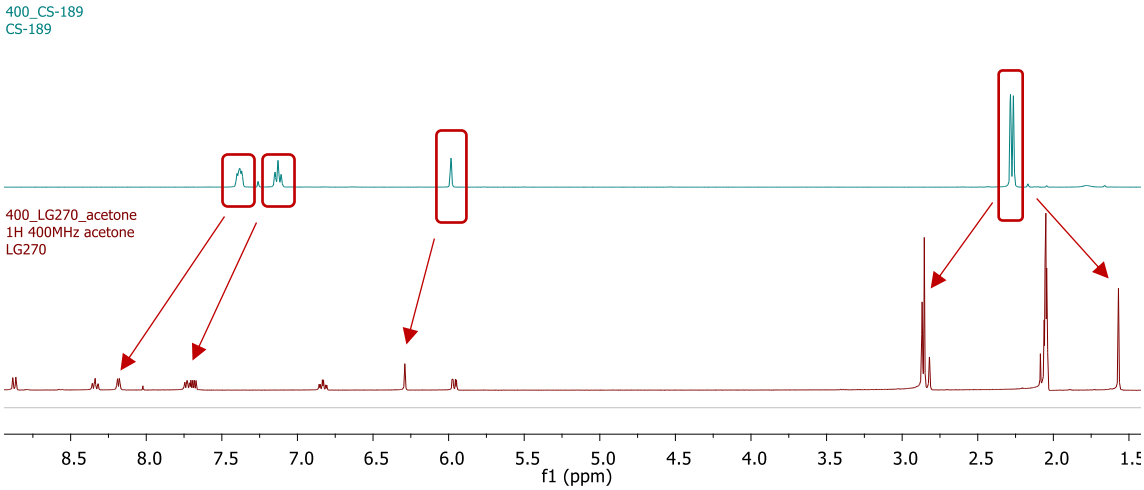

Figure 4.15:[1]H NMR spectrum of ppz-5 (top) and [Ir(ppz-5)$_2$(bipy)]BF$_4$ (bottom)

Slight differences are observed when comparing ppz-2 and [Ir(ppz-2)$_2$(bipy)]BF$_4$. As previously seen, the additional aromatic protons associated with the cyclometalating ligand are observed. The characteristic methyl groups (2.34 and 2.30 ppm in ppz-2) have again shifted to 2.98 and 1.63 ppm respectively. In this case, however, the three proton multiplet (7.68 – 7.53 ppm) observed in ppz-2 becomes two doublets, each integrating to two protons at 7.14 and 6.59 ppm. In addition, the aromatic singlet (7.74 ppm) observed for ppz-2 remains a singlet at 7.82 ppm (Figure 4.17).

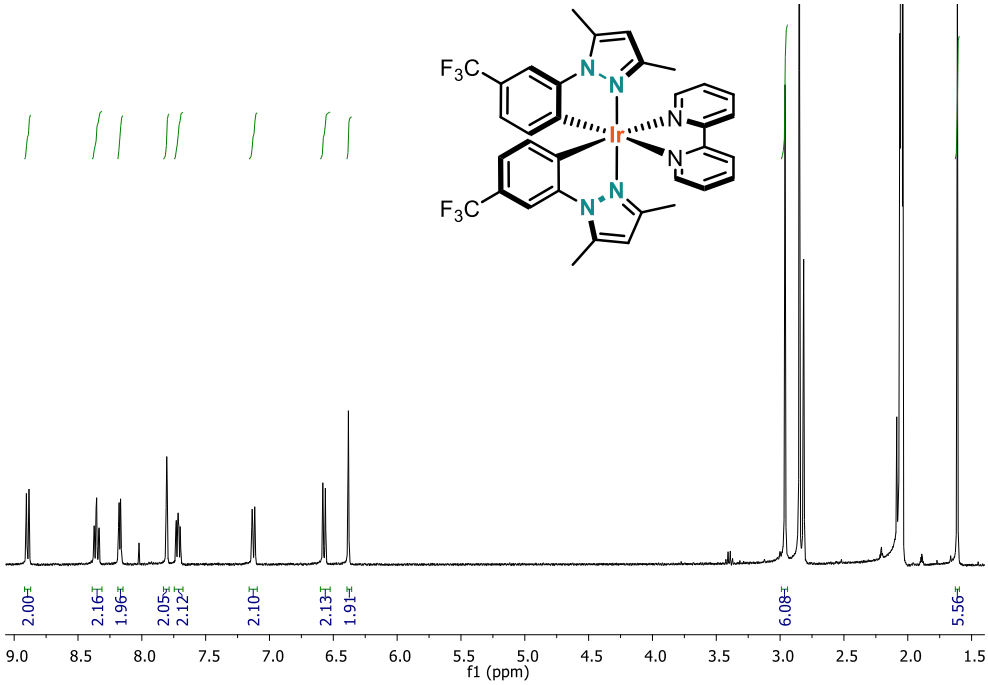

Figure 4.16: [1]H NMR spectrum of [Ir(ppz-2)$_2$(bipy)]BF$_4$

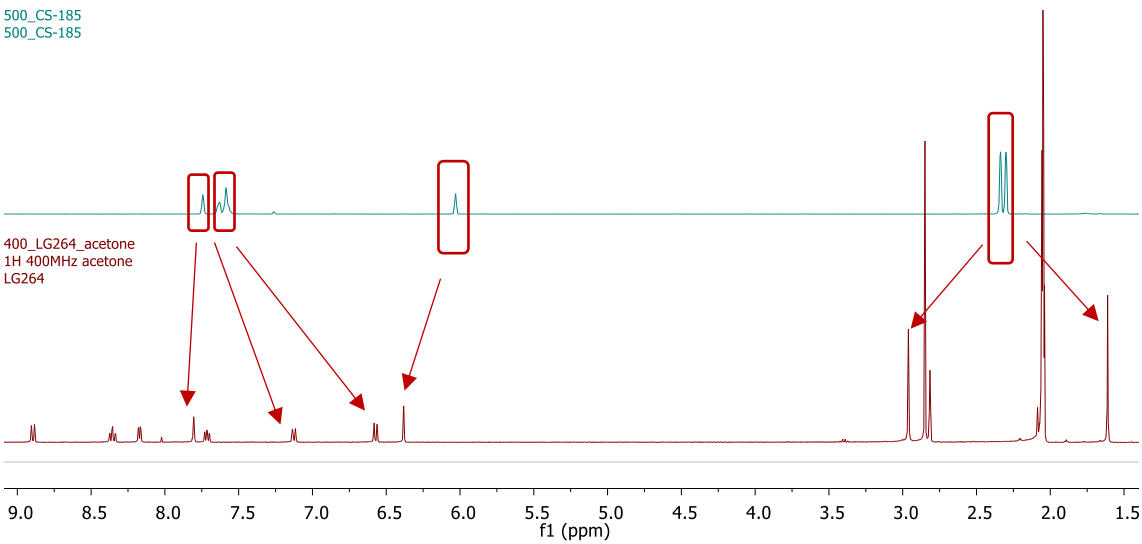

Figure 4.17:[1]H NMR spectrum of ppz-2 (top) and [Ir(ppz-2)$_2$(bipy)]BF$_4$ (bottom)

Similar trends in the ^{1}H NMR spectra are seen for the remaining complexes. In all cases, the proposed molecular formula was supported by HMRS (ES$^+$), each showing the [M^+ - C_2H_6] peak with a representative Ir(III) isotope pattern (Figure 4.18). IR studies of ligands and their corresponding complexes show the addition of several peaks within the fingerprint region of the spectrum, presumably attributed to the cyclometallation and additional bipy ligand associated with the complexes.

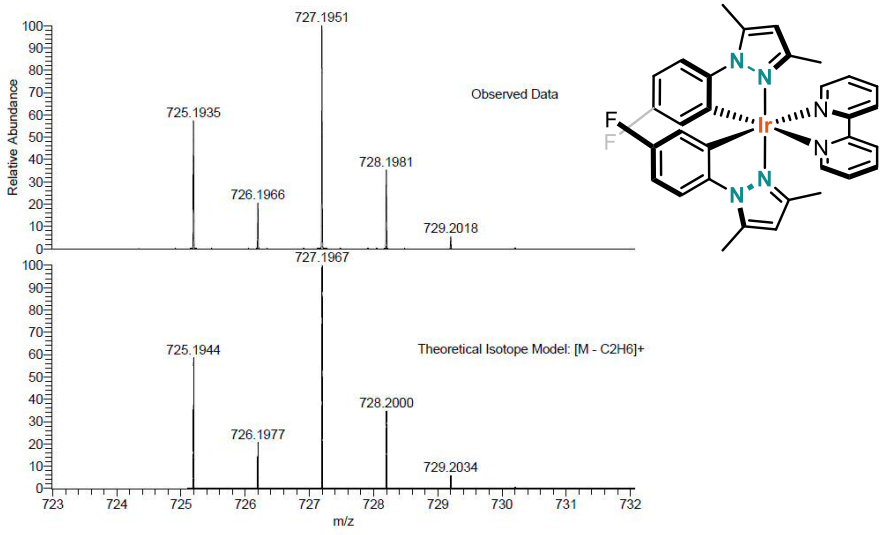

Figure 4.18: HMRS of [Ir(ppz-5)$_2$(bipy)]BF$_4$

4.3.3 X-ray Crystallographic Structural Studies

As well as solution state characterization, single crystal structure determinations were obtained for $[Ir(ppz\text{-}3)_2(bipy)]BF_4$ and $[Ir(ppz\text{-}6)_2(bipy)]BF_4$ in order to further confirm the structure of the complexes (Figure 4.19). Crystals suitable for X-ray diffraction were obtained by room temperature vapour diffusion of diethyl ether into concentrated MeCN solutions of the aforementioned complexes. Data collection, refinement and structure solution was conducted by Dr. Peter Horton at the UK National Crystallography Service, Southampton. Data collection parameters are shown in Table 4.1, together with supporting bond length (Table 4.2) and bond angle data (Table 4.3).

These structures revealed the anticipated formulations for both complexes and demonstrate retention of the different pyrazolato substituents, as well as the addition of bipy. In both cases the cyclometalating units are arranged with the coordinated C atoms in a *cis* arrangement. Bond lengths for the pyrazole ligands in both complexes range between Ir-N = 2.034-2.036 Å and Ir-C = 2.006(5)-2.016(4) Å, both ranges which are in agreement with similar literature examples.[16] In addition, the Ir-N bond angles in the bipy ligand (2.128(4)-2.135(4) Å) show correlation with reported values and ranges.[70] The bond angles show a distorted octahedral geometry at Ir(III) in both cases, which is again in agreement with previous literature examples.[29]

Compound	$[Ir(ppz\text{-}3)_2(bipy)]BF_4$	$[Ir(ppz\text{-}6)_2(bipy)]BF_4$
Formula	$C_{34}H_{28}F_6IrN_6$, BF_4, ½(C_2H_3N)	$C_{32}H_{28}F_{10}IrN_6S_2$, 2/3($C_4H_{10}O$), BF_4, 1/3(H_2O), 1/3(C_2H_3N)
$D_{calc.}$/ g cm^{-3}	1.652	1.790
μ/mm^{-1}	3.639	3.481
Formula Weight	934.16	1098.84
Colour	Yellow	yellow
Shape	Plate	cut needle
Size/mm^3	0.120×0.080×0.030	0.150×0.035×0.015
T/K	100(2)	100(2)
Crystal System	Monoclinic	triclinic
Space Group	$P2_1/n$	P-1
a/Å	10.71171(18)	14.25526(20)
b/Å	20.5811(3)	19.1140(4)
c/Å	17.8555(3)	23.8726(3)
α/°	90	70.9389(16)
β/°	107.3999(18)	84.0222(11)
γ/°	90	88.0894(14)
V/Å^3	3756.27(11)	6114.61(18)
Z	4	6
Z'	1	3
Wavelength/Å	0.71073	0.71073
Radiation type	MoK_α	MoK_α
Θ_{min}/°	2.225	1.825
Θ_{max}/°	27.482	27.484
Measured Refl.	48865	107412
Independent Refl.	8604	28021
Reflections Used	7659	23235
R_{int}	0.0299	0.0413
Parameters	522	1643
Restraints	531	1707
Largest Peak	1.836	2.455
Deepest Hole	-1.134	-2.187
GooF	1.055	1.047
wR_2 (all data)	0.1120	0.0953
wR_2	0.1080	0.0901
R_1 (all data)	0.0446	0.0576
R_1	0.0386	0.0433

Table 4.1: X-ray data collection parameters for the complexes

$[Ir(ppz\text{-}3)_2(bipy)]BF_4$			$[Ir(ppz\text{-}6)_2(bipy)]BF_4$		
Atom	Atom	Length/Å	Atom	Atom	Length/Å
Ir1	N1	2.036(4)	Ir1	N1	2.035(4)
Ir1	N21	2.034(4)	Ir1	N21	2.036(4)
Ir1	N41	2.135(4)	Ir1	N41	2.134(4)
Ir1	N42	2.130(4)	Ir1	N42	2.128(4)
Ir1	C1	2.016(4)	Ir1	C1	2.006(4)
Ir1	C21	2.006(5)	Ir1	C21	2.015(5)
			Ir2	N51	2.041(4)
			Ir2	N71	2.037(4)
			Ir2	N91	2.140(4)
			Ir2	N92	2.124(4)
			Ir2	C51	2.003(5)
			Ir2	C71	2.011(4)

Table 4.2: Bond lengths for the complexes

$[Ir(ppz\text{-}3)_2(bipy)]BF_4$				$[Ir(ppz\text{-}6)_2(bipy)]BF_4$			
Atom	**Atom**	**Atom**	**Angle/˚**	**Atom**	**Atom**	**Atom**	**Angle/˚**
N1	Ir1	N41	101.43(15)	N1	Ir1	N21	171.40(16)
N1	Ir1	N42	84.63(16)	N1	Ir1	N41	100.41(16)
N21	Ir1	N1	170.33(15)	N1	Ir1	N42	86.98(15)
N21	Ir1	N41	86.92(15)	N21	Ir1	N41	86.71(16)
N21	Ir1	N42	102.15(16)	N21	Ir1	N42	99.45(15)
N42	Ir1	N41	77.14(16)	N42	Ir1	N41	76.58(16)
C1	Ir1	N1	79.31(18)	C1	Ir1	N1	79.44(17)
C1	Ir1	N21	92.90(17)	C1	Ir1	N21	94.04(17)
C1	Ir1	N41	174.00(17)	C1	Ir1	N41	173.52(17)
C1	Ir1	N42	97.06(17)	C1	Ir1	N42	96.95(16)
C21	Ir1	N1	94.38(19)	C1	Ir1	C21	86.66(18)
C21	Ir1	N21	79.79(19)	C21	Ir1	N1	94.18(17)
C21	Ir1	N41	95.86(17)	C21	Ir1	N21	79.75(17)
C21	Ir1	N42	172.55(17)	C21	Ir1	N41	99.81(18)
C21	Ir1	C1	90.00(18)	C21	Ir1	N42	176.36(17)
				N51	Ir2	N91	102.70(17)

[Ir(ppz-3)$_2$(bipy)]BF$_4$				[Ir(ppz-6)$_2$(bipy)]BF$_4$			
Atom	**Atom**	**Atom**	**Angle/˚**	**Atom**	**Atom**	**Atom**	**Angle/˚**
				N51	Ir2	N92	88.43(16)
				N71	Ir2	N51	170.24(15)
				N71	Ir2	N91	84.54(16)
				N71	Ir2	N92	99.65(16)
				N92	Ir2	N91	77.29(15)
				C51	Ir2	N51	79.57(19)
				C51	Ir2	N71	94.14(18)
				C51	Ir2	N91	172.09(16)
				C51	Ir2	N92	95.29(16)
				C51	Ir2	C71	89.89(17)
				C71	Ir2	N51	93.05(18)
				C71	Ir2	N71	79.39(17)
				C71	Ir2	N91	97.51(16)
				C71	Ir2	N92	174.78(16)
				N71	Ir2	N91	84.54(16)
				N71	Ir2	N92	99.65(16)

Table 4.3: Bond angles for the complexes

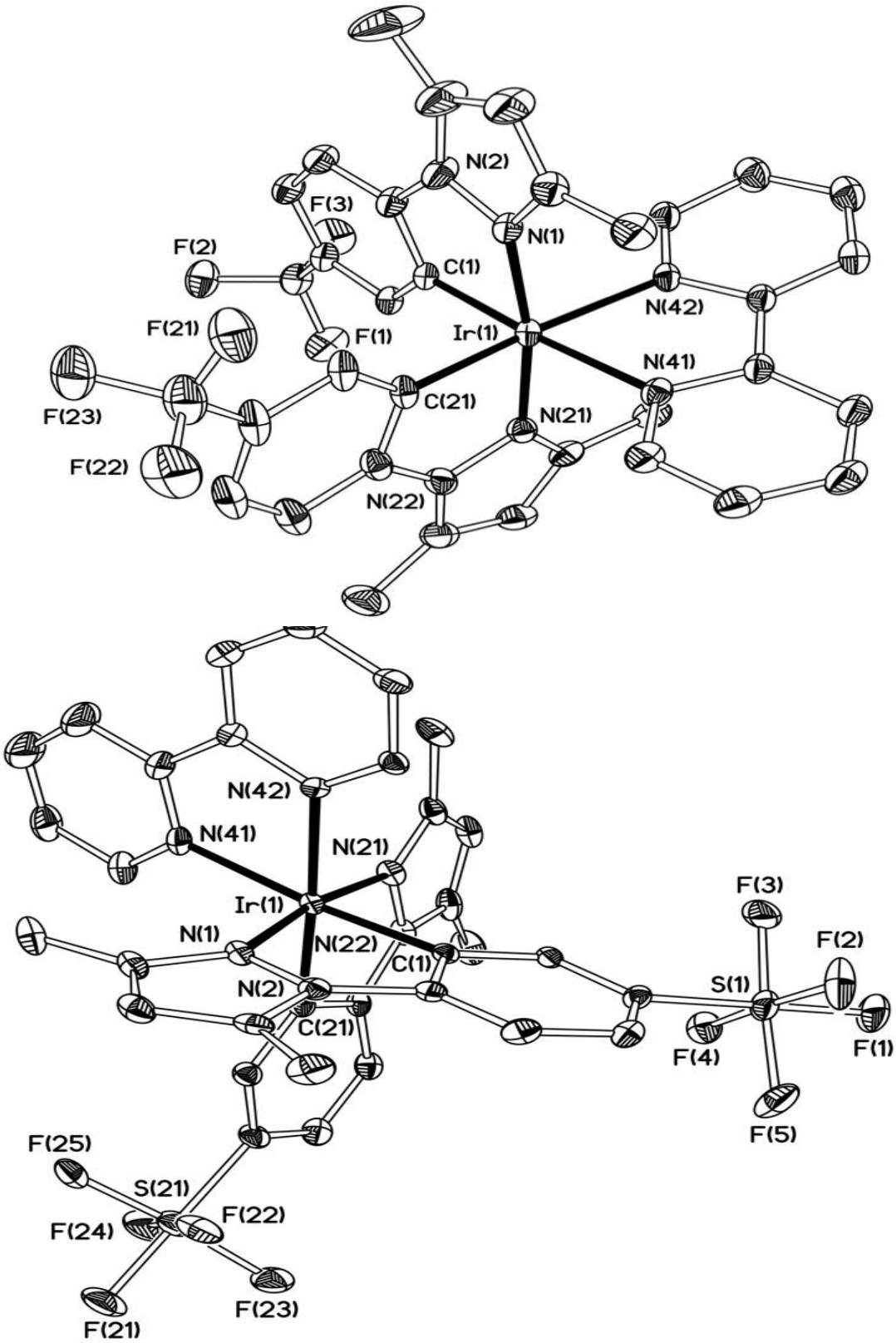

Figure 4.19:Molecular structures of the iridium complexes (top: [Ir(ppz-3)$_2$(bipy)]BF$_4$; bottom: [Ir(ppz-6)$_2$(bipy)]BF$_4$). Thermal ellipsoids drawn at the 30% probability level. Hydrogen atoms, anions and solvent molecules are omitted for clarity

4.3.4 Density functional theory (DFT) studies

Please note that all density functional theory studies were carried out by Dr. Jamie Platts.

Frontier molecular orbital data for the six Ir(III) complexes, calculated after full geometry optimisation, are reported in Table 4.4. They show a consistent HOMO-LUMO gap of around 3 eV with minor changes due to the nature and position of the fluorinated substituents on the cyclometalated ligand fragments. This is in broad agreement with the electrochemical data discussed later (Table 4.6), but with a slight overestimation. In all cases, the HOMO has mixed iridium *5d* (12.5 to 21.9%) and pyrazolate π-character, with the $-SF_5$ substituents increasing the Ir contribution, while the LUMO is wholly located on the ancillary bipyridine ligand, as shown in Figure 4.20.

Complex	E_{HOMO} / eV	E_{LUMO} / eV	$E_{Bandgap}$ / eV	% *5d* (HOMO)
$[Ir(ppz\text{-}1)_2(bipy)]BF_4$	-8.31	-5.39	2.92	17.3
$[Ir(ppz\text{-}2)_2(bipy)]BF_4$	-8.46	-5.47	2.99	12.5
$[Ir(ppz\text{-}3)_2(bipy)]BF_4$	-8.40	-5.42	2.98	14.7
$[Ir(ppz\text{-}4)_2(bipy)]BF_4$	-8.68	-5.59	3.09	21.9
$[Ir(ppz\text{-}5)_2(bipy)]BF_4$	-8.15	-5.33	2.82	13.5
$[Ir(ppz\text{-}6)_2(bipy)]BF_4$	-8.61	-5.54	3.07	21.8

Table 4.4:Calculated HOMO and LUMO energies and % 5d orbital character of the HOMO for each complex

To probe the spectroscopy of these complexes in more detail, TD-DFT calculations were carried out on $[Ir(ppz\text{-}5)_2(bipy)]^+$, using the CAM-B3LYP functional. Strong singlet transitions were predicted to lie in the range of 270 to 300 nm, the most intense of which at 272 nm is dominated by a π-π* transition within the bipyridine ligand. Lower energy triplet absorption bands are also predicted at 422 and 388 nm: at the scalar relativistic level used for these calculations, such bands are formally forbidden with an intensity of exactly zero. The orbital make-up of the 422 nm band is complex, with MOs

as low as HOMO-16 (metal *5d* / bipy π) contributing, but it is interesting to note that the predicted dominant contribution is HOMO-6 → LUMO, which is also a π-π^* transition within bipyridine. This data therefore suggests that the shoulder seen in absorption spectra could comprise a $^3IL_{bipy}$ transition, which is presumably weakly allowed due to spin-orbit coupling that stems from smaller contributions from a ^{3}MLCT transition. TD-DFT was also used to examine emission from the geometry optimised lowest triplet excited state of $[Ir(ppz\text{-}5)_2(bipy)]^+$. Once again, such bands are formally forbidden so no information on intensity is available, but this approach predicts emission at 510 nm, again in qualitative agreement with the experimental data. However, as with the triplet absorption, this band is dominated by intra-ligand transitions within the bipyridine with smaller ^{3}MLCT type contributions also noted, the latter a much more likely assignment to the broad featureless emission observed in the experiments.

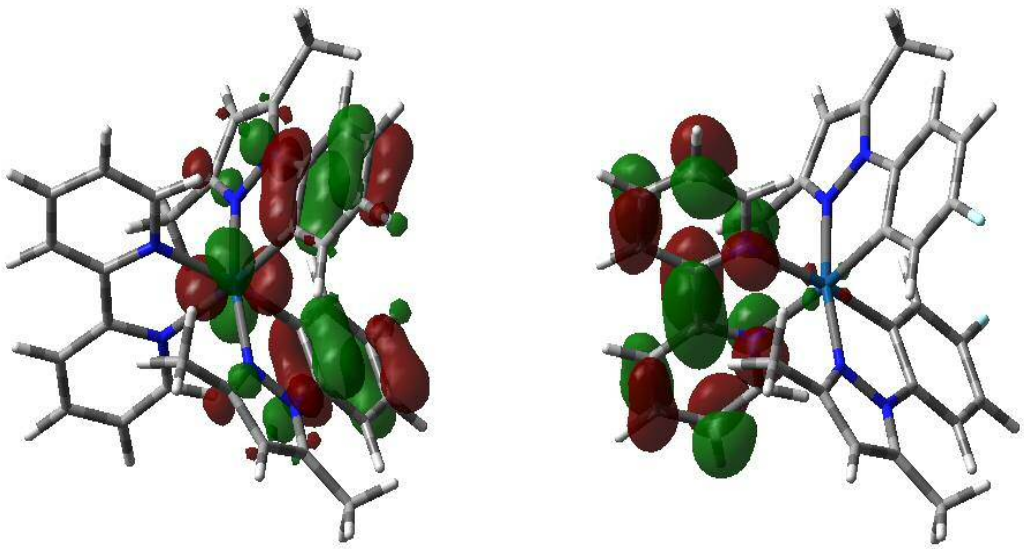

Figure 4.20:Isosurface plots for HOMO (left) and LUMO (right) of $[Ir(ppz\text{-}5)_2(bipy)]^+$, displayed at 0.04 au.

4.3.5 Photophysical Properties of the Complexes

The photophysical properties of the complexes were measured in aerated acetonitrile solutions. The UV-vis absorption spectra of the complexes (Figure 4.21) show several

common features between 250 and 450 nm. Ligand-centred ($^1\pi$-π^*) transitions dominate, with high molar absorption coefficients, <320 nm. A much weaker feature, present as a shoulder between 400 and 450 nm is tentatively assigned as a ^{1}MLCT transition with the possibility of a spin forbidden ^{3}MLCT also contributing. The position of the MLCT band(s) appear to be relatively insensitive to the variations in substituent (nature and position) that are present on the cyclometalated pyrazole ligand. Previous related iridium-pyrazole complexes by Chen *et al.* are comparable, and show ligand centred transitions between 271 and 378 nm, as well as a lower energy shoulder attributed to MLCT transitions.[16] Similar absorption values have been observed for Ir(III) complexes containing bipy ligands.[43, 69]

Complex	λ_{em} / nm [a,b]	τ / ns [a,c]	Φ_{em} [a]	k_r / s^{-1} $\times10^6$	k_{nr} / s^{-1} $\times10^6$
$[Ir(ppz\text{-}1)_2(bipy)]BF_4$	543 (484)	92 (107)	0.10	1.09	9.78
$[Ir(ppz\text{-}2)_2(bipy)]BF_4$	528 (488)	109 (113)	0.15	1.37	7.80
$[Ir(ppz\text{-}3)_2(bipy)]BF_4$	537 (484)	101 (103)	0.11	1.09	8.81
$[Ir(ppz\text{-}4)_2(bipy)]BF_4$	516 (484)	123 (133)	0.19	1.54	6.59
$[Ir(ppz\text{-}5)_2(bipy)]BF_4$	557 (497)	77 (90)	0.05	0.65	12.34
$[Ir(ppz\text{-}6)_2(bipy)]BF_4$	520 (485)	112 (127)	0.15	1.34	7.59

Table 4.5: Photophysical properties of the $[Ir(ppz)_2(bipy)]BF_4$ complexes. [a] recorded at RT in aerated MeCN (λ_{ex} = 405 nm); [b] values in parentheses were obtained at 77K (1:1 MeOH/EtOH glass); [c] values in parentheses are the lifetimes obtained from time-resolved transient absorption measurements.

Luminescence spectra were also obtained on aerated acetonitrile solutions (Table 4.5). Using an excitation wavelength of 380 nm the complexes revealed a broad featureless emission peak that ranged between 510 and 560 nm (Figure 4.22) depending upon the nature of the pyrazole ligand. For comparison, $[Ir(ppy)_2(bipy)]PF_6$ (ppy = 2-phenylpyridine) emits at 602 nm from a mixed ^{3}MLCT/^{3}LLCT excited state;[71] the more closely related $[Ir(ppz)_2(bipy)]PF_6$ (ppz = 2-phenylpyrazole) emits at 563 nm in MeCN.[13] In this work, the most red-shifted emission was induced by *para*-fluorination of the cyclometalating ligand in $[Ir(ppz\text{-}5)_2(bipy)]BF_4$, whilst the blue-shifted variants were the pentafluorosulfanyl derivatives $[Ir(ppz\text{-}4)_2(bipy)]BF_4$ and $[Ir(ppz\text{-}6)_2(bipy)]BF_4$ (*meta* substitution induced the highest energy emission). It is noteworthy that

pentafluorosulfanyl-substituted $[Ir(ppy)_2(bipy)]^+$ species have recently been shown to possess blue-shifted emission properties.[72] In addition, other closely related complexes of $[Ir(R\text{-}ppz)_2(bipy)][PF_6]$ (R = H, Me, CF_3) exhibit emission wavelengths ranging between 504 and 587 nm.[18]

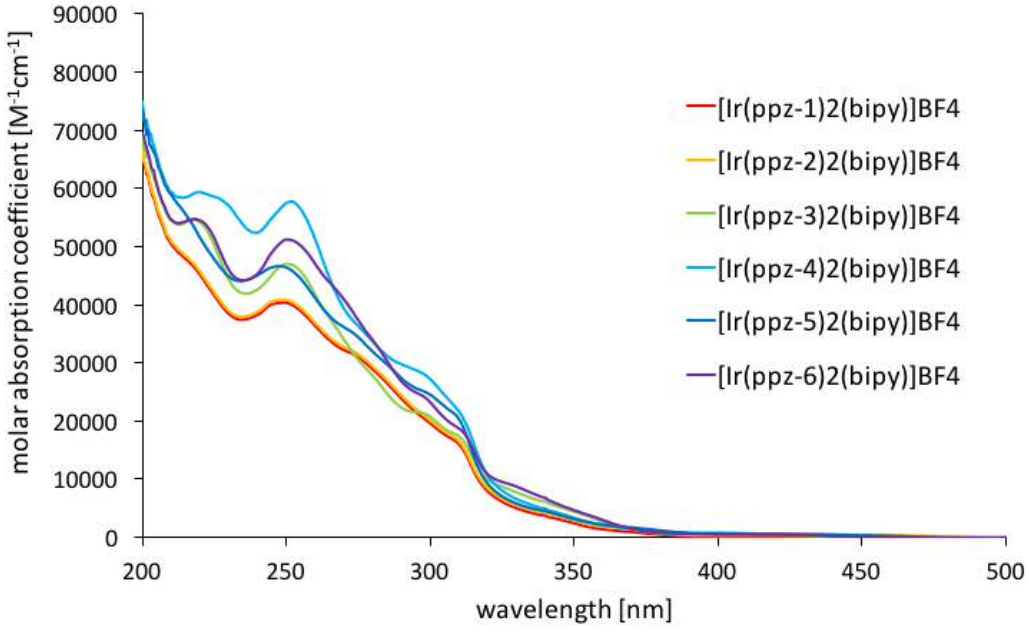

Figure 4.21:Comparison of the UV-vis. spectra for the complexes (in MeCN)

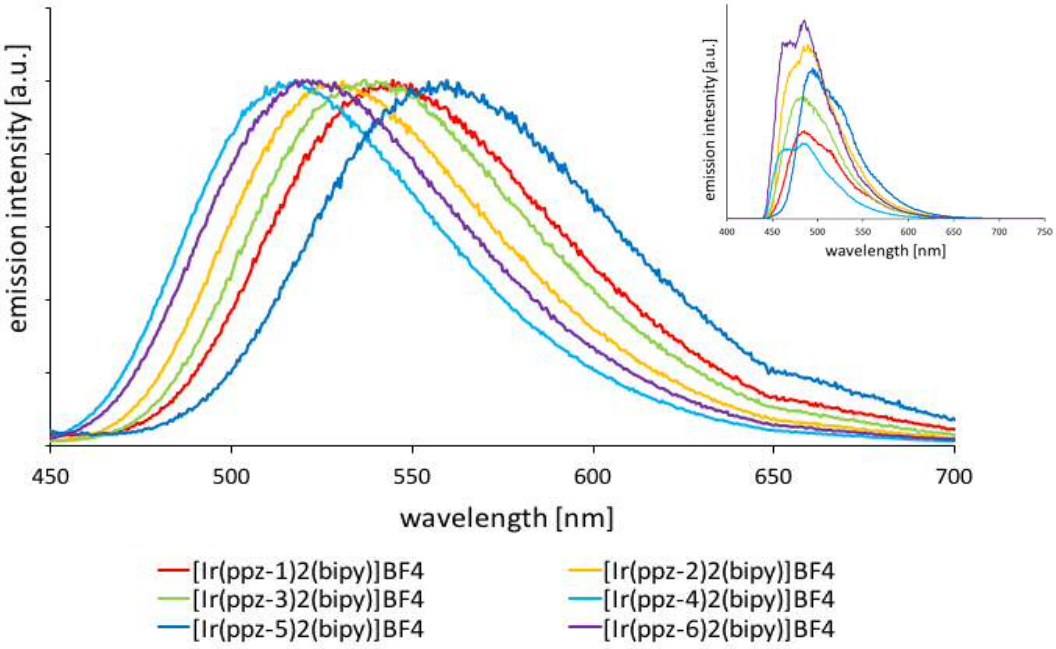

Figure 4.22:Main: Normalised emission spectra of the complexes (MeCN, λex = 380 nm). Foreground: emission spectra at 77K (MeOH/EtOH glass, λex = 380 nm).

These λ_{em} trends are supported by the $E_{Bandgap}$ data from the TD-DFT calculations (Table 4.4). Low temperature (77K) spectra revealed a general hyposchromic shift in the emission maxima together with stronger vibrational features in the peak appearance (Fig. 4.22 inset). The aerated, solution state quantum yields (5-19%) were also obtained together with the luminescence lifetimes (Table 4.5), which lie in the range 77-123 ns. The lifetimes were indicative of phosphorescence in all cases, with data best fitting a single exponential decay, thus indicating single component emission. These data are consistent with related previously reported examples.[16, 69] From these values, k_r and k_{nr} were determined for the different complexes (Table 4.5) and the resultant data shows a clear correlation between the energy of the emission maximum and k_{nr} (and thus in accordance with the energy gap law). Therefore, for these complexes the nature of the emitting state, which is attributed to a strong ^{3}MLCT character, is likely to be closely comparable across the series. The data suggests that in these complexes the electron withdrawing capacity of -SF_5 is greater than -CF_3, -OCF_3 and -F.

4.3.6 Transient Absorption Spectroscopy

Transient absorption (TA) spectroscopy, carried out by Dr Joseph Beames, was also conducted (using a pump wavelength of 266 nm) on the complexes under the same solvent conditions as described above for the UV-vis. and luminescence measurements. The spectral appearance of all six samples is very similar and contains a bleach (or reduction) in optical density (OD) at λ ~ 310 nm and three positive features at λ ~ 380, 490 and 760 nm (Figure 4.24). Closer inspection of the individual peaks shows very little variation in wavelength position across the six complexes. Time-resolved analysis of the transient features at λ = 380 nm give lifetimes that compare well, both in magnitude and trend, to those obtained in the luminescence studies.

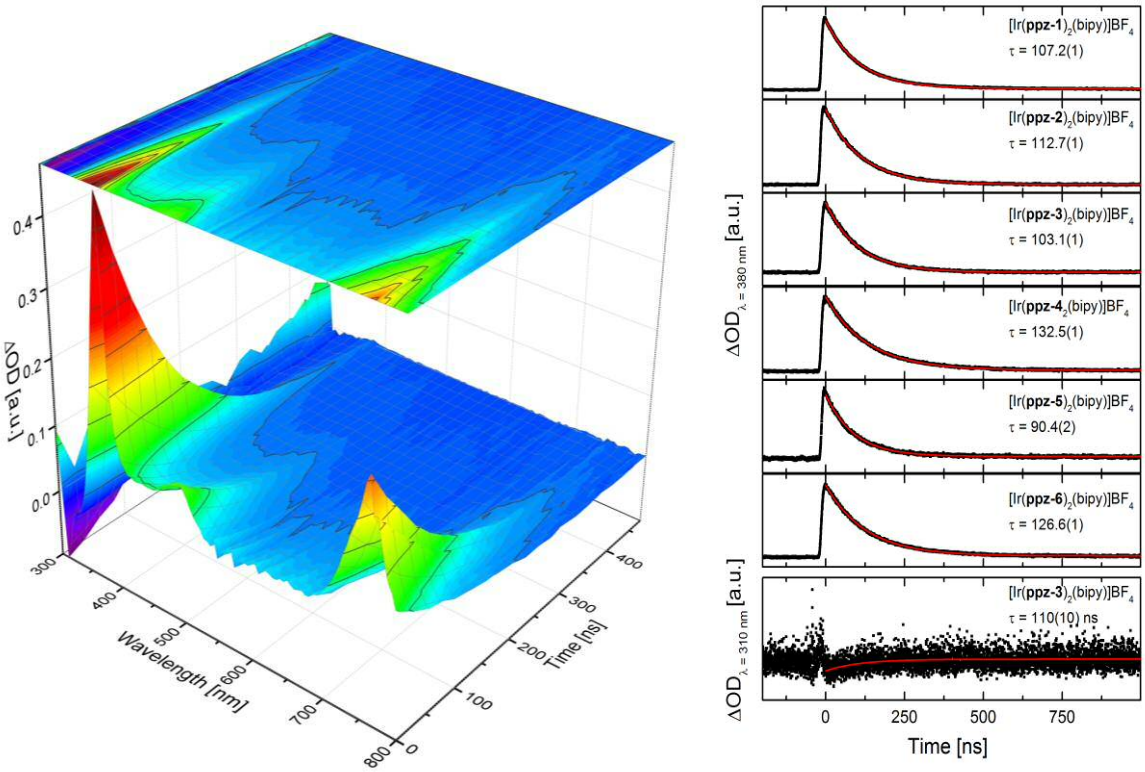

Figure 4.23:Transient absorption spectra and data. Left: a 3D time-resolved plot for [Ir(ppz-3)$_2$(bipy)]BF$_4$. Right: fitted (red trace) lifetime profiles for the different Ir(III) complexes. The lowest panel shows, as an example, the recovery of the spectral feature assigned as a bleach at λ=310 nm for [Ir(ppz-3)$_2$(bipy)]BF$_4$. The recovery of the bleach occurs on a timescale similar to the decay of the absorption features at longer wavelengths.

Analysis of the time-resolved decay of the peaks at λ = 760 nm for each sample revealed similar lifetimes, each of which correlates reasonably well with their respective lifetimes at λ = 380 nm. These TA spectral features could, therefore, originate from the same excitation and intersystem crossing processes that produce the emissive ^{3}MLCT states and, based on the state lifetimes, suggest excited states for the series of complexes that are very similar in nature.[73] Careful analysis of the features at λ = 760 nm suggest that this peak has two underlying components and is a doublet. The data are presented as a 3D contour plot (Figure 4.23) for $[Ir(ppz\text{-}3)_2(bipy)]BF_4$.

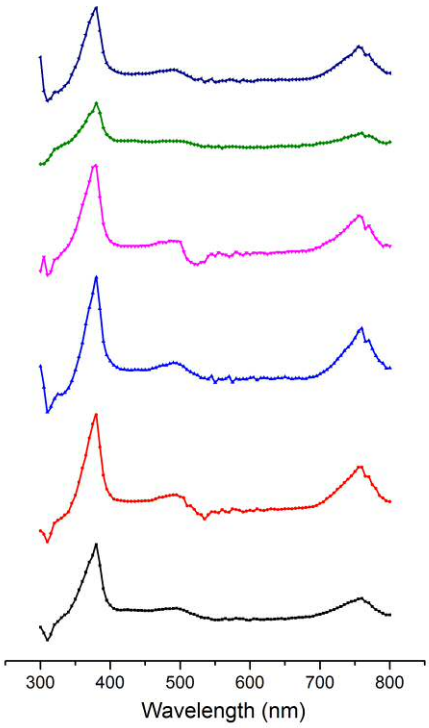

Figure 4.24: Comparative early time transient absorption spectra of the six iridium complexes (top-to-bottom: $[Ir(ppz\text{-}1)(bipy)_2]BF_4$ to $[Ir(ppz\text{-}6)(bipy)_2]BF_4$)

4.3.7 Electrochemistry

The electrochemical characteristics of the six $[Ir(ppz)_2(bipy)]BF_4$ complexes (Table 4.6) were studied in de-oxygenated dichloromethane. The cyclic voltammograms were measured using a platinum disc electrode (scan rate υ = 200 mV s^{-1}, 1 × 10^{-3} M solutions, 0.1 M $[NBu_4][PF_6]$ as a supporting electrolyte) and each complex showed one non-fully or fully reversible oxidation (Table 4.6) at +1.47 to + 1.75 V ascribed to the $Ir^{3+/4+}$ couple.

Each complex also showed one partially reversible or irreversible reduction wave, which was assigned to a ligand-centred process. The small differences in E_{ox} are probably due to the nature of the substituent on the cyclometalating ligand that can influence the electron density at the iridium centre. This data is again in correspondance with previous related examples.[18, 44]

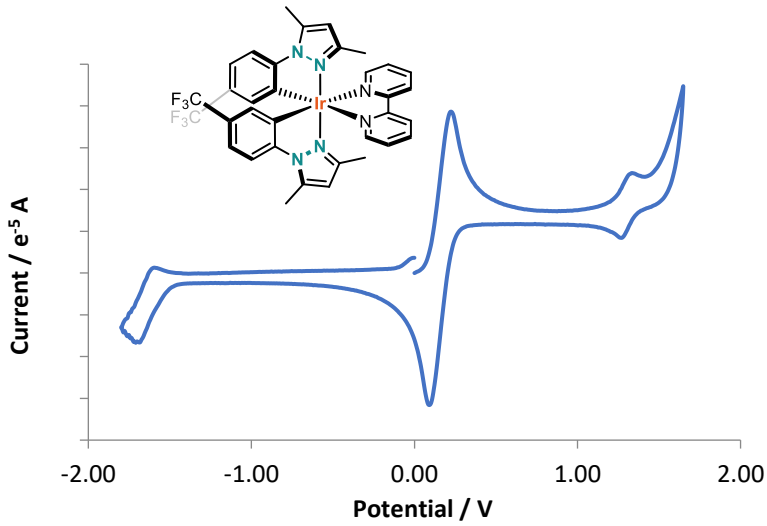

Figure 4.25: Example cyclic voltammogram of [Ir(ppz-3)$_2$(bipy)]BF$_4$ in MeCN solution, at 200mVs^{-1} with 0.1M [NBu$_4$][PF$_6$] as the supporting electrolyte, calibrated with FeCp$_2$

Complex	E_{ox} / V[a]	E_{red} / V[a]	HOMO / eV [d]	LUMO / eV[f]	$E_{bandgap}$ / eV[e]
[Ir(ppz-1)$_2$(bipy)]BF$_4$	+1.62[b]	-1.33[b]	-5.96	-3.43	2.53
[Ir(ppz-2)$_2$(bipy)]BF$_4$	+1.66[b]	-1.32[c]	-6.00	-3.44	2.56
[Ir(ppz-3)$_2$(bipy)]BF$_4$	+1.60[c]	-1.35[c]	-5.94	-3.39	2.55
[Ir(ppz-4)$_2$(bipy)]BF$_4$	+1.74[b]	-1.30[c]	-6.08	-3.52	2.56
[Ir(ppz-5)$_2$(bipy)]BF$_4$	+1.47[c]	-1.47[b]	-5.81	-3.30	2.51
[Ir(ppz-6)$_2$(bipy)]BF$_4$	+1.75[b]	-1.30[b]	-6.09	-3.47	2.62

Table 4.6:Electrochemical properties of the [Ir(ppz)2(bipy)]BF4 complex. [a] oxidation potentials were measured as dichloromethane solutions at 200 mVs^{-1} with 0.1 M [NBu$_4$][PF$_6$] as supporting electrolyte calibrated with Fc/Fc$^+$ at +0.46 V; [b] irreversible wave; [c] reversible wave; [d] the HOMO energy level was calculated using the equation $-E_{HOMO}$ (eV) = $E_{ox} - E_{Fc/Fc+} + 4.8$; [e] $E_{bandgap}$ was determined from the absorption edge of the iridium complexes; [f] the LUMO energy level was calculated using the equation E_{LUMO} (eV) = $E_{HOMO} + E_{bandgap}$

For example, $[Ir(ppz\text{-}5)_2(bipy)]BF_4$ showed the lowest E_{ox} value in the series, suggesting that *para*-fluorination of the pyrazole ligands renders the Ir^{3+} more easily oxidisable. The pentafluorosulfanyl derived complexes gave the highest oxidation potentials. Using the oxidation ($Ir^{3+/4+}$) potential gave the HOMO energy levels (E_{HOMO}), from which E_{LUMO} was also determined. The calculated $E_{bandgap}$ values again revealed a lowest value for $[Ir(ppz\text{-}5)_2(bipy)]BF_4$, with both $[Ir(ppz\text{-}4)_2(bipy)]BF_4$ and $[Ir(ppz\text{-}6)_2(bipy)]BF_4$ at the largest values, which was supported by TD-DFT.

4.4 Conclusions

In conclusion, this chapter reports the comparative syntheses of six new phenyl-1*H*-pyrazoles and their corresponding cyclometalated iridium(III) complexes using both batch and, successfully applied, flow-microwave methodologies. The machine-assisted technology approach clearly delivers improvements on safety, versatility and time. Specifically, microwave-assisted syntheses for the Ir(III) complexes allows isolation of spectroscopically pure species in less than 1 hour of reaction time from $IrCl_3$. All new complexes were explored photophysically (including nanosecond time-resolved transient absorption spectroscopy), electrochemically and by TD-DFT studies which show that the complexes possess ligand-dependent, and thus, tuneable green-yellow luminescence (500-560 nm), with quantum yields in the range 5-15 %. This photophysical evaluation of the complexes show that varying the position and nature of the fluorine-containing substituents on the cyclometalated phenyl-1*H*-pyrazolate can easily tune the emission wavelength of the iridium-based phosphors across the green-yellow part of the visible spectrum.

Future improvements could emanate from connecting the two production phases (ligand *and* complex) into one machine (which would likely require an automated purification phase at the connecting junction) and include the ability to automatically screen the luminescent properties of the formed products. A third-generation approach could then use feedback and optimisation algorithms to deliver a discovery platform for the rapid generation of new metal-ligand phosphors with tunable and targeted luminescence properties.

4.5 Experimental Procedures

4.5.1 General Experimental Considerations

All reagents and solvents were commercially available and were used without further purification if not stated otherwise. Petroleum ether refers to the 40-60 °C fraction. For the measurement of ^{1}H, ^{13}C and ^{19}F NMR spectra a Bruker Fourier^{300} (250, 300 MHz), 400 UltraShield^{TM} (400 MHz) or Ascend^{TM}500 (500 MHz) was used. The obtained chemical shifts δ are reported in ppm and are referenced to the residual solvent signal. ^{19}F NMR signals are reported uncorrected. Spin-spin coupling constants *J* are given in Hz.

The flow setup consisted of perfluoroalkoxy (PFA) tubing of an 0.8 mm ID and two syringe and two Knauer pumps. The residence coils were made from the tubing by taking the appropriate length for the desired volume. The microwave used was a CEM Discover SP. Column chromatography was performed using 60 A (40-64 micron) silica and solvent mixtures of petroleum ether and ethyl acetate.

Low-resolution mass spectra were obtained by the staff at Cardiff University. High-resolution mass spectra were carried out at the EPSRC National Mass Spectrometry Facility at Swansea University. High resolution mass spectral (HRMS) data were obtained on a Waters MALDI-TOF mx at Cardiff University or on a Thermo Scientific LTQ Orbitrap XL by the EPSRC UK National Mass Spectrometry Facility at Swansea University. IR spectra were obtained from a Shimadzu IR-Affinity-1S FTIR. UV-Vis studies were performed on a Jasco V-570 spectrophotometer as MeCN solutions (2.5 or 5×10^{-5} M). Photophysical data were obtained on a JobinYvon–Horiba Fluorolog spectrometer fitted with a JY TBX picosecond photodetection module as MeCN solutions. Emission spectra were uncorrected and excitation spectra were instrument corrected. The pulsed source was a Nano-LED configured for 459 nm output operating at 1 MHz. Luminescence lifetime profiles were obtained using the JobinYvon–Horiba FluoroHub single photon counting module and the data fits yielded the lifetime values using the provided DAS6 deconvolution software. Quantum yield measurements were obtained on aerated

MeCN solutions of the complexes using $[Ru(bpy)_3](PF_6)_2$ in aerated MeCN as a standard (Φ = 0.016). [23]

4.5.2 X-ray Diffraction

For both samples, a suitable crystal was selected and mounted on a MITIGEN holder in oil on a Rigaku FRE+ (45.0 kV, 55.0 mA) equipped with HF Varimax confocal mirrors (100µm focus) and an AFC12 goniometer and HG Saturn 724+ detector diffractometer. The crystals were kept at T = 100(2) K during data collection. Data were measured using profile data from ω-scans using MoK_α radiation. Cell determination and data collection were carried out using CrystalClear. With the data reduction, cell refinement and absorption correction using CrystalisPro. Using Olex2, the structures were solved with the ShelXT structure solution program and the models were refined with version 2014/7 of ShelXL using Least Squares minimisation. All non-hydrogen atoms were refined anisotropically. Hydrogen atom positions were calculated geometrically and refined using the riding model.

For sample $[Ir(ppz\text{-}3)_2(bpy)]BF_4$, the BF_4 anions are disordered over symmetry sites and each contributes half an ion to the asymmetric unit. Also one of the CF_3 groups is disordered over two positions. As such various geometrical (SADI, SAME, BUMP) restraints and displacement (RIGU) restraints were employed, along with displacement constraints (EADP).

For sample $[Ir(ppz\text{-}6)_2(bpy)]BF_4$, a general displacement restraint (RIGU) has been employed due to the number of readily disordered moieties in the asymmetric unit. Also there is a molecule of MeCN for which displacement constraints (EADP) have been employed.

4.5.3 DFT calculations

The geometry of all complexes was fully optimised without symmetry constraint using the B3LYP functional and a basis set consisting of 6-31G(d) on light atoms with Stuttgart-

Dresden core potential and basis set on Ir. Frontier orbital properties were calculated with the same functional and a 6-31+G(d,p) basis on light atoms. TD-DFT used the CAM-B3LYP functional known to perform well for charge transfer transitions, with 6-31+G(d,p) on light atoms and Stuttgart-Dresden potential/basis on Ir. All DFT calculations were performed using the Gaussian09 package.

4.5.4 Transient Absorption

Transient absorption (TA) UV-Vis spectra were collected at Cardiff University using an Edinburgh Instruments LP920 laser flash photolysis spectrometer. All spectra were generated by exciting the samples (prepared as for UV-Vis studies described above) at 266 nm (4^{th} harmonic of a Continuum Surelite II Nd:YAG laser, operated at 10 Hz) and collecting subsequent transient absorption spectra between 300 nm $< \lambda <$ 800 nm (a Xenon lamp provides probe wavelengths). Wavelength dependent TA data was recorded in 5 nm steps using an in-built monochromator, with a bandwidth of 1 nm. Data presented in this manuscript show early time spectra (t < 1 μs post excitation), however no additional TA features were observed over longer timescales (t < 10 ms). TA spectra are presented as $\Delta OD_{Xenon\ lamp}$, hereafter simply referred to as ΔOD, constructed by averaging the first 50 ns of data after the pump laser pulse. Lifetime data was created by fitting the raw experimental data using the Origin 2015 software package. Each fit is created using a single exponential decay function, with no evidence for multiexponential components.

4.5.5 Electrochemistry

Electrochemical studies were carried out using a Parstat 2273 potentiostat in conjunction with a three-electrode cell. The auxiliary electrode was a platinum wire and the working electrode a platinum (1.0 mm diameter) disc. The reference was a silver wire separated from the test solution by a fine porosity frit and an agar bridge saturated with KCl. Solutions (10 ml CH_2Cl_2) were 1.0×10^{-3} mol dm^{-3} in the test compound and 0.1 mol dm^{-3} in $[NBu^n_4][PF_6]$ as the supporting electrolyte. Under these conditions, $E^{0\prime}$ for

the one-electron oxidation of [Fe(η-C_5H_5)$_2$], added to the test solutions as an internal calibrant, is +0.46 V. [36] Unless specified, all electrochemical values are at υ = 200 mV s^{-1}.

4.5.6 Synthesis

For details of ligand synthesis and characterisation, please refer to the associated published paper.[74]

Preparation of fluorinated pyrazole-Iridium complexes in batch

Synthesis of *[Ir(ppz-1)$_2$(bipy)]BF_4*

$IrCl_3.xH_2O$ (180 mg, 0.6 mmol), **ppz-1** (310 mg, 1.2 mmol) and H_2O (2 mL) were heated at reflux in 2-methoxyethanol (6 mL) under argon for 48 hours. The solution was cooled and H_2O added (~20 mL). The resulting grey precipitate was filtered and oven dried to give presumed chloro-bridged dimer [Ir(ppz-1)$_2$(μ-Cl)$_2$(ppz-1)$_2$]. The dimer [Ir(ppz-1)$_2$(μ-Cl)$_2$(ppz-1)$_2$] (100 mg, 0.07 mmol) was split by stirring for 2 hours at reflux in the presence of $AgBF_4$ (27 mg, 0.14 mmol) with MeCN (15 mL) as solvent. The solution was cooled, filtered through cotton wool and the solvent removed *in vacuo*. The crude complex was precipitated from minimal dichloromethane and hexane as a grey oil, [Ir(ppz-1)$_2$(MeCN)$_2$]BF_4. The [Ir(ppz-1)$_2$(MeCN)$_2$]BF_4 (140 mg, 0.16 mmol) and 2,2'-bipyridine (26 mg, 0.16 mmol) were dissolved in $CHCl_3$ (7 ml) and heated at reflux under argon for 24 hours. The solution was cooled and the solvent removed *in vacuo*. The crude solid was dissolved in minimal dichloromethane and added drop wise to stirring Et_2O (15 mL) at 0°C. The resultant precipitate was filtered to give [Ir(ppz-1)$_2$(bipy)]BF_4 as a yellow solid (91 mg, 60%). ^{1}H NMR (500 MHz, $CDCl_3$, 25°C): δ= 8.86 (d, $^3J_{HH}$ = 8.2 Hz, 2H), 8.17 (t, $^3J_{HH}$ = 7.8 Hz, 2H), 7.80 (d, $^3J_{HH}$ = 5.2 Hz, 2H), 7.41 – 7.36 (m, 4H), 6.86 (d, $^3J_{HH}$ = 8.1 Hz, 2H), 6.00 (s, 2H), 5.96 (s, 2H), 2.73 (s, 6H), 1.39 (s, 6H) ppm; ^{13}C{^{1}H} NMR (100 MHz, $CDCl_3$, 25°C): δ= 156.3, 150.2, 149.6, 146.1, 142.6, 141.5, 140.3, 135.0, 127.9, 125.6, 124.9, 115.2, 113.2, 110.6, 14.2, 12.0 ppm; IR (solid): ν bar = 2976, 2359, 1607, 1574, 1558, 1472, 1445, 1248, 1217, 1186, 1155, 1053, 804, 768, 664, 588, 521, 449 cm^{-}

^{1}; UV-vis (MeCN): λ_{max} (ε) = 340 (6800) sh, 310 (18300) sh, 297 (24400), 252 nm (51000 $M^{-1}cm^{-1}$); HRMS: *m/z*: 859.1786, calc. 859.1802 for $[M - C_2H_6]^+$.

Synthesis of [Ir(ppz-2)$_2$(bipy)]BF$_4$

Following the general procedure (GP3), with $IrCl_3.xH_2O$ (156 mg, 0.53 mmol) and **ppz-2** (252 mg, 1.05 mmol). [Ir(ppz-2)$_2$(bipy)]BF_4 was isolated as a light yellow solid (130 mg, 84%). ^{1}H NMR (400 MHz, [D6]acetone, 25°C): δ= 8.91 (d, $^{3}J_{HH}$ = 8.2 Hz, 2H), 8.37 (app. td, J_{HH} = 8.0, 1.5 Hz, 2H), 8.19 (d, $^{3}J_{HH}$ = 4.5 Hz, 2H), 7.82 (s, 2H), 7.76 – 7.70 (m, 2H), 7.14 (d, $^{3}J_{HH}$ = 8.1 Hz, 2H), 6.59 (d, $^{3}J_{HH}$ = 7.9 Hz, 2H), 6.40 (s, 2H), 2.98 (s, 6H), 1.63 (s, 6H) ppm; $^{13}C\{^{1}H\}$ NMR (100 MHz, [D6]acetone, 25°C): δ= 157.5, 152.1, 151.8, 146.0, 143.9, 141.1, 140.5, 135.1, 129.7, 125.9, 122.8 (q, J_{CF} = 3.6 Hz), 112.2, 110.1 (q, J_{CF} = 4.1 Hz), 14.4, 12.4 ppm; IR (solid): ν bar = 2979, 2359, 1605, 1557, 1429, 1294,1327, 1159, 1119, 1082, 1051, 1026, 829, 772, 702; UV-vis (MeCN): λ_{max} (ε) = 339 sh (4600), 310 sh (17500), 276 nm (30900 $M^{-1}cm^{-1}$); HRMS: *m/z*: 827.1887, calc. 827.1905 for $[M - C_2H_6]^+$.

Synthesis of [Ir(ppz-3)$_2$(bipy)]BF$_4$

Following the general procedure (GP3) with $IrCl_3.xH_2O$ (151 mg, 0.5 mmol) and **ppz-3** (243 mg, 1.0 mmol). [Ir(L^3)$_2$(bipy)]BF_4 was isolated as a green/yellow solid (100 mg, 71 %). ^{1}H NMR (400 MHz, [D6]acetone, 25°C): δ= 8.76 (d, $^{3}J_{HH}$ = 8.2 Hz, 2H), 8.22 (td, $^{3}J_{HH}$ = 8.0, 1.6 Hz, 2H), 8.03 (dd, J_{HH} = 5.5, 0.8 Hz, 2H), 7.71 (d, $^{3}J_{HH}$ = 8.6 Hz, 2H), 7.59 (ddd, $^{3}J_{HH}$ = 7.6, 5.5, 1.2 Hz, 2H), 7.28 (dd, J_{HH} = 8.5, 1.4 Hz, 2H), 6.44 (d, $^{3}J_{HH}$ = 1.9 Hz, 2H), 6.27 (s, 2H), 2.80 (s, 6H), 1.49 (s, 6H) ppm; $^{13}C\{^{1}H\}$ NMR (100 MHz, [D6]acetone, 25°C): δ= 157.5, 152.4, 151.7, 148.5, 144.4, 141.0, 134.6, 130.1 (q, J_{CF} = 3.8 Hz), 127.3 (q, $^{1}J_{CF}$ = 31.1 Hz), 125.9, 121.8 (q, J_{CF} = 4.0 Hz), 114.2, 112.0, 14.5, 12.4 ppm; IR (solid): ν bar = 2976, 1604, 1557, 1472, 1400, 1323, 1267, 1078, 1055, 897, 816, 767, 702, 648 cm^{-1}; UV-vis (MeCN): λ_{max} (ε) = 341 sh (6600), 310 sh (18700), 297 sh (21500), 277 nm (32400 $M^{-1}cm^{-1}$) HRMS: *m/z*: 827.1883, calc. 827.1905 for $[M - C_2H_6]^+$.

Synthesis of [Ir(ppz-4)$_2$(bipy)]BF$_4$

Following the general procedure (GP3) with $IrCl_3.xH_2O$ (122 mg, 0.4 mmol) and **ppz-4** (243 mg, 0.8 mmol). [Ir(ppz-4)$_2$(bipy)]BF_4 was isolated as an off-white solid (116 mg, 52 %). ^{1}H NMR (400 MHz, [D6]acetone, 25°C): δ= 8.92 (d, $^{3}J_{HH}$ = 8.0 Hz, 2H), 8.38 (td, $^{3}J_{HH}$ =

8.0, 1.5 Hz, 2H), 8.23 (d, $^3J_{HH}$ = 4.7 Hz, 2H), 7.97 (d, $^3J_{HH}$ = 2.1 Hz, 2H), 7.78 – 7.69 (m, 2H), 7.31 (dd, J_{HH} = 8.4, 2.1 Hz, 2H), 6.59 (d, $^3J_{HH}$ = 8.3 Hz, 2H), 6.42 (s, 2H), 2.97 (s, 6H), 1.64 (s, 6H) ppm; $^{13}C\{^1H\}$ NMR (150 MHz, CD_3CN, 25°C): δ= 157.0, 152.4, 152.0, 145.5, 144.2, 140.8, 140.5, 134.4, 129.4, 125.7, 123.1, 111.8, 111.6, 111.1, 14.4, 12.4 ppm; IR (solid): ν bar = 2982, 1607, 1553, 1470, 1427, 1080, 1051, 1035, 854, 833, 795, 771, 723, 656, 594, 567, 519 cm^{-1}; UV-vis (MeCN): λ_{max} (ε) = 342 sh (6300), 308 sh (21400), 297 sh (28300), 276 nm (36600 $M^{-1}cm^{-1}$); HRMS: *m/z*: 943.1254, calc. 943.1280 for $[M - C_2H_6]^+$.

Synthesis of [Ir(ppz-5)$_2$(bipy)]BF$_4$

Following the general procedure (GP3) with $IrCl_3.xH_2O$ (200 mg, 0.7 mmol) and **ppz-5** (256 mg, 1.3 mmol). [Ir(ppz-5)$_2$(bipy)]BF_4 was isolated as a yellow solid (121 mg, 56 %). ^1H NMR (400 MHz, [D6]acetone, 25°C): δ 8.87 (d, *J* = 8.1 Hz, 2H), 8.38 – 8.28 (m, 2H), 8.18 (d, *J* = 4.7 Hz, 2H), 7.78 – 7.59 (m, 4H), 6.83 (td, *J* = 8.7, 2.8 Hz, 2H), 6.29 (s, 2H), 5.96 (dd, *J* = 9.0, 2.9 Hz, 2H), 2.85 (s, 6H), 1.57 (s, 6H).; $^{13}C\{^1H\}$ NMR (100 MHz, $CDCl_3$, 25°C): δ= 156.6, 150.0 (d, J_{CF} = 13.7 Hz), 141.0, 140.6, 128.0, 125.9, 120.1, 119.9, 113.8, 113.7, 110.7, 110.0, 109.7, 14.6, 12.4 ppm; IR (solid): ν bar = 1603, 1574, 1553, 1472, 1441, 1260, 1194, 1051, 868, 814, 768, 750, 737, 615 cm^{-1}; UV-vis (MeCN): λ_{max} (ε) = 341 sh (4300), 308 sh (21600), 272 nm (35700 $M^{-1}cm^{-1}$); HRMS: *m/z*: 727.1951, calc. 727.1967 for $[M - C_2H_6]^+$.

Synthesis of [Ir(ppz-6)$_2$(bipy)]BF$_4$

Following the general procedure (GP3) with $IrCl_3.xH_2O$ (117 mg, 0.4 mmol) and **ppz-6** (234 mg, 0.8 mmol). [Ir(ppz-6)$_2$(bipy)]BF_4 was isolated as a yellow solid (161 mg, 78 %). ^1H NMR (400 MHz, [D6]acetone, 25°C): δ= 8.78 (d, $^3J_{HH}$ = 8.1 Hz, 2H), 8.27 – 8.20 (m, 2H), 8.07 (ddd, $^3J_{HH}$ = 5.5, 1.5, 0.7 Hz, 2H), 7.72 (d, $^3J_{HH}$ = 8.9 Hz, 2H), 7.61 (ddd, $^3J_{HH}$ = 7.6, 5.5, 1.2 Hz, 2H), 7.46 (dd, J_{HH} = 9.0, 2.6 Hz, 2H), 6.46 (d, $^3J_{HH}$ = 2.6 Hz, 2H), 6.32 (s, 2H), 2.80 (s, 6H), 1.51 (s, 6H) ppm; $^{13}C\{^1H\}$ NMR (100 MHz, [D6]acetone, 25°C): δ= 157.5, 152.9, 151.8, 147.6, 144.9, 141.2, 140.2, 134.3, 130.2, 129.7, 126.0, 122.6, 114.1, 112.2, 14.3, 12.3 ppm; IR (solid): ν bar = 2971, 1470, 1439, 1421, 1396, 1371, 1105, 1063, 1028, 839, 831, 787, 766, 725, 658, 592 cm^{-1}; UV-vis (MeCN): λ_{max} (ε) = 340 sh (6800), 310 sh (18300), 297 sh (24400), 272 nm (37100 $M^{-1}cm^{-1}$); HRMS: *m/z*: 943.1251, calc. 943.1280 for $[M - C_2H_6]^+$.

Preparation of fluorinated pyrazole-Iridium complexes using microwave irradiation

Synthesis of [Ir(ppz-1)$_2$(bipy)]BF$_4$

$IrCl_3.xH_2O$ (180 mg, 0.6 mmol), **ppz-1** (310 mg, 1.2 mmol), H_2O (2 mL) and 2-methoxyethanol (6 mL) were heated in a microwave for 15 min at 180 °C. The solution was cooled and H_2O added (~20 mL). The resulting grey precipitate was filtered and oven dried to give chloro-bridged dimer [Ir(ppz-1)$_2$(μ-Cl)$_2$(ppz-1)$_2$]. [Ir(ppz-1)$_2$(μ-Cl)$_2$(ppz-1)$_2$] (270 mg, 0.19 mmol) was split using MeCN (5 mL) and $AgBF_4$ (74 mg, 0.38 mmol) heating in the microwave at 120 °C for 10 min. The solution was cooled, filtered through cotton wool and the solvent removed *in vacuo*. The crude complex was precipitated from minimal dichloromethane and hexane as a grey oily solid, [Ir(ppz-1)$_2$(MeCN)$_2$]BF$_4$. [Ir(ppz-1)$_2$(MeCN)$_2$]BF$_4$ (260 mg, 0.31 mmol) and 2,2'-bipyridine (49 mg, 0.31 mmol) were dissolved in $CHCl_3$ (7 mL) and heated in the microwave at 130 °C for 15 min. The solution was cooled and the solvent removed *in vacuo*. The crude solid was dissolved in minimal dichloromethane and added drop wise to stirring Et_2O (15 mL) at 0°C. Further purification was achieved using column chromatography (silica) and eluting with 99:1 DCM/MeOH. The resultant precipitate was filtered to give [Ir(ppz-1)$_2$(bipy)]BF$_4$ as a yellow solid (110 mg, 40%).

Synthesis of [Ir(ppz-2)$_2$(bipy)]BF$_4$

Following the general procedure (GP4) with [Ir(ppz-2)$_2$(MeCN)$_2$]BF$_4$ (42 mg, 0.050 mmol). [Ir(ppz-2)$_2$(bipy)]BF$_4$ was isolated as a light yellow solid (26 mg, 57%).

Synthesis of [Ir(ppz-3)$_2$(bipy)]BF$_4$

Following the general procedure (GP3) with [Ir(ppz-3)$_2$(MeCN)$_2$]BF$_4$ (318 mg, 0.38 mmol). Further purification was achieved using column chromatography (silica) and eluting with 99:1 DCM/MeOH. [Ir(ppz-3)$_2$(bipy)]BF$_4$ was isolated as a green/yellow solid (26 mg, 22%).

Synthesis of [Ir(ppz-4)$_2$(bipy)]BF$_4$

Following the general procedure (GP3) with $[Ir(ppz\text{-}4)_2(MeCN)_2]BF_4$ (111 mg, 0.116 mmol). $[Ir(ppz\text{-}4)_2(bipy)]BF_4$ was isolated as an off-white solid (167 mg, 76%).

Synthesis of $[Ir(ppz\text{-}5)_2(bipy)]BF_4$

Following the general procedure (GP3) with $[Ir(ppz\text{-}5)_2(MeCN)_2]BF_4$ (50 mg, 0.067 mmol). $[Ir(ppz\text{-}5)_2(bipy)]BF_4$ was isolated as a yellow solid (29 mg, 53%).

Synthesis of $[Ir(ppz\text{-}6)_2(bipy)]BF_4$

Following the general procedure (GP3) with $[Ir(ppz\text{-}6)_2(MeCN)_2]BF_4$ (85 mg, 0.089 mmol). $[Ir(ppz\text{-}6)_2(bipy)]BF_4$ was isolated as a yellow solid (64 mg, 71%).

1 J. S. Poh, D. L. Browne, S. V. Ley, React. *Chem. Eng*. 2016, **1**, 101-105

2 a) S. Fustero, M. Sánchez-Roselló, P. Barrio and A. Simón- Fuentes, *Chem. Rev*., 2011, **111**, 6984-7034; b) Y. L. Janin, *Chem. Rev*., 2012, **112**, 3924-3958; c) T. Eicher, S. Hauptmann and A. Speicher, *The Chemistry of Heterocycles: Structures, Reactions, Synthesis, and Applications,* Wiley-VCH, 3rd edn, 2012; d) J. A. Joule and K. Mills, *Heterocyclic Chemistry,* Wiley- Blackwell, 5th edn, 2010, For examples of continuous flow approaches towards pyrazoles see: e) I. R. Baxendale, S. C. Schou, J. Sedelmeier and S. V. Ley, *Chem. Eur. J.,* 2010, **16**, 89-94; f) C. J. Smith, F. J. Iglesias-Sigüenza, I. R. Baxendale and S. V. Ley, Org. *Biomol. Chem*., 2007, **5**, 2758-2761

3 R. J. Lundgren and M. Stradiotto, Angew. *Chem., Int*. Ed., 2010, **49**, 8686-8690.

4 A. DeAngelis, D.-H. Wang and S. L. Buchwald, *Angew. Chem., Int. Ed*., 2013, **52**, 3434-3437.

5 B. Li, D. Widlicka, S. Boucher, C. Hayward, J. Lucas, J. C. Murray, B. T. O'Neil, D. Pfisterer, L. Samp, J. VanAlsten, Y. Xiang, J. Young, *Org. Process Res. Dev.,* 2012, **16**, 2031-2037

6 For methods utilising sodium sulfite, see: (a) G. H. Coleman, *Org. Synth.,* 1922, **2**, 71; (b) J. P. Koilpillai, M. Subramanian, U. Mallela, V. B. Boddu, R. Dandala and S. Meenakshisunderam, Aurobindo Pharma Ltd., WO Pat., 2008/075163, 26 June 2008; (c) Z. Yu, G. Tong, X. Xie, P. Zhou, Y. Lv and W. Su, *Org. Process Res. Dev.,* 2015, **19**, 892-896., For methods utilising L-ascorbic acid, see: (d) M. Marinozzi, G. Marcelli, A. Carotti and B. Natalini, *RSC Adv.,* 2014, **4**, 7019-7023; e) C. P. Ashcroft, P. Hellier, A. Pettman and S. Watkinson, *Org. Process Res. Dev.,* 2011, **15**, 98-103; f) T. Norris, C. Bezze, S. Z. Franz and M. Stivanello, *Org. Process Res. Dev.,* 2009, **13**, 354-357; g) D. L. Browne, I. R. Baxendale and S. V. Ley, *Tetrahedron,* 2011, **67**, 10296-10303

7 X. Zhang, J. Kang, P. Niu, J. Wu, W. Yu, and J. Chang, *J. Org. Chem*., 2014, **79**, 10170−10178

8 R. Mukherjee, *Coordination Chemistry Reviews,* 2000, **203**, 151–218

9 S. Trofimenko, *J. Am. Chem. Soc.* 1966, **88**, 1842-1844

10 F. Estevan, P. Hirva, A. Ofori, M. Sanaú, T. Špec, and M. Úbeda, *Inorg. Chem*. 2016, **55**, 2101−2113

11 R. Costa, E. Orti, H. J. Bolink, S. Graber, C. E. Housecroft, E. C. Constable, *J. Am. Chem. Soc*., 2010, **132**, 5978-5980

12 A. B. Tamayo, B. D. Alleyne, P. I. Djurovich, S. Lamansky, I. Tsyba, N. N. Ho, R. Bau, M. E. Thompson, *J. Am. Chem. Soc.* 2003, **125**, 7377-7387

13 A. B. Tamayo, S. Garon, T. Sajoto, P. I. Djurovich, I. M. Tsyba, R. Bau, M. E. Thompson, *Inorg. Chem.* 2005, **44**, 8723-8732

14 A. Martinez, M. Fabra, M. P. Garcı´a, F. J. Lahoz, L. A. Oro, S. J. Teat, *Inorganica Chimica Acta*, 2005, **358**, 1635–1644

15 D. Han, X. Wang, L. Zhao, C. Pang, Q. Wang and G. Zhang, *Molecular Physics,* 2016, **114**, 2265-2271

16 K. Chen, C. Yang, Y. Chi, C. Liu, C. Chang, C. Chen, C. Wu, M. Chung, Y. Cheng, G. Lee, and P. Chou, *Chem. Eur. J.* 2010, **16**, 4315 – 4327

17 G. G. Shan, H-B. Li, H-Z. Sun, D-X. Zhu, H-T. Cao and Z-M. Su., *J. Mater. Chem.* C, 2013, **1**, 1440-1449

18 D. L. Davies, M. P. Lowe, K. S. Ryder, K. Singh and S. Singh, *Dalton Trans.* 2011, **40,** 1028-1030

19 D. Lloyd, M. P Coogan, S. J. A. Pope, *Reviews in Fluorescence*, Vol 7, Springer: New York, 2010, 15-44

20 Kenneth Kam-Wing Lo. Steve Po-Yam Li and Kenneth Yin Zhang, *New. J. Chem.,* 2011, 256-287

21 I.V Alilov, P.Minoofar, J. Cornil, and L. De Cole, *J. Am. Chem. Soc*., 2007, **129**, 8247-8258

22 M. Licini and J. A G. Williams, *Chem. Commun.,* 1999, **19**, 1943-1944

23 S. Obara, M. Itabashi, F. Okuda, S. Tamaki, Y. Tanabe, Y Ishii, K. Nozaki and M. Haga, *Inorg. Chem*, 2006, **45**, 8907-8921

24 P. Didier, I. Ortmans, A. Kirsch-De Mesmaeker and R. J. Watts, *Inorg. Chem*., 1993, **32**, 5239-5245

25 a) J. Sun, W. Wu, H. Guo, and J. Zhao, *Eur. J. Inorg. Chem*, 2011, **21**, 165-3173, b) K. J Castor, K. L Metera, U. M Tefashe, C. J. Serpell, J. Mauzeroll and H. F. Sleiman., *Inorg. Chem*., 2015, **54**, 6958-6967. c) J. Jayabharathi, R. Sathishkumar, V. Thanikachalam and K. Jayamoorthy, *J. Fluoresc.,* 2014, **24**, 445-453. d) S. Mandal, K. D. Poria, R. Ghosh, P. S. Ray and P. Gupta, *Dalton Trans*., 2014, **43**, 17463-17474.

26 a) H. Tang, Y. Li, B. Zhao, W. Yang, H. Wu and Y. Cao., *Organic Electronics*, 2012, **13**, 3211-3219. b) S. K. Seth, S. Mandal, P. Purkayastha and P. Gupta, *Polyhedron*, 2015, **95**, 14-23

27 M. S. Lowry and S. Bernhard, *Chem. Eur. J.,* 2006, **12**, 7970-7977

28 a) Q, Zhao, S. Lui, M. Shi, F. Li, H. Jing, T. Yi, and C. Huang, *Organometallics,* 2007, **26**, 5922-530. b) C. Jin, J. Lui, Y. Chen, L. Zeng, R, Guan, C. Ouyang, L. Ji and H. Chao,

Chem. Eur. J. 2015, **21**, 12000-12010. c) D. Todera, A. Pertegas, N. M. Shavaleev, R. Scopelliti, E. Orti, H. J. Bolink, E. Baranoff, M. Gratzel and M. K. Nazeeruddin, *J. Mater. Chem*, 2012, **22**, 19264-19268

29 C. H. Yang, Y. M Cheng, Y. Chi, C. J. Hsu, F. C. Fang, K. T. Wong, I. T. Chou, C. H. Chang, M. H Tsai, C. C Wu, *Angew. Chem.* 2007*,* **119**, 2470 –2473

30 C. H. Yang, J. Beltran, V. Lemaur, J. Cornil, D. Hartmann, W. Sarfert, R. Frohlich, C. Bizzarri and L. De Cola, *Inorg. Chem.,* 2010, **49**, 9891-9901

31 For example: a) J. I. Goldsmith, W. R. Hudson, M. S. Lowry, T. H. Anderson, S. Bernhard, *J. Am. Chem. Soc.* 2005, **127**, 7502-7510; b) S.-Y. Takizawa, R. Aboshi, S. Murata, *Photochem. Photobiol. Sci.* 2011, **10**, 895-903; c) A. J. Hallett, N. White, W. Wu, X. Cui, P. N. Horton, S. J. Coles, J. Zhao, S. J. A. Pope, *Chem. Commun*. 2012, **48**, 10838-10840.

32 J. D. Blakemore, N. D. Schley, D. Balcells, J. F. Hull, G. W. Olack, C. D. Incarvito, O. Eisenstein, G. W. Brudvig, and R. H. Crabtree *J. Am. Chem. Soc.*, 2010, **132**, 6017–16029

33 For example: a) T. S-M. Tang, K-K. Leung, M-W. Louie, H-W. Liu, S. H. Cheng, K.K-W. Lo, Dalton Trans. 2015, **44**, 4945-4956; b) C. Li, M. Yu, Y. Sun, Y. Wu, C. Huang, F. Li, *J. Am. Chem. Soc.* 2011, **133**, 11231-11239; c) A. Jana, E. Baggaley, A. J. Amoroso, M. D. Ward, *Chem. Commun.* 2015, **51**, 8833-8836

34 G.-G. Shan, H.-B. Li, H.-T. Cao, D.-X. Zhu, P. Li, Z.-M. Su, Y. Liao, *Chem. Commun.*, 2012, **48**, 2000-2002

35 H. Sun, S. Liu, W. Lin, K. Y. Zhang, W. Lv, X. Huang, F. Huo, H. Yang, G. Jenkins, Q. Zhao, W. Huang, *Nat. Commun.* 2014, **5**, 3601

36 S. Lamansky, P. Djurovich, D. Murphy, F. Abdel-Razzaq, H.-E. Lee, C. Adachi, P. E. Burrows, S. R. Forrest, M. E. Thompson, *J. Am. Chem. Soc.* 2001, **123**, 4304-4312;

37 A. Tsuboyama, H. Iwawaki, M. Furugori, T. Mukaide, J. Kamatani, S. Igawa, T. Moriyama, S. Miura, T. Takiguchi, S. Okada, M. Hoshino, K. Ueno, *J. Am. Chem. Soc.* 2003, **125**, 12971-12979

38 W.-Y.Wong, G.-J. Zhou, X.-M. Yu, H.-S. Kwok, B.-Z. Tang, *Adv. Funct. Mater.,* 2006, **16**, 838-846

39 R. Guo , D. Zhong, C. Ou, G. Xiong, X. Zhao, Y. Sun, M. Jurow, J. Kang, Y. Zhao, S. Li, L. You, L. Wang, Y. Lui, W. Huang,. *Inorg Chem.*, 2017, **56 (14),** 8397–8407

40 Z. Zhao, G. Yu, Q. Chang, X. Liu, Y. Liu, L. Wang, Z. Liu, Z. Bian, W. Liu and C. Huang*, J. Mater. Chem. C*, Accepted Manuscript, 2017, **56 (14),** 8397–8407

41 a) C. W. Lee and J. Y. Lee, *Adv. Mater.*, 2013, **25**, 5450-5454. b) H. Shin, S. Lee, K.-H. Kim, C.-K. Moon, S.-J. Yoo, J.-H. Lee and J.-J. Kim, *Adv. Mater.*, 2014, **26**, 4730-4734. c) E. Baranoff and B. F. E. Curchod, *Dalton Trans.*, 2015, **44**, 8318-8329. d) J.-H. Lee, S.-H. Cheng, S.-J. Yoo, H. Shin, J.-H. Chang, C.-I. Wu, K.-T. Wong and J.-J. Kim, *Adv. Funct. Mater.*, 2015, **25**, 361-366.

42 J. D. Slinker, A. A. Gorodetsky, M. S. Lowry, J. J. Wang, S. Parker, R. Rohl, S. Bernhard and G. G. Malliaras, *J. Am. Chem. Soc.,* 2004, **126**, 2763-2767

43 S. Evariste, M. Sandroni, T. Rees, C. Roldan-Carmona, L. Gil-Escrig, H. Bolink, E. Baranoff and E. Zysman-Colman, *J. Mater. Chem. C*, 2014, **2**, 5793-5804

44 J. M. Fernandez-Hernandez, S. Ladouceur, Y. Shen, A. Iordache, X. Wang, L. Donato, S. Gallagher-Duval, M. de Anda Villa, J. D. Slinker, L. De Cola and E. Zysman-Colman, *J. Mater. Chem.* C, 2013, **1**, 7440-7445

45 K. Lo, C. Chung, *Organometallics* 2001, ***20***, 4999- 5001.

46 K. Lo, C. Chung, T. K. Lee, L. Lui, K. H. Tsang, N. Zhu, *Inorg. Chem.* 2003, ***42***, 6886-6897

47 K. Lo, C. Chung, N. Zhu, *Chem.-Eur. J.* 2006, ***12***, 1500-1512.

48 H. Chen, Q. Zhao, Y. Wu, F. Li, H. Yang, T. Yi, and C. Huang, *Inorg. Chem.,* 2007, **46**, 11075-11081

49 D. Ma, H. J. Zhong, W-C. Fu, D. Chan, H-Y. Kwan, W-F. Fong, L-H. Chung, C-Y. Wong, C-H. Leung. *PLoS One.* 2013, **8**, e55751

50 D. L. Ma, W. L. Wong, W. H. Chung, F. Y. Chan, P. K. So, Angew. Chem. Int. Ed. Engl., 2008, **47**, 3735–3739

51 K. Qiu, M. Ouyang, Y. Liu, H. Huang, C. Liu, Y. Chen, L. Ji and H. Chao*, J. Mater. Chem. B*, 2017, Advance Article. DOI: 10.1039/C7TB00731K

52 R. A. Smith, E. C. Stokes, E. E. Langdon-Jones, J.A. Platts, B. M Kariuki, A. J. Hallett and S. J. A. Pope, *Dalton Trans.,* 2013, **42**, 10347-10357

53 M. Li, P. Jiao, W. He, C. Yi, C. Li, X. Chen, G. Chen and M. Yang*, Eur. J. Inorg. Chem*. 2011, **2**, 197–200

54 S. Po-Yam Li, Hua-Wei Liu, K. Yin Zhang, and K. Kam-Wing Lo. *Chem. Eur. J*. 2010, **16**, 8329 – 8339

55 S. Zanarini, M. Felici, G. Valenti, M. Marcaccio, L. Prodi, S. Bonacchi, P. Contreras-Carballada, R.M. Williams, M. C. Feiters, R. J. M. Nolte, L. De Cola, and F. Paolucci, *Chem. Eur. J.* 2011, **17**, 4640 – 4647

56 M. Licini and J. A. G Williams, *Chem. Commun.,* 1999, **19**, 1943-1944

57 B. Lou, Z. Q Chen, Z. Q Bian and C.H Huang. *New. J. Chem.,* 2010, **0,** 617-622

58 K. Kam-Wing Lo, S. Po-Yam Li and Y. Zhang, *New. J. Chem,* 2011, **0,** 256-287

59 For some examples of papers describing the incorporation of machines in to synthetic chemistry see: a) A. McNally, C. K. Prier and D. W. C. MacMillan, *Science*, 2011, **344**, 1114-1117; b) S. V. Ley, D. E. Fitzpatrick, R. M. Myers, C. Battilocchio and R. J. Ingham, Angew. *Chem. Int. Ed.* 2015, **54**, 10122-10136; c) S. V. Ley, R. J. Ingham, M. O'Brien and S. V. Ley, Beistein *J. Org. Chem.* 2013, **9**, 1051-1072; d) A. Adamo, R. L. Beingessner, M. Behnam, J. Chen, T. F. Jamison, K. F. Jensen, J.-C. M. Monbaliu, A. S. Myerson, E. M. Revalor, D. R. Snead, T. Stelzer, N. Weeranoppanant, S. Y. Wong and P. Zhang, *Science*, 2016, **352**, 61-67.

60 R. Adamo, L. Beingessner, M. Behnam, J. Chen, T. F. Jamison, K. F. Jensen, J.-C. M. Monbaliu, A. S. Myerson, E. M. Revalor, D. R. Snead, T. Stelzer, N. Weeranoppanant, S. Y. Wong and P. Zhang, *Science*, 2016, **352**, 61-67

61 a) S. Ceylan, L. Coutable, J. Wegner, A. Kirschning, Chem. Eur. J. 2011, **17**, 1884–1893. b) J. Hartwig, S. Ceylan, L. Kupracz, L. Coutable, A. Kirschning, *Angew. Chem. Int. Ed.* 2013, **52**, 9813–9817; Angew. Chem. 2013, **125**, 9995–9999; c) S. R. Chaudhuri, J. Hartwig, L. Kupracz, T. Kodanek, J. Wegner, A. Kirschning, *Adv. Synth. Catal.* 2014, **356**, 3530–3538; d) L. Kupracz, A. Kirschning, Adv. Synth. Catal. 2013, **355**, 3375–3380; d) L. Kupracz, A. Kirschning, *J. Flow Chem.* 2013, **3**, 10– 16.

62 For examples of papers reporting inline analytics see: a) S. Schwolow, F. Braun, M. Rädle, N. Kockmann and T. Röder, *Org. Process Res. Dev*., 2015, **19**, 1286-1292; b) K. L. A. Chan, S. Gulati, J. B. Edel, A. J. de Mello and S. G. Kazarian, *Lab Chip,* 2009, **9**, 2909–2913. c) C. F. Carter, H. Lange, S. V. Ley, I. R. Baxendale, B. Wittkamp, J. G. Goode and N. L. Gaunt, *Org. Process Res. Dev.,* 2010, **14**, 393-404. d) S. Newton, C. F. Carter, C. M. Pearson, L. D. Alves, H. Lange, P. Thansandote and S. V. Ley, Angew. *Chem., Int. Ed.,* 2014, **53**, 4915-4920. e) D. L. Browne, S.

Wright, B. J. Deadman, S. Dunnage, I. R. Baxendale, R. M. Turner and S. V. Ley, Rapid Commun. *Mass Spectrom*., 2012, **26**, 1999-2010.

63 For examples of papers reporting/discussing self optimization and the use of intelligent algorithms see: a) V. Sans and L. Cronin, *Chem. Soc. Rev.,* 2016, **45**, 2032-2043. b) D. C. Fabry, E. Suiono and M. Rueping, *React. Chem. Eng.,* 2016, **1**, 129-133. c) J. Parrott, R. A. Bourne, G. R. Akien, D. J. Irvine and M. Poliakoff, *Angew. Chem., Int. Ed.,* 2011, **50**, 3788-3792. d) R. A. Skilton, R. A. Bourne, Z. Amara, R. Horvath, J. Jin, M. J. Scully, E. Streng, S. L. Y. Tang, P. A. Summers, J. Wang, E. Pérez, N. Asfaw, G. L. P. Aydos, J. Dupont, G. Comak, M. W. George and M. Poliakoff*, Nat. Chem*., 2015, **7**, 1–5.

64 For papers reporting synthesis and biological screening machine platforms, see: a) C. Battilocchio, L. Guetzoyan, C. Cervetto, L. D. C. Mannelli, D. Frattaroli, I. R. Baxendale, G. Maura, A. Rossi, L. Sautebin, M. Biava, C. Ghelardini, M. Marcoli and S. V. Ley, *ACS Med. Chem. Lett*., 2013, **4**, 704-709; b) L. Guetzoyan, N. Nikbin, I. R. Baxendale and S. V. Ley, *Chem. Sci.,* 2013, **4**, 764-769; c) W. Czechtizky, J. Dedio, B. Desai, K. Dixon, E. Farrant, Q. Feng, T. Morgan, D. M. Parry, M. K. Ramjee, C. N. Selway, T. Schmidt, G. J. Tarver, and A. G. Wright, *ACS Med. Chem. Lett.,* 2013, **4**, 768-772

65 For examples of the formation of metal/ligand complexes (of iridium) under continuous flow or microwave conditions, see: a) J. G. Krabbe, A. R. Boer, G. Van der Zwan, H. Lingerman, W. M. A. Niessen and H. Irth, *J. Am. Chem. Soc. Mass Spectrom.* 2007, **18**, 707-713; b) H. Konno and Y. Sasaki, *Chem. Lett.* 2003, **32**, 252. c) B. Beyer, C. Ulbricht, A. Winter, M. D. Hager, R. Hoogenboom, N. Herzer, S. O. Baumann, G. Kickelbick, H. Görls and U. S. Schubert, *New J. Chem.* 2010, **34**, 2622-2628

66 T. M. Monos, A. C. Sun, R. C. McAtee, J. J. Devery III, C. R. J. Stephenson, *J. Org. Chem.* 2016, **81**, 6988-6994

67 A. F. Henwood, E. Zysman-Colman, *Chem. Commun*. 2017, **53**, 807-826.

68 M. Nonoyama, Bull. *Chem. Soc. Jpn.* 1974, **47**, 767-768

69 E. C. Stokes, E. E. Langdon-Jones, L. M. Groves, J. A. Platts, P. N. Horton, I. A. Fallis, S. J. Coles and S. J. A. Pope, *Dalton Trans.,* 2015, **44**, 8488-8496

70 R. D. Costa, E. Orti, H. J. Bolink, S. Graber, S. Schaffner, M. Neuburger, C. Housecroft, E. C. Constable., *Adv. Funct. Mater.,* 2009, **19**, 3456-3463

71 R.D. Costa, E. Orti, D. Tordera, A. Pertegas, H.J. Bolink, S. Graber, C.E. Housecroft, L. Sachno, M. Neuburger, E.C. Constable, *Adv. Energy Mater.,* 2011, **1**, 282-286

72 N.M. Shavaleev, G. Xie, S. Varghese, D.B. Cordes, A.M.Z. Slawin, C. Momblona, E. Orti, H.J. Bolink, I.D.W. Samuel, E. Zysman-Colman, *Inorg. Chem.,* 2015, **54**, 5907-5914

73 L. Flamigni, B. Ventura, F. Barigelletti, E. Baranoff, J-P. Collin, J-P. Sauvage, Eur. *J. Inorg. Chem.,* 2005, **36**, 1312-1318

74 L. Groves, C. Schotten, J. Beames, J. A. Platts, S. J. Coles, P. N. Horton, D. L. Browne, S. J. Pope, *Chem. Eur. J.* 2017, **23**, 9407-9418

Chapter 5 – Synthetic Development and Spectroscopic Analysis of Ferrocene 1,8-Naphthalimide Derivatives for Electrochemical Biosensors Applications

5.1 Introduction

5.1.1 Electrochemical Biosensors

Biosensors are used to determine specific analytes as well as investigate chemical interactions of biomolecules such as DNA. They represent a measuring instrument requiring no additional reagents, thus providing selective qualitative and/or quantitative analytical information using a biological recognition element which is retained in spatial contact with a transduction element.[1] The application of the biosensor depends on selection of its building blocks, where construction is tailored for a specific purpose. In particular, detection involving biomacromolecules such as DNA requires a biosensor with a rational and complex construction. DNA-based electrochemical biosensors comprise a nucleic acid recognition layer, which is immobilized over an electrode as the transducer converts the DNA response into an electronic signal. This type of biosensor can be applied in a variety of diagnostics of serious diseases, whilst typically offering high sensitivity, acceptable selectivity, easy automation and easy portability; leading to low running and investment costs.[1]

5.1.2 Electrochemical Clostridium Difficile Detection

Clostridium difficile (CDF) is a spore-forming, ubiquitous bacterium that is present in the human colon of 2-5% of the adult population.[2] CDF has significant antibiotic resistance, and upon commencement of antibiotic therapy the natural equilibrium of the gut is disturbed. This allows CDF to opportunistically dominate the colon, aiding the CDF infection (CDI). The symptoms of this disease are diarrhoea and inflammation,[3] and can range from mild disease to life-threatening pseudomembranous colitis. With an 8% mortality rate, CDI led to 0.8% of all hospital deaths in 2012.[4]

The current clinical method of diagnosis begins with a two-step algorithm: initial screening for glutamate dehydrogenase (detects the presence of the organism), followed by an enzyme immunoassay test for the presence of disease causing toxins.[5] This diagnostic method is lacking in terms of time-to-result, sensitivity and specificity. A

proposal based on a GW4 collaboration involving groups in Cardiff, Bristol and Bath universities aims to develop a diagnostic bedside test able to give a definitive result within ten minutes, thus allowing appropriate treatment to be given in a shorter time frame.

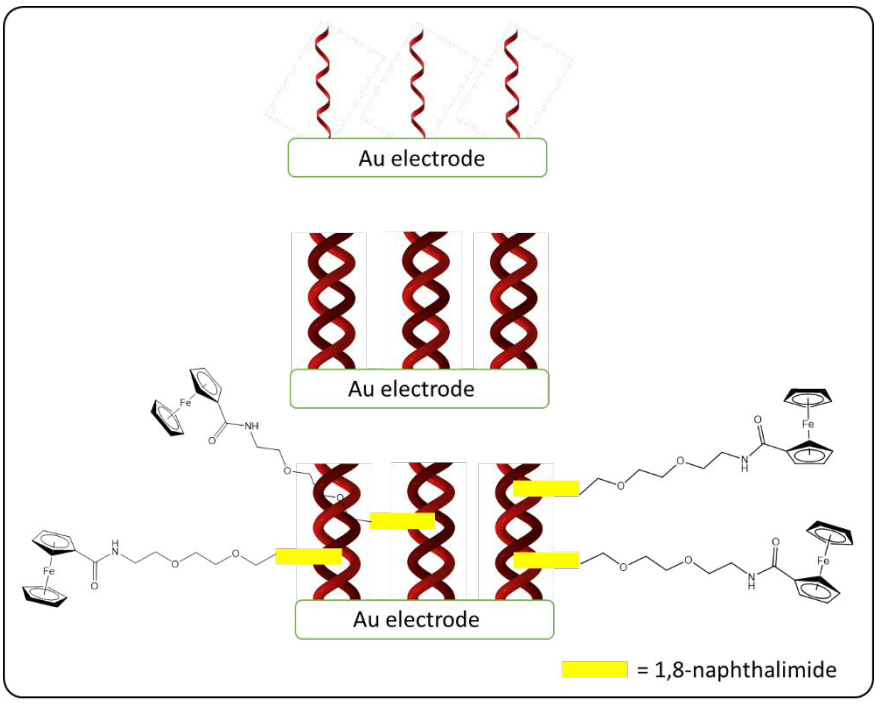

Figure 5.1:Schematic showing hypothesised detection method for CDF

The methodology for this bedside test is shown in Figure 5.1. A capture strand of DNA is used that is immobilised on a gold electrode, where the single stranded DNA is made up of complimentary base pairs to selectively target the DNA of CDF. If CDF is present, hybridisation will occur with the capture strand and form a double helix. This will in turn trigger one or more of the electronically active probes to bind to the DNA duplex on the electrode. This brings the redox-active element into proximity of the gold electrode and creates a detectable electrochemical signal for electrochemical impedance spectroscopy. This will perturb the typical signal of the gold electrode therefore causing the probe to act as a sensitiser for electrochemical detection of the DNA strand. An example of a suitable redox-active element is ferrocene, due to the facile redox properties of the ferrocene/ferrocenium couple, as displayed in Figure 5.2.

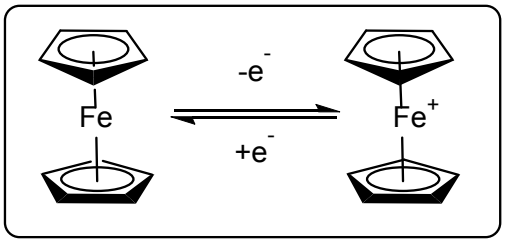

Figure 5.2: Ferrocene/ferrocenium redox couple

5.1.3 Naphthalimide Derivatives with Specific DNA Sequence Selectivity

Small molecules are able to be highly selective towards a specific DNA sequence through binding modes including intercalation, electrostatic and hydrogen bonding interactions. This characteristic is invaluable when developing new diagnostic and therapeutic agents.[6] It is possible for naphthalimide derivatives to achieve DNA binding by joining known minor groove-binding agents. For example, DNA-directed alkylating agents have been established that link naphthalimide, nitrogen mustard and lexitropsin moieties.[7] Lexitropsin is a known DNA binding ligand which is commonly used to admininster antibiotics.[8,9] However in this research the most biologically active compound unexpectedly lacked the lexitropsin unit.

In other research, the intercalation effect of a 1,8-naphthalimide chromophore was combined with the minor groove-binding characteristics of a range of pyrrole-imidazole polyamides.[10] The binding affinity and specificity of naturally occurring DNA binding proteins is mimicked by the pyrrole-imidazole polyamides: 8 membered ring systems containing a three-letter amino acid code.[11] Therefore, the naphthalimide moiety ensures the molecule intercalated tightly with DNA and the pyrrole-imidazole unit directed the molecule to specifically bind to the topoisomerase II gene promoter sequence. Figure 5.3 displays compounds 2 and 3 from the study, where the naphthalimide unit in compound 3 improved the sequence selectivity for the ICB2 site by simultaneous intercalation and minor-groove binding. Following this, other research has successfully developed 1,8-naphthalimide units linked to peptide chains to ensure selective DNA binding.

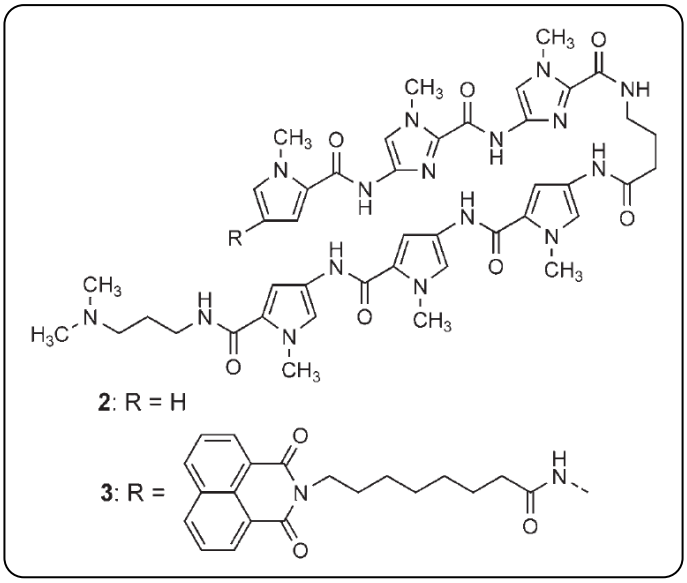

Figure 5.3: Pyrrole-imidazole polyamides by Lee et al.[10] *Copyright 2006 John Wiley & Sons*

5.1.4 Biological Applications of Ferrocene

Metallocenes have found applications in a wide variety of biological applications. There are three main characteristics that make them suitable for these applications. Firstly, they are small, rigid, hydrophobic molecules that can easily diffuse across the phospholipid bilayer of the cell membrane;[12] a characteristic that is maintained when the metallocene is functionalised with polar substituents. There are a number of *in vitro* and *in vivo* investigations available for this genre of compounds.[12] Secondly, the top surface of a metallocene bears resemblance to an aromatic system and hence they are able to mimic the binding of small aromatic molecules. However, due to their increased thickness they block further enzymatic sites, thus inhibiting enzyme-catalysed processes.[12] Finally, the inherent thermodynamic stability of metallocenes ensures that the metal centre cannot be displaced without destroying the structure. As a result, the metal centre can act as a tracer, especially when the metal is redox active, for example Fe(II)[13] or radioactive ^{87}Ru.

In particular, ferrocene has been widely used as an organometallic scaffold for the synthesis of many functionalised derivatives which have synthetic and medicinal applications.[14] Ferrocene's employment for a vast number of fields is due to a number of reasons: it is aromatic and readily functionalised; it has an electron rich Fe(II) centre; good solubility and ease of undergoing iron oxidation. In relation to these properties,

areas in which ferrocene has found use are electrochemistry, biochemistry, drug design mediators of protein redox reactions,[15,16] internal standards in electrochemistry[17,18] and organic synthesis,[19] as in the functionalisation of cyclopentadienyl ligands.[20,21] Derivatives are generally stable aerobically, thermodynamically and photochemically and hence a wide range of chemical behaviour can be explored.[22] Due to a positive combination of chemical and physical properties, ferrocene derivatives have also found applications as electronic materials, metallic coatings, high-octane additives to motor fuel and hematopoietic substances.[23] In addition, ferrocene-based polymers have also been explored in the fields of biosensing,[24,25] biomedical engineering,[26] biophysics and surface science.

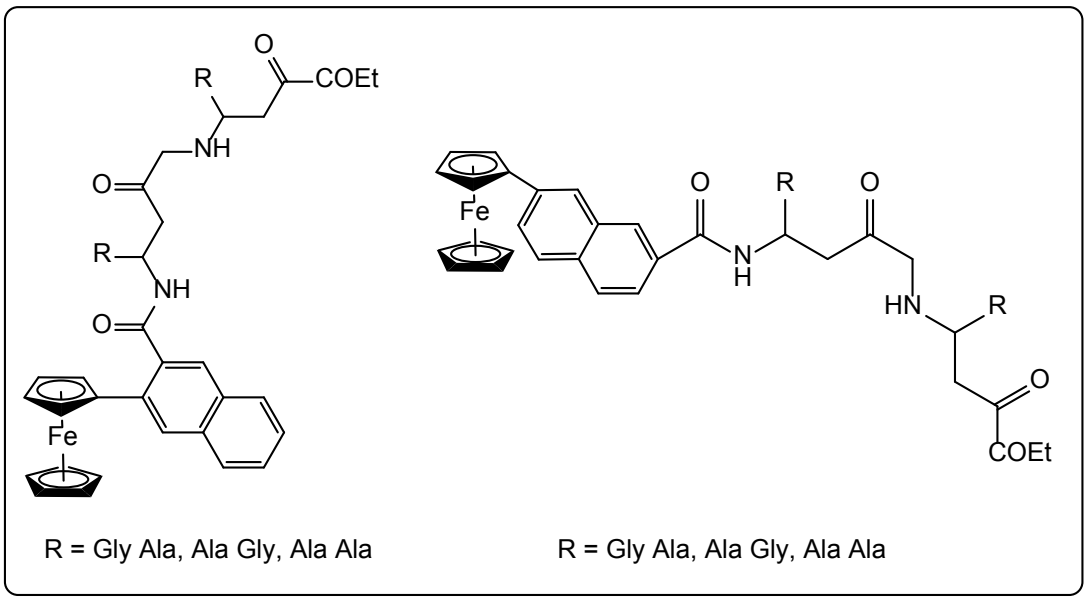

Figure 5.4: N-(ferrocenyl)naphthoyl derivatives investigated in terms of cytotoxicity towards H1299 cells[27]

Biological applications of ferrocene include analgesic, antineoplastic, anticonvulsant, anti-HIV, antitumour, antimalarial, antioxidant, antimicrobial and DNA-cleaving activities.[23] In particular, the applications of ferrocene derivatives as promising targets for cancer disease have been extensively reviewed.[23] Known compounds that are excellent anticancer and antimalarial agents include ferrocifen, tamoxifen[28] and ferroquine. For example, ferrocifens were the first anticancer agents to be active against both hormone-dependant and hormone-independent breast cancer.[29] In more recent

work, the N-(ferrocenyl)naphthoyl derivatives shown in Figure 5.4 were investigated for their cytotoxic activity against the human lung carcinoma cell line, H1299. All derivatives were found to be more cytotoxic *in vitro* than the clinically used anticancer drug carboplatin.[27]

In recent years, the development of DNA-biosensors has played a significant role in diagnostics and biomedicine, as well as forensics.[23] For example, electrochemical DNA biosensors have been used to predict drug-DNA interactions, where the techniques used are fast, high-throughput and low cost[30] thus giving rise to the ability to speed up the drug screening process. Oxidation reactions that take place at an electrode show similar behaviour to those in the body, which is why it is possible for electrochemical and biological reactions to be compared. For the same reason, an electrochemical signal related to DNA-drug interaction can provide information on interaction mechanism, binding constant, binding bite size and the role of free radicals generated during the interaction.[23]

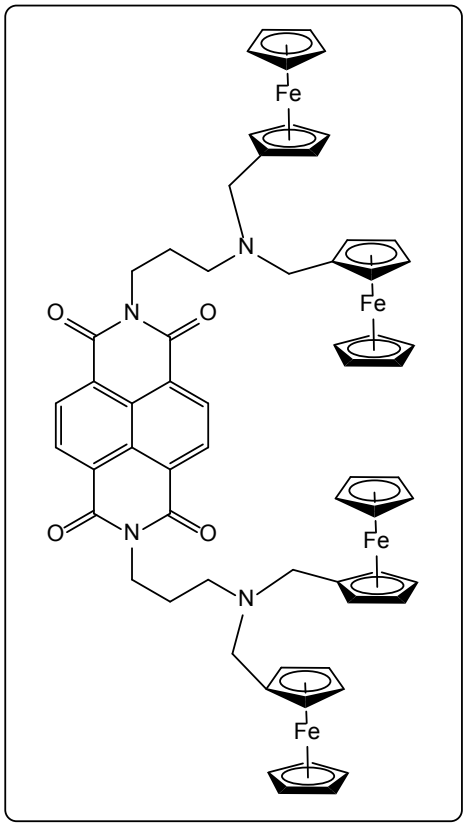

Figure 5.5: F_4ND hybridisation indicator[31]

One example of a ferrocene derivative being applied as an electrochemical gene detector is provided by Sato *et al*., who developed a new naphthalene diimide F_4ND hybridisation indicator (Figure 5.5).[31] Although the compound had bulky substituents, F_4ND showed binding to double-stranded DNA with intercalation mode therefore distorting the duplex. Methylated and unmethylated sites on the target DNA caused differences in the rate of dissociation of the F_4ND which allowed distinction between these sites. As a consequence, an electrode was perturbed allowing identification of sites through an electrochemical detection system.

5.1.5 1,8-Naphthalimide Ferrocene Complexes

Multi-state fluorimetric logic gates with redox-active ferrocene groups have been developed and offer dual mode chemical and electrochromic contrast agents.[32,33] For example, Magri *et al*., utilised naphthalimide based ferrocene complexes as logic gates

that combine acid-base and redox equilibria allowing simultaneous monitoring of redox potential and the pH of a system (Figure 5.6).[34] These derivatives were found to emit fluorescence upon oxidation of the ferrocene unit and protonation of the tertiary amine to an almost 13-fold enhancement. These compounds exhibited a reasonable sensitivity between pH 5.5 and pH 7.5, and demonstrated a highly favourable driving force of -1.59eV during PeT from ferrocene to the excited state fluorophore.

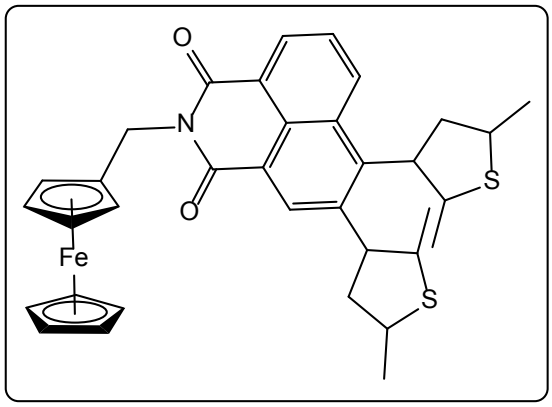

Figure 5.6: Compound by Magri et al.[34]

5.2 Aims

As discussed above, 1,8-naphthalimides intercalate selectively with DNA double helices and exhibit fluorescence, both attributes that facilitate the detection of CDF by eliminating the need for a covalently labelled analyte, thus making them suitable for this application. In addition to an intercalating fluorophore, the technique requires a redox-active element to introduce electrochemical functionality to the probe. Ferrocene is a suitable derivative due to the facile redox properties of the ferrocene/ferrocenium couple. The aim of this work, therefore, was to create a synthetic protocol for a luminescent, water soluble, 1,8-naphthalimide derivative coupled to a ferrocene moiety, in turn developing a fluorescent biosensor with an additional redox element.

Once synthesised, spectroscopic and analytical characterisation would be carried out to provide data indicating the synthesis of the novel compounds, where ^{1}H NMR spectroscopy is of particular significance to confirm the structural integrity of both the naphthalimide and ferrocene units. Study of the electrochemical and photophysical properties is also imperative due to the potential electrochemical application. In addition, preliminary fluorescence microscopy investigations have been carried out.

5.3 Results and Discussion

5.3.1 Synthetic Protocol Investigations

The general hypothesis required a covalently linked ferrocene unit with a naphthalimide. A variety of experimental procedures were attempted before a viable protocol synthesised the desired target compounds. Presentations of the considerations of these abandoned synthetic routes provides context and a rationale for the final route that was devised.

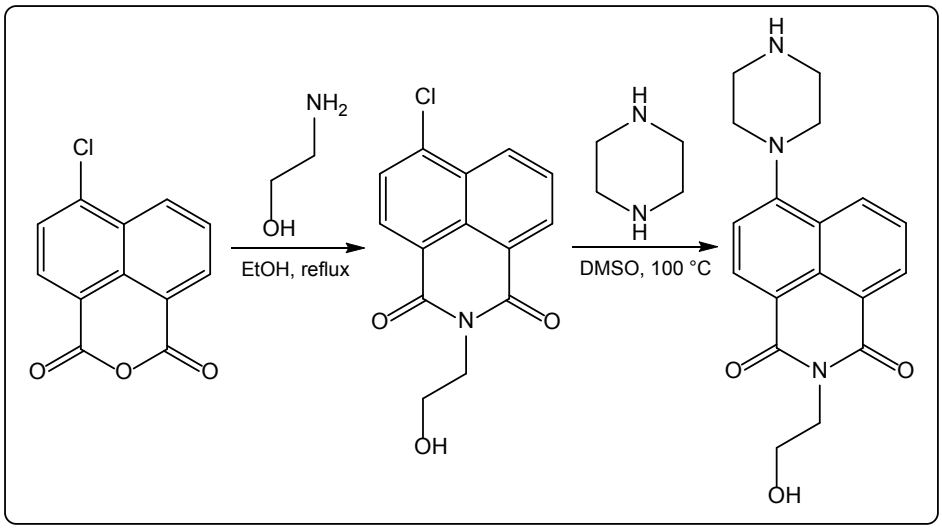

Scheme 5.1: Synthesis of a 4-substituted-1,8-naphthalimide

The first step in Scheme 5.1 followed adapted standard methodologies[35] from commercially available 4-chloro-1,8-naphthalic anhydride, where a yield of 30% was obtained. The second step also followed literature examples, and involved the addition

of piperidine at the 4-position of the 1,8-naphthalimide via a S_NAr mechanism.[36] A yield of 42% was obtained.

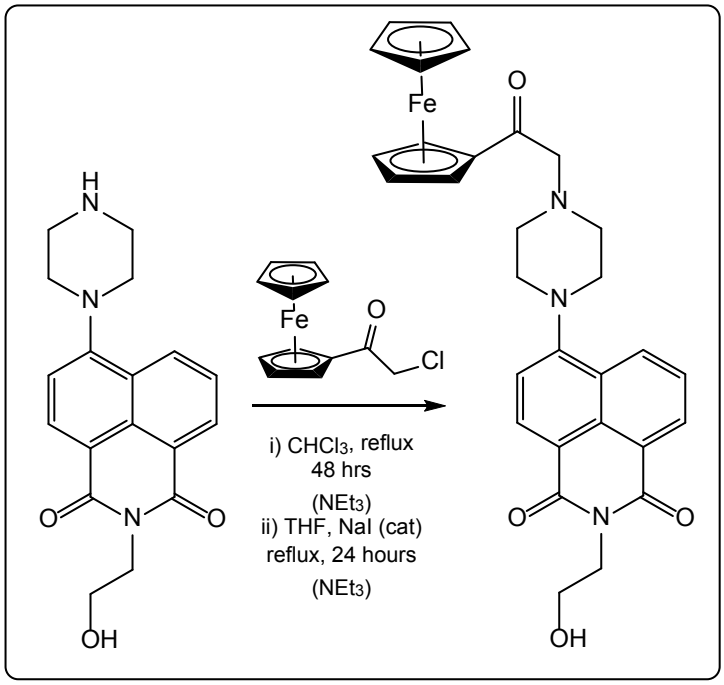

Scheme 5.2: Reaction of a 1,8-naphthalimide with 2-chloroferrocenyl ethanone

A S_N2 reaction was attempted in two ways with the product of Scheme 5.1 and 2-chloroferrocenyl ethanone (synthesised by Dr. Samuel Adams[37]), described in Scheme 5.2. Initially, this was carried out in chloroform using triethylamine (NEt_3) to deprotonate the ammonium cation intermediate resulting in a crude, brown oil. This was determined to be a mixture of starting materials through ^1H NMR spectroscopic analysis. The reaction was repeated using THF as the solvent, along with the addition of a catalytic amount of sodium iodide (NaI), as iodide is a better leaving group than chloride.[38] However, the brown oil produced was found to be only starting material through TLC and ^1H NMR spectroscopy.

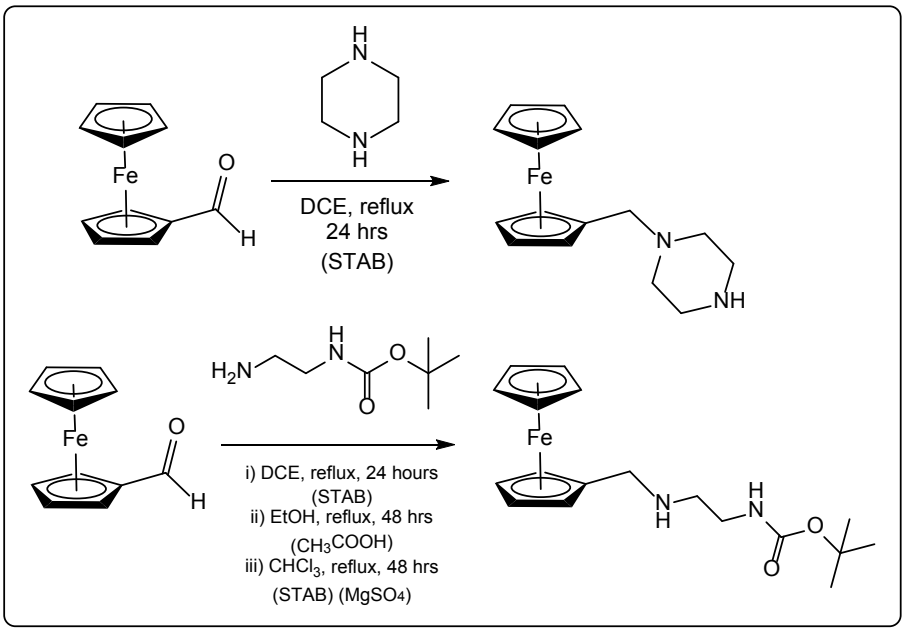

Scheme 5.3: Reactions with ferrocene carboxaldehyde

Following this, a more reactive alternative to 2-chloroferrocenyl ethanone was sought. Ferrocene carboxaldehyde was used as an alternative reagent, as shown in Scheme 5.3. Rather than adding the ferrocene unit in the final step, the synthesis was altered to build from the ferrocene starting material and adding the naphthalimide in subsequent steps.

Firstly, ferrocene carboxaldehyde was reacted with piperazine using a one-pot reductive amination approach. DCE was used as a solvent and 1.5 equivalents of sodium triacetoxyborohydride (STAB) were added after 2 hours. STAB acts as the reducing agent to reduce the imine intermediate, leading to the amine product.[39] This reaction was also unsuccessful and no product formation was observed.

The amine was changed from piperazine to mono-BOC-protected ethylene diamine in an attempt to eliminate the possibility that the reductive amination was ineffective because of the steric hindrance associated with piperazine. Three different reactions were attempted with varying conditions, described in Scheme 5.3. Firstly, analogous reaction conditions to those used with piperazine were attempted;[39] this was unsuccessful. Alternative conditions were attempted in ethanol with the addition of a catalytic amount of glacial acetic acid.[40] It was thought that the acetic acid would act as a catalyst by protonating the carbonyl oxygen, thus increasing the electrophilicity of the carbonyl carbon.[41] Once again this led to only starting material. In addition, the reaction

was carried out in chloroform with STAB as the reducing agent. After 3 hours at reflux under N_2, magnesium sulphate was added as a drying agent as water is formed as a by-product of a reductive amination reaction. Again, starting materials were observed following the reaction attempt.

A further attempt using an adaptation of research by Richards *et al.* was carried out.[42] This involved the use of Dean-Stark apparatus along with molecular sieves; both designed to collect and remove water from the reaction medium. A proof of concept reaction using benzylamine was conducted using the exact reaction conditions depicted in the literature, as shown in Scheme 5.4.

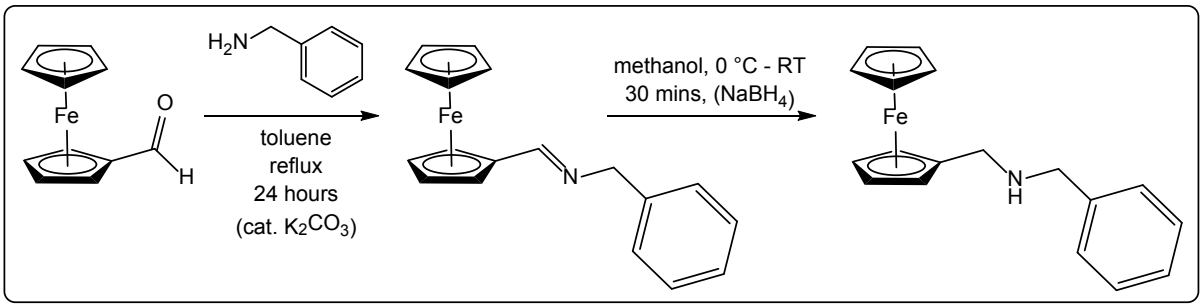

Scheme 5.4: Reaction using Dean-Stark apparatus

This reaction was successful, producing results that are comparable to the aforementioned literature.[42] Identical reaction conditions were thus applied to an amino 1,8-naphthalimide derivative shown in Scheme 5.5. TLC analysis suggested that the imine formation was successful but no product was isolated following the reduction step.

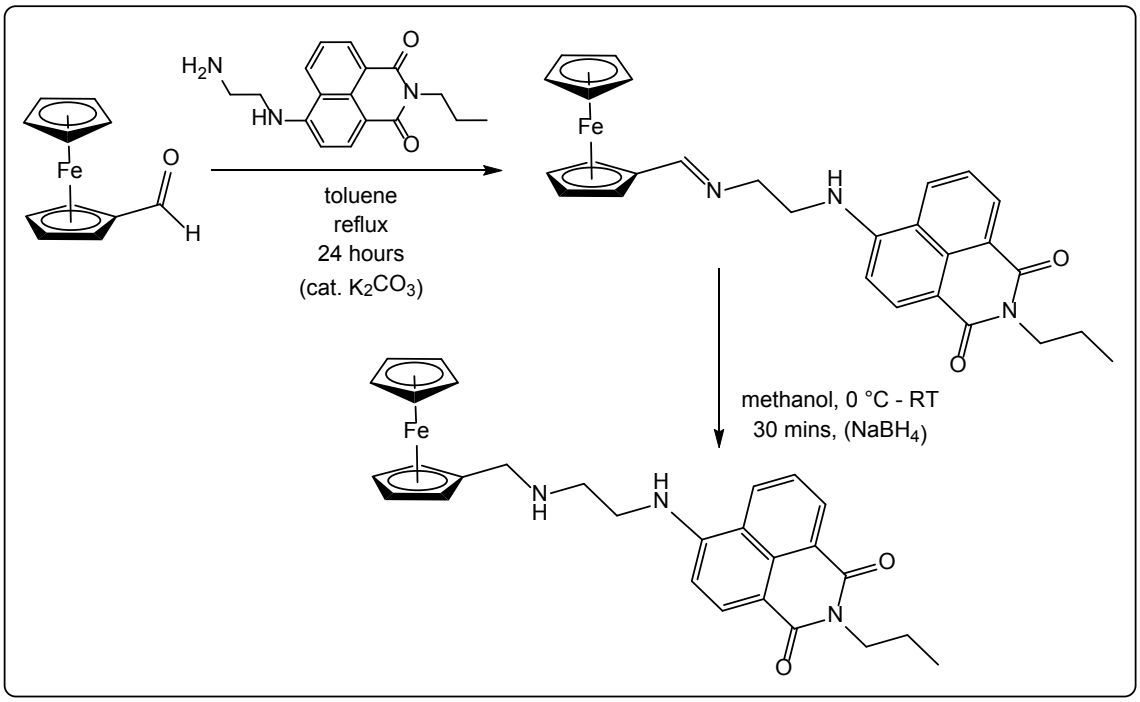

Scheme 5.5: Further reaction using Dean-Stark apparatus

5.3.2 Final Experimental Procedure

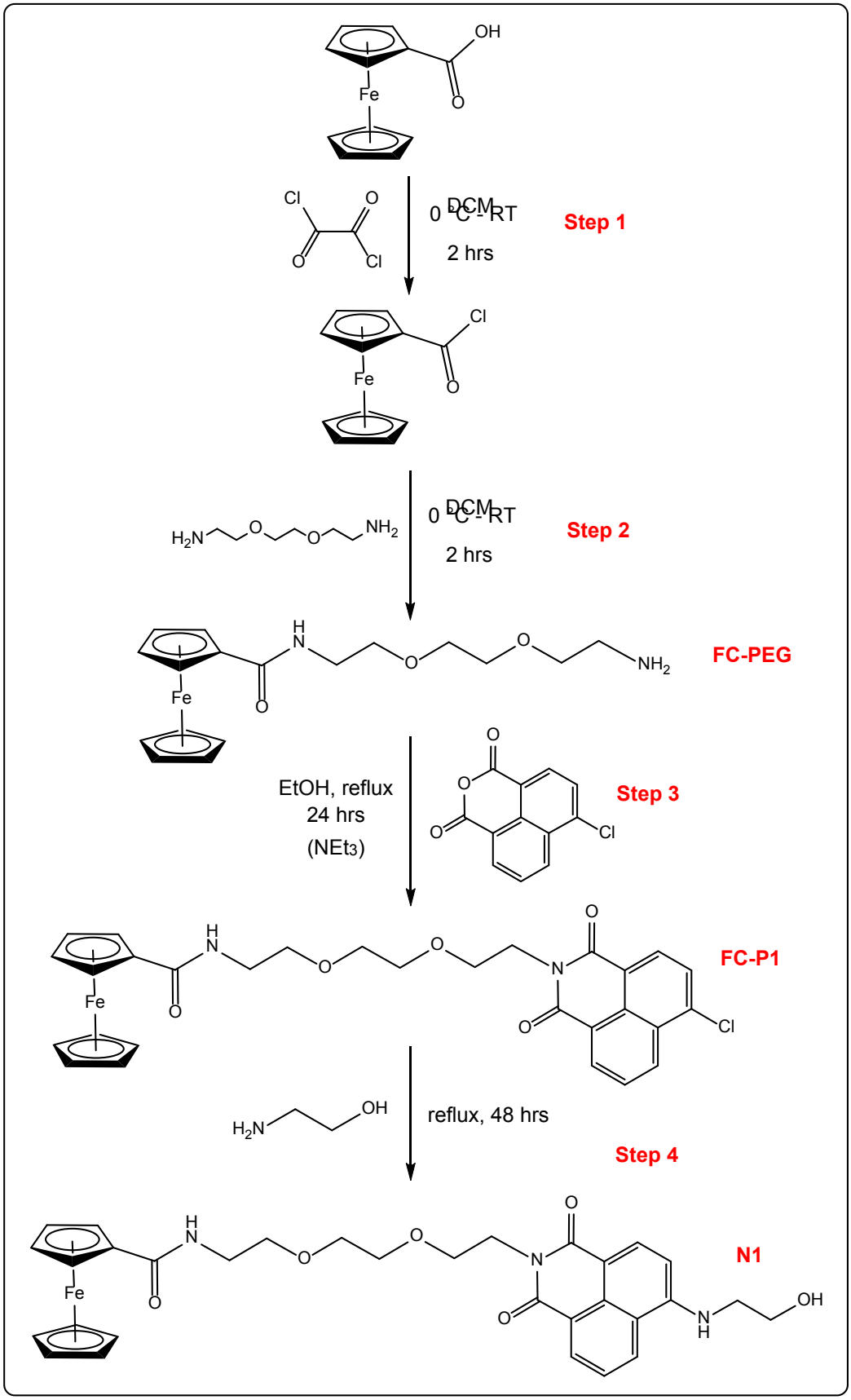

Scheme 5.6: Final experimental protocol for N1

Ferrocene carboxylic acid was then used as an alternative starting material. Step 1 of Scheme 5.6 involves the carboxylic acid moiety undergoing a nucleophilic substitution reaction with oxalyl chloride,[43] thus replacing the –OH group with a –Cl group to form a more reactive acyl chloride.[38] In Step 2 the acid chloride reacted with 2,2[I]-(ethylenedioxy)bisethylamine[43] to form an amide bond. The mechanism of this reaction is shown in Figure 5.7. This step produced FC-PEG with a yield of 84%.

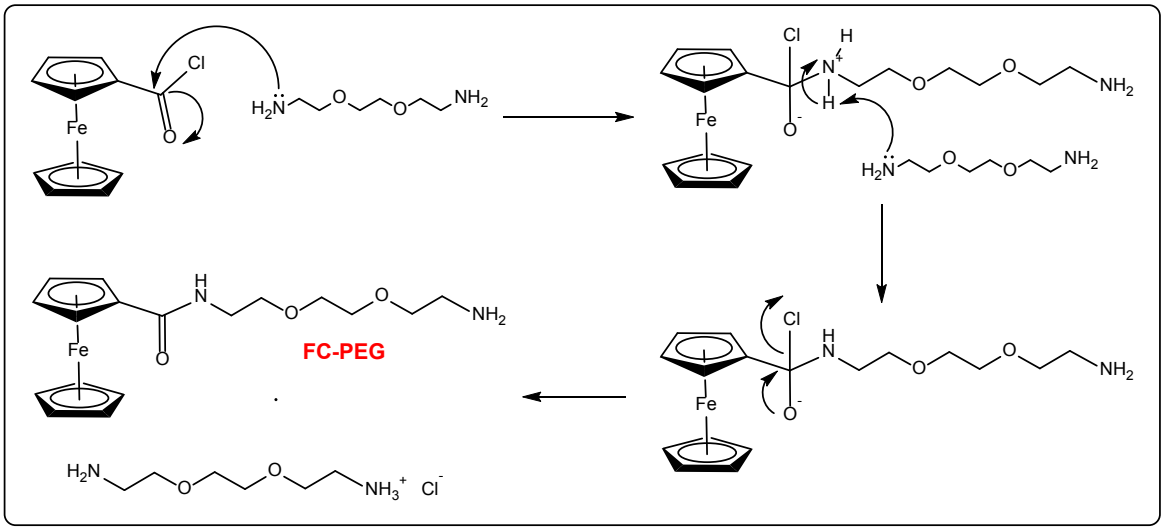

Figure 5.7: Mechanism of reaction between ferrocene acid chloride and 2,2-(ethylenedioxy)bisethylamine

FC-PEG was then reacted with 4-chloro-1,8-naphthalic anhydride in Step 3 using analogous conditions to above,[35] where an excess of triethylamine was used as a base. This condensation reaction at the imide position on the naphthalic anhydride produces FC-P1, with a yield of 92%. Further functionalization with ethanolamine at the 4-position of the naphthalimide was successful (Step 4 – Scheme 5.6), and aimed to introduce intramolecular charge transfer (ICT) and water solubility to N1. This step was initially carried out using DMSO and had a yield of 21%.

Due to the water-soluble nature of N1, the typical DMSO aqueous work-up used in Step 4 led to the low yield mentioned above. For this reason, ethanolamine was employed as both the nucleophile and the solvent in this reaction, thus eliminating the difficult extraction from DMSO. This resulted in an improved yield for N1 of 55%.

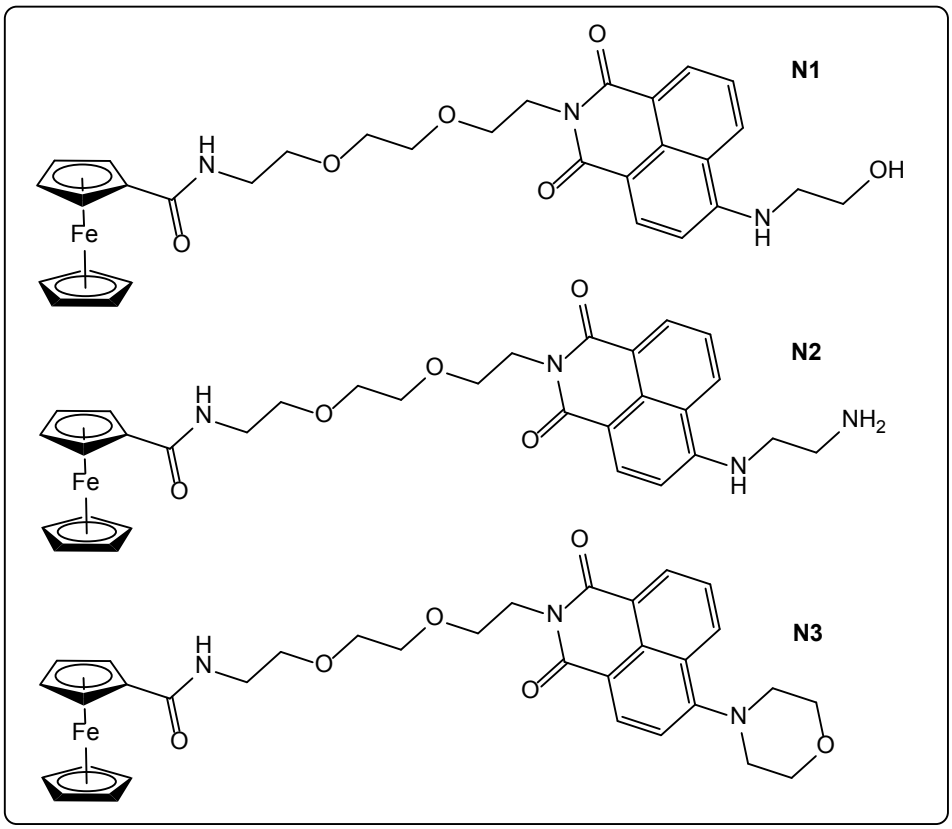

Figure 5.8: Structures of final compounds isolated in this chapter: N1-N3

For N2 and N3, the synthetic procedure was common for Steps 1-3. However, for N2, 2-methoxyethanol was used to replace DMSO in Step 4. This is because ethylenediamine shows higher levels of acute toxicity when compared to ethanolamine, hence it should be used in as smaller quantity as possible. For N3, the final step of the reaction was carried out in DMSO due to the decreased water solubility of the final product.

5.3.3 Spectroscopic Characterisation

FC-P1 and N1-N3 were fully characterised using ^{1}H NMR, ^{13}C NMR, UV-Vis, IR and HRMS. ^{1}H NMR spectroscopy was obtained due to all of the compounds' high solubility in chloroform, obtaining well resolved spectra with the expected peak multiplicities. The ^{1}H NMR of FC-PEG was comparable to that seen in the literature.[43]

^{1}H NMR was informative when confirming the formation of FC-P1 (Figure 5.9). The peaks residing in the aromatic region, between 8.6 - 7.7 ppm are characteristic of the five

protons associated with the 1,8-naphthalimide moiety, as shown in Figure 5.9. Three distinctive singlets present between 4.2 – 4.0 ppm corresponding to the ferrocene group and integrate as 2:2:5 protons. Since the naphthalimide and ferrocene environments are in a 1:1 ratio to one another, product formation is suggested. In addition, the broad triplet at 6.4 ppm is characteristic of a naphthalimide N-*H* resonance following formation of the amide bond (Figure 5.9).

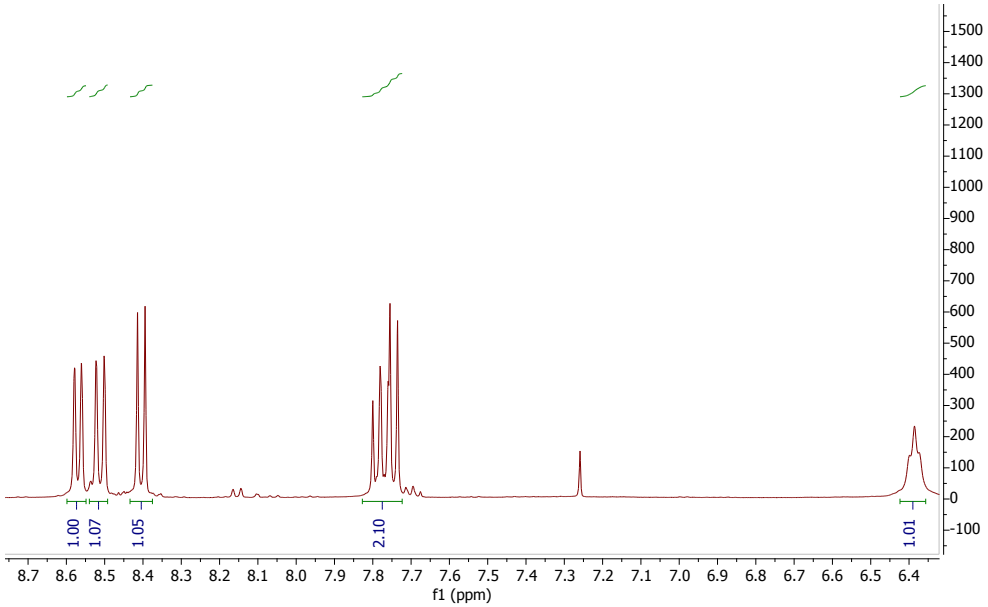

Figure 5.9: ^{1}H NMR spectrum of aromatic region of FC-P1

Comparison of the ^{1}H NMR spectra for FC-P1 and N1 confirmed the substitution of chloride for ethanolamine at the 4-position. The aromatic peaks present for FC-P1 have shifted and the multiplet present at 7.77 ppm has separated due to the shielding effects of the amine compared to the chloride. This has the most significant effect on the proton in the β-position to the amine, which has been shifted to 6.6 ppm, as shown in Figure 5.10. There is also an additional N-H resonance at 5.9 ppm that integrates to one proton, thus confirming that ethanolamine is present at the 4-position. There are also additional peaks in the aliphatic region at 4.03 and 3.27 ppm which correspond to ethanolamine. All of the changes in spectra mentioned above indicate the successful formation of N1. Similar trends in the ^{1}H NMR spectra were observed for the formation of N2 and N3.

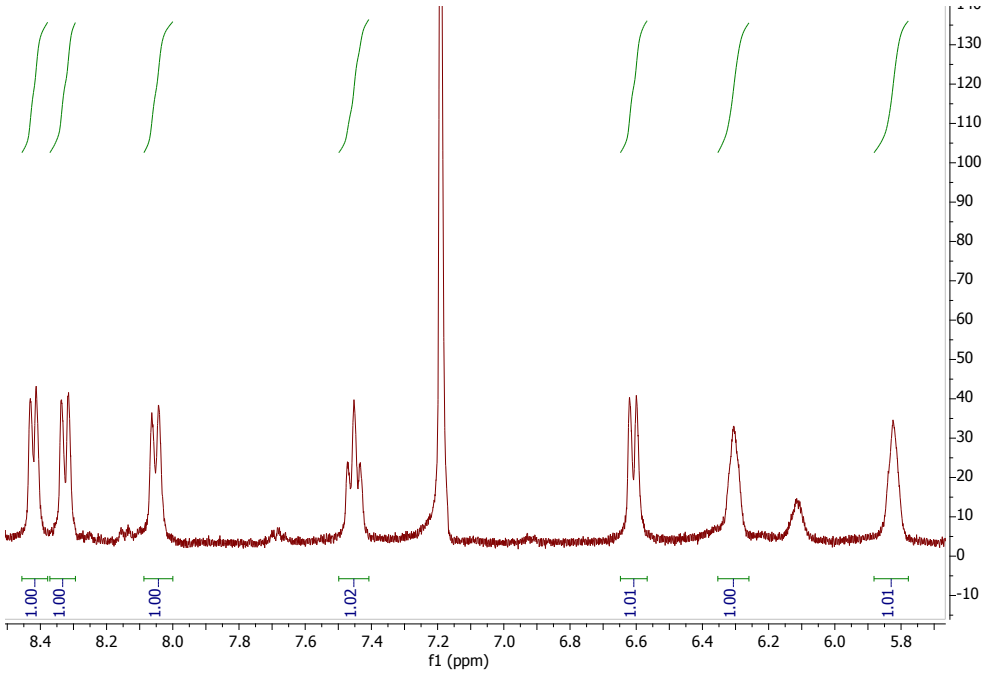

Figure 5.10: ^{1}H NMR spectrum of the aromatic region of N1

In all cases N1-N3, the proposed molecular formula for the target compounds was supported by HRMS (ES^{+}), each showing the expected $[M+H]^{+}$ peak. IR spectroscopy further illustrated the formation of N1-N3. Comparison of the IR spectra of FC-P1 and N1 (Figure 5.11) illustrates product formation due to the new broad O-H stretch at 3345 cm^{-1} assigned to the terminal alcohol on ethanolamine.

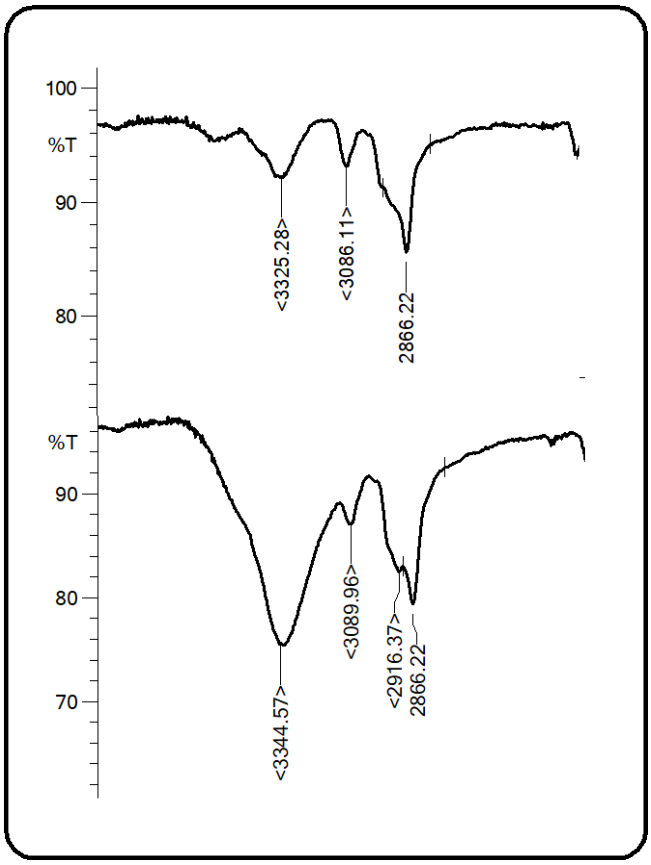

Figure 5.11: IR spectra of FC-P1 (top) and N1 (bottom)

5.3.4 Photophysical Properties

The photophysical properties of N1-N3 were investigated *via* UV-vis., steady state luminescence, luminescence lifetimes and quantum yields, and were measured in aerated solutions of acetonitrile in all cases. A summary of the photophysical properties are shown in Table 5.1.

Compound	λ_{max} / nm[a]	λ_{em} / nm	τ_{obs} / ns[b]	ϕ [c]
FC-P1	353	-	-	-
N1	430	524	9.7	13.9
N2	433	521	8.3	11.0
N3	395	524	3.9	8.0

Table 5.1: Absorption and emission data for the FC-P1 and N1-N3: [a] measurements obtained in MeCN solutions; [b] using λ_{ex}= 295 nm.; [c] for quantum yield measurements using $[Ru(bpy)_3](PF_6)_2$ as reference of 0.016 in aerated MeCN

The absorption profiles of FC-P1 and N1-N3 are displayed in Figure 5.12. In the case of FC-P1, the absorption spectra is dominated by $\pi \rightarrow \pi^*$ absorbances associated with the naphthalimide unit. The two intense bands between 200-250 nm correlate to high energy transitions, and the weaker, vibronically structured absorption at 300-360 nm are additional $\pi \rightarrow \pi^*$ transitions. When compared to N1-N3, the $\pi \rightarrow \pi^*$ absorbances are hypsochromically shifted to appear between 200 and 300 nm. Upon substitution at the 4-position of the naphthalimide, in N1-N3, intramolecular charge transfer (ICT) gives rise to an additional absorption 395-430 nm, as seen with other related systems.[44] Of the three systems, N3 has the ICT band ar highest energy due to the presence of a morpholine derivative. It is also worth noting that the absorption profile of ferrocene contains peaks at ca 320 and 430 nm. However due to extremely low molar extinction coefficients they are not visible in this case.[45,46]

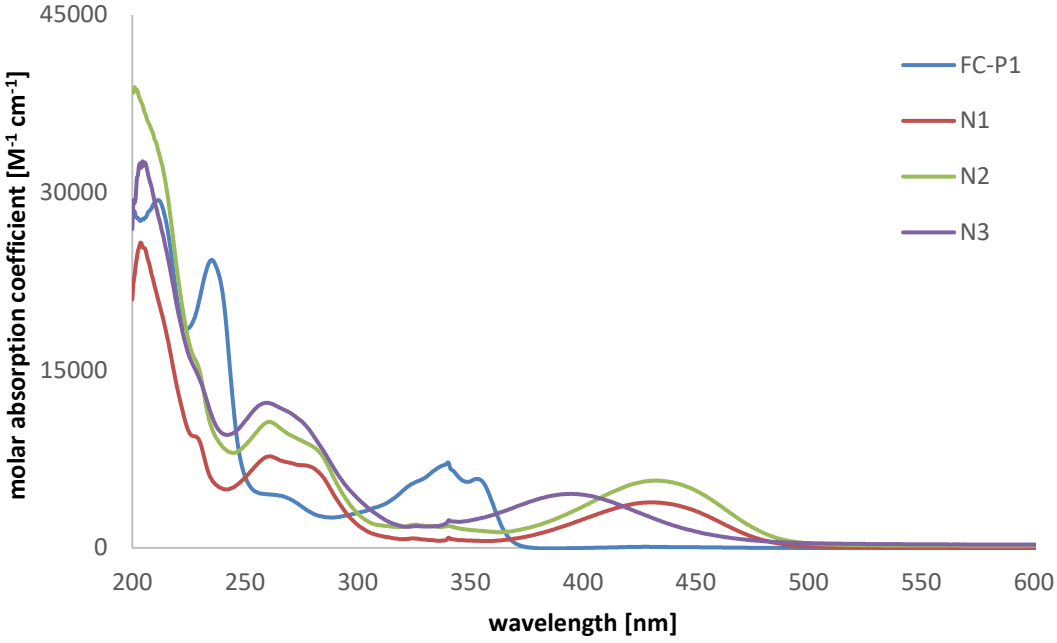

Figure 5.12: Absorption profiles of FC-P1 and N1-N3

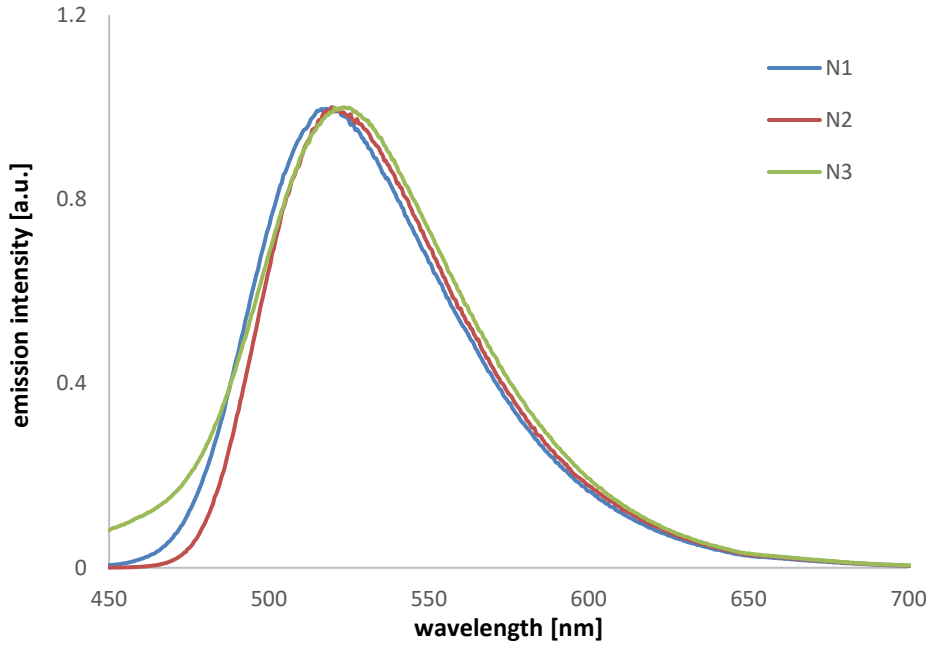

Figure 5.13: Emission profiles of N1-N3

Each of the compounds, N1-N3, was shown to be fluorescent in solution, with emission wavelengths between 520-525, indicating that the nature of the group at the 4-position has little effect on the emission wavelength (Figure 5.13). The data are very typical of previously reported naphthalimide fluorophores.[47] Time-resolved measurements (λ_{ex} = 295 nm) revealed lifetimes that were consistent with fluorescence emission from the ICT excited state in all cases (Table 5.1). Quantum yields range from 8-14%. For N3, a shorter lifetime and lower quantum yield are observed, suggesting that efficiency of the emission of the compound is not as significant. This may be due to the presence of a morpholine moiety at the 4-position and its differing electronic properties. Overall, the photophysical data from this series of ferrocene coupled naphthalimides demonstrated that the presence of the ferrocene moiety did not appear to quench the luminescent properties that are commonly associated with the naphthalmide unit.

5.3.5 Bioimaging Studies

Confocal fluorescence microscopy was performed using MCF7 cells. MCF-7 cells were grown on circular glass coverslips for 5-7 days in RPMI-1640 medium, supplemented

with 5% foetal calf serum (heat inactivated) and 100 U/ml penicillin/streptomycin solution, until around 70-90% confluent. For experiments, culture medium was replaced with 1 ml fresh RPMI-1640 and cells were incubated with 100 ug/ml of compound N1. This compound was incubated with the cells for 30 minutes at 37 °C, then washed in warmed PBS before imaging using an excitation wavelength of 405 nm.

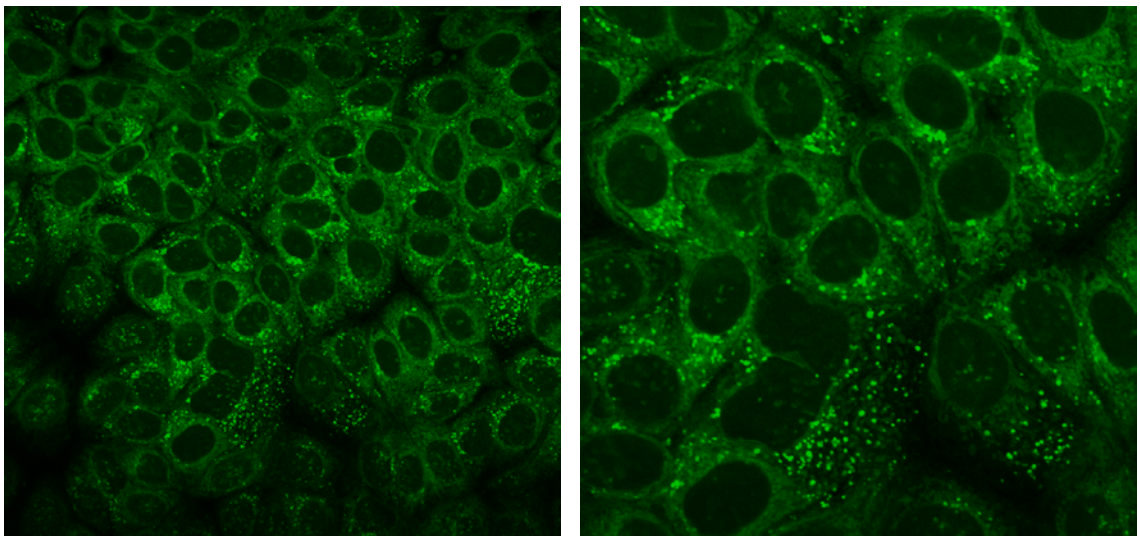

Figure 5.14: CFM images of N1 with MCF-7 cells

This preliminary study found that uptake into the cells was very fast and very bright images were obtained (Figure 5.14). These studies therefore provide clear evidence of the biocompatibility of N1 towards cell imaging using confocal fluorescence microscopy. Further studies are required to investigate the precise localisation and cytotoxicity of N1.

5.3.6 Electrochemical Properties

Complex	*Component*	E_{ox} / V	E_{red} / V
N1	Ferrocene	+0.60	+0.55
	Naphthalimide	+1.19	-
N2	Ferrocene	+0.47	+0.37
	Naphthalimide	+1.16	-
N3	Ferrocene	+0.59	+0.51
	Naphthalimide	+1.26	-1.39

Table 5.2: Electrochemical data for N1-N3

The electrochemical characteristics of N1-3 were studied in deoxygenated DCM (Table 5.2). The cyclic voltammograms were measured using a platinum disc electrode; scan rate υ = 200 mV s^{-1}, 1 x 10^{-3} M solutions, 0.1 M [NBu_4][PF_6] as a supporting electrode calibrated with Fc/Fc^+ at +0.47 V. N1-N3 all demonstrated fully reversible one-electron oxidation at +0.47-0.60 V ascribed to the ferrocene/ferrocenium couple, this showed a reversible reduction wave at +0.37-0.55V attributed to the reformation of the ferrocene unit. For N1 and N3 the anodic and cathodic wave of the ferrocene unit is shifted to a higher potential than the reference ferrocene, suggesting that these compounds are harder to oxidise than ferrocene.[48] For N2, the waves associated with ferrocene in N2 is superimposed with that of the reference ferrocene. This may be due to the ferrocene derivative on N2 being more electron deficient due to the electron withdrawing ability of the amide attached to the ferrocene group. The additional anodic wave residing between +1.16-1.26 V is thought to correspond with the oxidisation of 1,8-naphthalimide present in N1-N3. This peak has no mirroring cathodic wave, implying this is an irreversible process. For N1 and N2, there are no anodic or cathodic waves present at a negative potential, suggesting neither the ferrocene nor the naphthalimide unit are reducible within the voltage range explored. This is not the case for N3, where a reductive wave is observed at -1.39 V and attributed to a naphthalimide localised process.

Consequently, N1-N3 have illustrated distinguishable electrochemical properties suggesting it would be able to perturb a gold electrode signal as desired in the aim of this chapter. N1 has been sent to our collaborators Prof. Martin Cryan and Dr. Pedro Estrela at the Universities of Bristol and Bath, respectively, for further investigations into its suitability for electrochemical detection of CDF.

5.4 Conclusions

This chapter has described the determination of a successful synthetic route to, and spectroscopic analysis of, a series of fluorescent biosensors that incorporate both a redox active ferrocene unit and a naphthalimide moiety. Three novel target compounds were generated, N1-N3, as well as a novel precursor, FC-P1.

The effective synthetic protocol was as follows: ferrocene carboxylic acid reacted with oxalyl chloride in a nucleophilic substitution reaction; the resultant acid chloride reacted with 2,2'-(ethylenedioxy)bisethylamine to form an amide bond (FC-PEG); FC-PEG was reacted with 4-chloro-1,8-naphthalic anhydride to form a naphthalimide (FC-P1); FC-P1 was reacted with an amine (ethanolamine, ethylenediamine or morpholine) in a nucleophilic aromatic substitution reaction to form N1-N3. This approach proved to be a superior route over a number of alternatives, including the use of a 4-subsituted-1,8-naphthalimide, 2-chloroferrocenyl ethenone, as well as ferrocene carboxaldehyde, that did not yield the desired targets.

The resultant ^{1}H NMR spectra of each of the target compounds showed the correct number of peaks with anticipated multiplicities, including N-H resonances in the cases of N1 and N2. Retention of both the ferrocene and naphthalimide units during the final step of the synthetic protocol were confirmed in each case. The dyad compounds show their luminescent behaviour with naphthalimide-based emission attributed to the ICT character observed between 520-525 nm. The electrochemical properties of N1-N3 were also investigated and showed a fully reversible one-electron oxidation attributed to the ferrocene unit (E_{ox} = +0.47-0.60 V), in addition to an irreversible oxidation of the 1,8-naphthalimide moiety (E_{ox} = +1.16-1.26 V).

Future work will involve collaborating with Prof. Martin Cryan (University of Bristol) and Dr. Pedro Estrela (University of Bath) to investigate the viability of N1-3 for an electrochemical detection method for CDF. In addition, further bioimaging studies will be carried out to establish the organelle localisation of the compounds, as studied with related structures in Chapters 2 and 3.

5.5 Experimental

5.5.1 General Experimental Considerations

All reagents and solvents were commercially available and were used without further purification if not stated otherwise. For the measurement of ^{1}H and ^{13}C NMR spectra a Bruker Fourier^{300} (300 MHz), Bruker AVANCE HD III equipped with a BFFO SmartProbe^{TM} (400 MHz) or Bruker AVANCE III HD with BBO Prodigy CryoProbe (500 MHz) was used. The obtained chemical shifts δ are reported in ppm and are referenced to the residual solvent signal. Spin-spin coupling constants *J* are given in Hz.

Low-resolution mass spectra were obtained by the staff at Cardiff University. High-resolution mass spectra were carried out at the EPSRC National Mass Spectrometry Facility at Swansea University. High resolution mass spectral (HRMS) data were obtained on a Waters MALDI-TOF mx at Cardiff University or on a Thermo Scientific LTQ Orbitrap XL by the EPSRC UK National Mass Spectrometry Facility at Swansea University. IR spectra were obtained from a Shimadzu IR-Affinity-1S FTIR. UV-Vis studies were performed on a Shimadzu UV-1800 spectrophotometer as MeCN solutions (2.5 or 5 × 10^{-5} M) or $CHCl_3$ solutions (2.5 or 5 × 10^{-5} M). Photophysical data were obtained on a JobinYvon–Horiba Fluorolog spectrometer fitted with a JY TBX picosecond photodetection module as MeCN/$CHCl_3$ solutions. Emission spectra were uncorrected. The pulsed source was a Nano-LED configured for 459 nm output operating at 1 MHz. Luminescence lifetime profiles were obtained using the JobinYvon–Horiba FluoroHub single photon counting module and the data fits yielded the lifetime values using the provided DAS6 deconvolution software. Quantum yield measurements were obtained on aerated MeCN solutions of the complexes using $[Ru(bpy)_3](PF_6)_2$ in aerated MeCN as a standard (Φ = 0.016).[49]

5.5.2 Synthesis

Synthesis of FC-PEG

Ferrocenecarboxylic acid (1 g, 1 eq, 4.36 mmol) was dissolved in anhydrous DCM (50 mL) and oxalyl chloride (0.896 mL, 2.4 eq, 10.46 mmol) was added at 0°C. The mixture was allowed to warm to room temperature and left to stir for 2 hours under nitrogen. The solvent was removed *in vacuo* to give a crude brown solid; this was redissolved into anhydrous DCM (25 mL) and added dropwise at 0°C to a solution of 2,2[I]-(ethylenedioxy)bisethylamine (6.36 mL, 10 eq, 43.6 mmol) in anhydrous DCM (2 x 20 mL) over 10 minutes. The resulting solution was warmed to room temperature and left to stir under nitrogen for 2 hours. The reaction was quenched with $NaHCO_3$ (25 mL), extracted into DCM (30 mL) and washed with water (2 x 30 mL) and brine (30 mL). The solution was dried over magnesium sulphate and the solvent removed *in vacuo* to give FC-PEG as a brown solid (1.31 g, 84%). ^{1}H NMR (400 MHz, Chloroform-*d*) δ 6.32 (br. s, N-H, 1H), 4.69 (t, $^3J_{HH}$ = 4.0, 2H), 4.33 (t, 4.0, 2H), 4.20 (s, 5H), 3.65 (dd, $^3J_{HH}$ = 9.8, 3.2 Hz, 6H), 3.63 – 3.56 (m, 2H), 3.53 (t, $^3J_{HH}$ = 5.2 Hz, 2H), 2.89 (t, $^3J_{HH}$ = 5.2 Hz, 2H).

Synthesis of FC-P1

FC-PEG (1.31 g, 2 eq, 3.64 mmol) was dissolved in EtOH (50 mL) and 4-chloro-1,8-naphthalic anhydride (423 mg, 1 eq, 1.82 mmol) with triethylamine (1.79 mL, 7 eq, 12.74 mmol) was added. The solution was heated at reflux under nitrogen overnight. The solution was left to cool and the EtOH was removed *in vacuo*. The crude solid was redissolved into DCM, (40 mL) washed with H_2O (2 x 40 mL), washed with brine (2 x 40 mL) and dried over magnesium sulphate. The solvent was removed *in vacuo,* to give FC-P1 as a brown solid (961 mg, 92 %). ^{1}H NMR (400 MHz, $CDCl_3$) δ 8.57 (d, $^3J_{HH}$ = 7.1 Hz, 1H), 8.51 (d, $^3J_{HH}$ = 8.4 Hz, 1H), 8.40 (d, $^3J_{HH}$ = 7.9 Hz, 1H), 7.77 (dd, $^3J_{HH}$ = 18.1, 7.7 Hz, 2H), 6.39 (br. S, N-H, 1H), 4.65 (s, 2H), 4.41 (t, $^3J_{HH}$ = 5.9 Hz, 2H), 4.23 (s, 2H), 4.17 (s, 2H), 4.10 (s, 5H), 3.84 (t, $^3J_{HH}$ = 5.9 Hz, 2H), 3.60 (d, $^3J_{HH}$ = 4.8 Hz, 2H), 3.54 (d, $^3J_{HH}$ = 4.9 Hz, 2H), 3.46 (d, $^3J_{HH}$ = 4.9 Hz, 2H). ^{13}C NMR (400 MHz, $CDCl_3$) δ 170.2, 163.6, 163.4, 139.0, 131.9, 131.0, 130.6, 129.1, 128.9, 127.8, 127.3, 122.8, 121.3, 76.1, 70.4, 70.3, 70.2, 70.0, 69.8, 69.7, 69.7, 69.6, 68.2, 68.1, 67.9, 53.5, 39.2, 39.1, 30.9. HRMS found *m/z* 573.1108, calculated *m/z* 573.1083 for $[C_{29}H_{27}ClFeN_2O_5]^+$. UV-Vis (MeCN): λ_{max} {ε/dm^3 mol^{-1} cm^{-1}}:

353 {5260}, 340 {6660}, 265 (s) {3860}, 235 {23740}, 211.5 {28800}. IR (solid. V_{max})/cm^{-1}: 3325, 3086, 2866, 2237, 1701, 1659, 1634, 1589, 1574, 1531, 1404, 1371, 1342, 1296, 1234, 1188, 1105, 1051, 1001, 910, 820, 779, 750, 725, 667, 646, 567, 482, 417, 403.

Synthesis of N1

FC-P1 (306.6 mg, 1 eq, 0.534 mmol) was dissolved in ethanolamine (3 mL) and heated at reflux under nitrogen overnight. The solution was allowed to cool and extracted into DCM (2 x 20 mL), washed with water (2 x 20 mL), dried over magnesium sulphate, and the solvent removed *in vacuo* to give N1 as a brown oil. (177 mg, 55%). ^{1}H NMR (500 MHz, $CDCl_3$) δ 8.47 (d, $^{3}J_{HH}$ = 7.2 Hz, 1H), 8.38 (d, $^{3}J_{HH}$ = 8.4 Hz, 1H), 8.12 (d, $^{3}J_{HH}$ = 8.2 Hz, 1H), 7.50 (t, $^{3}J_{HH}$ = 7.8 Hz, 1H), 6.66 (d, $^{3}J_{HH}$ = 8.4 Hz, 1H), 6.42 (br. s, N-H, 1H), 5.95 (br. s, N-H, 1H), 4.66 (d, $^{3}J_{HH}$ = 7.3 Hz, 2H), 4.46 (t, $^{3}J_{HH}$ = 5.8 Hz, 2H), 4.26 (s, 2H), 4.20 (s, 2H), 4.13 (s, 5H), 3.89 (t, $^{3}J_{HH}$ = 5.8 Hz, 2H), 3.67 – 3.53 (m, 6H), 3.50 – 3.44 (m, 2H), 3.27 (q, $^{3}J_{HH}$ = 5.2 Hz, 2H). ^{13}C NMR (400 MHz $CDCl_3$) δ 169.6, 163.8, 163.2, 148.9, 133.5, 130.1, 128.7, 125.6, 123.5, 121.6, 119.4, 108.9, 103.4, 74.8, 69.5, 69.3, 69.2, 69.0, 68.8, 68.7, 67.2, 67.1, 59.1, 52.4, 44.7, 39.9, 38.2, 37.9, 29.9. HRMS found *m/z* 600.1777, calculated *m/z* 600.1752 for $[C_{31}H_{34}FeN_3O_6]^+$. UV-Vis (MeCN): λ_{max} {ε/dm^3 mol^{-1} cm^{-1}} 430.5 {3840}, 340.5 {860}, 324.5 {800}, 277.5 (s) {6940}, 261 {7720}, 227 (s) {9440}, 204 {25740}. IR (solid. V_{max})/cm^{-1}: 3345, 3090, 2916, 2866, 2234, 1682, 1634, 1576, 1541, 1452, 1425, 1366, 1341, 1296, 1246, 1190, 1105, 1055, 1022, 953, 910, 820, 772, 756, 727, 664, 644, 581, 482, 411.

Synthesis of N2

FC-P1 (347 mg, 0.60 mmol) and ethylenediamine (0.16 ml, 2.4 mmol) were dissolved in 2-methoxyethanol (7 ml) and heated at reflux under nitrogen overnight. The resulting solution was cooled and the solvent removed in *vacuo*. The crude solid was then dissolved in DCM (15 ml) and washed with water (2 x 15 ml). The organic layer was extracted and dried in *vacuo*. The crude solid was washed with hexane (15 ml) and dried in *vacuo* to yield N2 as an orange oil (221 mg, 61%). ^{1}H NMR (400 MHz, $CDCl_3$) δ 8.55 (d, *J* = 7.2 Hz, 1H), 8.43 (d, *J* = 8.4 Hz, 1H), 8.19 (d, *J* = 8.9 Hz, 1H), 7.60 (t, *J* = 7.8 Hz, 1H),

6.68 (d, *J* = 8.5 Hz, 1H), 6.63 (br. t, 1H, NH), 6.27 (br. t, 1H, NH), 4.73 (t, J = 1.9 Hz, 1H), 4.67 (t, J = 1.9 Hz, 1H), 4.46 (t, *J* = 6.0 Hz, 2H), 4.33 – 4.32 (m, 1H), 4.28 – 4.26 (m, 2H), 4.20 (s, 2H), 4.16 (s, 5H), 3.87 (t, *J* = 6.0 Hz, 2H), 3.74 – 3.70 (m, 2H), 3.65 – 3.53 (m, 6H), 3.17 (t, 1H). ^{13}C NMR (101 MHz, $CDCl_3$) δ 169.38, 163.83, 163.19, 148.93, 133.59, 130.15, 128.89, 125.62, 123.60, 121.80, 119.46, 108.84, 103.39, 69.44, 69.35, 69.28, 69.13, 68.95, 68.77, 68.73, 68.68, 67.22, 67.19, 67.17, 52.44, 43.96, 40.72, 39.12, 38.26, 37.83, 29.93. HRMS found *m/z* 599.1938, calculated *m/z* 599.1951 for $[C_{31}H_{35}FeN_4O_5]^+$. UV-Vis (MeCN): λ_{max} {ε/dm^3 mol^{-1} cm^{-1}}: 433 {5680}, 341 {1860}, 326 {1940}, 283 {8080}, 261 {10640}, 228 {16020}, 209 {35100}. IR (solid. V_{max})/cm^{-1}: 3509, 3331, 3094, 2963, 2920, 2868, 1676, 1632, 1576, 1539, 1449, 1425, 1364, 1342, 1296, 1188, 1096, 1059, 1037, 999, 818, 773, 756, 662, 579, 527, 482, 459, 413.

Synthesis of N3

FC-P1 (234 mg, 0.41 mmol) and morpholine (0.14 ml, 1.63 mmol) were dissolved in DMSO and heated at 100 °C under nitrogen for 48 hours. The solution was cooled, water was added, and the solution neutralised using 1M HCl. The resultant solution was extracted into DCM, washed with water and dried with $MgSO_4$. The solvent was removed in *vacuo* to yield N3 as a brown oil (92 mg, 37 %). ^{1}H NMR (400 MHz, $CDCl_3$) δ 8.51 (d, *J* = 7.3 Hz, 1H), 8.45 (d, *J* = 8.7 Hz, 1H), 8.35 (d, *J* = 8.6 Hz, 1H), 7.63 (t, 1H), 7.15 (d, *J* = 7.7 Hz, 1H), 6.38 (br. s, 1H, NH), 4.64 (br. t, 1H), 4.40 (t, J = 6.9 Hz, 2H), 4.21 (s, 2H), 4.14 (s, 1H), 4.08 (s, 5H), 3.98 – 3.93 (m, 4H), 3.81 (t, J = 4.9 Hz, 2H), 3.70 – 3.54 (m, 8H), 3.23 – 3.14 (m, 4H). ^{13}C NMR (101 MHz, $CDCl_3$) δ 169.42, 163.10, 154.77, 131.65, 130.32, 130.26, 130.19, 129.26, 128.96, 128.94, 125.11, 124.85, 124.79, 122.14, 121.08, 117.41, 115.91, 113.95, 75.08, 69.35, 69.28, 69.24, 68.90, 68.78, 68.66, 67.21, 67.08, 65.93, 52.40, 39.92, 38.22, 37.98, 28.67. HRMS found *m/z* 626.1947, calculated *m/z* 626.1948 for $[C_{33}H_{36}FeN_3O_6]^+$. UV-Vis (MeCN): λ_{max} {ε/dm^3 mol^{-1} cm^{-1}} 395 {2060}, 375 (s) {6980}, 341 {860}, 326 {780}, 260 {7680}, 205 {25400}. IR (solid. V_{max})/cm^{-1}: 2961, 2922, 2857, 1694, 1653, 1585, 1574, 1537, 1518, 1452, 1422, 1375, 1348, 1296, 1260, 1236, 1188, 103, 1086, 1043, 1016, 868, 785, 758, 700, 669, 658, 590, 536, 503, 480, 457, 401.

1 V. Svitková and J. Labuda, *Monatshefte für Chemie - Chem. Mon.*, 2017, **148**, 1569–1579.

2 K. J. Ryan and C. G. Ray, *Sherris Medical Microbiology*, McGraw Hill, New York., 4th edn., 2004.

3 W. K. Smits, D. Lyras, D. B. Lacy, M. H. Wilcox and E. J. Kuijper, *Nat. Rev. Dis. Prim.*, 2016, **2**, 16021.

4 L. Mulcahy, Deaths Involving Clostridium difficile, England and Wales: 2012 - Office for National Statistics, https://www.ons.gov.uk/peoplepopulationandcommunity/birthsdeathsandmarriages/deaths/bulletins/deathsinvolvingclostridiumdifficileenglandandwales/2013-08-22, (accessed 13 September 2017).

5 M. J. Crobach, O. M. Dekkers, M. H. Wilcox and E. J. Kuijper, *Clin. Microbiol. Infect.*, 2009, **15**, 1053–1066.

6 S. Banerjee, E. B. Veale, C. M. Phelan, S. A. Murphy, G. M. Tocci, L. J. Gillespie, D. O. Frimannsson, J. M. Kelly, T. Gunnlaugsson, J. Kluza, D. Hochhauser, J. A. Hartley, M. Lee, F. Darro, R. Kiss, R. J. Diamond, R. J. McRipley, R. J. Page and J. L. Gross, *Chem. Soc. Rev.*, 2013, **42**, 1601–1618.

7 R. Gupta, L. Jixiang, X. Guojian and J. W. Lown, *Anticancer Drug Discov.*, 1996, **11**, 581–596.

8 S. M. Sondhi, B. S. Praveen Reddy and J. W. Lown, *Curr. Med. Chem.*

9 D. S. Goodsell, H. L. Ng, M. L. Kopka, J. W. Lown and R. E. Dickerson, *Biochemistry*, 1995, **34**, 16654–16661.

10 L. V. Flores, A. M. Staples, H. Mackay , C. M. Howard, P. B. Uthe, J. S. Sexton, K. L. Buchmueller, W. D. Wilson, C. O'Hare, J. Kluza, D. Hochhauser, J. A. Hartley and M. Lee , *ChemBioChem*, 2006, **7**, 1722–1729.

11 P. Dervan, *Bioorg. Med. Chem.*, 2001, **9**, 2215–2235.

12 K. E. Dombrowski, W. Baldwin and J. E. Sheats, *J. Organomet. Chem.*, 1986, **302**, 281–306.

13 C. M. Cardona and A. E. Kaifer, *J. Am. Chem. Soc.*, 1998, **120**, 4023–4024.

14 P. Stepnicka, *Ferrocenes: Ligands, Materials, and Biomolecules*, John Wiley & Sons Inc: New York, 2008.

15 G. Jaouen, *Bioorganometallics: Biomolecules, Labelling and Medicine*, John Wiley & Sons, Ltd, 2006.

16 Z. H. Dai, J. Ni, X. H. Huang, G. F. Lu and J. C. Bao, *Bioelectrochemistry*, 2007, **70**, 250–256.

17 M. Carney, J. Lesniak, M. Likar and J. Pladziewicz, *J. Am. Chem. Soc.*, 1984, **106**, 2565–2569.

18 Miguel A. Fuertes, and Carlos Alonso and José. M. Pérez, 2003, **103**, 645–662.

19 A. Goel, D. Savage, S. R. Alley, P. N. Kelly, D. O'Sullivan, H. Mueller-Bunz and P. T. M. Kenny, *J. Organomet. Chem.*, 2007, **692**, 1292–1299.

20 E. W. Neuse, J. R. Woodhouse, G. Montaudo and C. Puglisi, *Appl. Organomet. Chem.*, 1988, **2**, 53–57.

21 B.-X. Ye, L.-J. Yuan, C. Chen and J.-C. Tao, *Electroanalysis*, 2005, **17**, 1523–1528.

22 F. Carso and M. Rossi, *Mini-Rev. Med. Chem.*, 2004, **4**, 49.

23 F. A. Larik, A. Saeed, T. A. Fattah, U. Muqadar and P. A. Channar, *Appl. Organomet. Chem.*, 2017, **31**, 1–22.

24 D. Li, S. Song and C. Fan, *Acc. Chem. Res.*, 2010, **43**, 631–641.

25 Y. Wu, S. Liu and L. He, *Anal. Chem.*, 2009, **81**, 7015–7021.

26 H. N. Cheng and R. A. Gross, *ACS Symp. Ser.*, 2005, **900**, 1.

27 X. Qiu, H. Zhao and M. Lan, *J. Organomet. Chem.*, 2009, **694**, 3958–3964.

28 S. Top, A. Vessières, G. Leclercq, J. Quivy, J. Tang, J. Vaissermann, M. Huché and G. Jaouen, *Chem. - A Eur. J.*, 2003, **9**, 5223–5236.

29 H. Yu, L. Wang, J. Huo, J. Ding and Q. Tan, *J. Appl. Polym. Sci.*, 2008, **110**, 1594–

1599.

30 A. M. O. Brett, S. H. Serrano, T. A. Macedo, D. Raimundo, M. Helena Marques and M. A. La-Scalea, *Electroanalysis*, 1996, **8**, 995–995.

31 S. Sato, M. Tsueda and S. Takenaka, *J. Organomet. Chem.*, 2010, **695**, 1858–1862.

32 H. Li, J.-N. Zhang, W. Zhou, H. Zhang, Q. Zhang, D.-H. Qu and H. Tian, *Org. Lett.*, 2013, **15**, 3070–3073.

33 W. Zhu, L. Song, Y. Yang and H. Tian, *Chem. - A Eur. J.*, 2012, **18**, 13388–13394.

34 J. C. Spiteri, J. S. Schembri, D. C. Magri, S. Selcuk, S. Koleman, G. Gulseren, T. Nalbantoglu, H. Boyaci, E. U. Akkaya, K. R. A. S. Sandanayake and J.-P. Soumillion, *New J. Chem.*, 2015, **39**, 3349–3352.

35 K. N. de Oliveira, P. Costa, J. R. Santin, L. Mazzambani, C. Bürger, C. Mora, R. J. Nunes and M. M. de Souza, *Bioorg. Med. Chem.*, 2011, **19**, 4295–4306.

36 R. Stolarski, *Fibres Text. East. Eur.*, 2002, **71**, 91.95.

37 A. P. Ferreira, J. L. F. da Silva, M. T. Duarte, M. F. M. da Piedade, M. P. Robalo, S. G. Harjivan, C. Marzano, V. Gandin and M. M. Marques, *Organometallics*, 2009, **28**, 5412–5423.

38 J. Clayden, N. Greeves, S. Warren and P. Worthers, *Organic Chemistry*, Oxford University Press, 1st ed., 2001.

39 Ahmed F. Abdel-Magid, Kenneth G. Carson, Bruce D. Harris, and Cynthia A. Maryanoff and R. D. Shah, *J. Org. Chem.*, 1996, **61**, 3849–3862.

40 F. Allouch, N. Dwadnia, N. V. Vologdin, Y. V. Svyaschenko, H. Cattey, M.-J. Penouilh, J. Roger, D. Naoufal, R. Ben Salem, N. Pirio and J.-C. Hierso, *Organometallics*, 2015, **34**, 5015–5028.

41 S. Gomez, J. A. Peters and T. Maschmeyer, *Adv. Synth. Catal.*, 2003, **344**, 1037–1058.

42 R. A. Arthurs, P. N. Horton, S. J. Coles and C. J. Richards, *Eur. J. Inorg. Chem.*,

2017, **2017**, 229–232.

43 Z. Yang, M. A. d'Auriac, S. Goggins, B. Kasprzyk-Hordern, K. V. Thomas, C. G. Frost and P. Estrela, *Environ. Sci. Technol.*, 2015, **49**, 5609–5617.

44 E. E. Langdon-Jones, N. O. Symonds, S. E. Yates, A. J. Hayes, D. Lloyd, R. Williams, S. J. Coles, P. N. Horton and S. J. A. Pope, *Inorg. Chem.*, 2014, **53**, 3788–3797.

45 K. Tahara, T. Akita, S. Katao and J. Kikuchi, *Dalton+- Trans.*, 2014, **43**, 1368–1379.

46 M. A. Vorotyntsev, V. A. Zinovyeva, D. V. Konev, M. Picquet, L. Gaillon and C. Rizzi, *J. Phys. Chem. B*, 2009, **113**, 1085–1099.

47 D.-Y. Liu, J. Qi, X.-Y. Liu, H.-R. He, J.-T. Chen and G.-M. Yang, *Inorg. Chem. Commun.*, 2014, **43**, 173–178.

48 C. H. Hamann, A. Hamnett and W. Vielstich, *Electrochemistry*, Wiley-VCH, 2007.

49 M. Frank, M. Nieger, F. Vögtle, P. Belser, A. von Zelewsky, L. De Cola, V. Balzani, F. Barigelletti and L. Flamigni, *Inorganica Chim. Acta*, 1996, **242**, 281–291.